

THE INTERACTION BETWEEN 6 MV X-RAYS AND $p(66)/\text{Be}$
NEUTRONS WITH SPHERICAL GOLD NANOPARTICLES TO
INDUCE CELLULAR DAMAGE



MONIQUE ENGELBRECHT

2016

**THE INTERACTION BETWEEN 6 MV X-RAYS AND p(66)/Be NEUTRONS WITH
SPHERICAL GOLD NANOPARTICLES TO INDUCE CELLULAR DAMAGE**

by

MONIQUE ENGELBRECHT

Submitted in partial fulfilment for the degree

Magister Scientiae

(Nanoscience)



in the

Department of Medical Bioscience, Faculty of Science

WESTERN CAPE

at the

University of the Western Cape

Bellville

South Africa

Supervisor: Prof. M. de Kock

Co-supervisor: Prof. J. P. Slabbert

Submitted: November 2016

DECLARATION

I, the undersigned, hereby declare that the work contained in this thesis titled **The interaction between 6 MV X-rays and p(66)/Be neutrons with spherical gold nanoparticles to induce cellular damage** is my own work and has not previously been submitted for any degree or assessment at any university. All the sources that I have used or quoted have been indicated and acknowledged by means of complete references.



M. Engelbrecht

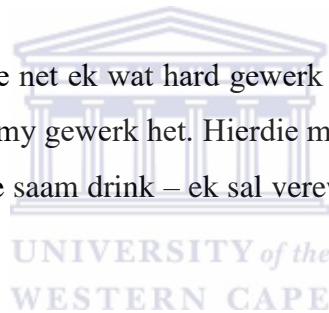
Date

ACKNOWLEDGEMENTS

Ek sal nooit weer sê: “Ek kan nie,” want “Ek is tot alles in staat deur Hom wat my krag gee.”

- Filip. 4:13

In 'n projek soos hierdie is dit nie net ek wat hard gewerk het nie – dis die mense wat in die agtergrond net so hard saam met my gewerk het. Hierdie mense het almal 'n bydrae gehad, al was dit net moed inpraat of koffie saam drink – ek sal verewig dankbaar wees vir mense soos julle.



Die “mense soos julle” vir wie ek 'n baie groot dankie wil sê is die volgende:

My wonderlike promotor, Prof. Maryna de Kock. Sonder Prof sou hierdie projek nooit op die been gekom het nie. Ek is oneindig dankbaar dat ek die geleentheid gekry het om saam met Prof te kon werk aan projekte – ek sou nie met enige ander professor so lekker kon saamwerk nie. Mag ander studente net so gelukkig wees soos ek om saam met 'n puik professor soos Prof te werk.

Aan my iThemba gesin:

Julle is die aangenaamste mense wat ek al ooit teëgekom het. Baie dankie Prof. Kobus Slabbert vir al Prof se leiding en advies – ek waardeer dit opreg! Prof se briljante kennis verstom my elke dag. Mag ek eendag net soveel leiding vir iemand kan bied.

Mej. Xanthe Miles, jy is een van die dierbaarste mense! Dankie dat jy my altyd gehelp het en vir al die wenke wat jy my gegee het oor hoe om iets op die regte manier te doen, of vir die “probeer lievers hierdie tegniek”. Dankie vir die motivering om al daardie selle te tel. Jy was my regter- EN linkerhand. Uit hierdie proses van eksperimente doen, het ons ’n vriendskapsband gesmee – baie dankie daarvoor.

Verder, baie dankie aan Dr. Charlot Vandevoorde vir al jou hulp met *foci* – jy is ’n boffin! Ook baie dankie aan Philip Beukes vir al die bestraling-optogte wat ons moes doen. Julle gewilligheid en die tyd wat julle afgestaan het om my te help, was altyd opreg waardeer.

My vriende naaste aan my hart (julle weet wie julle is) – dankie vir julle motivering en “kom ons gaan vir ’n vinnige enetjie”, al het dit nooit by een gebly nie. Ek wil ook dankie sê aan Helen vir haar hulp met die proeflees van hierdie tesis.

Aan my oupa en ouma (Dirk en Annie Coetzee): Dankie vir oupa se besorgdheid oor my navorsing. “Hoe het dit vandag by die *lab* gegaan?” “Was dit toe suksesvol?” Al dié skynbaar klein vragies oor my werk is wat saak maak. Dankie ouma vir die ondersteuning, asook omgee oor my studies en dat ouma altyd wil hê ek beter moet doen.

WESTERN CAPE

Laaste, maar nie die minste nie – my ouers, Eric en Madelein Engelbrecht. Dankie vir AL die ondersteuning, motivering en konstante aanmoediging om nooit tou op te gooi nie. Ek kon nie vir beter ouers vra nie, al gee ek julle soms grys hare!

TRANSLATED TO ENGLISH

I can do all things because of Christ who strengthens me.

– Philippians. 4:13

With a project such as this, it is not only me who has worked hard – it is also those who worked just as hard behind the scenes. These people all contributed in one way or another, whether it was just giving me a pep talk or going for a cup of coffee – I’ll be eternally grateful for people like you.

The “people like you” to whom I owe a huge thank you, are the following:

My wonderful supervisor, Prof Maryna de Kock. Without you this project would have never seen the light of day. I am eternally grateful for the opportunity to work on projects with you – I would not have worked as well with any other professor. May other students be as lucky to be able to work with such an outstanding professor such as yourself.

To my iThemba family:

You are the most pleasant group of people that I have ever had the pleasure of meeting. Thank you for your guidance and advice Prof Kobus Slabbert – I really appreciate it! Your expert knowledge never ceases to amaze me. May I be able to one day provide someone with the same type of guidance.

Miss Xanthene Miles, you are one of the most loveable people! Thank you for always helping me, for all the tips you gave me on how to do something the right way, or for the “rather try this technique”. Thank you for motivating me to count all those cells. You were my right hand, as well as the left! By doing all these experiments, we forged a bond of friendship – thank you for that.

Furthermore, I would like to thank Dr Charlot Vandevoorde for your help with foci – you are a genius! I would also like to thank Philip Beukes for the irradiation of my samples. Your willingness and the time you sacrificed to help me was always greatly appreciated.

The friends nearest and dearest to me (you know who you are) – thank you for your motivation and the “let’s just go for a quick one”, even though it never was just one. Also, thank you to Helen for assisting with the proofreading of this thesis.

To my grandparents (Dirk en Annie Coetzee): Thank you grandpa for being so concerned about my research. “How did it go at the lab today?” “Was it successful?” It’s these seemingly unimportant questions about my work that truly matters to me. Thank you for your support grandma, as well as for caring about my studies and for always wanting me to be better.

Last, but definitely not least, my parents – Eric en Madelein Engelbrecht. Thank you for ALL of the support, motivation and constant encouragement to never throw in the towel. I could not have asked for better parents, even though I am the cause of your grey hair!

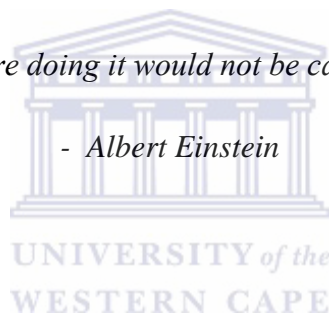


DEDICATION

I dedicate my dissertation work to my family and friends – with their encouragement, affection and love is what made me able to achieve success.

“If we knew what we were doing it would not be called research, would it?”

- Albert Einstein



“I would rather die of passion than boredom.”

- Van Gogh.

TABLE OF CONTENTS

DECLARATION	i
ACKNOWLEDGEMENTS	ii
DEDICATION	vi
TABLE OF CONTENTS	vii
ABBREVIATIONS	xi
LIST OF TABLES	xix
LIST OF FIGURES	xxiv
ABSTRACT	1
CHAPTER 1:	3
LITERATURE REVIEW	3
1.1 Nanotechnology	3
1.2 Gold nanoparticles (AuNPs)	5
1.2.1 History of gold	5
1.2.2 Gold as medicine	5
1.2.3 Synthesis of AuNPs	6
1.2.4 Characterisation and properties of AuNPs	6
1.2.5 <i>In vitro</i> and <i>in vivo</i> studies	8
1.3 Cancer	8
1.3.1 Breast cancer	9
1.3.2 Breast cancer treatment	10
1.4 Radiation	11
1.5 Ionising radiation (IR)	12
1.5.1 X-ray radiation	12
1.5.2 p(66)/Be neutron radiation	13
1.6 Application of AuNPs in cancer	14
1.6.1 Radiosensitisers	14
1.6.2 AuNPs accumulation and clearance	15
1.6.3 AuNPs sensitisation in cell line and animal models	17
	vii



1.7 Overview of cell cycle	18
1.7.1 The cell cycle	18
1.7.2 Cell cycle phases	19
1.7.2.1 The G ₁ phase	19
1.7.2.2 The S phase	20
1.7.2.3 The G ₂ /M phase	20
1.7.3 Cell cycle checkpoints	21
1.7.3.1 G ₁ /S checkpoint	21
1.7.3.2 G ₂ /M checkpoint	22
1.7.3.3 Mitotic checkpoint	22
1.8 Cell cycle and radiation	22
1.9 Aims of the study	23
CHAPTER 2:	24
MATERIALS AND METHODS	24
2.1 Materials and Methods	24
2.1.1 Reagents and cells	24
2.1.1.1 Chinese Hamster Ovary (CHO-K1) cells	25
2.1.1.2 Brain endothelial (BEnd5) cells	25
2.1.1.3 Michigan Cancer Foundation-7 (MCF-7) cells	25
2.1.1.4 Michigan Cancer Foundation-10A (MCF-10A) cells	25
2.1.2 Gold nanoparticles (AuNPs)	26
2.1.3 Sample collection and isolation of lymphocytes for γ -H2AX foci assay	26
2.1.4 General cell culture procedures	26
2.1.5 Characterisation of AuNPs	27
2.1.5.1 UV-visible (vis) absorption spectrophotometry	27
2.1.5.2 Zeta (Z) potential dynamic light scattering (DLS) and polydispersity index (PDI)	27
2.1.5.3 Transmission electron microscopy (TEM)	28
2.1.5.3.1 AuNPs within cells	28
2.1.6 Experimental set-up for irradiation procedures	29
2.1.6.1 X-ray radiation	29
2.1.6.2 p(66)/Be neutron radiation	30
2.1.7 γ -H2AX foci assay	31
2.1.8 Cytokinesis-block Micronucleus (CBMN) assay	32

2.1.9 Cell viability assay	35
2.1.10 Cell cycle analysis	36
2.1.11 Statistical analyses	38
2.1.11.1 γ -H2AX foci assay	38
2.1.11.2 Cytokinesis-block Micronucleus (CBMN) assay	38
2.1.11.3 Cell viability assay	38
2.1.11.4 Cell cycle analysis	39
CHAPTER 3:	40
RESULTS	40
3.1 Characterisation of AuNPs	40
3.1.1 UV-visible (vis) absorption spectrophotometry	40
3.1.2 Zeta (Z) potential, dynamic light scattering (DLS) and polydispersity index (PDI)	41
3.1.3 Transmission electron microscopy (TEM)	43
3.1.3.1 AuNPs within MCF-7 & MCF-10A cells	43
3.2 DNA double-strand breaks	45
3.3 Cytogenetic damage	46
3.3.1 Visualisation of MNi with binucleated cells (BNCs)	46
3.3.1.1 Cells incubated for 4 hours with 50 μ g/ml of AuNPs and 2 Gy X-ray radiation	46
3.3.1.2 Cells incubated for 4 hours with 50 μ g/ml of AuNPs and 4 Gy X-ray radiation	49
3.3.1.3 Cells incubated for 4 hours with 2.5 μ g/ml of AuNPs and 2 Gy X-ray radiation	50
3.3.1.4 Cells incubated for 4 hours with 50 μ g/ml of AuNPs and 1 Gy p(66)/Be neutron radiation	52
3.3.1.5 Cells incubated for 4 hours with 50 μ g/ml of AuNPs and 2 Gy p(66)/Be neutron radiation	53
3.3.2 Quantification of cellular kinetics and MNi	55
3.4 Cell viability assays	68
3.5 Flow cytometry	72
CHAPTER 4:	77
DISCUSSION	77
4.1 Introduction	77
4.2 Characterisation of AuNPs	78

4.2.1 UV-visible (vis) absorption spectrometry	78
4.2.2 Zeta (Z) potential dynamic light scattering (DLS) and polydispersity index (PDI)	78
4.2.3 Transmission electron microscopy (TEM)	79
4.3 γ -H2AX foci assay	82
4.4 Cytokinesis-Block Micronucleus (CBMN) assay	83
4.5 Cell viability assay	86
4.6 Flow cytometry (Propidium iodide)	88
SUMMARY AND CONCLUSION	91
REFERENCES	93
ADDENDUM	



ABBREVIATIONS

α	alpha
γ	gamma
γ H2AX	phosphorylated H2AX
λ_{\max}	maximum wavelength
%	percentage
3-D	three-dimensional
7-AAD	7-aminoactinomycin D
$^{\circ}\text{C}$	degree Celsius
>	greater than
<	smaller than

A

Ab	antibody
AF	auranofin
ANOVA	Analysis of variance
AO	Acridine Orange
APC/C	Anaphase-Promoting Complex/Cyclosome

ATCC	American Type Culture Collection
ATM	Ataxia Telangiectasia Mutated
ATP	adenosine triphosphate
ATR	ATM and Rad3-related
Au	gold (bulk)
AuNPs	gold nanoparticles

B

BBB	blood-brain barrier
BC	Before Christ
BEnd5	brain endothelial cells
BNC(s)	binucleated cell(s)
BRCA 1	Breast cancer gene 1
BRCA 2	Breast cancer gene 2
bromodeoyuridine	BrdU
BSA	bovine serum albumin

C

CBMN	cytokinesis-block micronucleus assay
Cdc	cell division cycle
Cdc25A	cell division cycle 25A
Cdc25C	cell division cycle 25C

CDK	cyclin-dependent kinase
Cdt 1	Cdc10-dependent transcript 1
CHK1	checkpoint kinases 1
CHK2	checkpoint kinases 2
CHO-K1	Chinese Hamster Ovary cells
CKI	CDK inhibitors

D

DAPI	4',6-Diamidino-2-Phenylindolo
dH ₂ O	distilled water
DLS	dynamic light scattering
DMEM	Dulbecco's Modified Eagle Medium
DMSO	dimethyl sulfoxide
DNA	deoxyribonucleic acid
DSB(s)	double strand break(s)

E

e.g.	'for example'
E2F	transcription factor
EGF	epidermal growth factor
EPR	enhanced permeability and retention
ER	estrogen receptor

et al. 'and other'
EtOH ethanol
eV electron Volt

F

FACS fluorescence-activated cell sorting
FBS fetal bovine serum
FITC fluorescein isothiocyanate
FSC forward scatter

G

G_(0,1 and 2) gap phase
Gy Gray



UNIVERSITY of the
WESTERN CAPE

H

H⁺ hydrogen ions
H₂O₂ hydrogen peroxide
H2AX H2A histone family, member X

I

ICP-AES inductively coupled plasma atomic emission spectroscopy
i.e. 'that is'

IR ionising radiation

J

J joule

K

K562 human leukemic cells

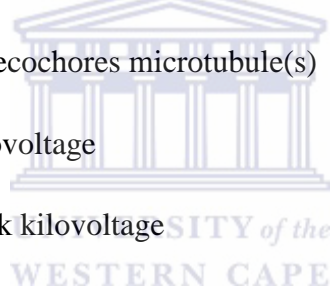
keV kiloelectron volts

keV/ μ m kiloelectron volts/micrometer

K-MT(s) kinetochore microtubule(s)

kV kilovoltage

kVp peak kilovoltage

The logo of the University of the Western Cape, featuring a classical building with columns and a pediment, with the text 'UNIVERSITY of the WESTERN CAPE' below it.

L

LET linear energy transfer

LINAC linear accelerator

M

M phase mitosis phase

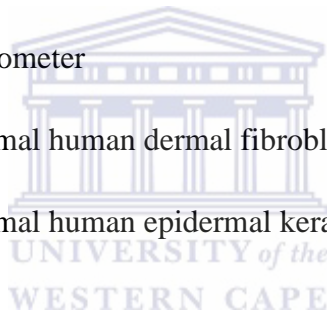
MCF-7 human breast adenocarcinoma cell line

MCF-10A non-tumourgenic human breast epithelial cell line

MCM2-7	minichromosome maintenance subunits 2-7
MN(i)	micronucleus (micronuclei)
MT(s)	microtubule(s)
MTT	3-(4,5-Dimethylthiazol-2-yl)-2,5-diphenyltetrazolium bromide
MeV	megaelectron-volts
mV	millivolts
MV	mega volts

N

nm	nanometer
NHDF	normal human dermal fibroblasts
NHEK	normal human epidermal keratinocytes



O

OH [•]	hydroxyl radicals
-----------------	-------------------

P

p(66)/Be	neutron beam
p21 ^{cip1}	protein encoded by the CDK1NA gene
p27 ^{kip1}	protein encoded by the CDKN1B gene.
p53	tumour protein 53
PBS	phosphate buffered saline

PC-3	human prostate cancer cell line
PCD	programmed cell death
PDI	polydispersity index
pH	measure of the acidity or basicity of a solution
PI	propidium iodide
pRB	retinoblastoma protein
preRC	pre-replicative complexes

R

RB	retinoblastoma
RBE	relative biological effectiveness
REM	receptor-mediated endocytosis
RES	reticuloendothelial system
rpm	revolutions per minute
ROS	reactive oxygen species
RT	radiotherapy

S

S phase	synthesis phase
SEER	Surveillance, Epidemiology, and End Results Program
SERS	Surface Enhanced Raman Scattering
SPR	surface plasmon resonance

SSB(s) single-strand break(s)

SSC side scatter

T

TB tuberculosis

TEM transmission electron microscopy

Thr Threonine

TRITC Tetramethyl Rhodamine Isothiocyanate

U

UV ultraviolet



V

vis visible

W

WHO World Health Organisation

Z

Z zeta

LIST OF TABLES

CHAPTER 3

Page

- Table 3.1** Shows the percentage distribution of CHO-K1 controls, AuNPs and irradiated AuNPs treated cells in the different cell cycle phases. PI staining detected by flow cytometry was utilized to investigate the effects of AuNPs and X-ray radiation on the cell cycle distribution. DNA content analysis showed a significant increase in the number of CHO-K1 cells in the S phase (38.2%) and in the G₂/M phase (37.9%), after radiation, when compared to the control cells in S (27.4%) and G₂/M (28.2%) (Fig. 3.34 A & B). Exposure to 5 and 10 nm AuNPs respectively increased the number of cells in G₂/M (37.3% and 42.5%) when compared to control cells (Fig 3.34 C & E). Radiated cells with 5 nm AuNPs increased the number of cells in the G₂/M phase even more (48.1%) and the cells treated with 10 nm AuNPs showed an increase in the S phase (42.4%).
- Table 3.2** **Table 3.2:** Shows the percentage distribution of BEnd5 controls, AuNPs and irradiated AuNPs treated cells in the different cell cycle phases. DNA content analysis displayed a significant increase in the number of BEnd5 cells in the G₂/M phase (28.2%) after radiation when compared to the control cells in G₂/M (21.9%) (Fig. 3.35 A & B). No major difference in number of cells in S phase (15.3%), after radiation, when compared to control cells were observed (Fig. 3.34 A & B). Exposure to 5 and 10 nm AuNPs respectively increased the number of cells in G₂/M (34.1% and 35.4%) when compared to control cells (Fig 3.35 C & E).

Table 3.3 **Table 3.3: Shows the percentage distribution of MCF-7 controls, AuNPs and irradiated AuNPs treated cells in the different cell cycle phases.** PI staining detected by flow cytometry was utilized to investigate the effects of AuNPs and X-ray radiation on the cell cycle distribution. DNA content analysis showed a significant increase in the number of MCF-7 cells in the G₂/M phase (51.7%), after radiation, when compared to the control cells G₂/M (33.7%) (Fig. 3.36 A & B). Exposure to 5 and 10 nm AuNPs respectively increased the number of cells in G₂/M (45.7% and 47.1%) when compared to control cells in G₂/M phase (33.7%). Cells incubated with 5 nm AuNPs, followed by 2 Gy X-ray radiation showed a significant increased the number of cells in the G₂/M phase (63.2%) when compared to control cells in G₂/M phase (33.7%). Cells exposed to 10 nm AuNPs and irradiated 10 nm AuNPs displayed a small decrease in the number of cells (47.5% and 45.5%, respectively) (Fig. 3.36 E & F).

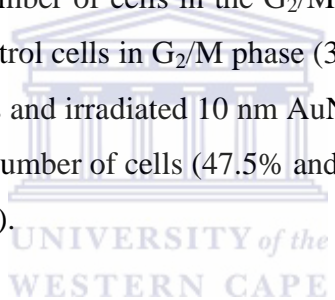


Table 3.4 **Table 3.4: Shows the percentage distribution of MCF-10A controls, AuNPs and irradiated AuNPs treated cells in the different cell cycle phases.** DNA content analysis showed a significant increase in the number of MCF-10A cells in the S phase (20.4%) after radiation when compared to the control cells in S (10.4%) (Fig. 3.37 A & B). Exposure to 5 and 10 nm AuNPs respectively increased the number of cells in G₂/M (37.3% and 42.5%) when compared to control cells (Fig 3.34 C & E). Radiated cells with 5 nm and 10 nm AuNPs respectively increased the number of cells in the S phase (22.5% & 17.6 %) when compared to the control S phase (10.4%).

CHAPTER 4 **Page**

Table 4.1 **Flow cytometry.** This latter was used to investigate cell cycle progression in CHO-K1, BEnd5, MCF-7 and MCF-10A cells. **88**

ADDENDUM **Page**

Table 5.3 **Average number of foci per isolated human lymphocytes incubated with 50 µg/ml AuNPs for 4 hours.** Kruskal-Wallis test was used to determine the significant difference between the control means and experimental groups. **127**

Table 5.4 **% of cell viability in CHO-K1 cells incubated with 50 µg/ml AuNPs for 4 hours.** Kruskal-Wallis test was used to determine the significant difference between the control means and experimental groups. **127**

Table 5.5 **% of cell viability in CHO-K1 cells incubated with 50 µg/ml AuNPs for 4 hours followed by 4 Gy X-ray radiation.** Kruskal-Wallis test was used to determine the significant difference between the control means and experimental groups. **128**

Table 5.6 **% of cell viability in CHO-K1 cells incubated with 50 µg/ml AuNPs for 24 hours.** Kruskal-Wallis test was used to determine the significant difference between the control means and experimental groups. **128**

Table 5.7 **% of cell viability in BEnd5 cells incubated with 50 µg/ml AuNPs for 4 hours.** Kruskal-Wallis test was used to determine the significant difference between the control means and experimental groups. **129**

Table 5.8 **% of cell viability in BEnd5 cells incubated with 50 µg/ml** **129**

AuNPs for 4 hours followed by 4 Gy X-ray radiation. Kruskal-Wallis test was used to determine the significant difference between the control means and experimental groups.

Table 5.9	% of cell viability in BEnd5 cells incubated with 50 µg/ml AuNPs for 24 hours. Kruskal-Wallis test was used to determine the significant difference between the control means and experimental groups.	130
Table 5.10	% of cell viability in MCF-7 cells incubated with 50 µg/ml AuNPs for 4 hours. Kruskal-Wallis test was used to determine the significant difference between the control means and experimental groups.	130
Table 5.11	% of cell viability in MCF-7 cells incubated with 50 µg/ml AuNPs for 4 hours followed by 4 Gy X-ray radiation. Kruskal-Wallis test was used to determine the significant difference between the control means and experimental groups.	131
Table 5.12	% of cell viability in MCF-7 cells incubated with 50 µg/ml AuNPs for 24 hours. Kruskal-Wallis test was used to determine the significant difference between the control means and experimental groups.	131
Table 5.13	% of cell viability in MCF-10A cells incubated with 50 µg/ml AuNPs for 4 hours. Kruskal-Wallis test was used to determine the significant difference between the control means and experimental groups.	132
Table 5.14	% of cell viability in MCF-10A cells incubated with 50 µg/ml AuNPs for 4 hours followed by 4 Gy X-ray radiation. Kruskal-Wallis test was used to determine the significant difference between the control means and experimental groups.	132

Table 5.15 **% of cell viability in MCF-10A cells incubated with 50** **133**
µg/ml AuNPs for 24 hours. Kruskal-Wallis test was used to
determine the significant difference between the control means
and experimental groups.



LIST OF FIGURES

CHAPTER 1		Page
Figure 1.1	Logarithmical length scale showing size of nanoparticles compared to biological components and description of 'nano' and 'micro' sizes. Relative sizes of nanoparticles compared to common biological structures. Diagram of nanoparticle size as compared to common biological structures and their linked length scale. An electron microscope is required to envision structures that are submicrometer in size (Ediriwickrema & Saltzman, 2015).	3
Figure 1.2	Examples of nanoparticles. Several nanoparticles have been scrutinized for biomedical applications targeting cancer (Cai et al., 2008).	4
Figure 1.3	The Lycurus Cup. This cup was designed and made by Romans in the 40th century (Heiligtag & Niederberger, 2013).	5
Figure 1.4	Synthesis equation for synthesis of AuNPs. Schematic representation of reduction of the chloraurate ions by sodium citrate at 100°C (Faraday, 1875) to produce AuNPs.	6
Figure 1.5	Types of IR. The penetrating ability of five major types of IR (http://www.nrc.gov/about-nrc/radiation/health-	12

effects/radiation-basics.html).

- Figure 1.6** **Examples of radiation damage to DNA resulting from both direct and indirect effects.** **15**
During the indirect effect, secondary electrons for instance, a water molecule (H₂O) to produce a hydroxyl radical (OH[•]), which in turn produces damage to DNA (Hall & Giaccia, 2006).
- Figure 1.7** **Size dependent accumulation.** Schematic representation of size dependent accumulation and clearance of AuNPs bioconjugates in the organs of mice. (Zhang et al., 2011; Barchanski, 2016). **17**
- Figure 1.8** **Diagram illustrating the four phases of the cell cycle.** **19**
The cell cycle is the series of events that takes place in cells, which leads to cell division and replication. In eukaryotes, the cell cycle has two main phases: interphase and the mitotic phase. Interphase is the stage during which the cell prepares, grows and accumulates nutrients essential for mitosis and also replicates the DNA (Nurse, 1994). In the mitotic phase, the cell divides into two separate cells known as 'daughter cells' and the final phase is cytokinesis, where the newly formed cells are fully divided (<http://biology.tutorvista.com/cell/cell-cycle.html>).
- Figure 1.9** **Schematic representation of the RB/E2F pathway.** **20**
Phosphorylation by cyclin D-CDK 4 and cyclin E-CDK 2, causes changes to the RB structure and releases E2F to activate cell division genes. *Adapted from Freeman & Co (2004), Life: The Science of Biology, 7th Edition.*

CHAPTER 2	Page	
Figure 2.1	X-ray experimental set-up. (A) The red arrow shows the 20x20 cm Shonka chambers. The yellow arrow displays the distance from the gantry to the samples, which is 100 cm. (B) The red arrow shows the depth of the Shonka chamber (iThemba LABS, Somerset West, South Africa).	31
Figure 2.2	p(66)/Be neutron radiation set up. (A) The red arrow shows the 30x30 cm radiation field. (B) The yellow arrow shows the samples in petri dishes and the red arrow shows three Perspex blocks, each block is 3 cm thick (iThemba LABS, Somerset West, South Africa).	32
Figure 2.3	The Metafer 4 System set-up. (A) The complete Metafer 4 System (Metasystems) equipped with a 40x objective. The white arrow shows the stage of the inverted fluorescence microscope (Zeiss) that can contain 8 slides. (B) Detailed image to show precisely the location of the cell containing DNA DSBs, on the slide – indicated by the white arrow (iThemba LABS, Somerset West, South Africa).	33
Figure 2.4	Different types of BNCs in the CBMN assay. (A) Ideal BNC, (B) a BNC with touching nuclei, (C) BNC with thin nucleoplasmic bridge between nuclei and (D) BNC with rather thick nucleoplasmic bridge (Fenech et al., 2003).	35
Figure 2.5	The characteristic appearance and relative size of MNi in BNCs. (A) BNC with two MNi containing viable MNi varying un sizes between 1/3 to 1/9 of the main nuclei. (B) BNC with three MNi touching, but not overlapping the main nuclei. (C) A BNC with nucleoplasmic bridge	36

between main nuclei and two MNi. **(D)** A BNC with six MNi varying in sizes (Fenech et al., 2003).

Figure 2.6 **Example of MTT assay.** 96 well plate, in which the MTT solution was removed and the formazan solvent DMSO was added, resulting in a purple colour. **37**

Figure 2.7 **Mechanisms of flow cytometry.** There are four general components of a flow cytometer: fluidics, optics, detectors and electronics. Cells in suspension flow in single-file through an illuminated volume, where they scatter light and emit fluorescence that is collected, filter and converted to digital numbers that are stored on a computer (Brown et al., 2002). **38**

CHAPTER 3

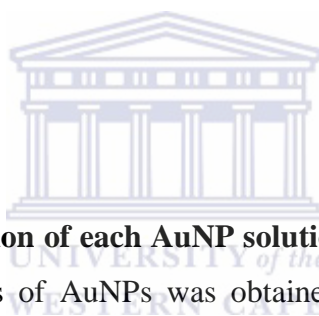


Figure 3.1 **The absorption of each AuNP solution.** UV-vis spectrum of both types of AuNPs was obtained using the Agilent 8453. Absorbance profiles were measured between 525–580 nm, with an SPR of 525 nm occurring for 5 nm AuNPs **(A)** and 10 nm AuNPs **(B)**. The red vertical line represents the λ_{max} at 525 nm and indicates the successful production of AuNPs. **40**

Figure 3.2.1 **Zeta (Z) potential measurements of 5 nm and 10 nm AuNPs.** The Z-potential of 5 **(A)** and 10 **(B)** nm AuNPs was -24.5 mV and -23.2 mV, respectively. The negative Z-potential values present the necessary repulsive forces for the particles to remain stable in the solution. Nanoparticles with Z-potential < -30 mV are regarded as strongly anionic, whereas nanoparticles with a Z-potential > +30 mV are regarded as strongly cationic. Data was obtained in phase **41**

analysis light scattering mode at 25 °C and pH 7.4 (Addendum: Table 5.1).

Figure 3.2.2 **PDI represents the size distribution width, whereas DLS (Z-average) displays the hydrodynamic core size of both 5 and 10 nm AuNPs.** A PDI value of 0.1–0.25 suggests that the nanoparticles have a uniform size distribution, whilst a PDI > 0.5 indicates a very broad distribution. Results conducted shows that both sizes of AuNPs have a uniformity size width distribution. DLS measurements (Z-average) show that the 5 nm AuNPs are 38.12 nm in diameter (**A**), whilst 10 nm AuNPs are 48.50 nm in diameter (**B**). These larger sizes in diameter may be due to the agglomeration state of nanoparticles as a function of time or suspending solution. Data was obtained in phase analysis light scattering mode at 25 °C and pH 7.4 (Addendum: Fig. 5.2).

Figure 3.3 **TEM micrographs of 50 µg/ml of 10 nm AuNPs within MCF-7 cells (A–F) and within the MCF-10A cells (G–L).** A large number of vesicles transporting AuNPs were observed in the MCF-7 cells. After the 4 hour incubation period, some AuNPs were observed in the vicinity of the nucleus. Red arrows indicate the nuclear membrane of the cell, blue arrows indicate possible autophagosomes or transport vesicles, yellow arrows represents the 10 nm AuNPs, pink arrows shows swollen mitochondria and the green arrows indicate possible lysosomal bodies. The swollen mitochondria could possibly be due to AuNP induced cytotoxic stress. AuNPs are taken up by endocytosis which is clearly indicated by the orange arrows (**J**), (**E**) and (**F**), which indicates the distance from the AuNPs to the nuclear membrane; 0.12 µm, 0.15 µm and

0.49 μm , respectively. 0.01 μm TEM measurement of the AuNPs itself to illustrate that it is indeed 10 nm in diameter (G). AuNPs were observed in the nucleus (A and B), within the cells and near the nuclear membranes of the cells. The MCF-7 cells consistently displayed a greater number of AuNPs in the cells, in comparison to the MCF-10A cells which displayed far less AuNPs.

- Figure 3.4** **γ -H2AX foci assay.** Examples of isolated human lymphocytes after the γ -H2AX foci assay, wherein (A–C) illustrates non-irradiated control samples, (D–F) non-irradiated lymphocytes incubated with 5 nm AuNPs, (G–I) lymphocytes incubated irradiated with 5 nm AuNPs, (J–L) non-irradiated lymphocytes incubated with 10 nm AuNPs and (M–O) lymphocytes incubated irradiated with 10 nm AuNPs. The blue area represents the isolated human lymphocyte and the green ‘dots’ shows the foci, which represent the amount of DNA DSBs in the cell. All samples were treated with 50 $\mu\text{g}/\text{ml}$ of AuNPs and irradiated with 1 Gy X-rays. **45**
- Figure 3.5** **Box-and-Whisker plot representing γ -H2AX foci in isolated lymphocytes.** Box-and-Whisker plots represents the quantification of effects of isolated human lymphocytes incubated with culture media containing 50 $\mu\text{g}/\text{ml}$ of AuNPs for 4 hours followed by 1 Gy X-rays and 1 Gy p(66)/Be neutron radiation, respectively. Significant increases ($p < 0.000001$) in foci are observed in the overall cell count compared to the control. * represents only two data points obtained for the p(66)/Be neutron radiation experiment (Addendum: Table 5.3). **46**
- Figure 3.6** CHO-K1 cells after CBMN assay, wherein (A) illustrates a BNC, (B) two BNC, each with one micronuclei (MNi), (C) **47**

a characteristic apoptotic cell indicated via a blue arrow, **(D)** a BNC with one MNi, **(E)** a BNC with three MNi and **(F)** a BNC with four MNi. White arrows indicate MNi within BNCs.

- Figure 3.7** BEnd5 cells after CBMN assay, wherein **(A)** illustrates a two BNCs, **(B)** two mononucleated cells, and a BNC with one MNi, **(C)** and **(D)** a BNC with one MNi, **(E)** a mononucleated cell, and a BNC with three MNi and **(F)** two BNC, one with two MNi. White arrows indicate MNi within BNCs. **47**
- Figure 3.8** MCF-7 cells after CBMN assay, wherein **(A)** illustrates a BNC, **(B)** a BNC with three MNi, **(C)** two BNC with four and five MNi, respectively, **(D)** a BNC with an anaphase bridge between the cells, **(E)** a BNC and a possible apoptotic cell and **(F)** a BNC with multiple MNi. White arrows indicate MNi within BNCs, blue arrow indicates a characteristic apoptotic cell and pink arrows indicate an anaphase bridge. **48**
- Figure 3.9** MCF-10A cells after CBMN assay, wherein **(A)** illustrates two BNCs, **(B)** a BNC with two MNi, **(C)** two BNCs, **(D)** a BNC, **(E)** a mononucleated cell, and a BNC with three MNi and **(F)** a BNC with one MNi. White arrows indicate MNi within BNCs and the pink arrow indicate an anaphase bridge. **48**
- Figure 3.10** CHO-K1 cells after CBMN assay, wherein **(A)** illustrates a BNC, **(B)** a BNC with multiple MNi, **(C)** a BNC with two MNi, **(D)** a BNC, and **(E)** and **(F)** a BNC with multiple MNi. White arrows indicate MNi within BNCs, the blue arrow illustrates a characteristic apoptotic cell and yellow **49**

arrow indicates cell blebbing.

- Figure 3.11** MCF-7 cells after CBMN assay, wherein (A) illustrates a BNC, (B) four BNCs with multiple MNi, (C) a BNC with two MNi, (D) a BNC with four MNi, (E) a BNC with two MNi, and (F) two distinctive apoptotic cells. White arrows indicate MNi within BNCs, the blue arrow illustrates a distinctive apoptotic cell and pink arrow indicates an anaphase bridge. **50**
- Figure 3.12** CHO-K1 cells after CBMN assay, wherein (A) illustrates two BNCs, (B) two BNCs; one with one MNi, (C) two BNC, and a cell in prometaphase, (D) and (E) four BNC, and (F) a BNC with one MNi, and a cell in early anaphase. White arrows indicate MNi within BNCs, the blue arrows indicate distinctive apoptotic cells, orange arrows indicate metaphases, and the purple arrow shows that the cells are pyktonic. **51**
- Figure 3.13** MCF-7 cells after CBMN assay, wherein (A) illustrates two BNCs, (B) a BNC with two MNi, (C) two BNCs, (D) two BNCs; one with one MNi, (E) six BNCs, (F) three BNCs; one with two MNi. White arrows indicate MNi within BNCs and the pink arrow points to an anaphase bridge. **51**
- Figure 3.14** CHO-K1 cells after CBMN assay, wherein (A) illustrates three BNCs, (B) three BNCs; one with three MNi, (C) and (D) a BNC with one MNi, and (E) and (F) a BNC with an anaphase bridge between the cells. White arrows indicate MNi within BNCs, a yellow arrow shows blebbing of the cell and pink arrow shows a distinctive anaphase bridge. **52**

- Figure 3.15** MCF-7 cells after CBMN assay, wherein (A) illustrates two BNCs, (B) a BNC with different sizes of MNi, (C) BNCs with one MNi and one without MNi, (D) two BNCs, both containing two MNi, (E) a BNC with four MNi, and (F) three BNCs with various sizes and quantities of MNi. White arrows indicate MNi within BNCs and the pink arrow shows a distinctive anaphase bridge. **53**
- Figure 3.16** CHO-K1 cells after CBMN assay, wherein (A) illustrates three BNCs, (B) multiple apoptotic cells, (C) and (D) BNCs with one MNi, (E) a BNC with multiple MNi, and (F) a BNC with four MNi. White arrows indicate MNi within BNCs and blue arrows indicate possible apoptotic events. **54**
- Figure 3.17** MCF-7 cells after CBMN assay, wherein (A) illustrates two BNCs, (B) a number of MNi with BNCs, (C) two BNCs; one cell containing one MNi, (D) two BNCs both having two MNi, (E) a number of MNi with BNC, and (F) two BNCs with two and four MNi, respectively. White arrows indicate MNi within BNCs and the pink arrow indicates an anaphase bridge. **54**
- Figure 3.18** (A) Cellular kinetics of the CHO-K1 cells was determined by scoring 400 AO stained BNCs and expressed as a percentage (%). Cells treated with 50 µg/ml AuNPs and/or irradiated with 2 Gy X-rays showed an overall decrease in cellular kinetics in comparison to the control. (B) Mean cumulative frequency of MNi present determined via the CBMN assay in CHO-K1 cells after 4 hour incubation with 50 µg/ml AuNPs followed by 2 Gy X-ray radiation. Control cells treated with AuNPs showed a small number of MNi, whilst an outspoken increase of MNi within cells **55**

treated with AuNPs and radiated with 2 Gy X-rays was apparent. The interaction indices for AuNPs and 6 MV X-rays in CHO-K1 cells are 1.6 to 1.7, thus $>$ Unity (Unity = 1).

Figure 3.19

(A) Cellular kinetics of the BEnd5 cells was determined by scoring 400 AO stained BNCs and expressed as a percentage (%). Cells treated with 50 $\mu\text{g/ml}$ AuNPs and/or irradiated with 2 Gy X-rays showed an overall decrease in cellular kinetics in comparison to the control. (B) Mean cumulative frequency of MNi present determined via the CBMN assay in BEnd5 cells after 4 hour incubation with 50 $\mu\text{g/ml}$ AuNPs followed by 2 Gy X-ray radiation. Control cells treated with AuNPs showed a negligible number of MNi, whilst a noticeable increase of MNi within cells treated with AuNPs and radiated with 2 Gy X-rays was apparent. The interaction indices for AuNPs and 6 MV X-rays of 0.92 to 1.06 determined for BEnd5 cells was differed from Unity (Unity = 1).

56

Figure 3.20

(A) Cellular kinetics of MCF-7 cells was determined by scoring 400 AO stained BNCs and expressed as a percentage (%). Cells treated with 50 $\mu\text{g/ml}$ AuNPs and/or irradiated with 2 Gy X-rays showed an overall decrease in cellular kinetics in comparison to the control. (B) Mean cumulative frequency of MNi present determined via the CBMN assay in MCF-7 cells after 4 hour incubation with 50 $\mu\text{g/ml}$ AuNPs followed by 2 Gy X-ray radiation. Control cells treated with AuNPs displayed an insignificant number of MNi, whilst an outspoken increase of MNi within cells treated with AuNPs and radiated with 2 Gy X-rays was apparent. The interaction indices for AuNPs and 6 MV X-rays of 1.3 to 1.4 were determined for MCF-7 cells,

57

which is $>$ Unity (Unity = 1).

Figure 3.21

(A) Cellular kinetics of MCF-10A cells was determined by scoring 400 AO stained BNCs and expressed as a percentage (%). Cells treated with 50 $\mu\text{g/ml}$ AuNPs, excluding cells treated with 10 nm AuNPs and/or irradiated with 2 Gy X-rays showed an overall decrease in cellular kinetics in comparison to the control. (B) Mean cumulative frequency of MNi present determined via the CBMN assay in MCF-10A cells after 4 hour incubation with 50 $\mu\text{g/ml}$ AuNPs followed by 2 Gy X-ray radiation. Control cells treated with AuNPs showed an insignificant number of MNi in control, whilst a noticeable increase of MNi within cells treated with AuNPs and radiated with 2 Gy X-rays was apparent. The interaction indices for AuNPs and 6 MV X-rays of 0.87 to 0.97 determined for MCF-10A cells, which is $<$ Unity (Unity = 1).

58

Figure 3.22

(A) Cellular kinetics of CHO-K1 cells was determined by scoring 400 AO stained BNCs and expressed as a percentage (%). Cells treated with 50 $\mu\text{g/ml}$ AuNPs and/or irradiated with 4 Gy X-rays showed an overall decrease in cellular kinetics in comparison to the control. (B) Mean cumulative frequency of MNi present determined via the CBMN assay in CHO-K1 cells after 4 hour incubation with 50 $\mu\text{g/ml}$ AuNPs followed by 4 Gy X-ray radiation. Control cells treated with AuNPs caused an insignificant number of MNi, whilst a clear increase of MNi within cells treated with AuNPs and radiated with 4 Gy X-rays was observed. The interaction indices for AuNPs and 6 MV 4 Gy X-rays of 1.04 to 1.13 have been determined for CHO-K1 cells is lower than the interaction indices after 2 Gy, in comparison to 2 Gy X-rays.

60

Figure 3.23

(A) Cellular kinetics of MCF-7 cells was determined by scoring 400 AO stained BNCs and expressed as a percentage (%). Cells treated with 50 µg/ml AuNPs and/or irradiated with 4 Gy X-rays showed an overall decrease in cellular kinetics in comparison to the control. (B) Mean cumulative frequency of MNi present determined via the CBMN assay in MCF-7 cells after 4 hour incubation with 50 µg/ml AuNPs followed by 4 Gy X-ray radiation. Control cells treated with AuNPs displayed a few caused MNi, whilst an observable increase of MNi within cells treated with AuNPs and radiated with 4 Gy X-rays was apparent. The interaction indices for AuNPs and 4 Gy X-rays of 0.74 to 0.77 is lower than the interaction indices after 2 Gy X-rays.

61**Figure 3.24**

(A) Cellular kinetics of CHO-K1 cells was determined by scoring 400 AO stained BNCs and expressed as a percentage (%). Cells treated with 2.5 µg/ml AuNPs and/or irradiated with 2 Gy X-rays showed no change in cellular kinetics in comparison to the control. (B) Mean cumulative frequency of MNi present determined via the CBMN assay in CHO-K1 cells after 4 hour incubation with 2.5 µg/ml AuNPs followed by 2 Gy X-ray radiation. The radiated samples treated with AuNPs showed a number of MNi, but no difference between the control and the AuNP treated samples were observed. The interaction indices for AuNPs and 2 Gy X-rays of 0.89 to 1.00 is lower than the interaction indices after 50 µg/ml AuNPs.

62**Figure 3.25**

(A) Cellular kinetics of MCF-7 cells was determined by scoring 400 AO stained BNCs and expressed as a percentage (%). Cells treated with 2.5 µg/ml AuNPs and/or

63

irradiated with 2 Gy X-rays showed no change in cellular kinetics in comparison to the control. **(B)** Mean cumulative frequency of MNi present determined via the CBMN assay in MCF-7 cells after 4 hour incubation with 2.5 µg/ml AuNPs followed by 2 Gy X-ray radiation. A visible increase of MNi within cells treated with AuNPs and radiated with 2 Gy X-rays was evident in comparison to the radiated control. The interaction indices for AuNPs and 2 Gy X-rays of 1.10 to 1.19 are lower than the interaction indices after 50 µg/ml AuNPs.

Figure 3.26

(A) Cellular kinetics of CHO-K1 cells was determined by scoring 400 AO stained BNCs and expressed as a percentage (%). Cells treated with 50 µg/ml AuNPs and/or irradiated with 1 Gy p(66)/Be neutrons showed an overall decrease in cellular kinetics in comparison to the control. **(B)** Mean cumulative frequency of MNi present were determined via the CBMN assay in CHO-K1 cells after 4 hour incubation with 50 µg/ml AuNPs followed by 1 Gy p(66)/Be neutrons. Control cells treated with AuNPs displayed an insignificant number of MNi, whilst a visible increase of MNi within cells treated with AuNPs and radiated with 1 Gy p(66)/Be neutrons was evident. The interaction indices for AuNPs and 1 Gy p(66)/Be neutrons of 1.06 to 1.16 is lower than the interaction indices after 2 X-rays.

64

Figure 3.27

(A) Cellular kinetics of MCF-7 cells was determined by scoring 400 AO stained BNCs and expressed as a percentage (%). Cells treated with 50 µg/ml AuNPs showed a decrease in cellular kinetics in comparison to the control, whilst the irradiated cells with 1 Gy p(66)/Be neutrons did not differ from the radiated control. **(B)** Mean

65

cumulative frequency of MNi present determined via the CBMN assay in MCF-7 cells after 4 hour incubation with 50 µg/ml AuNPs followed by 1 Gy p(66)/Be neutrons. No difference in the number of MNi within cells treated with AuNPs and radiated with 1 Gy p(66)/Be neutrons and the radiated control was noticeable. The interaction indices for AuNPs and 1 Gy p(66)/Be neutrons of 0.88 to 0.95 is lower than the interaction indices after 2 Gy X-rays.

Figure 3.28

(A) Cellular kinetics of CHO-K1 cells was determined by scoring 400 AO stained BNCs and expressed as a percentage (%). Cells treated with 50 µg/ml AuNPs and/or irradiated with 2 Gy p(66)/Be neutrons showed an overall decrease in cellular kinetics in comparison to the control. (B) Mean cumulative frequency of MNi present determined via the CBMN assay in CHO-K1 cells after 4 hour incubation with 50 µg/ml AuNPs followed by 2 Gy p(66)/Be neutrons. All the samples radiated with 2 Gy p(66)/Be neutrons showed an increase in the number of MNi, however no clear increase was observed in the samples treated with AuNPs. The interaction indices for AuNPs and 2 Gy p(66)/Be neutrons of 1.00 to 1.02 is lower than he interaction indices after 2 Gy X-rays.

66

Figure 3.29

(A) Cellular kinetics of MCF-7 cells was determined by scoring 400 AO stained BNCs and expressed as a percentage (%). Cells treated with 50 µg/ml AuNPs and/or irradiated with 2 Gy p(66)/Be neutrons showed a small decrease in cellular kinetics in comparison to the control. (B) Mean cumulative frequency of MNi present determined via the CBMN assay in MCF-7 cells after 4 hour incubation with 50 µg/ml AuNPs followed by 2 Gy p(66)/Be neutrons. Control cells treated with AuNPs

67

showed an irrelevant number of MNi. No difference between the radiated control and the AuNPs samples after 2 Gy p(66)/Be neutrons – was obvious. The interaction indices for AuNPs and 2 Gy p(66)/Be neutrons of 0.86 to 0.94 is lower than the interaction indices after 2 Gy X-rays.

Figure 3.30 **Box-and-Whisker plots showing the % cell viability in CHO-K1 cells as determined by MTT in 96 well plates.** **68**

(A) Cells incubated with AuNPs for 4 hours, (B) cells incubated with AuNPs for 4 hours followed by 4 Gy 6 MV X-ray radiation, and (C) cells incubated with AuNPs for 24 hours. 5 and 10 nm AuNPs, at 50 µg/ml, caused a significant decrease in cell proliferation ($p < 0.05$) in all three different conditions, namely A, B and C (Addendum: Tables 5.4–5.6).

Figure 3.31 **Box-and-Whisker plots showing the % cell viability in CHO-K1 cells as determined by MTT in 96 well plates.** **69**

(A) Cells incubated with AuNPs for 4 hours, (B) cells incubated with AuNPs for 4 hours followed by 4 Gy X-ray radiation, and (C) cells incubated with AuNPs for 24 hours. 5 and 10 nm AuNPs, at 50 µg/ml, caused a significant decrease in cell proliferation ($p < 0.05$) in all three different conditions, namely A, B and C (Addendum: Tables 5.7–5.9).

Figure 3.32 **Box-and-Whisker plots showing the % cell viability in MCF-7 cells as determined by MTT in 96 well plates.** **70**

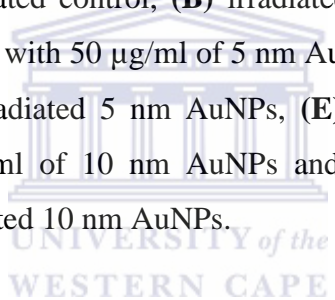
(A) Cells incubated with AuNPs for 4 hours, (B) cells incubated with AuNPs for 4 hours followed by 4 Gy X-ray radiation, and (C) cells incubated with AuNPs for 24 hours. 5 and 10 nm AuNPs, at 50 µg/ml, caused a significant decrease in cell proliferation ($p < 0.05$) in all

three different conditions, namely **A**, **B** and **C** (Addendum: Tables 5.10–5.12).

- Figure 3.33** **Box-and-Whisker plots showing the % cell viability in MCF-10A cells as determined by MTT in 96 well plates.** **71**
- (A) Cells incubated with AuNPs for 4 hours, (B) cells incubated with AuNPs for 4 hours followed by 4 Gy X-ray radiation, and (C) cells incubated with AuNPs for 24 hours. 5 and 10 nm AuNPs, at 50 µg/ml, caused a significant decrease in cell proliferation ($p < 0.05$), except in condition C (Addendum: Tables 5.13–5.15).
- Figure 3.34** **Flow cytometry was used to investigate the cell cycle progression in CHO-K1 cells.** The DNA histograms show the effect of AuNPs on the CHO-K1 cells after a 4 hour exposure period, followed by 2 Gy X-ray radiation. (A) non-radiated control, (B) irradiated control, (C) non-radiated cells with 50 µg/ml of 5 nm AuNPs, (D) cells with 50 µg/ml irradiated 5 nm AuNPs, (E) non-radiated cells with 50 µg/ml of 10 nm AuNPs and (F) cells with 50 µg/ml irradiated 10 nm AuNPs. **72**
- Figure 3.35** **Flow cytometry was used to investigate the cell cycle progression in BEnd5 cells.** The DNA histograms show the effect of AuNPs on the BEnd5 cells after a 4 hour exposure period, followed by 2 Gy X-ray radiation. (A) non-radiated control, (B) irradiated control, (C) non-radiated cells with 50 µg/ml of 5 nm AuNPs, (D) cells with 50 µg/ml irradiated 5 nm AuNPs, (E) non-radiated cells with 50 µg/ml of 10 nm AuNPs and (F) cells with 50 µg/ml irradiated 10 nm AuNPs. **73**
- Figure 3.36** **Flow cytometry was used to investigate the cell cycle** **73**

progression in MCF-7 cells. The DNA histograms show the effect of AuNPs on the MCF-7 cells after a 4 hour exposure period, followed by 2 Gy X-ray radiation. **(A)** non-radiated control, **(B)** irradiated control, **(C)** non-radiated cells with 50 µg/ml of 5 nm AuNPs, **(D)** cells with 50 µg/ml irradiated 5 nm AuNPs, **(E)** non-radiated cells with 50 µg/ml of 10 nm AuNPs and **(F)** cells with 50 µg/ml irradiated 10 nm AuNPs.

Figure 3.37	Flow cytometry was used to investigate the cell cycle progression in MCF-10A cells. The DNA histograms show the effect of AuNPs on the MCF-10A cells after a 4 hour exposure period, followed by 2 Gy X-ray radiation. (A) non-radiated control, (B) irradiated control, (C) non-radiated cells with 50 µg/ml of 5 nm AuNPs, (D) cells with 50 µg/ml irradiated 5 nm AuNPs, (E) non-radiated cells with 50 µg/ml of 10 nm AuNPs and (F) cells with 50 µg/ml irradiated 10 nm AuNPs.	74
--------------------	--	-----------



ADDENDUM		Page
Figure 5.1	Expert advice for the zeta potential measurements of AuNPs using Malvern Instruments' Zetasizer Nano ZS. (A) represents the 5 nm AuNPs and (B) the 10 nm AuNPs.	125
Figure 5.2	Expert advice for the size measurements of AuNPs using Malvern Instruments' Zetasizer Nano ZS. (A) represents the 5 nm AuNPS and (B) the 10 nm AuNPs.	126

ABSTRACT

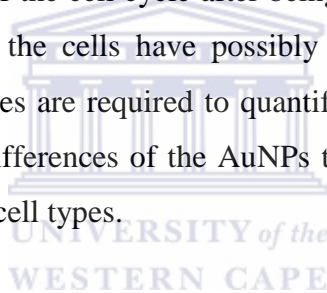
Despite the advances in therapies such as chemotherapy and radiotherapy, tumours have been shown to be resistant to the treatments. Gold nanoparticles (AuNPs) have been recognized as effective radiosensitizers of low energy (e.g. 200–500 kV) X-rays, leading to the emission of Auger electrons that cause highly localised ionizing damage to cells.

Spherical AuNPs were synthesised via the reduction of the chloroaurate ions by sodium citrate. Characterisation of AuNPs involved UV-visible spectrophotometry, zeta (Z) potential, dynamic light scattering (DLS) and polydispersity index (PDI) measurements for determination of surface plasmon resonance (SPR), surface charge and stability, as well as transmission electron microscopy (TEM) for hydrodynamic core sizes, size distribution width and shape of AuNPs. Both the 5 and 10 nm AuNPs were found to be anionic with λ_{\max} absorbance of 525 nm and uniform size distribution. DLS measurement at 38.12 nm and 48.50 nm, respectively for 5 nm and 10 nm AuNPs, points to aggregation of the AuNPs. However, TEM measurements confirmed the core size of the 10 nm AuNPs. Non-malignant Chinese hamster ovary (CHO-K1), brain endothelial (BEnd5), breast (MCF-10A), isolated human lymphocytes and malignant breast (MCF-7) cell lines were treated with 50 $\mu\text{g}/\text{ml}$ of AuNPs, and irradiated with either 1, 2 or 4 Gy X-rays or 1 or 2 Gy p(66)/Be neutron radiation. The γ -H2AX foci assay, cytokinesis-block micronucleus assay, MTT assay and fluorescence-activated cell sorting (FACS) was used to determine that amount of double stranded breaks (DSBs) in isolated lymphocytes, the presence and number of micronuclei (MNi) within binucleated cells (BNCs), cell viability and cell cycle progression, respectively.

Preliminary experiments that established the reliability of the study regarding the induction of DNA damage after the bombardment of AuNPs by scattered low kV X-rays, were carried out on lymphocytes. Combined treatment (AuNPs and radiation) resulted in more endogenous foci in comparison to lymphocytes that were treated with AuNPs only. The CHO-K1 and MCF-7 cells showed higher MNi frequencies after the combination treatment of AuNPs and

radiation compared to the number of MNi in samples exposed to AuNPs and radiation separately. The AuNPs alone influenced the cellular kinetics of all cell types. Interaction indices, which is the enhancement factor of AuNPs in combination with radiation, for AuNPs and 6 MV 2 Gy X-rays of 1.6 to 1.7 and 1.3 to 1.4 have respectively been determined for CHO-K1 and MCF-7 cells, whilst that for the other cell types used in the study were not different from Unity. As expected, the interaction indices between AuNPs and p(66)/Be neutrons was lower than the interaction indices after 2 Gy X-rays, as p(66)/Be neutrons interact only with the nuclei of the AuNP's atoms and the X-ray photons interact with the orbital electrons of the atoms of the AuNPs leading to Auger electron emission.

The cell viability assay showed that 50 µg/ml of AuNPs had an inhibitory effect on cellular proliferation, in all four cell lines whereas the lower concentrations (2.5, 5 and 10 µg/ml) had no effect. Results in this study, revealed an increase in the accumulation of CHO-K1 and MCF-7 cells in the G₂/M phase of the cell cycle after being treated with AuNPs followed by X-ray radiation, suggesting that the cells have possibly been sensitised to the damaging effects of radiation. Further studies are required to quantify internalised AuNPs and to then link the possible concentration differences of the AuNPs to differences in radiation damage effects observed for the different cell types.



CHAPTER 1:

LITERATURE REVIEW

1.1 Nanotechnology

Nanotechnology is a promising field that involves the deliberate engineering of materials at the atomic or molecular level to create new materials, known as nanomaterial or nanoparticles that have unique and novel properties. Nanoparticles are defined as materials with external dimensions in the size range of approximately 1 - 100 nanometer (Fig. 1.1) (Oberdörster, 2010).

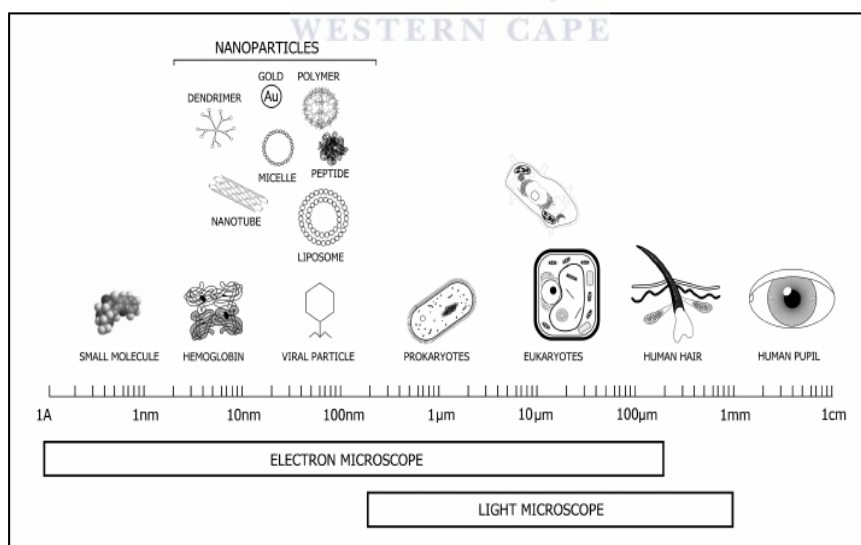


Figure 1.1: Logarithmical length scale showing size of nanoparticles compared to biological components and description of 'nano' and 'micro' sizes. Relative sizes of nanoparticles compared to common biological structures. Diagram of nanoparticle size as compared to common biological structures and their linked length scale. An electron microscope is required to envision structures that are submicrometer in size (Ediriwickrema & Saltzman, 2015).

Research in the use of nanoparticles for targeted drug delivery, detection and treatment of cancer is motivated by the unique features, such as surface to mass ratio that is much larger than that of other particles, their quantum properties, and the ability of the nanoparticles to increase interaction between the themselves and the surface of cells (De Jong & Borm, 2008; Lim et al., 2013; Verma et al., 2014).

Nanoparticles can be engineered and created to encompass specific sizes, shapes, surface properties, stability and several other characteristics for a variety of applications, such as effective and targeted delivery of drugs and enhancing imaging techniques by infiltrating the biological, biophysical and biomedical barriers (Cai & Chen, 2007; Cai, et al., 2008). Research is moving towards the use of modern nanodevices, such as nanochips and nanosensors (Grodzinski et al., 2006; Sahoo et al., 2007), but studies on their biocompatibility, *in vivo* kinetics, acute and chronic toxicity, and competence to escape the reticuloendothelial system (RES) are on-going challenges that still have to be overcome by nanotechnology (Panchangam & Dutta, 2015).

The nanoparticles mostly studied in biomedical applications, include quantum dots (Gao et al., 2004; Michalet et al., 2005), carbon nanotubes (Zhang et al., 2009; Elhissi et al., 2012), paramagnetic nanoparticles (Neuberger et al., 2005), liposomes (Cho et al., 2008; Malam et al., 2009) and gold nanoparticles (AuNPs) (Huang et al., 2007; Tiwari et al., 2011) (Fig. 1.2).

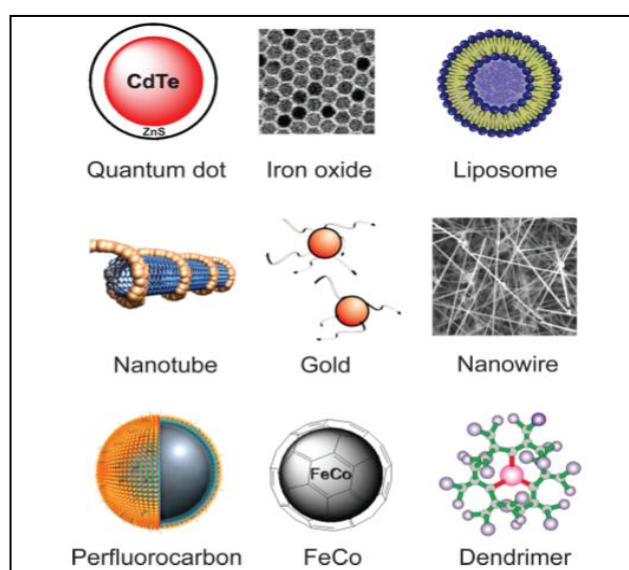


Figure 1.2: Examples of nanoparticles. Several nanoparticles have been scrutinized for biomedical applications targeting cancer (Cai et al., 2008).

1.2 Gold nanoparticles (AuNPs)

1.2.1 History of gold

Dykman and Khlebtsove (2011) reported that the first data on colloidal gold can be found in dissertations by Chinese, Arabian, and Indian scientists, who obtained colloidal gold in the V–IV centuries BC. Scientists used gold (Au) for medical purposes, while alchemists used it to introduce prominent red colours to glass. An example of this is the Lycurus Cup in the British Museum (Heiligtag & Niederberger, 2013) that is observed as a green in daylight (Fig. 1.3, left), but changes to a red colour (Fig. 1.3, right), when illuminated from the inside. Colloidal gold also known as AuNPs (Rohiman et al., 2011) are exceptionally small parts of gold which cannot be seen with the naked eye. Due to the small size they display a different colour from normal gold (Eustis and El-Sayed, 2005).



Figure 1.3: The Lycurus Cup. This cup was designed and made by Romans in the 40th century (Heiligtag & Niederberger, 2013).

1.2.2 Gold as medicine

The element, gold has a long medical history, used for people suffering from nervous conditions (Fricker & Buckley, 1996), epilepsy in the 16th century, syphilis (Daniel & Astruc, 2004), tuberculosis (TB) in the beginning of the 19th century, and in 1925 gold complexes

were being used to treat arthritis of all types especially, rheumatic diseases (Aaseth et al., 1998; Kean et al., 1987; Shaw, 1999; Shedbalkar et al., 2014). A number of side effects have been linked with prolonged exposure to gold complex drugs, which include nephrotoxicity, skin irritation, mouth ulcers, liver toxicity and blood disorders (Bhattacharya & Mukherjee, 2008). However, currently a second generation gold drug, auranofin (AF) used to treat rheumatoid arthritis, with limited adverse side effects and increased efficacy has been produced (Glennes et al., 1997; Daniel & Astruc, 2004; Panyala et al., 2009).

1.2.3 Synthesis of AuNPs

The synthesis of spherical AuNPs is performed via citrate reduction method applications, known as the Turkevich method (Turkevich et al., 1951; DiScipio, 1996). Chloroaurate ions are reduced by sodium citrate at 100°C (Fig. 1.4) resulting in the synthesis of monodispersed spherical AuNPs, which are electrostatically stabilised by citrate ions bound to surface of AuNPs. Size variation of AuNPs can be achieved by changing the temperature and/or gold/reducing agents' ratios; with smaller particles yielded as the amount of reducing agents increases (Frens, 1875; Turkevich et al., 1951; Verma et al., 2014). Various other types of AuNPs exist, namely nanorods, nanoshells, nanocages, nanosphere, and Surface Enhanced Raman Scattering (SERS) nanoparticles (Cai et al., 2008).

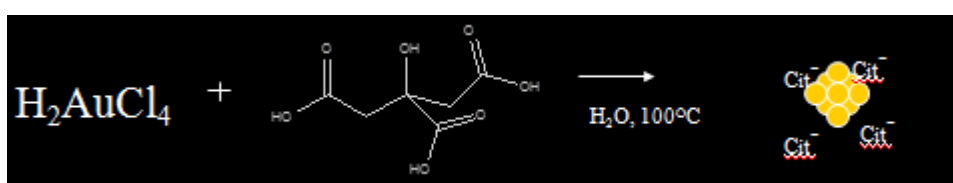


Figure 1.4: Synthesis equation for synthesis of AuNPs. Schematic representation of reduction of the chloroaurate ions by sodium citrate at 100°C (Faraday, 1875) to produce AuNPs.

1.2.4 Characterisation and properties of AuNPs

The AuNPs are generally characterised via UV-visible (vis) spectrophotometry, zeta (Z) potential measurements, dynamic light scattering (DLS), polydispersity index (PDI) and transmission electron microscopy (TEM) (Chithrani et al., 2006; Torres-Chavolla et al.,

2010). The absorption of AuNP solution is measured via UV-vis spectrophotometry as a single absorption peak in the visible range between 510 – 550 nm, for the analysis of surface plasmon resonance (SPR) to determine AuNPs presence. AuNPs exhibit unique optical properties, which include SPR and the ability to bind amine and thiol groups, allowing surface modification and use in biomedical applications (Aillon et al., 2009). When AuNPs are excited by a specific wavelength of light, it will cause the conduction of electrons on the surface of the particles surface and will lead to SPR, whilst 2 nm AuNPs do not display SPR (Eustis & El-Sayed, 2005; Huang & El-Sayed, 2010). Z-potential measurements reveal the stability of any nanoparticles in suspension. Z-potential measurements between -10 and +10 mV are regarded as neutral, whilst Z-potential of $> +30$ mV or < -30 mV suggest that the nanoparticles are strongly cationic and strongly anionic, respectively (Clogston & Partri, 2011; Abbott, 2014). An extremely positive or negative zeta potential value can cause larger repulsion forces whereas repulsion between particles with analogous electrical charge prevents aggregation (Honary & Zahir, 2013). The DLS technique can be used to determine the hydrodynamic size of small particles in suspension. The PDI represents the size distribution width of the AuNPs. A PDI value of 0.1–0.25 suggests that the nanoparticles possess uniform size distribution, while a PDI value greater than 0.5 indicates a very broad distribution and aggregation (Yeo, 2013). It is essential to maintain the PDI parameter as low as possible, to accomplish long-term stability of the AuNP solution.

The size and shape of synthesised nanoparticles, quantum mechanics, electric, optical and chemical characteristics, can vary considerably from that of bulk solids (Burda et al., 2005). In addition, minor divergence in the size and shape of the AuNPs can have major effects on the properties of AuNPs. The behavior of the AuNPs depends on the ratio of surface area: as the ratio of surface area to volume increase, the behavior of the surface atoms assumes dominance over the composition of the nanoparticles itself (Arvizo et al., 2010; Yah, 2013).

AuNPs have been consistently described as both non-toxic (Connor et al., 2005; Shukla et al., 2005) and toxic (Goodman et al., 2004; Pernodet et al., 2006; Pan et al., 2007; Zhang et al., 2011), depending on the size and surface charge of these nanoparticles. Pan et al. (2007) reported that the size of AuNPs plays a major role in toxicity and found that 15 nm AuNPs are non-toxic at all concentrations, whilst 1–2 nm AuNPs cause rapid cell death by necrosis at low concentrations. Furthermore, AuNPs smaller than 4–5 nm in diameter may be toxic due to their ability to penetrate the nuclear membrane of the cell (Soenen et al., 2011).

Panyala and colleagues (2009) reported that metallic Au is non-toxic, however gold chloride or potassium gold cyanide is toxic to organs. Despite reports that cationic AuNPs are more toxic than anionic AuNPs (Wang et al., 2011; Logan & Ly, 2013), other researchers have shown that both cationic and anionic AuNPs are toxic to cells (Schaeublin et al., 2011), and that both positively and negatively charged AuNPs can induce alterations of the mitochondrial membrane leading to oxidative stress (Schaeublin et al., 2011).

1.2.5 *In vitro* and *in vivo* studies

In vitro studies of AuNPs are dissimilar in cell types, whereas *in vivo* studies examine toxicity to a disease, bio-imaging, possible routes of administration, biodistribution, translocation and clearance of AuNPs (Alkilany & Murphy, 2010; Khlebtsov & Dykman, 2011; Verma et al., 2014). Freese and co-workers (2012), showed that the cell viability and the proliferation of endothelial cells decreased after exposure to AuNPs, particularly at high concentrations. A study by Chen et al. (2013) administered 21 nm AuNPs intravenously into mice models to investigate the distribution, organ toxicity and changes in inflammatory cytokines within the adipose tissue after AuNPs exposure. They reported no measureable organ or cell toxicity in the mice, but considerable fat loss and suppression of inflammation was observed due to the reducing agent sodium citrate. Therefore, to comprehend the chemical and physical interaction of AuNPs with biological media is of great importance to establish suitable biological models to investigate cytotoxic effects.

1.3 Cancer

According to World Health Organisation (WHO) (2008), cancer is the primary cause of death in economically developed countries and the second leading cause of death in developing countries. Miller et al. (2016) reported that the 3 most common cancers in 2016 were prostate (3 306 760), colon and rectum (724 690), and melanoma (614 460) amongst males in the United States of America (USA). Amongst females it was breast (3 560 570), uterine corpus (757 190), and colon and rectum (727 350) (Miller et al., 2016). South Africa is one of the countries with the highest cancer incidence and prevalence on the World Cancer Research Fund's list of countries (Fourie et al., 2014). As a consequence of population aging and

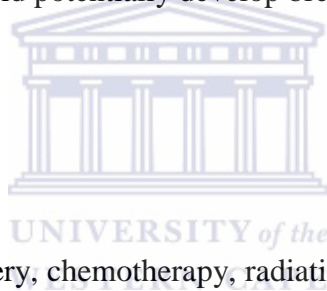
growth, with an increase in cancer-associated lifestyle choices, such as smoking, alcohol consumption, physical inactivity and unhealthy diets, the burden of cancer is rising in economically developing countries. It is predicted that a 78% increase in cancer cases by 2030 can be expected (Morhason-Bello et al., 2014). Despite our knowledge and advances in cancer biology, the personal and economic burden of cancer is escalating, which emphasizes the critical need for intensified research efforts in developing treatments.

1.3.1 Breast cancer

In 2016, 1 685 210 new cancer cases and 595 690 cancer deaths were estimated to occur in the United States (US) (Siegel et al., 2016). According to the American Cancer Society (2016), the most common type of cancer is breast cancer, with more than 249 000 cases being expected in US. Breast cancer is the second leading cause of cancer death after lung cancer amongst African American women. Regardless of all the improvements that have been made in the area of breast cancer research, African American women suffer excessively from the effects of this disease (Jones & Chilton, 2002; Jemal et al., 2011). Miller et al. (2016) reported worldwide that 75% of breast cancer survivors are of 60 years or older, whilst 7% are younger than 50 years; 19% of breast cancers are diagnosed in women aged of 30 to 49 years, and 44% occur amongst women who are 65 years or older.

According to Jemal et al. (2011) and the American Cancer Society (2013), breast cancer mortality among African American women is nearly 28% higher than in White women. This difference between the mortality rates of African American and White women can be related to a later stage of diagnosis or being diagnosed with an aggressive estrogen receptor tumour in African American women. Furthermore, black women have a lower survival rate within each stage due a slighter chance to be diagnosed at a local breast cancer stage, compared to white women (53% versus 62%) (Howlander et al., 2015). This is due to diversity of socioeconomic concerns and difference in comorbidities, lack of premium medical care among black women, and biological variations in cancers (e.g. higher occurrence of triple negative cancer in black women) (Curtis et al., 2008; Vona-Davis & Rose, 2009; Danforth et al., 2013).

The common risk factors that may be linked to the development of breast cancer include: alcohol abuse, cigarette smoke, early menstruation, lack of exercise and obesity which also affects the prognosis of breast cancer (Chen et al., 2011). Besides lifestyle and environmental factors, there are a number of genes that may contribute toward the development of breast cancer. These genes include the BREast CANcer (BRCA) 1 and BRCA 2 gene. It is believed that 5–10% of breast cancers are hereditary and caused by mutations in the BRCA 1 and BRCA 2 genes (Apostolou & Fostira, 2013). BRCA 1 and BRCA 2 are human genes that produce tumour suppressor proteins and participate in the repair of damaged deoxyribonucleic acid (DNA) to maintain the stability of the cell's genetic material (Welch & King, 2001; Silver & Livingston, 2012). A mutation in the BRCA 1/2 genes, inhibits the DNA repair process leading to unchecked cell proliferation which could contribute towards the development of cancer. According to SEER Cancer Statistics Review (2013), 55–65% of women who inherit a mutation in the BRCA 1 gene and ~45% of women who inherit a mutation in the BRCA 2 gene could potentially develop breast cancer by the age of 70 years.



1.3.2 Breast cancer treatment

A combination of therapies (surgery, chemotherapy, radiation, targeted and hormone therapy) is available to treat cancer. However, negative effects of these treatments can adversely impact on the person's ability to function and their quality of life.

According to the American Cancer Society (2015), women have a 12% chance of developing invasive breast cancer and a 3% chance of dying from it. Breast cancer treatment entails surgical removal of the tumour that is followed by chemotherapy with or without radiation (Lim et al., 2011). For any stage of breast cancer, 79% of patients receives hormonal therapy. Miller et al. (2016) reported that 61% of women diagnosed with stage I or II breast cancer will undergo breast conserving surgery, while 36% will undergo a mastectomy. Among women diagnosed with stage III, 21 % undergo breast conserving surgery, whereas 72% undergo mastectomy. In women diagnosed with stage IV, 48% of patients receive chemotherapy only and/or radiation.

The primary treatment and prevention for breast cancer in women, frequently includes prophylactic mastectomy, which is used to remove one or both breasts, and lumpectomy, to remove the tumour (breast lump) and a surrounding margin of normal tissue. In early stage, long-term survival is the same as with mastectomy, when breast cancer surgery is followed by radiation to the breast, and suitable for localised cancers (Jatoi & Proschan, 2005; Litiere et al., 2012). Some patients require a mastectomy due to the characteristics of tumours (e.g. size, stage and number of tumours), and in some cases post-surgery radiation is inadvisable due to comorbid medical conditions (e.g. active connective tissue disease) or other obstructions. American women younger than 40, as well as patients with larger and/or more aggressive tumours are more likely to undergo a mastectomy (McGuire et al., 2009; Freedman et al., 2012). Worldwide, woman are increasingly choosing mastectomy above other treatments for a variety of reasons, such as refusal or unwillingness to undergo radiation therapy and dread of recurrence (McGuire et al., 2009).



1.4 Radiation

Based on how radiation affects matter, it can be classified as either being ionising or non-ionising radiation. Non-ionising radiation is low-frequency radiation, including visible light, heat, radar, microwaves, and radio waves (Gherardini et al., 2014). This type of radiation comprises photons that do not have sufficient energy to break chemical bonds or ionise biological molecules (Kattou et al., 2014).

The linear energy transfer (LET) is a physical quantity used to portray the quality of the radiation (Yukihara, & McKeever, 2011). The LET of a particular type of radiation is a measure of the average energy deposited along the track of a particle per unit length and is expressed in keV/ μm (Hill, 1999). In essence, it reflects the mean ionisation density and represents a microdosimetric parameter. The LET depends on several parameters including the mass, charge and velocity/energy of the radiation (LaTorre Travis, 1989).

1.5 Ionising radiation (IR)

Radiation that possesses adequate energy to emit one or more orbital electrons from the atoms or molecules by which it interacts, thus creating ions, is referred to as ionising radiation (IR) (Christensen et al., 2014). The ionisations and/or excitations are resultant from the course of radiation through cells initiating a series of events that can lead to biological damage.

IR can be categorised into electromagnetic and particle radiation. Electromagnetic radiations include both X-rays and γ -rays (Hall & Giaccia, 2006). They have neither mass nor charge and as such they are considered either as waves or as discrete quanta of electromagnetic energy, called photons. Electromagnetic radiation is commonly used in experimental studies and in many clinical applications (Azeemi & Raza, 2005). Particle radiation comprises other types of radiation like protons, α -particles, negative π -mesons, heavy charged ions, and neutrons. As IR passes through material, it deposits sufficient energy to break molecular bonds and displace (or remove) electrons from atoms. This electron displacement generates two electrically charged particles, which may cause alterations in living cells of plants, animals, and people (Fig. 1.5).

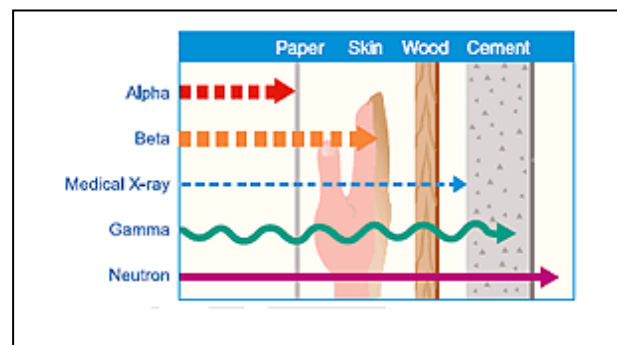
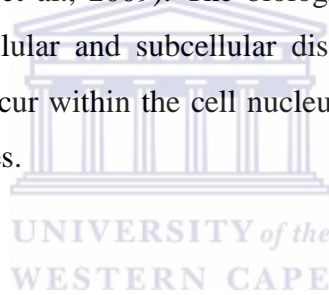


Figure 1.5: Types of IR. The penetrating ability of five major types of IR (<http://www.nrc.gov/about-nrc/radiation/health-effects/radiation-basics.html>).

1.5.1 X-ray radiation

Previous studies reported that contrast agents are taken up selectively by tumours leading to an enhanced therapeutic ratio by altering the lower energy photon interaction, thus delivering

a highly localised dose to the tumour (Mello et al., 1983; Mesa et al., 1999). This is accomplished by loading the target volume with contrast agents and irradiating the target with kV X-rays where photoelectric effects are dominant. Contrast agents, materials of certain atomic numbers interact with radiation, with high-atomic-number (Z) includes, iodine ($Z = 53$), gadolinium ($Z = 64$) and gold ($Z = 79$) provide a high possibility for photon interaction by photoelectric effect (Mesa et al., 1999; Robar et al., 2002). In addition, the photoelectric effect produces high-LET and short range of photoelectric interaction products and Auger electrons to cause a highly localised dose enhancement in the tumour (Rahman et al., 2009). Auger electrons are weakly bound electrons with characteristic energies ejected from atoms in reaction to a descending transition by a different electron in the atom, resulting in the Auger effect. Auger electrons emit maximum energy of 0.5–25 KeV and travels short distance, typically 0.02–10 μm (Aktolun & Goldsmith, 2012). Therefore, they are only effective if the contrast agent or radiopharmaceutical is internalised in the cell, preferably close to the nucleus (Robertson et al., 2009). The biological effects of Auger emitters are highly dependent upon their cellular and subcellular distribution (Bingham et al., 2000). Auger electron emissions that occur within the cell nucleus generate effects similar to high-LET radiations, such as α -particles.



1.5.2 p(66)/Be neutron radiation

Neutrons are uncharged particles and can be produced artificially when a charged particle, such as a deuteron or a proton, is accelerated to high energy and strikes a suitable target material (Hall & Giaccia, 2006; Lehnert, 2008). A major treatment of cancer is low LET photons, which damage cells either directly or indirectly through the production of free radicals causing DNA single or double-stranded breaks (DSBs) whereas high-LET radiation predominantly damages the DNA directly by breaking chemical bonds. X-ray photons interact with the orbital electrons of atoms of the absorbing matter (Fig. 1.6) while neutrons interact with the nuclei of atoms of the absorbing matter and set fast recoil protons, α -particles and heavier nuclear fragments in motion (Hall & Giaccia, 2006; Aktolun & Goldsmith, 2012).

Many tumours contain hypoxic regions (Yu et al., 2003; Yu et al., 2008) that render cells to be more resistant to low LET radiation than their normoxic counterparts due to decreased free

radical damage mediated by oxygen (Yu et al., 2003). The relative efficiency at deactivating cells by high LET compared to low LET beams are described as relative biological effectiveness (RBE) (Franken et al., 2011). Neutrons and other high-LET particles are less dependent on oxygen to exert an effect and therefore hypoxic cells are less resistant to neutron irradiation. There are various forms of DNA damage, but DSBs are regarded as the most lethal lesions induced by IR. It has been assumed that the increased RBE for cell death results from enhanced efficiency of high-LET radiation to induce these lesions. However, neutrons do not appear to induce more DSBs than X-rays for a given dose (Barendsen, 1994; Prise et al., 1994; Britten & Murray, 1997). According to Li et al. (2001), neutrons are difficult to target onto the tumour, and cause more DNA damage than photons resulting into adverse side effects to normal tissue. Therefore, it is not used often in clinical practises.

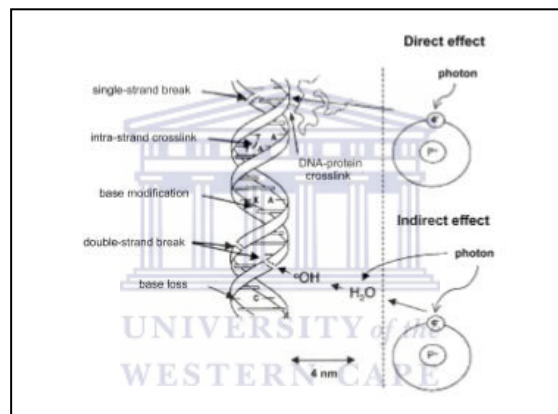


Figure 1.6: Examples of radiation damage to DNA resulting from both direct and indirect effects. During the indirect effect, secondary electrons for instance, a water molecule (H₂O) to produce a hydroxyl radical (OH[·]), which in turn produces damage to DNA (Hall & Giaccia, 2006).

1.6 Application of AuNPs in cancer

1.6.1 Radiosensitisers

The development of new AuNPs with biocompatible characteristics has stimulated and motivated research to pursue the application of AuNPs in combination with radiation therapy. In contrast to MV, kV X-rays have a limited penetration capacity. However, the use of AuNPs in combination with radiotherapy (RT) in numerous research studies with

orthovoltage X-rays have showed significant dose enhancement effects (Mousavie Anijdan et al., 2012). Orthovoltage X-rays are fairly low energy radiation sources (e. g. 150–200 kV) and at these energies, a considerably dose is deposited at the skin surface and 90% of the dose will occur at approximately 2 cm of depth in the tissue (Khan, 2003). The greatest challenge to treat underlying tumours is the limitation of radiation tolerance of the surrounding tissues; the skin dose becomes excessively large when adequate doses are to be delivered to underlying tumours (Khan, 2003; Medina et al., 2008). Disproportionate absorption of radiation in different types of tissues such as bone tissue opposed to soft tissue can result in damage to one type of tissue, in this example, bone damage. AuNPs are commonly used in radiation research applications, due to the high atomic number (Z) of gold ($Z=79$), which results in considerable differences in mass energy absorption properties in contrast to soft tissue (Kwatra et al. 2013). They have been proposed as excellent radiosensitisers by enhancing the vulnerability of the tumour tissue to radiation exposure without damaging healthy surrounding soft tissue (Kwatra et al., 2013).

The AuNPs can selectively scatter and/or absorb X-ray radiations providing an increased interaction between photons of the radiation for improved targeting of cellular components within the tumour causing localised damage (Park et al., 2006; Carter et al., 2007). According to Kwatra et al. (2013), a combined treatment consisting of AuNPs and X-ray radiation results in reduction in the therapeutic radiation dose, thus limiting the damage to the healthy soft tissue. The utilisation of AuNP radiosensitisers is termed Nanoparticle Enhanced X-ray Therapy or NEXT (Praetorius & Mandal, 2007).

1.6.2 AuNPs accumulation and clearance

As mentioned previously, AuNPs are biologically compatible and have a great application in cancer detection and treatment (Huang et al., 2007; Tomar & Garg, 2013). Long circulating AuNPs are prone to accumulate in tumours by penetrating the leaking tumour vasculature. This process is known as the enhanced permeability and retention (EPR) effect (Maeda et al., 2000; Maeda, 2010). After the nanoparticles leak out of these permeable blood vessels into the surrounding tissue, it is very difficult for the nanoparticles to be transported out again. Thus the presence of the nanoparticles allows doctors to visualise and locate the tumour by observing the site of nanoparticles.

It is of importance to note the distribution, biodistribution in organs, as well clearance from the body, of the AuNPs. Previous reports that the AuNPs accumulate in the liver and spleen suggest that they are recognised by phagocyte-rich reticuloendothelial system (RES) (Krpetic et al., 2009; Balasubramanian et al., 2010; Ema et al., 2010). Furthermore, nanoparticles that circulate for longer time periods, which are not small enough to be excreted via kidneys, are recognised and trapped by the RES (Kobayashi & Brechbiel, 2005). Sonavane et al. (2008) completed a size-dependent accumulation study (Fig. 1.7). In this study, AuNPs with 15, 50, 100 and 200 nm diameter were administered intravenously in mice. The smaller size (15 nm) particles yielded the highest amounts in organs, including the liver, lung, spleen, kidney, brain, heart and stomach. Furthermore, an *in vivo* study conducted by Zhang et al. (2011) reported that BSA-conjugated AuNPs aggregated in 40–80 nm sized clusters, and accumulated mainly in the liver and spleen, whilst glutathione-conjugated AuNPs of 5–30 nm clustered size were cleared by the kidneys. Another study showed that AuNPs were released into the urine after 5 hours through filtration by the glomeruli (kidneys) (Hainfeld et al., 2006).

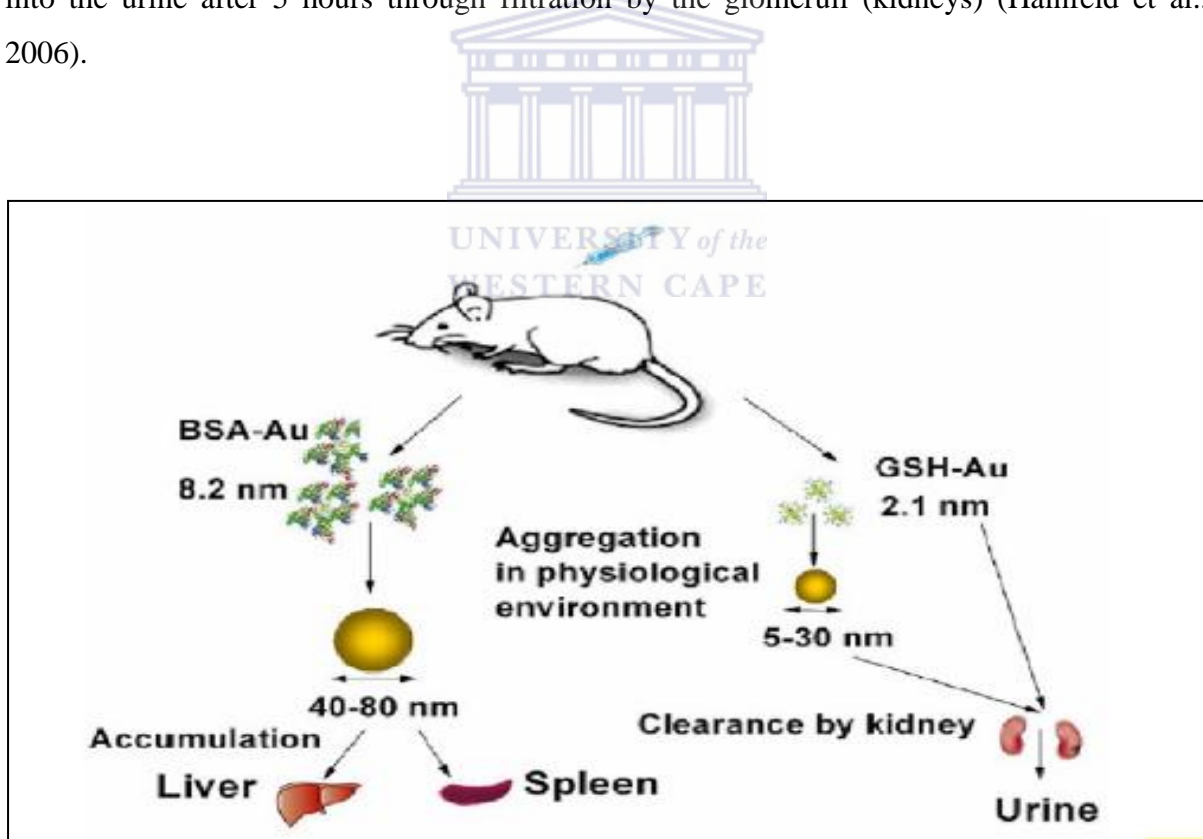


Figure 1.7: Size dependent accumulation. Schematic representation of size dependent accumulation and clearance of AuNPs bioconjugates in the organs of mice. (Zhang et al., 2011; Barchanski, 2016).

1.6.3 AuNPs sensitisation in cell line and animal models

In an *in vivo* study performed by Hainfeld et al. (2004), 6 mice with subcutaneous breast cancer tumours were divided in three groups and treated with AuNPs to enhance radiotherapy toxicity for cancerous cells in mice. The first group was treated with AuNPs before 250 kVp X-ray radiation, the second group only received radiation, and the last group was only treated with AuNPs. Results showed that the group that received the combined treatment had the highest one-year survival (86%), in comparison to the radiation alone group (20%), and AuNPs alone group (0%) (Hainfeld et al., 2004). Therefore, the AuNPs enhanced the radiotherapeutic effects (Mesbahi, 2010).

In an *in vitro* study conducted by Kong et al. (2008) thioglucose (Glu)-AuNPs were synthesised. The cell lines, MCF-7 (breast cancer cell line) and MCF-10A (non-cancerous breast cell line), were incubated with Glu-AuNPs and irradiated with 200 kVp X-rays. TEM micrographs showed that the uptake of Glu-AuNPs were significantly higher in MCF-7 cells. Furthermore, the results showed that the radiotherapy combined with AuNPs significantly induced cell death of MCF-7 cells, in comparison to MCF-10A cells and cells without AuNPs (Mesbahi, 2010). Targeting systems based on glucose receptors have been utilised to enhance the uptake of AuNPs into tumours allowing the distribution of high atomic mass atom with electron range for metal-enhanced radiation therapy, which can be implicated in further AuNPs studies (Hainfeld et al., 2006).

1.7 Overview of cell cycle

1.7.1 The cell cycle

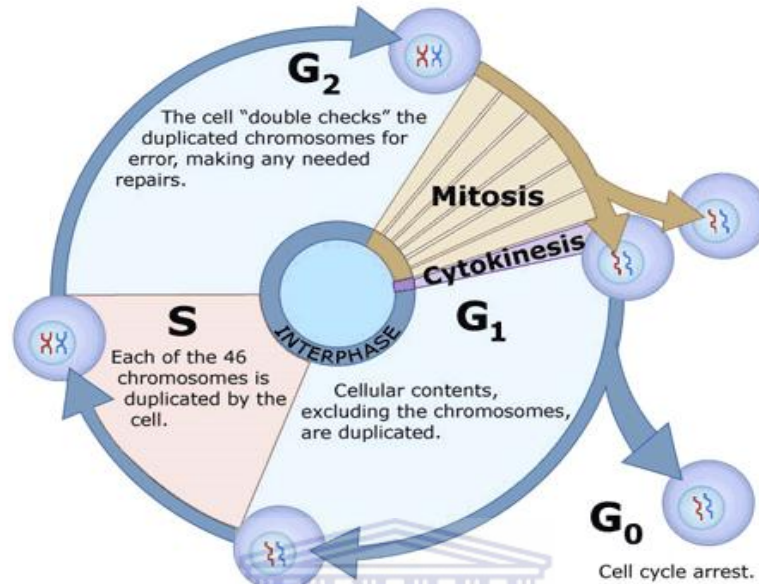


Figure 1.8: Diagram illustrating the four phases of the cell cycle. The cell cycle is the series of events that takes place in cells, which leads to cell division and replication. In eukaryotes, the cell cycle has two main phases: interphase and the mitotic phase. Interphase is the stage during which the cell prepares, grows and accumulates nutrients essential for mitosis and also replicates the DNA (Nurse, 1994). In the mitotic phase, the cell divides into two separate cells known as 'daughter cells' and the final phase is cytokinesis, where the newly formed cells are fully divided (<http://biology.tutorvista.com/cell/cell-cycle.html>).

The cell cycle consists of four phases, namely the synthesis phase (S), in which nuclear DNA is replicated and synthesised, and the mitotic phase (M), which is separated by two gap phases i.e. G_1 and G_2 (Fig. 1.8) (Imoto et al., 2011). Furthermore, after mitosis, a quiescent phase known as the G_0 phase can also occur (Cooper, 1998; Collier, 2007; Daignan-Fornier & Sagot, 2011). In the G_0 phase cells are at resting phase after mitosis, before the initiation of cell cycle (Fig. 1.8) (Cooper, 1998; Daignan-Fornier & Sagot, 2011). The main purpose of the cell cycle is to ensure that the DNA is replicated correctly in the S phase and that the division of two daughter cells are achieved during the M phase (Dalto, 1998; Blow & Tanaka, 2005).

Two key components of the cell cycle control system are cyclins and cyclin-dependent kinases (CDKs). CDKs are serine/threonine kinases that can phosphorylate multiple substrates (Dylnacht, 1997) leading to the regulation of cell cycle progression (Dubravka & Scott, 2000; Suryadinata, et al., 2010; Lim & Kaldis, 2013). The cell cycle cyclin-CDK activity is regulated by periodic synthesis of cyclins, proteolysis, phosphorylation of various protein substrates, inhibitory proteins, and tumour suppressor gene products, e.g. retinoblastoma protein (pRB) and p53.

1.7.2 Cell cycle phases

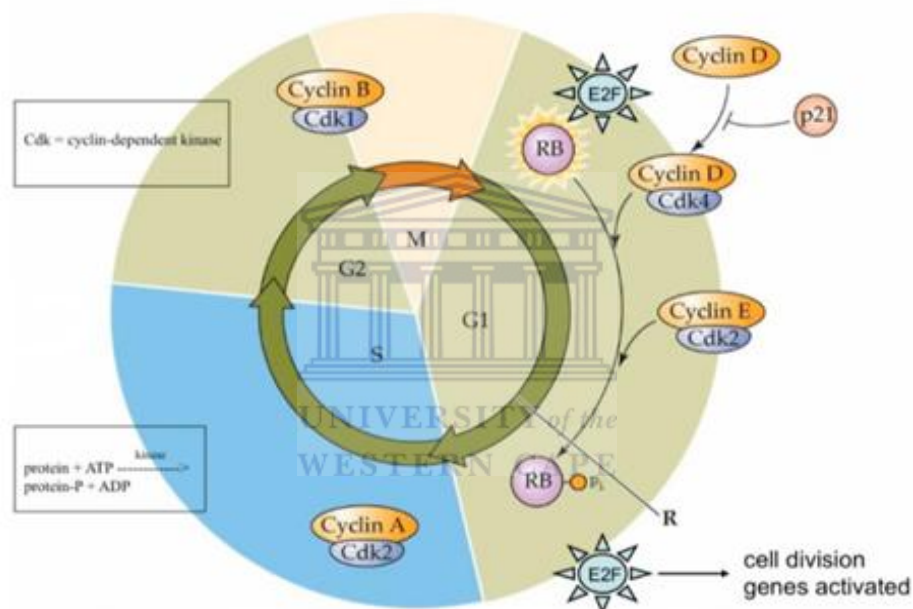


Figure 1.9: Schematic representation of the RB/E2F pathway. Phosphorylation by cyclin D-CDK 4 and cyclin E-CDK 2, causes changes to the RB structure and releases E2F to activate cell division genes. Adapted from Freeman & Co (2004), *Life: The Science of Biology*, 7th Edition.

1.7.2.1 The G₁ phase

The G₁ phase assess whether a cell is prepared to enter the S phase based on nutrients and the availability of growth factors (Saqcena, 2014). This is accomplished by means of the retinoblastoma (RB)/E2F pathway (Fig. 1.9). The pRB is a product of RB tumour suppressor gene. pRB plays an essential role in the regulation of the cell cycle through their control of the E2F family of transcription factors that regulate expression of a number of cell cycle components, such as cyclin E, cyclin A, Cdc25A and the transcription factor, E2F (Berride, 2012). In the G₁ phase extracellular signals, such as growth factors, stimulate the production

of cyclin D, due to the increase in cyclin D, CDK 4/6 start to associate within (Fig. 1.9) (Cobrinik, 2005). The transition through the cell cycle is controlled by phosphorylation of specific targets on kinases (Dorée & Galas, 1994; Hochegger et al., 2008). Therefore, cyclin D-CDK 4/6 complex is activated by phosphorylation on threonine 172 (Thr¹⁷²). The formation of the cyclin D-CDK 4/6 complex results in the confiscation of the CDK inhibitors (CKI), p21^{cip1} and p27^{kip1} (after this called p27) and thus leading to the late G₁ phase activation of cyclin E-CDK 2 (Sherr, 1994; Sherr & Roberts, 1999). The activated cyclin D-CDK 4/6 complex phosphorylates the tumour suppressor, RB, leading to the release of the transcription factor, E2F. The release of E2F can allow the cell by gene activation to progress through the restriction phase, into the S phase for DNA replication.

1.7.2.2 The S phase

During the S phase the genome is duplicated by DNA replication where each identical copy segregates into two daughter cells. Chromosome duplication is triggered by the activation of cyclin A-CDK 2, which activates proteins that unwind the DNA and initiate its replication at sites in the DNA called replication origins (Bertoli et al., 2013). The Cdc10-dependent transcript 1 (Cdt1) is required for formation of the pre-replicative complexes (preRC) and is an essential factor that binds to the recognition complex, and Cdc6 loads the minichromosome maintenance subunits 2-7 (MCM2-7) to initiate the complex for replication (Nishitani et al., 2001; Riialand et al., 2002; Soria & Gottifredi, 2010; Darzynkiewicz et al., 2015).

1.7.2.3 The G₂/M phase

The G₂ phase and S phase of the cell cycle is driven by activated cyclin A-CDK 1 and cyclin B-CDK 1 complexes. During G₂ phase the production of cyclin B is elevated and as cyclin B reaches threshold, the cell will enter mitosis (Lindqvist et al., 2009; Rhind & Russell, 2012). The activated cyclin B-CDK 1 triggers the assembly of the mitotic spindle leading to the segregation of the duplicated genome. The mitotic spindle is made up of microtubules (MTs) that can grow and shrink from their ends (Meunier & Vernos, 2012). These MTs can conjugate to chromosomes at specific sites known as kinetochores, which act as protein molecules that connect chromosomes to MTs and act as a signalling mechanism to coordinate

mitotic progression (Sacristan & Kops, 2015). A study conducted by Gayek & Ohi (2016), concluded that CDK 1 inhibition in G₂ phase can impair the subsequent mitosis through an unknown mechanism that eventually stabilizes kinetochores-MTs (K-MTs). Mitosis (M phase) consist of the following phases, namely prophase, metaphase, telophase and anaphase. The loss of CDK 1 activity results in the activation of mitotic exit and completion of cell cycle (Niederhuber et al., 2013).

1.7.3 Cell cycle checkpoints

1.7.3.1 G₁/S checkpoint

DNA damage can be in the form of DNA single-strand breaks (SSBs) and/or double-strand breaks (DSBs) that leads to unstable chromosome structure and induce DNA damage response. The G₁/S checkpoint is activated to avoid cells with damaged DNA occupied in the G₁ phase from entering the S phase. G₁/S checkpoint is more sensitive to a single DSB that can induce arrest, whilst a larger number is required to activate G₂/M checkpoint (D' Adda di Fagagna, 2008). The key molecular mechanisms of checkpoint pathways that are activated in response to DNA damage is the ataxia telangiectasia mutated (ATM) and Rad3-related (ATR) and subsequently downstream pathways causing the activation of p53 (Al-Ejeh et al., 2010). DSBs activate ATM, whilst ATR is activated by either SSBs or DSBs, and both mechanisms trigger a series of phosphorylations (Medema & Macurek, 2012). ATM phosphorylates the checkpoint kinase 2 (CHK2), while ATR phosphorylates the checkpoint kinase 1 (CHK1). Both CHK1 and CHK2 initiate the cell cycle arrest by phosphorylating cell division cycle 25A protein (CDC25A) that prevents the dephosphorylation of the cyclin D-CDK 4/6 and cyclin E-CDK 2 (Mombach et al., 2014). This latter ceases phosphorylation events of RB and prevents the release of E2F transcription factors which allows the cell by gene activation to progress through the restriction point into the S phase. ATR, ATM, CHK1 and CHK2 phosphorylate p53 that mediate the repairs at G₁/S checkpoint arrest via the activation of p21 (Hyun & Jang, 2015). This CDKI inhibits Cyclin D-CDK 4/6 and Cyclin E-CDK 2. Upon DNA repair, the complex Cyclin E-CDK 2 is activated and drives the cell from G₁ to S phase (Mombach et al., 2014).

1.7.3.2 G₂/M checkpoint

The G₂M checkpoint is an essential point that allows for a delay of cell cycle before segregation of chromosomes. Cyclin B-CDK 1 controls the entry into M phase (Tyner, 2009). Upon DNA damage, G₂ arrest is initiated via phosphorylation of Cdc25C by CHK1 and CHK2 kinases (see section 1.7.3.1 G₁/S checkpoint) preventing Cdc25C from activating CDK1 complex (Charrier-Savournin et al., 2004). Therefore, cyclin B-CDK1 complex remains in its inactive form and preventing entrance into M phase.

1.7.3.3 Mitotic checkpoint

The segregation of sister chromatids at anaphase is controlled by the mitotic spindle. The mitotic spindle is made up of microtubules (MTs) that can grow and shrink from their ends (Meunier & Vernos, 2012). These MTs can conjugate to chromosomes at specific sites known as kinetochores, which act as protein molecules that connect chromosomes to MTs and as signalling mechanism to coordinate mitotic progression (Sacristan & Kops, 2015). As all kinetochores are attached and aligned at the metaphase plate, anaphase can proceed as allowed by the activation of E3 ubiquitin ligase known as the Anaphase-Promoting Complex or Cyclosome (APC/C) (Barnum & O'Connell, 2014). The APC activity is controlled by Cdc20, which is utilised until the metaphase-anaphase, and Cdh1, which aids in the APC-mediated ubiquitination once cyclin degradation has started (McLean et al., 2011). When sister chromatid cohesion is released, spindle tension and the related motor proteins facilitate sister chromatids to move separately, forming identical daughter nuclei (McLean et al., 2011).

1.8 Cell cycle and radiation

Cells that are exposed to IR will initiate a complex response that includes the arrest of cell cycle progression in G₁ and G₂, apoptosis and DNA repair (Hwang & Muschel, 1998). Irradiated cells will result in an increased effect on the levels and activity of p53. The main purpose of p53-dependent G₁ arrest might be the removal of cells containing DNA damage, whilst G₂ arrest following radiation has been shown to be important in protecting cells from

death (Hwang & Muschel, 1998; Teyssier et al., 1999). Thus, radiation will cause a G₂ phase arrest mediated by p53. Moreover, radiation-induced G₂ arrest was shown to require inhibitory phosphorylation of the cdc2 via an ATM-dependent pathway (Teyssier et al., 1999). Therefore, the G₂ checkpoint can be used in future studies as an essential approach for cancer therapy.

1.9 Aims of the study

The aim of this study was to determine possible toxicity caused by AuNPs and to establish whether scattered 6 MV X-rays, as well as p(66)/Be neutron radiation, will biologically and physically interact with AuNPs. Since AuNPs have been indicated as excellent radiosensitisers and may enhance the radiotherapy effect in cancerous cells, the radiosensitising enhancement effect of AuNPs was examined on the Chinese hamster ovary (CHO-K1) cell line, brain endothelial (BEnd5) cell line, breast cancer (MCF-7) and non-cancerous breast (MCF-10A) cell line, by treating them with AuNPs. The treatment was followed by radiation of cells with 2 & 4 Gy X-rays and 1 & 2 Gy p(66)/Be neutrons, respectively. The objectives of this study were as follow:

- Characterisation of 5 nm and 10 nm AuNPs.
- To differentiate the reaction of non-malignant cells versus malignant cells treated with AuNPs, followed by radiation.
- To study and quantify chromosomal aberrations in the cells that has been treated with AuNPs followed by ionising radiation exposure.
- To evaluate AuNPs-treated cell proliferation.
- To determine cell cycle progression of the cells treated with AuNPs followed by radiation exposure.

CHAPTER 2:

MATERIALS AND METHODS

2.1 Materials and Methods

2.1.1 Reagents and cells

All chemicals and solutions, including dimethyl sulfoxide (DMSO), tetrazolium bromide (3-(4,5-dimethylazol-2-yl)-2,5-diphenyl-tetrazolium bromide, MTT), glutaraldehyde, osmium tetroxide, propylene, resin, uranyl acetate, propidium iodine (PI) and Acridine Orange (AO) were of analytical grade and purchased from Sigma-Aldrich (Johannesburg, South Africa).

Gamma irradiated fetal bovine serum (FBS) was supplied via GIBCO (Cat# 16000044). Phosphate buffered saline (PBS) without Ca^{+2} , Mg^{+2} or phenol red was purchased from WhiteSci (Cape Town, South Africa) and Trypsin (10X) was purchased from Sigma-Aldrich (Johannesburg, South Africa). Dulbecco's Modified Eagle Medium (DMEM), Ham's F-12 Medium and RPMI 1640 Medium for tissue culture, and penicillin-streptomycin were obtained from Thermo Fisher Scientific (Johannesburg, South Africa). Epidermal growth factor (EGF), hydrocortisone and insulin were purchased from Sigma-Aldrich (Johannesburg, South Africa). The Chinese hamster ovary cells (CHO-K1) and Brain Endothelial cells (BEnd5) were a gift from Prof. J. P. Slabbert, NRF-iThemba LABS (Somerset West, Cape Town), whereas human breast adenocarcinoma (MCF-7) and non-tumourgenic human breast epithelia cells (MCF-10A) were purchased from American Type Culture Collection (ATCC), Maryland, United States of America.

2.1.1.1 Chinese Hamster Ovary (CHO-K1) cells

This fast growing cell line is used as a standard model for experiments. The line of epithelial-like CHO cells was initiated by T.T. Puck in 1957. Since then, CHO cells have become a widely used mammalian expression system in science (Gamper et al., 2005).

2.1.1.2 Brain endothelial (BEnd5) cells

BEnd5 cell line is a polyoma middle T-oncogen-immortalized mouse brain endothelioma cell line (Steiner et al., 2011). BEnd5 cell culture model could provide a useful *in vitro* model of the blood–brain barrier (BBB) for AuNPs (i.e. drug delivery) and visualising pathological states such as cell death.

2.1.1.3 Michigan Cancer Foundation-7 (MCF-7) cells

MCF-7 cell lines are an estrogen receptor (ER) positive cells which are derived from a patient with metastatic breast cancer. The MCF-7 cell line is the most studied human breast cancer cell line in the world, and results obtained from this cell line have had an essential impact upon breast cancer research and patient outcomes (Lee et al., 2015). MCF-7 cells are sensitive to estrogen, as well as sensitive to cytokeratin. Once grown *in vitro*, the cell line is capable of forming domes (upper half of a sphere) and the epithelial like cells grow in monolayers. (<http://www.mcf7.com/>).

2.1.1.4 Michigan Cancer Foundation-10A (MCF-10A) cells

The MCF-10A cell line is a non-malignant breast epithelial cell line and is positive for epithelial sialomucins, cytokeratins and milk fat globule antigen (Imbalzano et al., 2009). These cells are cultured in three-dimensional (3-D) reconstituted basement membrane culture and form domes in confluent cultures (Imbalzano et al., 2009; Qu et al., 2015). MCF-10A cell line has a stable, near-diploid karyotype (Yoon et al., 2009) and expresses normal p53 (Debnath et al., 2003). MCF-7 and MCF-10A cells were used for comparison in this study.

2.1.2 Gold nanoparticles (AuNPs)

The 5 nm and 10 nm AuNPs, in a citrate buffer, were purchased from Sigma-Aldrich (Johannesburg, South Africa). The AuNPs were filtered by the use of syringe filters (0.2 μm) (Cat# 431219) and stored in sterile 50 ml tubes to ensure that no contamination could occur.

2.1.3 Sample collection and isolation of lymphocytes for γ -H2AX foci assay

Peripheral blood samples were collected in sodium heparin blood collection tubes (Cat# 368884 and BD Vactainer® PLUS) from healthy adult volunteers. Donors were non-smokers and had no history of radiotherapy treatment within the last ten years. CD3⁺ T cells were isolated from peripheral blood using the RosetteSep™ Human T Cell Enrichment Cocktail (Stemcell Technologies) by negative selection after density gradient centrifugation (Density: 1.081 g/ml, RosetteSep™ Density Medium, Stemcell Technologies). Unwanted cells were targeted for removal with Tetrameric Antibody Complexes recognizing CD16, CD19, CD36, CD56, CD66b and glycophorin A on red blood cells (RBCs), resulting in a highly enriched population of CD3 T-lymphocytes (purity > 98%) (Vandevoorde et al. 2016).

2.1.4 General cell culture procedures

The CHO-K1 cells were cultured using RPMI 1640 medium supplemented with 10% FBS. MCF-7 cells were cultured using Dulbecco's Modified Eagle's medium F-12 (DMEM F-12) supplemented with 10% FBS, penicillin (100 $\mu\text{g/l}$) and streptomycin (100 $\mu\text{g/ml}$). MCF-10A and BEnd5 cells were all cultured using Dulbecco's Modified Eagle's medium F-12 (DMEM F-12) and Ham's F-12 (50:50), supplemented with 5% Fetal Bovine Serum (FBS). Furthermore, the MCF-10A medium was supplemented with EGF (20 ng/ml final concentration), hydrocortisone (0.5 mg/ml final concentration), insulin (10 $\mu\text{g/ml}$ final concentration), penicillin (100 $\mu\text{g/l}$) and streptomycin (100 $\mu\text{g/ml}$) (Debnath et al., 2003). The aforementioned cell lines were incubated at 37 °C, 5% CO₂ air and humidified atmosphere. Tissue culture flasks, serological pipettes and filters were obtained from BIOCROM/Biotech.

Stock cultures of CHO-K1, MCF-7, MCF-10A and BEnd5 cells, taken from the -80°C freezer, were thawed quickly. The suspension was centrifuged at 900 rpm for 6 minutes, resulting in a pellet. The supernatant was aspirated and the pellet of cells was re-suspended in 2 ml of culture media. Each 1 ml of cell suspension was added to 4 ml of culture media in a tissue culture flask, respective to the type of cell line. The cell viability and cell density was determined by staining the trypsinized cells with trypan blue in a ratio of 1 part cells in medium : 3 part dye : 6 part culture media and was loaded onto a haemocytometer and counted (Strober, 2001). When needed media was replaced respective to the specific cell line.

When the culture flask reached ~75–80% confluence, the cells were trypsinised and some sub-cultured cells were placed in cryovials and stored at -80 °C to ensure a constant supply of low passage cells. The freeze media used to store the cells consisted of 70% culture media, 20% FBS and 10% DMSO.



2.1.5 Characterisation of AuNPs

2.1.5.1 UV-visible (vis) absorption spectrophotometry

The absorption of both AuNP solutions was measured via UV-vis spectrophotometry for the analysis of SPR to substantiate the presence of AuNPs, in addition to the estimated size and quantity. Samples were placed in cuvettes and the UV-vis spectra measurements were recorded within the 200–1000 nm wavelength range, using an Agilent 8453 spectrophotometer (GenTech Scientific Inc.) and a software program known as UV-visible ChemStation.

2.1.5.2 Zeta (Z) potential dynamic light scattering (DLS) and polydispersity index (PDI)

The Z-potential is the main indicator of attractive or repulsive forces between nanoparticles. Therefore, this Z-potential parameter can be used to forecast the stability of the nanoparticles dispersion over a long-term period. A DLS measurement represents the hydrodynamic core size of nanoparticles in suspension. In addition, PDI measurements were used to determine

the size distribution width of the AuNPs. AuNPs samples were placed in capillary tubes for Z-potential and, in cuvettes for PDI measurements of AuNPs were determined using Malvern Instruments' Zetasizer Nano ZS. The data was obtained in the phase analysis light scattering mode at 25 °C.

2.1.5.3 Transmission electron microscopy (TEM)

2.1.5.3.1 AuNPs within cells

A TEM analysis was done to observe the presence, as well as the infiltration of AuNPs within cells. MCF-7 cells were seeded into 25 cm² flasks, at 3x10⁵ cells per flask and the slow growing MCF-10A cells were seeded at 5x10⁵ cells per flask. Cells were allowed to attach overnight at 37 °C, 5% CO₂ air and relative humidified atmosphere. Afterwards, each flask of cells was treated with 50 µg/ml of 10 nm AuNP solution for 4 hours. Subsequent to incubation, the media was removed and the cells were washed with PBS. To each of these flasks, 2.5% glutaraldehyde diluted in PBS (pH 7.4) was added for fixation of the cells. The cells were harvested through scraping and centrifuged at 1000 rpm for 3 minutes to obtain a pellet.

Post-fixation, cells were washed thrice in 200 mM phosphate buffer for 5 minutes and stained with 1% osmium tetroxide diluted in 100 mM phosphate for 60 minutes. Afterwards, the cells were counter-stained with 1% uranyl acetate diluted in 100 mM phosphate. Both treated cell samples were washed with distilled water (dH₂O) to remove phosphate ions, and thereafter dehydrated in ethanol (EtOH) (50, 70, 90 and 100%) for 5 minutes. Ethanol was then replaced with propylene oxide, and the cells were washed in this solution to remove plastic residues. The solution was removed and replaced with 50% propylene oxide and 50% resin solution and dried for 2 hours. The 50% solution was removed and replaced with pure resin and dried for extra 2 hours. 1 µm thick sections of each sample were made using a microtome, and deposited on a Formvar coated 200-300 mesh copper grids and analysed (TEM JEOL JEM-1011). The fixation steps were performed by a medical echnologist (Electron Microscopy) namely, Mrs Nolan Muller, from NHLS Tygerberg Hospital. The TEM images were also captured by Mrs Muller using Software Imaging System (SIS).

2.1.6 Experimental set-up for irradiation procedures

All cell samples were irradiated as monolayers in 25 cm² culture flasks and 9 cm² petri dishes. The irradiation experiments were performed using a clinical linear accelerator (LINAC) operating at 6 MV peak photon energy mode and the p(66)/Be neutron beam with a mean neutron energy of 29 MeV at iThemba LABS (Somerset West, Cape Town, South Africa) (Fig 2.1 & 2.2). Gy can be defined as 1 joule (J) of energy deposited in 1 kilogram of mass.

2.1.6.1 X-ray radiation

X-ray radiation was conducted using a vertical beam (Philips SL 75-5 LINAC) directed downward through a 20x20 cm field of build-up material, referred to as a Shonka chamber, consisting of 20 mm polyethylene onto a 2 cm thick backscatter block of Perspex (Fig. 2.1). The LINAC was calibrated to use 6 MV X-rays, which was scattered by using a Shonka chamber to obtain lower energies X-rays to interact with the AuNPs. This procedure can be known as beam “softening”. The beam “softening” technique described by Berbeco (2012) was accomplished by using the Shonka chamber, mentioned above, to expect kV X-rays. The dose rate was 0.6 Gy/min for X-ray radiation. All the samples were placed at the machine’s isocenter and orthogonal to the central axis of the beam to ensure each sample was irradiated with the same dose. Following a 4 hour incubation period with AuNPs, cells were irradiated with a dose of 2 Gy or 4 Gy. According to Berbeco and co-workers (2012), AuNPs are of interest in radiotherapy for *in vitro* applications due to the high K-edge of Au (~81 keV), which can result in the emission of short-range photoelectrons upon radiation with low LET photons.

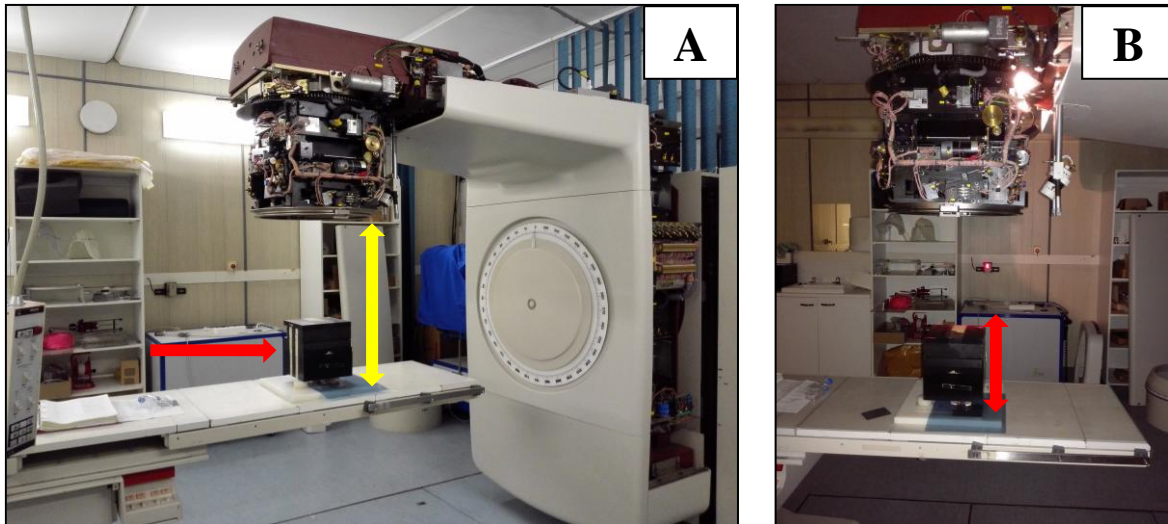


Figure 2.1: X-ray experimental set-up. (A) The red arrow shows the 20x20 cm Shonka chambers. The yellow arrow displays the distance from the gantry to the samples, which is 100 cm. (B) The red arrow shows the depth of the Shonka chamber (iThemba LABS, Somerset West, South Africa).

2.1.6.2 p(66)/Be neutron radiation

The p(66)/Be neutron radiation set-up was in a 30x30 cm field of build-up material that consisted of 2x3 cm deep nylon tissue-equivalent material, onto three 3 cm thick backscatter blocks of Perspex (Fig. 2.2). All the samples were placed under the radiation field as mentioned in section 2.1.6.1. The dose rate was 0.5 Gy/min for p(66)/Be neutron radiation. Following AuNP incubation, cells were irradiated with doses of 1 Gy or 2 Gy p(66)/Be neutron radiation. The chosen X-ray and neutron radiation doses reflect similar relative biological effectiveness (RBE) to cause the same level of effect, given that the same amount of energy is absorbed within the cells/tissue. Therefore, 1 Gy p(66)/Be neutron radiation is approximately equivalent to 2 Gy X-radiation, in addition to reflecting the dosages received by patients in a clinical set-up (Franken et al., 2011).

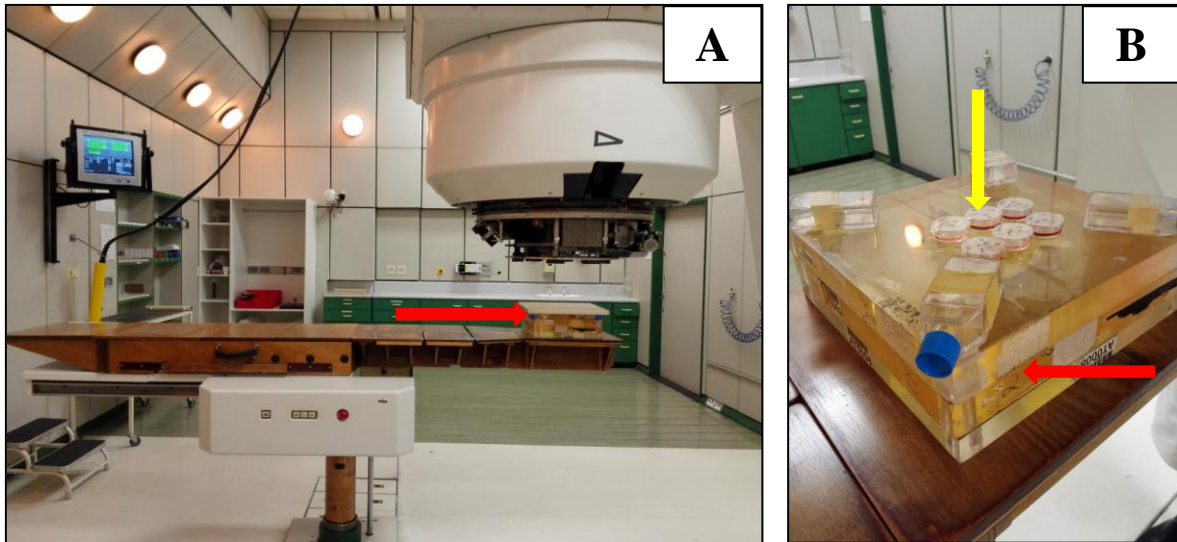


Figure 2.2: p(66)/Be neutron radiation set up. (A) The red arrow shows the 30x30 cm radiation field. (B) The yellow arrow shows the samples in petri dishes and the red arrow shows three Perspex blocks, each block is 3 cm thick (iThemba LABS, Somerset West, South Africa).

2.1.7 γ -H2AX foci assay

The γ -H2AX foci assay is commonly used for the quantitative evaluation of induced DNA double-strand breaks (DSBs) formation in lymphocytes (Olive & Banath, 2004). In general, analysis of H2AX expression can be used to detect the genotoxic effect of different toxic substances (Podhorecka et al., 2010). The γ -H2AX foci assay was carried out in isolated human lymphocytes only, to establish radiation damage following a 4 hour treatment with 50 $\mu\text{g/ml}$ AuNPs. This assay in lymphocytes is seen as a quick informative tool of early DNA damage. After incubation with AuNPs of two different diameters (5 nm and 10 nm) and irradiation with x-rays or neutrons, isolated lymphocyte cells were centrifuged on poly-L-lysine coated slides (VWR International) in a concentration of 6×10^5 cells/ml. The slides were fixed in PBS containing 3% paraformaldehyde (PFA) (Life Technologies) for 20 minutes and stored overnight in PBS (4 °C) containing 0.5% PFA. The next day, slides were washed with PBS for 10 minutes and treated with 0.2% (v/v) Triton X-100 solution (Life Technologies) in PBS for 10 minutes. Thereafter, cells were blocked by washing them three times for 10 minutes in PBS containing 1% Bovine Serum Albumin (BSA) obtained from Sigma-Aldrich (Johannesburg, South Africa). Immunohistochemistry staining was performed using a monoclonal primary antibody (Ab) against γ -H2AX (1:500, Mouse mAb, Life Technologies). Slides were incubated with the primary Ab for 1 hour at room temperature.

After washing the cells three times in PBS containing 1% BSA the slides were incubated for 1 hour at room temperature with Tetramethyl Rhodamine Isothiocyanate (TRITC) rabbit-anti-mouse Ab (1:1000, Life Technologies) as secondary Ab. Afterwards, the slides were rinsed three times in PBS and mounted in Fluoromount purchased from Sigma-Aldrich (Johannesburg, South Africa) containing 2% 4',6-Diamidino-2-Phenylindole (DAPI) (Life Technologies).

Slides were stored in a cool, dark place before image capturing to allow the mounting medium to dry and to avoid fading of the fluorescent signal. Slides were scanned by a Metafer 4 System (Metasystems) at iThemba LABS (Fig. 2.3). Metafer system is a special platform to automatically scan samples. Images were obtained automatically by using MetaCyte software (40x Magnification). In each experiment, at least 1000 cells were scored over two slides in randomly selected fields of view.



Figure 2.3: The Metafer 4 System set-up. (A) The complete Metafer 4 System (Metasystems) equipped with a 40x objective. The white arrow shows the stage of the inverted fluorescence microscope (Zeiss) that can contain 8 slides. (B) Detailed image to show precisely the location of the cell containing DNA DSBs, on the slide – indicated by the white arrow (iThemba LABS, Somerset West, South Africa).

2.1.8 Cytokinesis-block Micronucleus (CBMN) assay

The CBMN assay is a cytogenetic test for the measurement of chromosome breakage and loss in nucleated cells. The micronuclei (MNi) observed in binucleated cells (BNCs) are minute extracellular bodies, separated from the main nucleus, that consist of acentric fragments (Fig.

2.5) (Fenech et al., 2003). As a result, MNi present a consistent index of chromosome damage due to radiation damage at the G₀ phase of the cell cycle (Vral et al., 2011).

Exponentially growing CHO-K1, MCF-7, MCF-10A and BEnd5 cells were seeded on cover slips at 4×10^3 per 9 cm² petri dish and allowed to attach overnight. All the above mentioned cells were treated with 50 µg/ml with both types of AuNP and subsequently irradiated with X-ray and p(66)/Be neutron radiation respectively, after which the CBMN assay was performed. Controls consisted of a negative control (i.e. no AuNPs and no radiation), AuNP controls (i.e. no radiation) and radiation controls (i.e. no AuNPs) following 4 hours incubation. Irradiation was done by using the beam “softening” technique (Berbeco et al., 2012). The fraction of photons in a clinical megavoltage (MV) beam depends on the depth of material. Beam “softening” will occur at deeper measurement points as the contribution of low-energy scattered photons become more significant relative to the attenuated primary beam (Berbeco et al., 2012). Therefore, this application involves the use of 6 MV photon beam over a fairly large distance to enhance the production of low-energy scattered photons, with AuNPs penetrating into the cells, leading to damage enhancement as a function of amplified depth. Enhanced interaction indices between the AuNPs and scattered 6 MV 2 Gy X-rays were observed in the CHO-K1 and MCF-7 cells only. Therefore, only these two cell lines were further used in the study to validate and further investigate the interaction between the AuNPs and radiation. Further studies included a change in the radiation dose from 2 to 4 Gy X-rays and a decrease in the AuNP concentration from 50 µg/ml to 2.5 µg/ml. These AuNP treated cells were also irradiated with 1 Gy and 2 Gy neutrons (separate experiments) to establish whether the interaction between AuNPs and scattered 6 MV 2 Gy X-rays would still exist. Irradiation experiments were performed as described in sections 2.1.6, 2.1.6.1 and 2.1.6.2. The CBMN assay was performed by following the same protocol provided by iThemba LABS Somerset West. After radiation treatment, media with AuNPs was removed and fresh culture media was added to each cell line. 2.25 µg/ml cytochalasin B was added to each experimental sample, to inhibit cytoplasmic division to enable the observation of MNi after anaphase division, and incubated for 24 hours. Thereafter, the media was removed and the cells were washed with PBS (pH 7.4). This was followed by the addition of 1 ml cold methanol/acetic acid (3:1) for a 5 minute fixation. The fixative was removed and the cells were allowed to air-dry for 15 minutes. A 0.1% aqueous solution of acridine orange (AO) was prepared for staining, in which a stock solution of 0.24 mM of the stain was diluted in Gurr buffer (pH 6.8) (Gibco Cat# 10582-013 and 1 Gurr buffer tablet supplied from

ThermoFisher Scientific was dissolved in 1 L of DH₂O). The fixed cells on the cover slip were stained with AO for 1 minute and rinsed for 1 minute in Gurr buffer. The stained cover slips were placed on the centre of the labelled microscope slides, with the excess buffer being blotted, and the slides were sealed with Fixogum Rubber Cement (SMM Instruments, Cat# LK-071A).

Following the guidelines indicated by Fenech (2000), Fenech et al. (2003) and Vandersickel et al. (2010), scoring of 500 BNCs per slide was done manually using an inverted fluorescence microscope (Zeiss), and the FITC filter. MNi are counted within BNCs to ensure that any possible damage enhancement that has occurred will be observed as acentric fragments within the BNCs. The “scoring” of MNi within the BNCs was completed by counting the number of MNi within the BNCs and binning them as 0, 1, 2, 3, 4, etc., to generate a ratio of total MNi within the entire population of BNCs per slide.

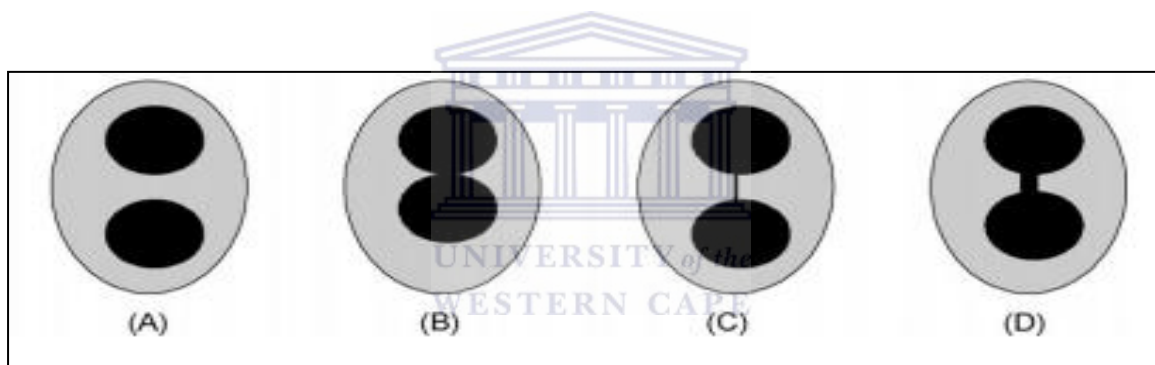


Figure 2.4: Different types of BNCs in the CBMN assay. (A) Ideal BNC, (B) a BNC with touching nuclei, (C) BNC with thin nucleoplasmic bridge between nuclei and (D) BNC with rather thick nucleoplasmic bridge (Fenech et al., 2003).

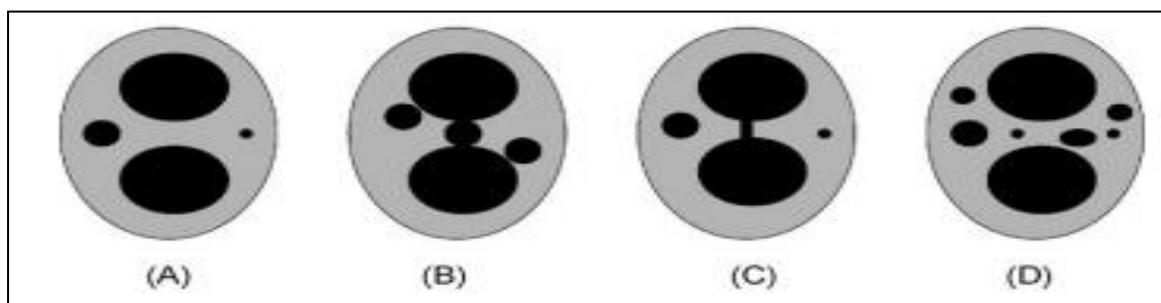


Figure 2.5: The characteristic appearance and relative size of MNi in BNCs. (A) BNC with two MNi containing viable MNi varying in sizes between 1/3 to 1/9 of the main nuclei. (B) BNC with three MNi touching, but not overlapping the main nuclei. (C) A BNC with nucleoplasmic bridge between main nuclei and two MNi. (D) A BNC with six MNi varying in sizes (Fenech et al., 2003).

2.1.9 Cell viability assay

Both CHO-K1 and BEnd5 cells were plated sub-confluent at 1×10^2 cells per well due to their fast growth nature. MCF-7 cells were plated sub-confluent at 7.5×10^3 cells per well and MCF-10A cells were plated at 10×10^3 cells per well. In the time and dose study, exponentially growing CHO-K1, MCF-7, MCF-10A and BEnd5 cells were plated into flat-bottomed 96-well tissue culture plates and allowed to attach overnight. Thereafter, cells were treated with different concentrations of the two types of AuNPs (2.5, 5, 10 and 50 $\mu\text{g/ml}$) for different times (4 hours non-irradiated, 4 hours irradiated with 4 Gy scattered 6 MV X-rays, and 24 hours non-irradiated) in triplicate. The cells were irradiated with 4 Gy X-rays to obtain the maximum effect on cellular proliferation after 4 hours. The average of all the experiments is shown as the cell-viability percentage in comparison with the control, which is the untreated cells and considered as 100%. The controls consisted of non-irradiated cells without AuNPs and irradiated cells without AuNPs. At the end of each treatment period, the toxicity level was measured by adding MTT (5 mg/ml), diluted in PBS (pH 7.4), to each well. The plates were covered with foil, due to light sensitivity, and incubated at 37 °C, 5% CO₂ air and relative humidified atmosphere for 4 hours. Following incubation, the MTT solution was removed and the formazan solvent DMSO, was added. The plate was covered again with foil and placed on a rocker for 15 minutes. The MTT assay was used to determine the AuNP effect on the cell viability by measurement of enzymatic reduction of yellow tetrazolium to a purple formazan by cellular mitochondria (Fig. 2.6) and detected by a whole plate read using PhotoRead Software via Apollo LB 913 (Berthold technologies) UV-vis spectrophotometer at 570 nm. The MTT assay followed the procedure as described by Riss et al. (2013) in the Assay Guidance Manual.

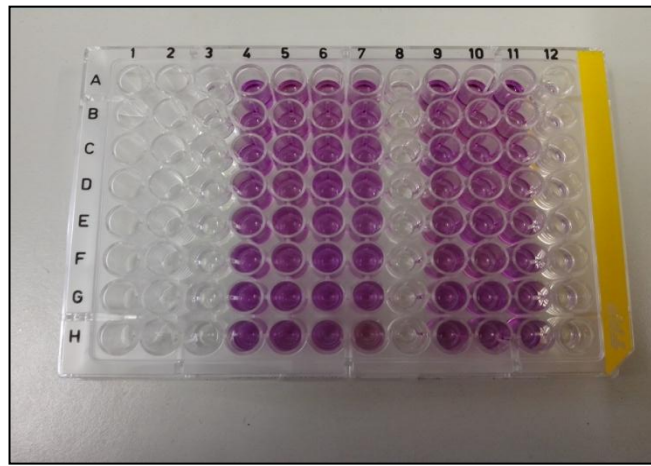


Figure 2.6: Example of MTT assay. 96 well plate, in which the MTT solution was removed and the formazan solvent DMSO was added, resulting in a purple colour.

2.1.10 Cell cycle analysis

Flow cytometry measures numerous types of individual particles flowing in single file in a stream of fluid (Fig. 2.7) (Brown and Wittwer, 2002). According to Brown and Wittwer (2002) physical properties like size, represents forward angle light scatter) and internal complexity which corresponds to right-angle scatter) and can determine cell populations. Flow cytometry can be used to analyse the progression of the cell cycle as the light scatters of the population of cells and excites the fluorescent probe to emit a certain colour (Krishan, 1975). This is quantified by a particular software program. In this study, propidium iodine (PI) was used to bind to double stranded (ds) DNA. The stained DNA will in this way emit fluorescence from stained cells as it passes through the laser beam. Flow cytometric analysis provides quantitative data and the ability to measure large numbers of cells swiftly.

Each cell line was seeded at 5×10^4 cells per 25 cm^2 flask and was allowed to attach overnight under the specific conditions described in section 2.1.4. The following day, it was exposed to $50 \text{ }\mu\text{g/ml}$ of either 5 nm or 10 nm AuNPs. Cells were harvested and then centrifuged (Jouan B4 Centrifuge) for 6 minutes at 900 rpm ($25 \text{ }^\circ\text{C}$) for pellet formation and washed with PBS (pH 7.4). Permeabilization of the cell membrane was achieved by fixing the cells in 3 ml of ice cold 99.5% EtOH. The fixed cell suspensions were stored at $-20 \text{ }^\circ\text{C}$ overnight. Subsequently, the EtOH was removed by centrifugation at 1400 rpm for 5 minutes and the cells were washed with PBS (pH 7.4) twice. The supernatant was removed without disturbing the pellet and the sediment was resuspended in 1 ml of the hypotonic DNA staining buffer

(20 µg/ml) and stored at 4°C protected from the light for 30 minutes, prior to utilization of the BD ACCURI-C6 flow cytometer. The flow cytometer used a BD FITC BrdU flow kit (Cat# 559619) and was equipped with a 488-nm laser, which excites FITC and 7-AAD. After data is collected, the BD ACCURI-C6 software Zoom function allows visualisation of data to set up specific gates and regions. For each cell sample 10 000 events were collected and aggregated cells were gated out. The PI staining method was provide by Prof. Slabbert from iThemba LABS, Somerset West.

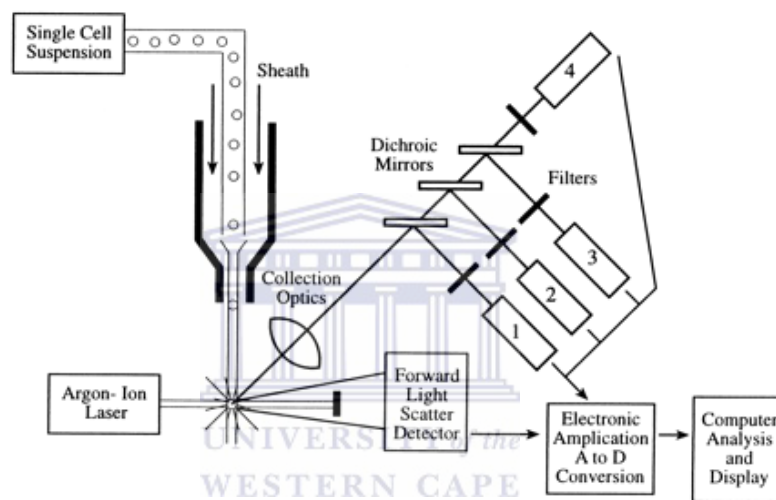
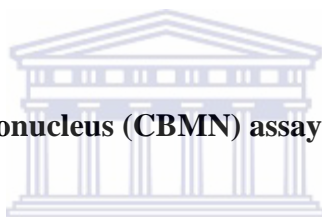


Figure 2.7: Mechanisms of flow cytometry. There are four general components of a flow cytometer: fluidics, optics, detectors and electronics. Cells in suspension flow in single-file through an illuminated volume, where they scatter light and emit fluorescence that is collected, filter and converted to digital numbers that are stored on a computer (Brown et al., 2002).

2.1.11 Statistical analyses

2.1.11.1 γ -H2AX foci assay

Automated scoring of ~1000 lymphocytes was completed via a Metafer 4 System. Statistical analysis was completed via MedCalc program (Version 14.8.1). Multiple comparison graphs (Box-and-Whisker plots) were used to visualise and quantify the influence of the AuNP types and radiation on each sample in an experimental group. The central box in the diagram (Box-and-Whisker) represents the lower and upper quartiles (25 to 75 percentile), therefore the box contains the middle 50% of the values. The middle line in the box represents the median. From each end of the box a line is drawn to the most remote point that is not an outlier. The Kruskal-Wallis test was performed to identify sample means that are significantly different from each other and results were considered statistically significant if $p < 0.05$.



2.1.11.2 Cytokinesis-block Micronucleus (CBMN) assay

Manual scoring of MNi from 500 BNCs per slide was completed as described above. The mean cumulative frequency for each experimental group (Control, X-ray and p(66)/Be neutron radiation) for both types of AuNPs was then calculated, and represented in bar graphs.

For the determination of cellular kinetics, 400 BNCs were counted per conditions and expressed as a percentage (%) of the total number of cells viewed. The % of cells whose nuclei were able to divide after treatment (cellular kinetics) for each experimental group (Control, X-ray and p(66)/Be neutron radiation) for both types of AuNPs was then calculated, and represented in bar graphs.

2.1.11.3 Cell viability assay

MedCalc statistical software version 14.8.1 was used to analyse data. One-way ANOVA (Kruskal-Wallis test) was used to determine the significant difference between the control means and experimental groups. Statistical analysis was completed via MedCalc program

(Version 14.8.1). Multiple comparison graphs (Box-and-Whisker plots) with bars were used to visualise and quantify the influence of the AuNPs types and radiation on each sample in an experimental group. Kruskal-Wallis tests were performed for all independent comparisons and results were considered statistically significant if $p < 0.05$.

2.1.11.4 Cell cycle analysis

Flow cytometry results obtained was determined by using BD ACCURI-C6 software Zoom.



CHAPTER 3:

RESULTS

3.1 Characterisation of AuNPs

3.1.1 UV-visible (vis) absorption spectrophotometry

The absorption of both AuNP solutions was measured via UV-vis spectrometry for the analysis of surface plasmon resonance (SPR) to confirm the presence of AuNPs, as well as approximate size and quantity.

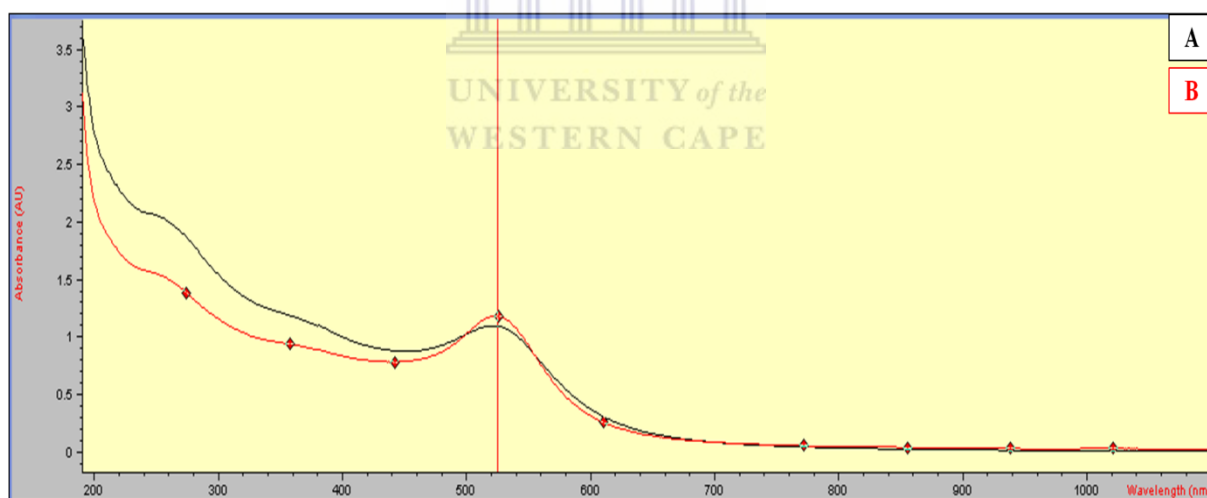


Figure 3.1: The absorption of each AuNP solution. UV-vis spectrum of both types of AuNPs was obtained using the Agilent 8453. Absorbance profiles were measured between 525–580 nm, with an SPR of 525 nm occurring for 5 nm AuNPs (A) and 10 nm AuNPs (B). The red vertical line represents the λ_{max} at 525 nm and indicates the presence of AuNPs.

3.1.2 Zeta (Z) potential, dynamic light scattering (DLS) and polydispersity index (PDI)

Z-potential is an indication of repulsive and attractive forces between nanoparticles and can predict the long-term stability of nanoparticles in the solution. PDI values represent the size distribution width of nanoparticles. Furthermore, DLS measurements were used to determine the hydrodynamic size of citrate-coated AuNPs.

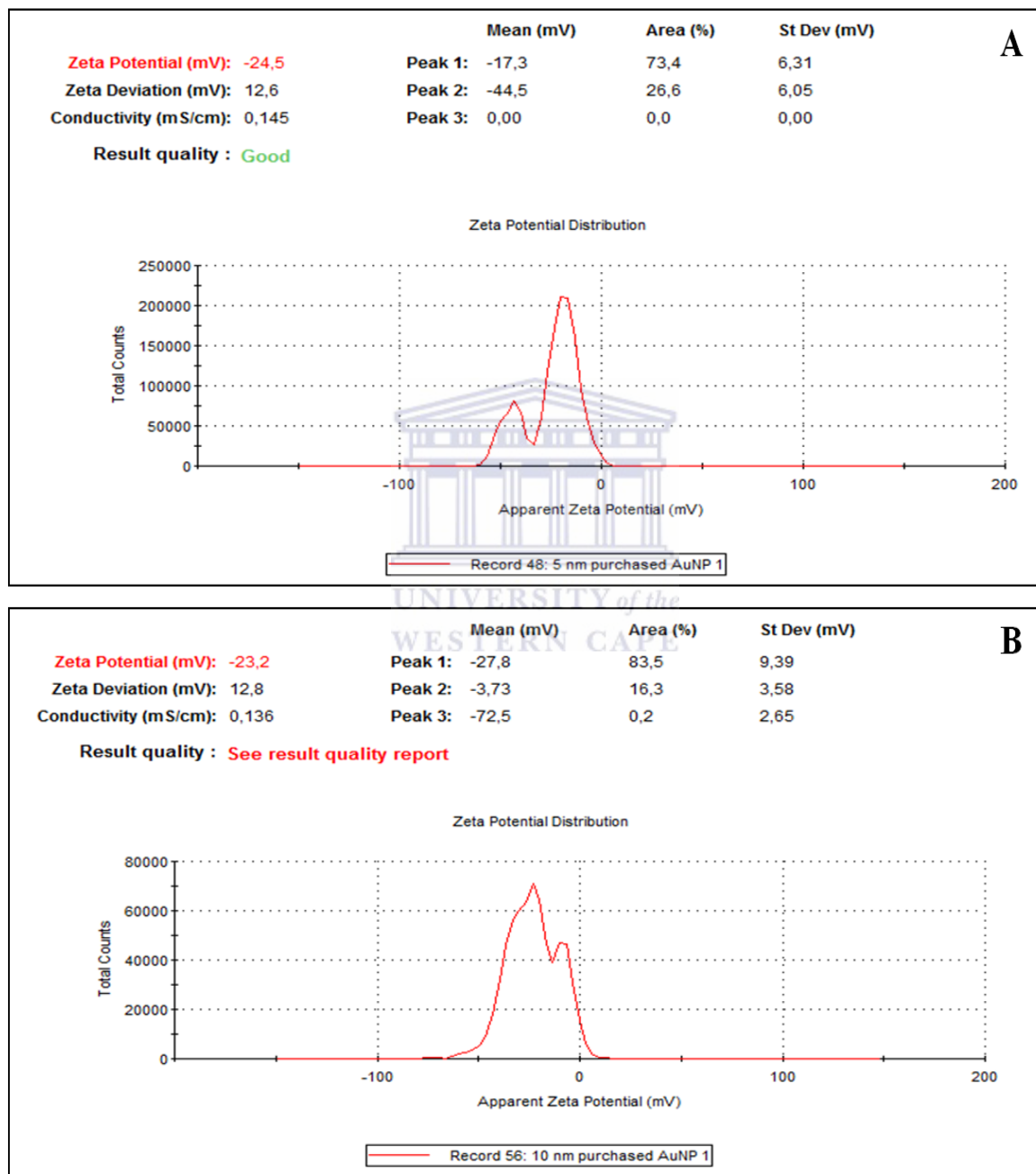


Figure 3.2.1: Zeta (Z) potential measurements of 5 nm and 10 nm AuNPs. The Z-potential of 5 (A) and 10 (B) nm AuNPs was -24.5 mV and -23.2 mV, respectively. The negative Z-potential values present the necessary repulsive forces for the particles to remain stable in the solution. Nanoparticles with Z-potential < -30 mV are regarded as strongly anionic, whereas nanoparticles with a Z-potential > +30 mV are regarded as strongly cationic. Data was obtained in phase analysis light scattering mode at 25 °C and pH 7.4 (Addendum: Fig. 5.1).

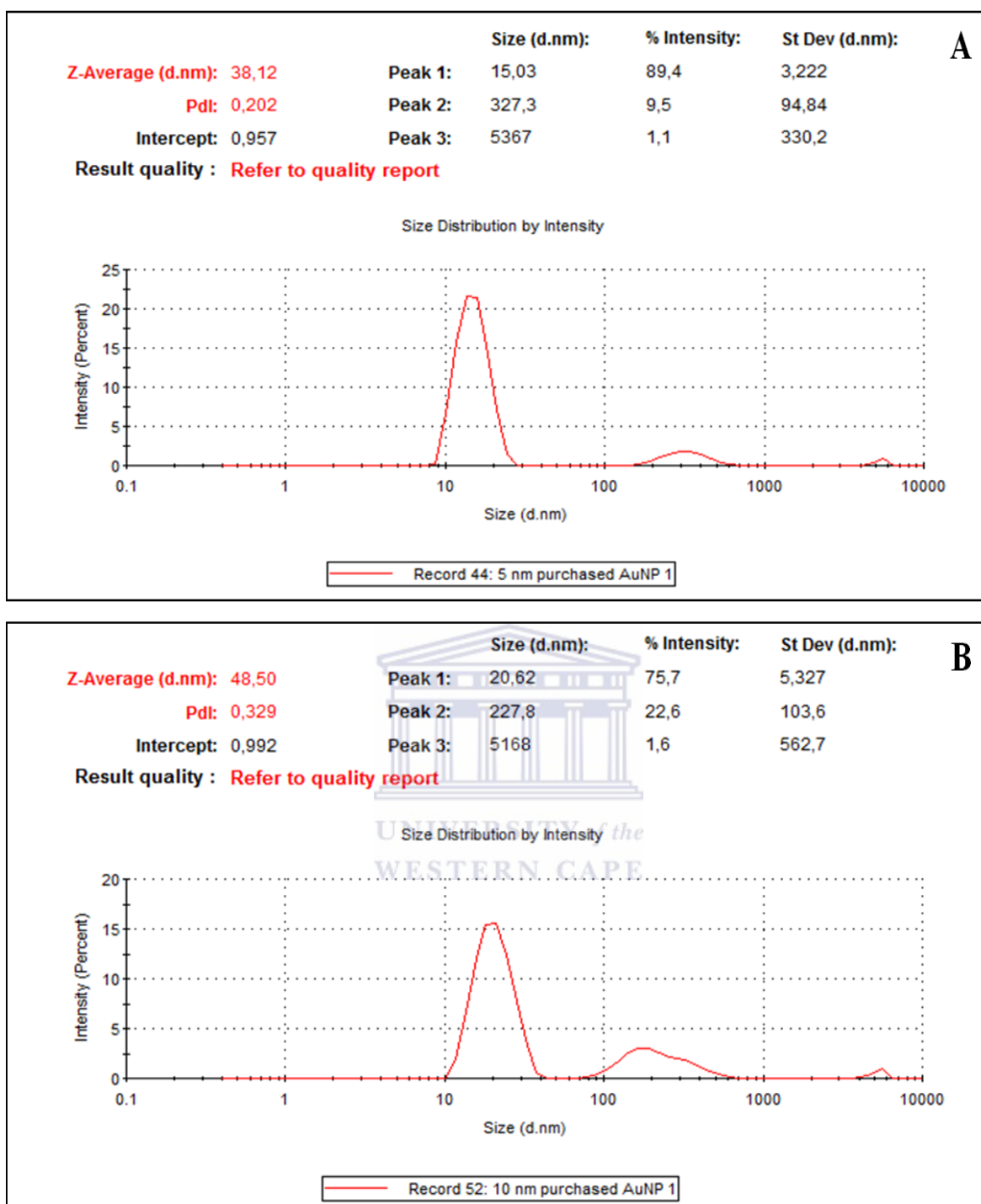
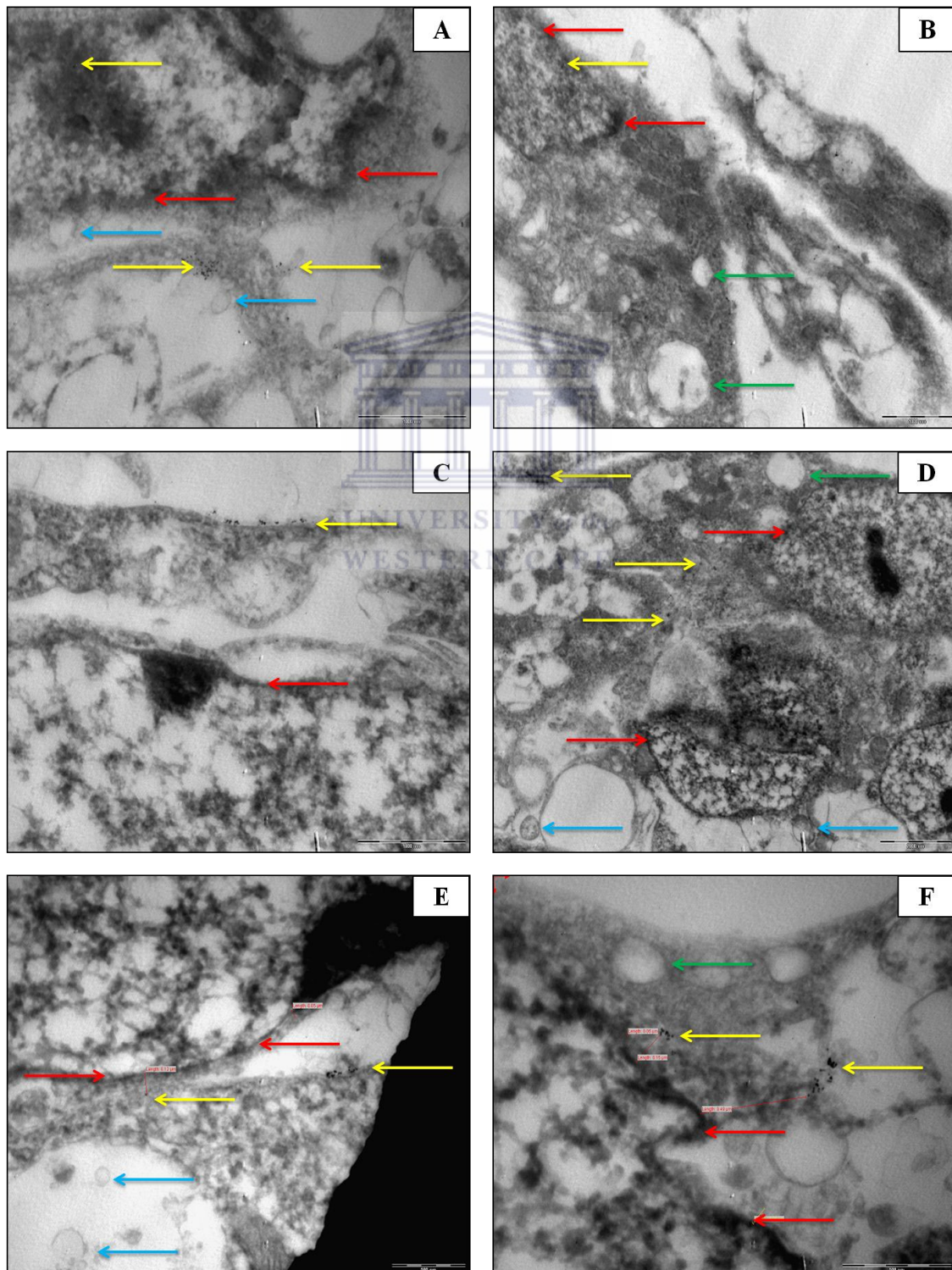


Figure 3.2.2: PDI represents the size distribution width, whereas DLS (Z-average) displays the hydrodynamic core size of both 5 and 10 nm AuNPs. A PDI value of 0.1–0.25 suggests that the nanoparticles have a uniform size distribution, whilst a PDI > 0.5 indicates a very broad distribution. Results conducted shows that both sizes of AuNPs have a uniformity size width distribution. DLS measurements (Z-average) show that the 5 nm AuNPs are 38.12 nm in diameter (A), whilst 10 nm AuNPs are 48.50 nm in diameter (B). These larger sizes in diameter may be due to the agglomeration state of nanoparticles as a function of time or suspending solution. Data was obtained in phase analysis light scattering mode at 25 °C and pH 7.4 (Addendum: Fig. 5.2).

3.1.3 Transmission electron microscopy (TEM)

TEM was used to determine the uptake and location of the AuNPs in two cell lines namely MCF-7 and MCF-10A cells.

3.1.3.1 AuNPs within MCF-7 & MCF-10A cells



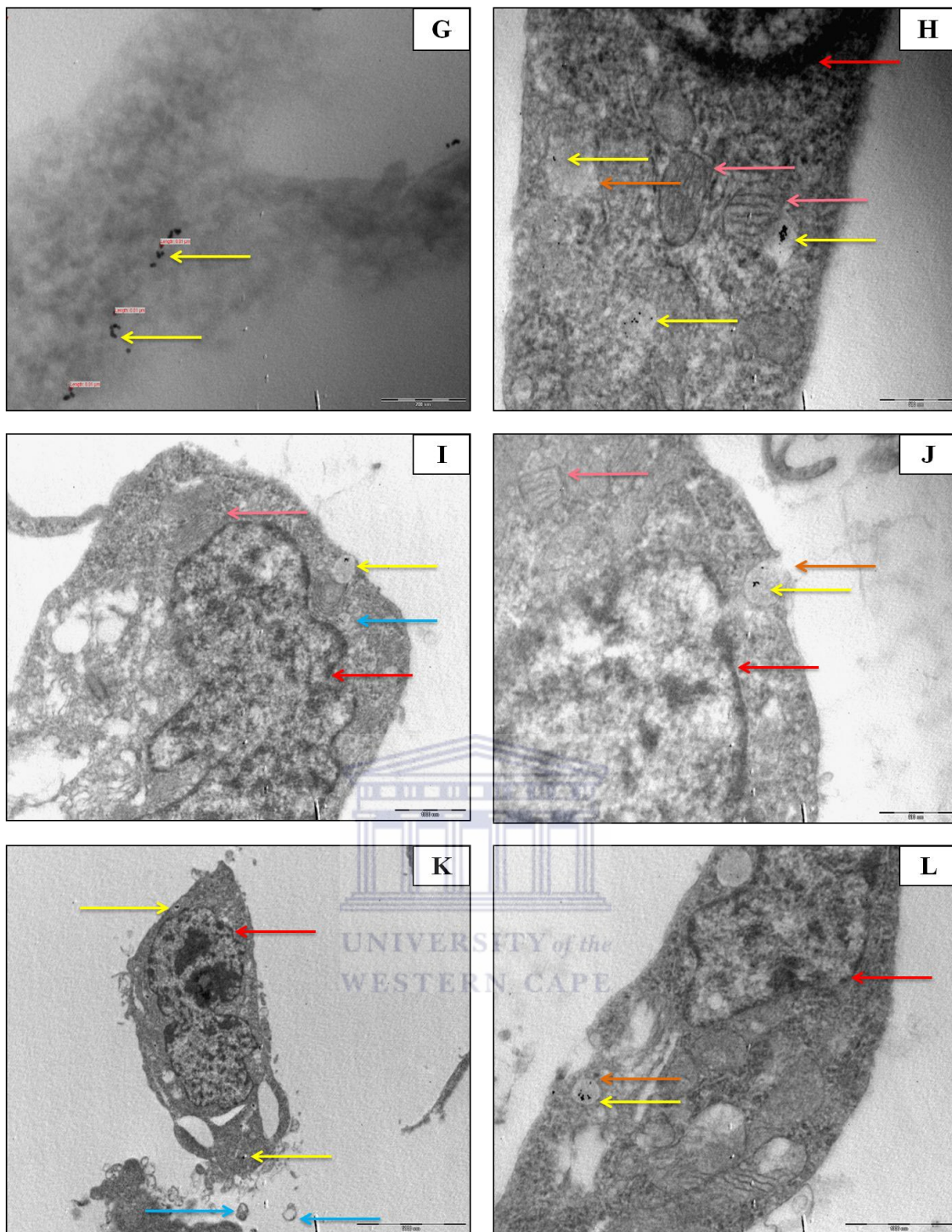


Figure 3.3: TEM micrographs of MCF-7 cells (A–F) and MCF-10A cells (G–L) tested with 50 µg/ml of 10 nm AuNPs. A large number of vesicles transporting AuNPs were observed in the MCF-7 cells. After the 4 hour incubation period, some AuNPs were observed in the vicinity of the nucleus. Red arrows indicate the nuclear membrane of the cell, blue arrows indicate possible autophagosomes or transport vesicles, yellow arrows represents the 10 nm AuNPs, pink arrows shows swollen mitochondria and the green arrows indicate possible lysosomal bodies. The swollen mitochondria could possibly be due to AuNP induced cytotoxic stress. AuNPs are taken up by endocytosis which is clearly indicated by the orange arrows (J), (E) and (F), which indicates the distance from the AuNPs to the nuclear membrane; 0.12 µm, 0.15 µm and 0.49 µm, respectively. The TEM measurement of the AuNPs via SIS confirmed that it is 10 nm in diameter (G). AuNPs were observed in the nucleus (A and B), within the cells and near the nuclear membranes of the cells.

3.2 DNA double-strand breaks

The γ -H2AX foci assay has been shown to be a reliable and sensitive indicator of radiation-induced DNA DSBs and has potential as a biodosimetry tool from hours to approximately 3 days post exposure. Radiation and AuNPs-induced DNA DSBs were assessed by automated microscopic scoring of γ -H2AX foci (Fig. 3.4), after low dose X-ray radiation exposure. The number of foci per cell increased for cells treated with AuNPs and X-ray and p(66)/Be neutron irradiations, as compared to the control (Fig. 3.5). The combined treatment (AuNPs and IR) obtained higher endogenous foci in lymphocytes, in comparison to lymphocytes that were only treated with AuNPs alone (Fig. 3.5)

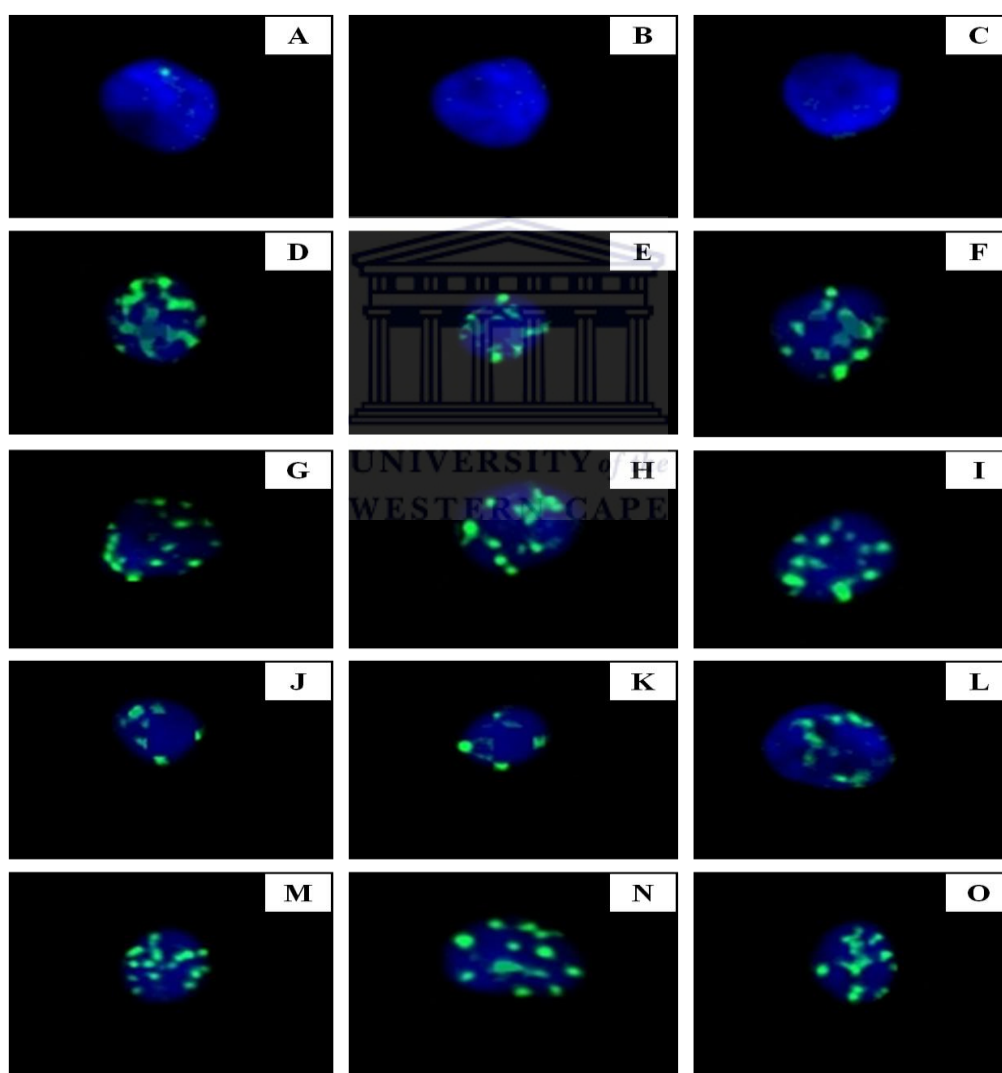


Figure 3.4: Visualisation of γ -H2AX foci. Examples of isolated human lymphocytes after the γ -H2AX foci assay, wherein (A–C) illustrates non-radiated control samples, (D–F) non-radiated lymphocytes incubated with 5 nm AuNPs, (G–I) lymphocytes irradiated with 5 nm AuNPs, (J–L) non-radiated lymphocytes incubated with 10 nm AuNPs and (M–O) lymphocytes irradiated with 10 nm AuNPs. The blue area represents the isolated

human lymphocyte nuclei and the green 'dots' show the foci, which represent the amount of DNA DSBs in the cell. All samples were treated with either 50 µg/ml of AuNPs or with AuNPs and 1 Gy X-rays.

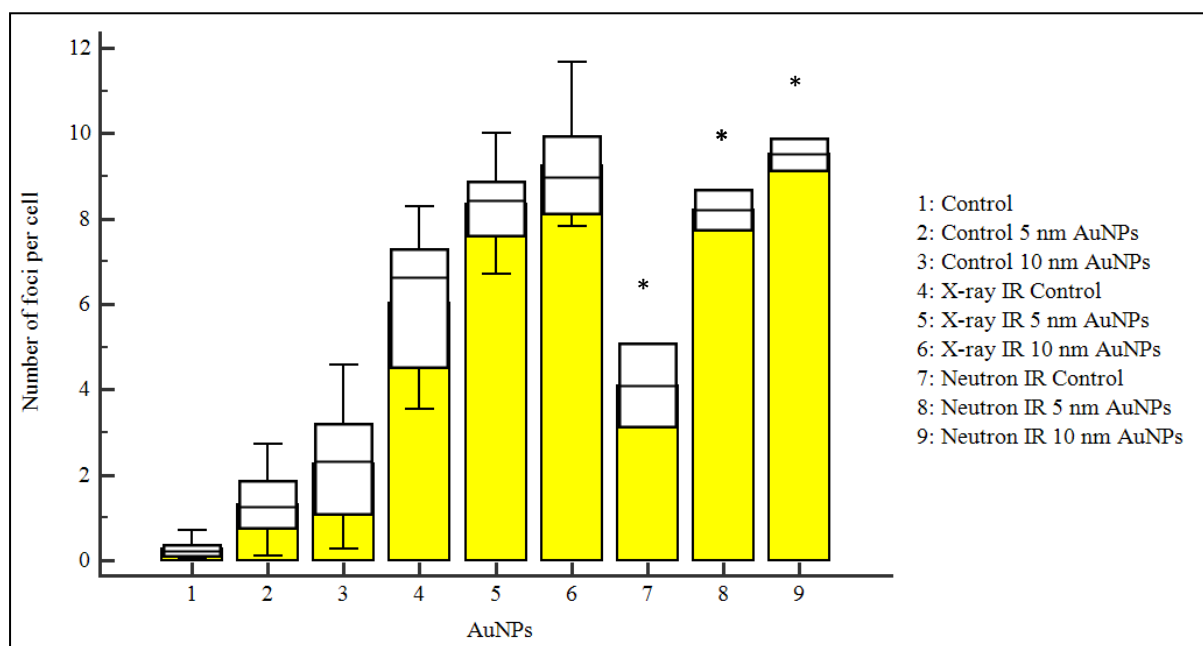


Figure 3.5: Box-and-Whisker plot representing γ -H2AX foci in isolated lymphocytes. Box-and-Whisker plots represents the quantification of effects of isolated human lymphocytes incubated with culture media containing 50 µg/ml of AuNPs for 4 hours followed by 1 Gy X-rays or 1 Gy p(66)/Be neutron radiation, respectively. Significant increases ($p < 0.000001$) in foci are observed in the overall cell count compared to the control. * represents only two data points obtained for the p(66)/Be neutron radiation experiment (Addendum: Table 5.3).

UNIVERSITY of the
WESTERN CAPE

3.3 Cytogenetic damage

Fig. 3.6–3.17 show fluorescent images of MNi with binucleated cells (BNCs) in different cell lines after exposure to different concentrations of AuNPs and either 2 or 4 Gy X-rays, as well as 1 or 2 Gy p(66)/Be neutrons. Quantification of cellular kinetics after treatment and MNi induction in these experiments are displayed in Fig 3.18–3.29.

3.3.1 Visualisation of MNi with binucleated cells (BNCs)

3.3.1.1 Cells incubated for 4 hours with 50 µg/ml of AuNPs and 2 Gy X-ray radiation

Fig. 3.6–3.9 shows acridine orange (AO) stained BNCs of CHO-K1, BEnd5, MCF-7 and MCF-10A cells exposed to 2 Gy X-rays. Each figure shows: (A) non-radiated control, (B) irradiated control, (C) non-radiated cells with 50 µg/ml of 5 nm AuNPs, (D) cells with 50

$\mu\text{g/ml}$ irradiated 5 nm AuNPs, (E) non-radiated cells with 50 $\mu\text{g/ml}$ of 10 nm AuNPs and (F) cells with 50 $\mu\text{g/ml}$ irradiated 10 nm AuNPs. All cell types (malignant and non-malignant) display a similar morphology once they have undergone the CBMN assay.

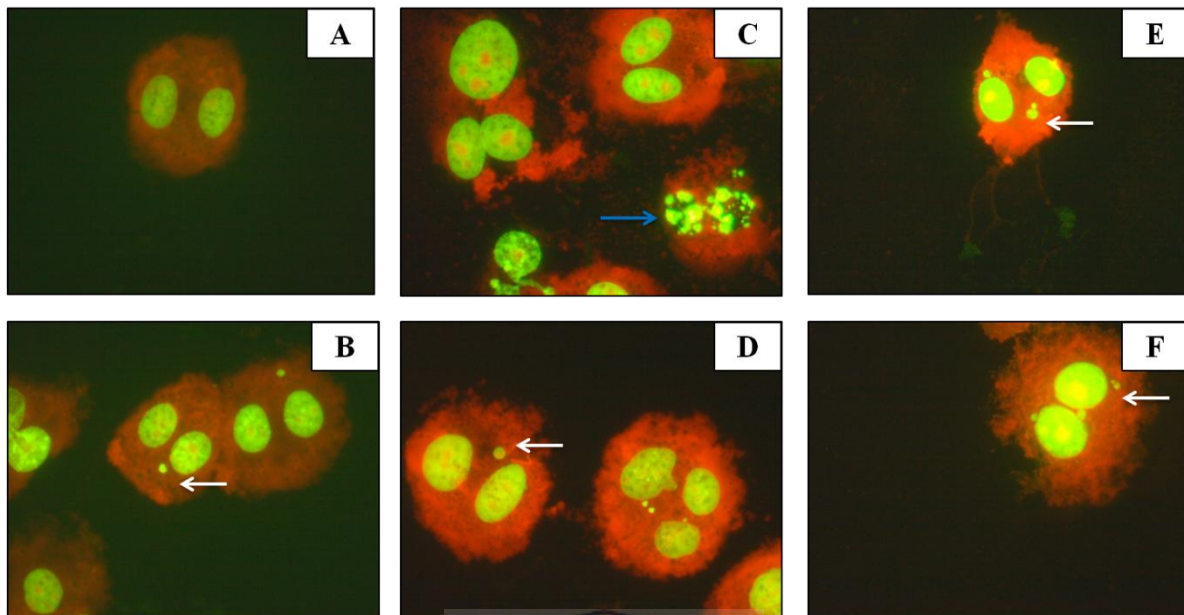


Figure 3.6: CHO-K1 cells after CBMN assay, wherein (A) illustrates a BNC, (B) two BNC, each with one micronuclei (MNI), (C) a characteristic apoptotic cell indicated via a blue arrow, (D) a BNC with one MNI, (E) a BNC with three MNI and (F) a BNC with four MNI. White arrows indicate MNI within BNCs.

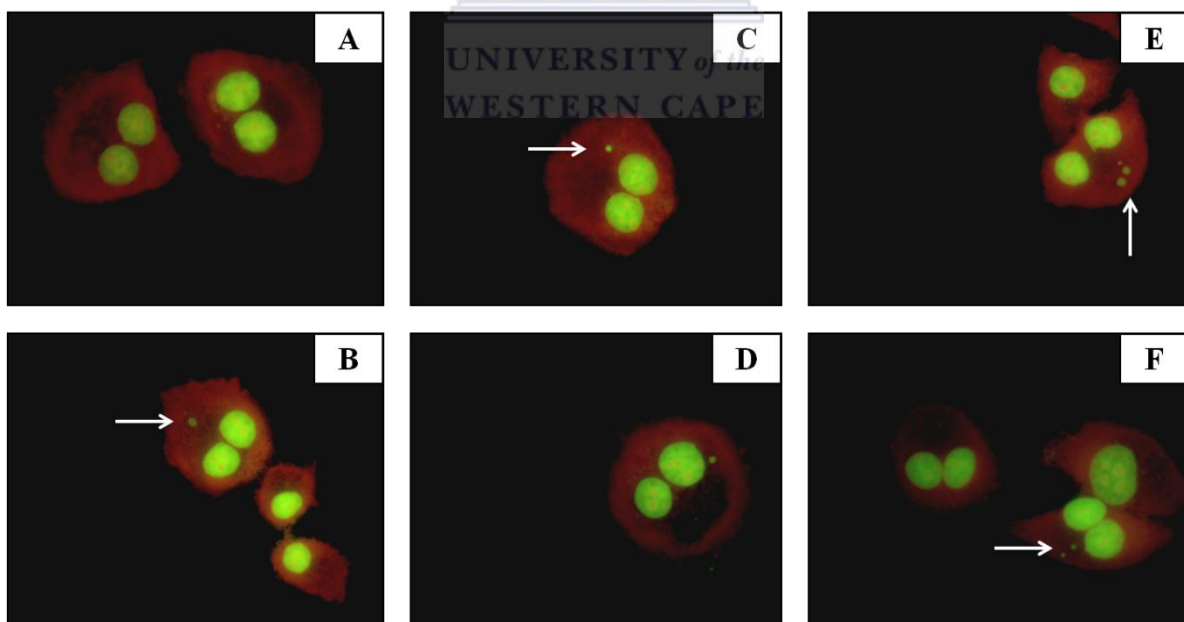


Figure 3.7: BEnd5 cells after CBMN assay, wherein (A) illustrates a two BNCs, (B) two mononucleated cells, and a BNC with one MNI, (C) and (D) a BNC with one MNI, (E) a mononucleated cell, and a BNC with three MNI and (F) two BNC, one with two MNI. White arrows indicate MNI within BNCs.

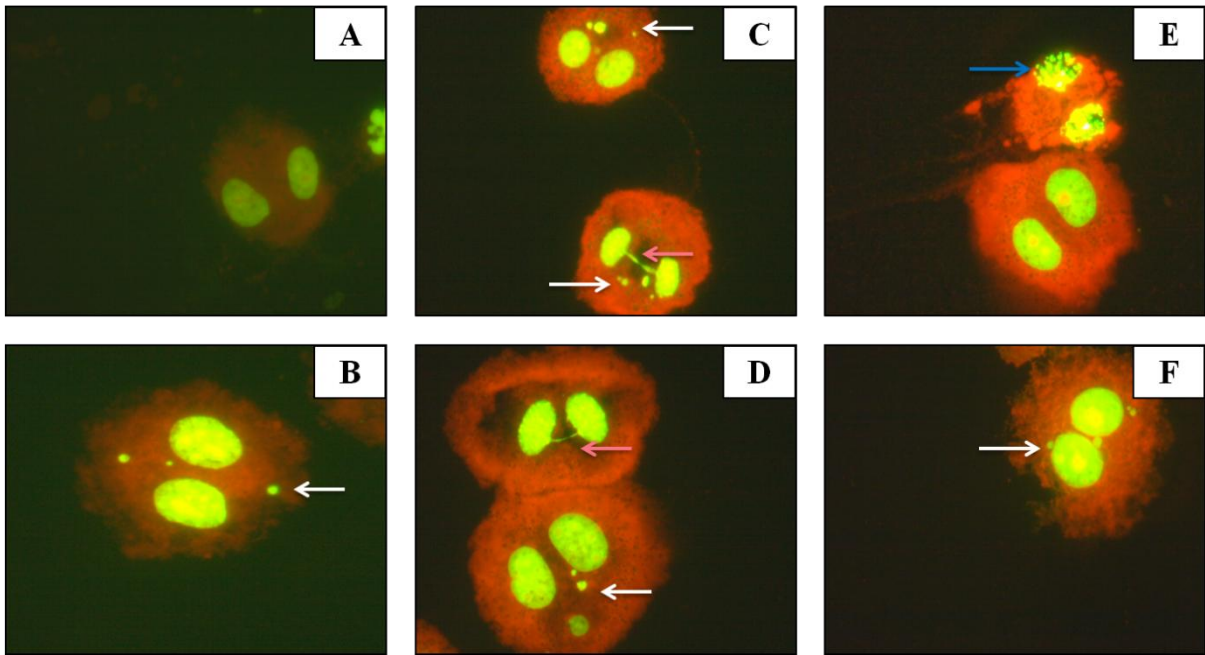


Figure 3.8: MCF-7 cells after CBMN assay, wherein (A) illustrates a BNC, (B) a BNC with three MNi, (C) two BNC with four and five MNi, respectively, (D) a BNC with an anaphase bridge between the cells, (E) a BNC and a possible apoptotic cell and (F) a BNC with multiple MNi. White arrows indicate MNi within BNCs, blue arrow indicates a characteristic apoptotic cell and pink arrows indicate an anaphase bridge.

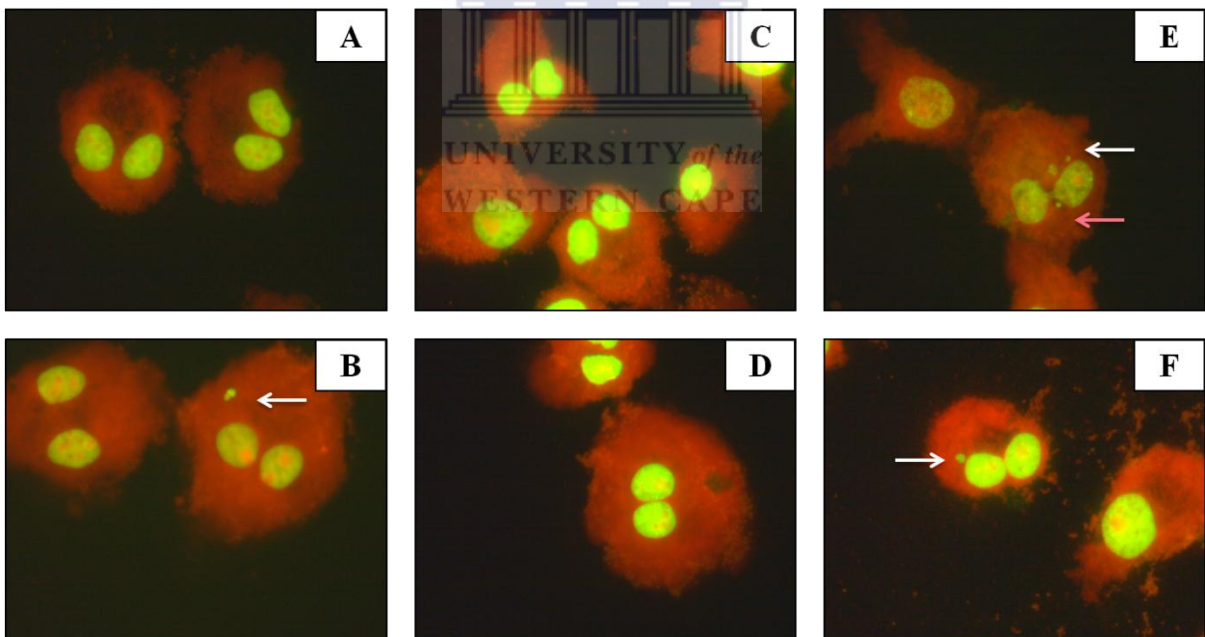


Figure 3.9: MCF-10A cells after CBMN assay, wherein (A) illustrates two BNCs, (B) a BNC with two MNi, (C) two BNCs, (D) a BNC, (E) a mononucleated cell, and a BNC with three MNi and (F) a BNC with one MNi. White arrows indicate MNi within BNCs and the pink arrow indicate an anaphase bridge.

Based on results showed in Fig. 3.18–3.22 an interaction between the AuNPs and 6 MV 2 Gy X-rays was only noted in two cell lines, namely CHO-K1 and MCF-7. Only CHO-K1 and MCF-7 cells lines were used for further investigation in the CBMN assay, since the interaction indices were greater than Unity ($Unity = 1$) (Fig. 3.18 & 3.20).

3.3.1.2 Cells incubated for 4 hours with 50 µg/ml of AuNPs and 4 Gy X-ray radiation

Fig. 3.10 and 3.11 shows AO stained BNCs of CHO-K1 and MCF-7 cells after an increased dose of radiation, namely 4 Gy. (A) non-radiated control, (B) irradiated control, (C) non-radiated cells with 50 µg/ml of 5 nm AuNPs, (D) cells with 50 µg/ml irradiated 5 nm AuNPs, (E) non-radiated cells with 50 µg/ml of 10 nm AuNPs and (F) cells with 50 µg/ml irradiated 10 nm AuNPs. No change in the morphology of both the CHO-K1 and MCF-7 cells could be observed after the CBMN assay.

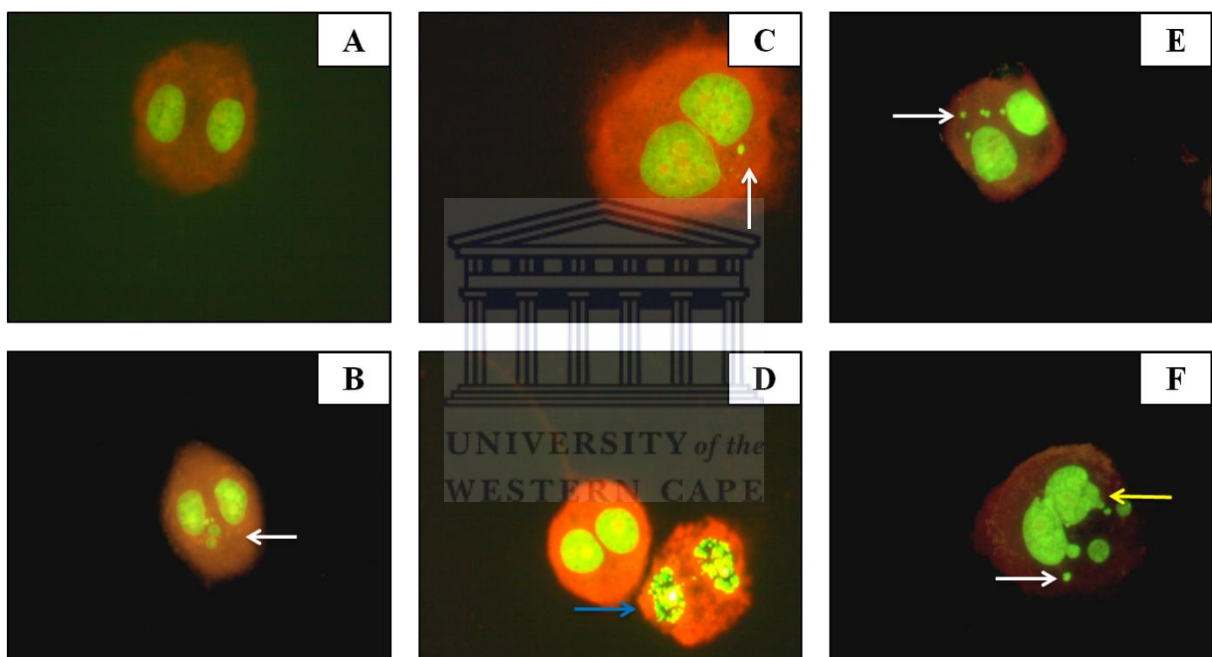


Figure 3.10: CHO-K1 cells after CBMN assay, wherein (A) illustrates a BNC, (B) a BNC with multiple MNi, (C) a BNC with two MNi, (D) a BNC, and (E) and (F) a BNC with multiple MNi. White arrows indicate MNi within BNCs, the blue arrow illustrates a characteristic apoptotic cell and yellow arrow indicates cell blebbing.

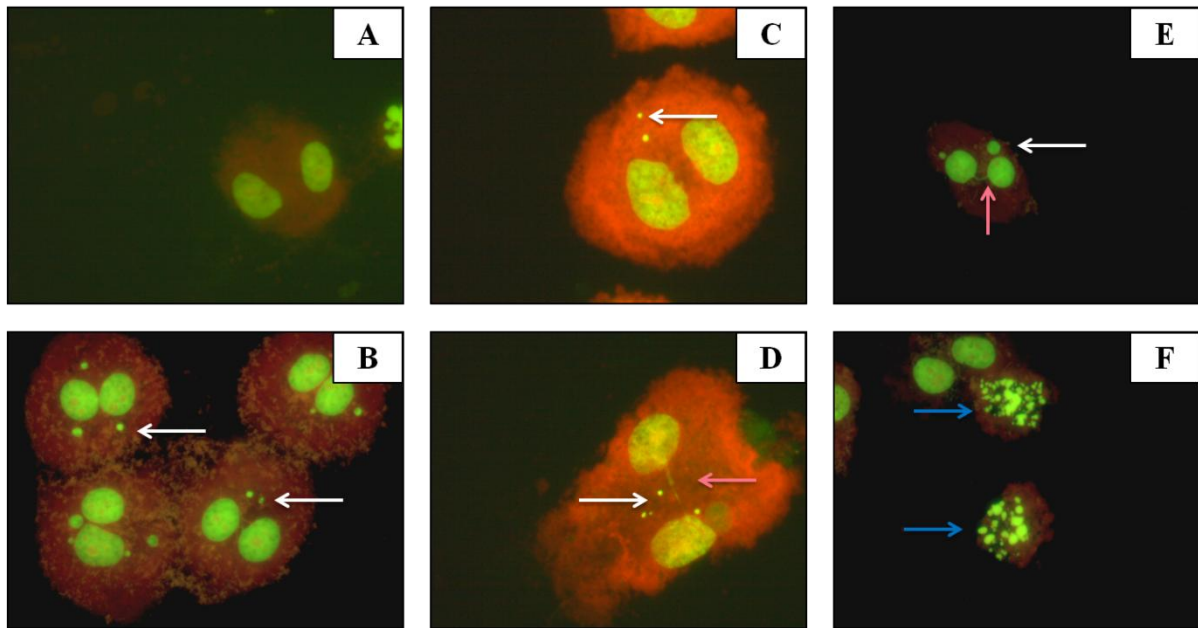


Figure 3.11: MCF-7 cells after CBMN assay, wherein (A) illustrates a BNC, (B) four BNCs with multiple MNi, (C) a BNC with two MNi, (D) a BNC with four MNi, (E) a BNC with two MNi, and (F) two distinctive apoptotic cells. White arrows indicate MNi within BNCs, the blue arrow illustrates a distinctive apoptotic cell and pink arrow indicates an anaphase bridge.

Considering all the cell types (Fig. 3.6 – 3.11), a low radiation dose yielded less MNi and a high radiation dose (4 Gy) yielded more MNi. A decrease in the interaction indices between AuNPs and 4 Gy X-rays is observed in CHO-K1 and MCF-7 cells (Fig 3.22 & 3.23). Based on the results from figures 3.19 and 3.21, the interaction indices between the AuNPs and 2 Gy X-rays in BEnd5 (0.92–1.06) and MCF-10A (0.87–0.97) is slightly higher, in comparison to the cells exposed to higher dose of radiation (4 Gy) (i.e. 0.74–1.04). Thus, the higher the radiation dose (e.g. 4 Gy), the smaller interaction indices between AuNPs and radiation.

3.3.1.3 Cells incubated for 4 hours with 2.5 µg/ml of AuNPs and 2 Gy X-ray radiation

Fig. 3.12 and 3.13 shows AO stained BNCs of CHO-K1 and MCF-7 cells exposed to a low concentration of AuNPs. Each figure shows: (A) non-irradiated control, (B) irradiated control, (C) non-irradiated cells with 2.5 µg/ml of 5 nm AuNPs, (D) cells with 2.5 µg/ml irradiated 5 nm AuNPs, (E) non-irradiated cells with 2.5 µg/ml of 10 nm AuNPs and (F) cells with 2.5 µg/ml irradiated 10 nm AuNPs. Both cell lines (non-malignant and malignant) display a similar morphology

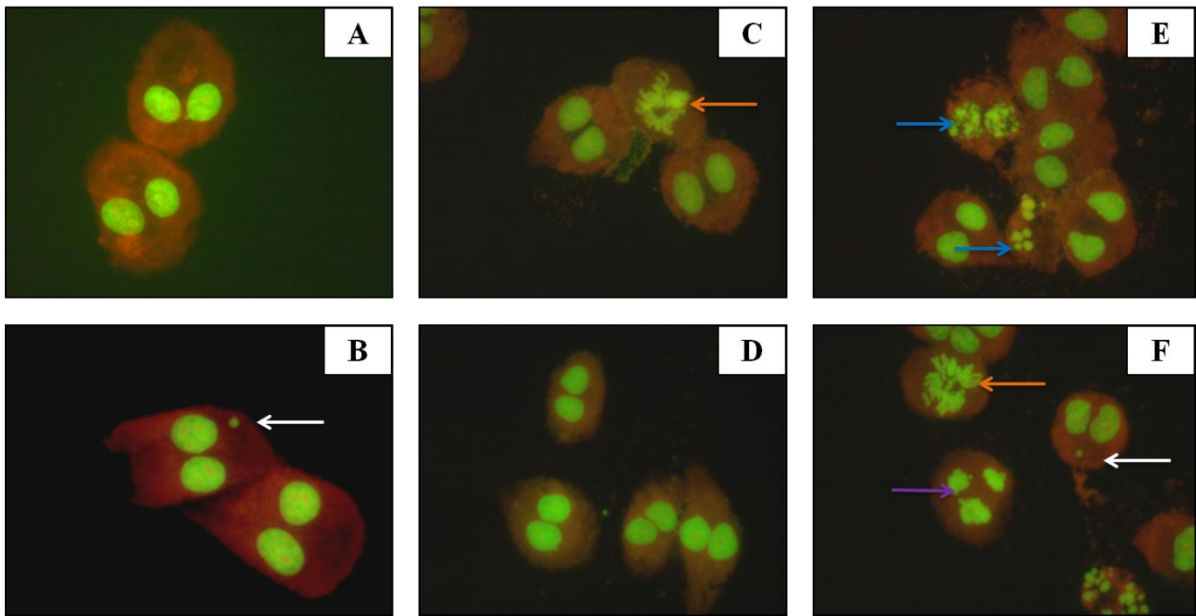


Figure 3.12: CHO-K1 cells after CBMN assay, wherein (A) illustrates two BNCs, (B) two BNCs; one with one MNi, (C) two BNC, and a cell in prometaphase, (D) and (E) four BNC, and (F) a BNC with one MNi, and a cell in early anaphase. White arrows indicate MNi within BNCs, the blue arrows indicate distinctive apoptotic cells, orange arrows indicate metaphases, and the purple arrow shows that the cells are pyktonic.

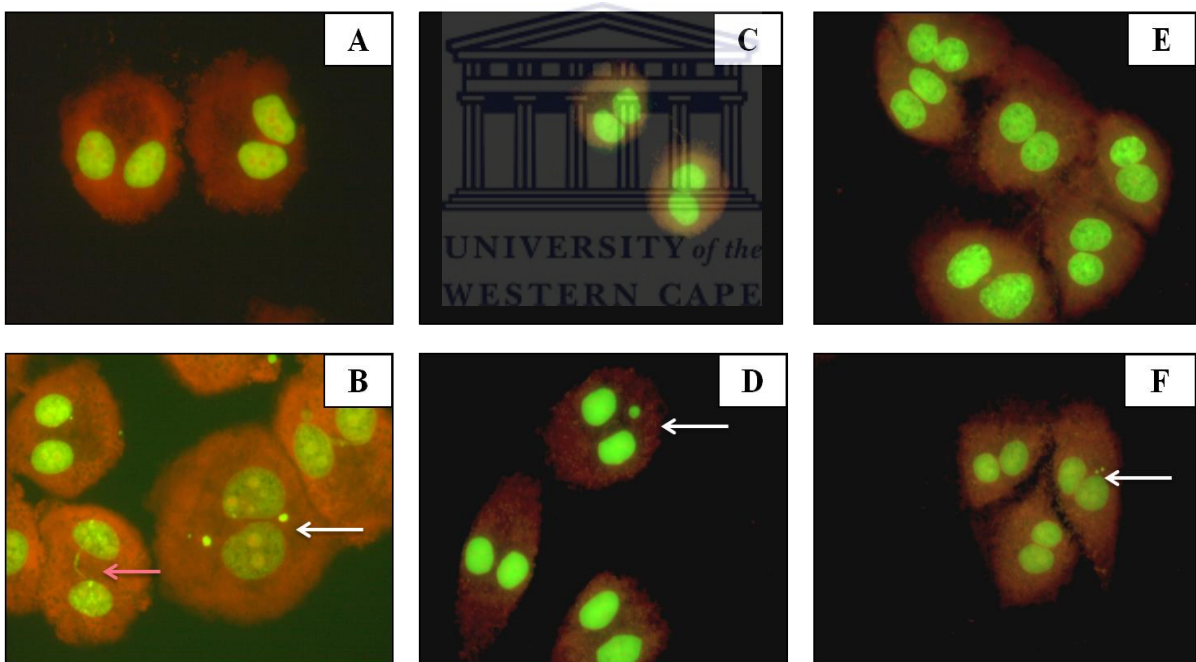


Figure 3.13: MCF-7 cells after CBMN assay, wherein (A) illustrates two BNCs, (B) a BNC with two MNi, (C) two BNCs, (D) two BNCs; one with one MNi, (E) six BNCs, (F) three BNCs; one with two MNi. White arrows indicate MNi within BNCs and the pink arrow points to an anaphase bridge.

The lower concentration (2.5 $\mu\text{g/ml}$) of AuNPs yielded less MNi in both CHO-K1 and MCF-7 BNCs, signifying a smaller amount of damage to the cells (Fig 3.24 B & 3.25 B). The non-irradiated or irradiated AuNPs (2.5 $\mu\text{g/ml}$) affected 20–30% of the CHO-K1 cellular kinetics (Fig. 3.24 A), whereas the 50 $\mu\text{g/ml}$ of AuNPs affected 60–70% (Fig. 3.18).

3.3.1.4 Cells incubated for 4 hours with 50 µg/ml of AuNPs and 1 Gy p(66)/Be neutron radiation

Fig. 3.14 and 3.15 shows AO stained BNCs of CHO-K1 and MCF-7 cells. (A) non-irradiated control, (B) irradiated control, (C) non-irradiated cells with 50 µg/ml of 5 nm AuNPs, (D) cells with 50 µg/ml irradiated 5 nm AuNPs, (E) non-irradiated cells with 50 µg/ml of 10 nm AuNPs and (F) cells with 50 µg/ml irradiated 10 nm AuNPs. Both CHO-K1 and MCF-7 cells (non-malignant and malignant) display a similar morphology once they have undergone the CBMN assay.

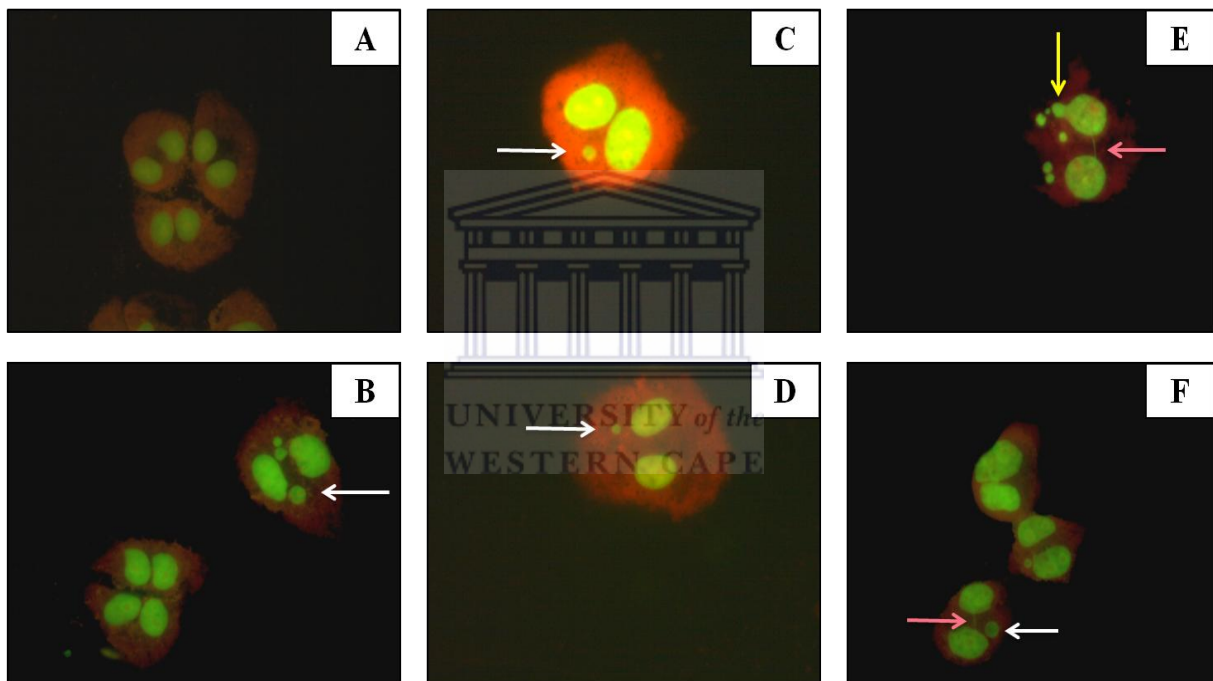


Figure 3.14 CHO-K1 cells after CBMN assay, wherein (A) illustrates three BNCs, (B) three BNCs; one with three MNi, (C) and (D) a BNC with one MNi, and (E) and (F) a BNC with an anaphase bridge between the cells. White arrows indicate MNi within BNCs, a yellow arrow shows blebbing of the cell and pink arrow shows a distinctive anaphase bridge.

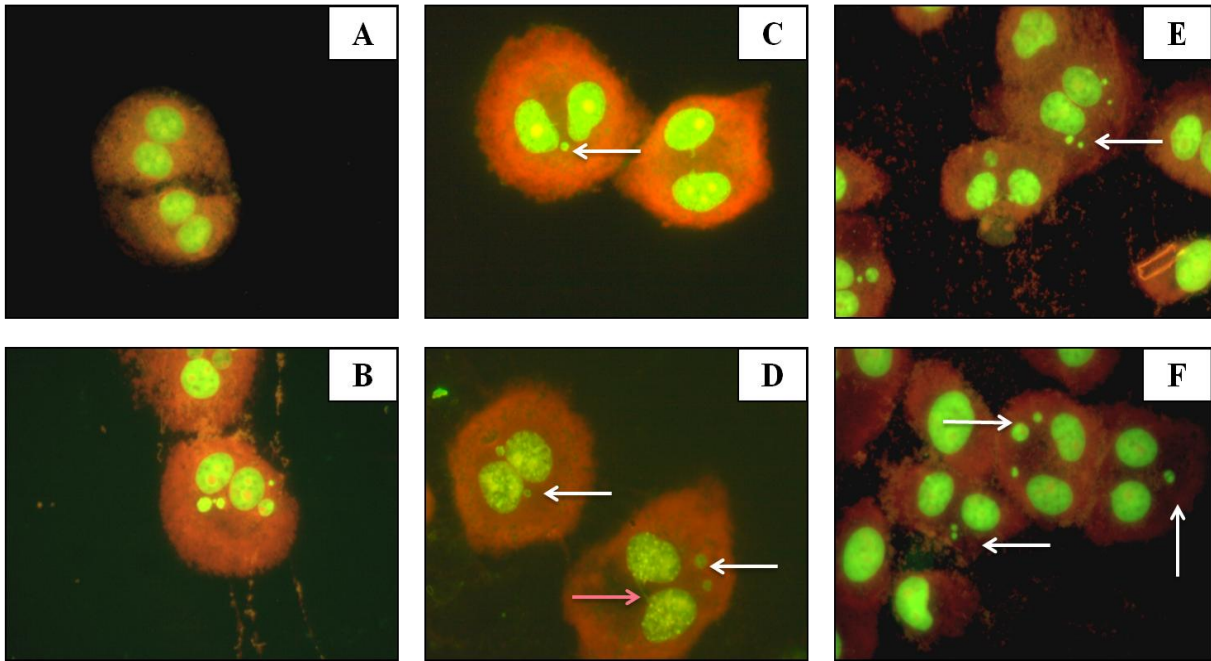


Figure 3.15: MCF-7 cells after CBMN assay, wherein (A) illustrates two BNCs, (B) a BNC with different sizes of MNi, (C) BNCs with one MNi and one without MNi, (D) two BNCs, both containing two MNi, (E) a BNC with four MNi, and (F) three BNCs with various sizes and quantities of MNi. White arrows indicate MNi within BNCs and the pink arrow shows a distinctive anaphase bridge.

The irradiated samples showed an increased number of MNi within the CHO-K1 and MCF-7 BNCs in comparison to the non-irradiated samples (Fig. 3.26 B & 3.27 B).

3.3.1.5 Cells incubated for 4 hours with 50 µg/ml of AuNPs and 2 Gy p(66)/Be neutron radiation

Fig. 3.16 and 3.17 shows AO stained BNCs of CHO-K1 and MCF-7 cells. Each figure shows the following micrographs: (A) non-radiated control, (B) irradiated control, (C) non-radiated cells with 50 µg/ml of 5 nm AuNPs, (D) cells with 50 µg/ml irradiated 5 nm AuNPs, (E) non-radiated cells with 50 µg/ml of 10 nm AuNPs and (F) cells with 50 µg/ml irradiated 10 nm AuNPs.

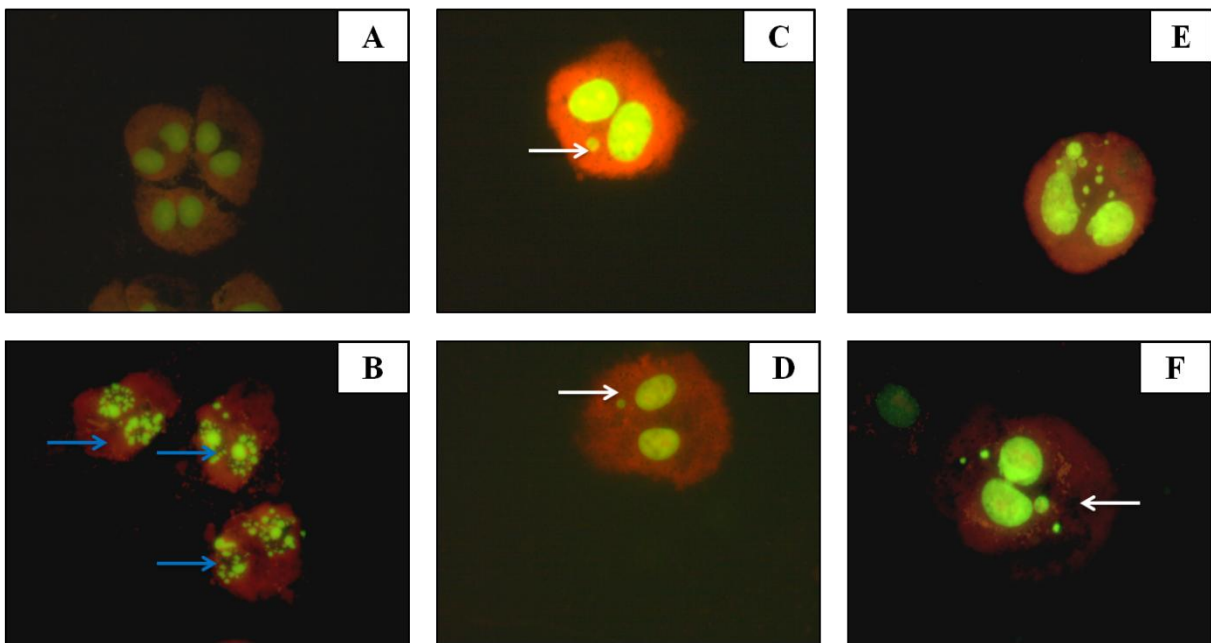


Figure 3.16: CHO-K1 cells after CBMN assay, wherein (A) illustrates three BNCs, (B) multiple apoptotic cells, (C) and (D) BNCs with one MNi, (E) a BNC with multiple MNi, and (F) a BNC with four MNi. White arrows indicate MNi within BNCs and blue arrows indicate possible apoptotic events.

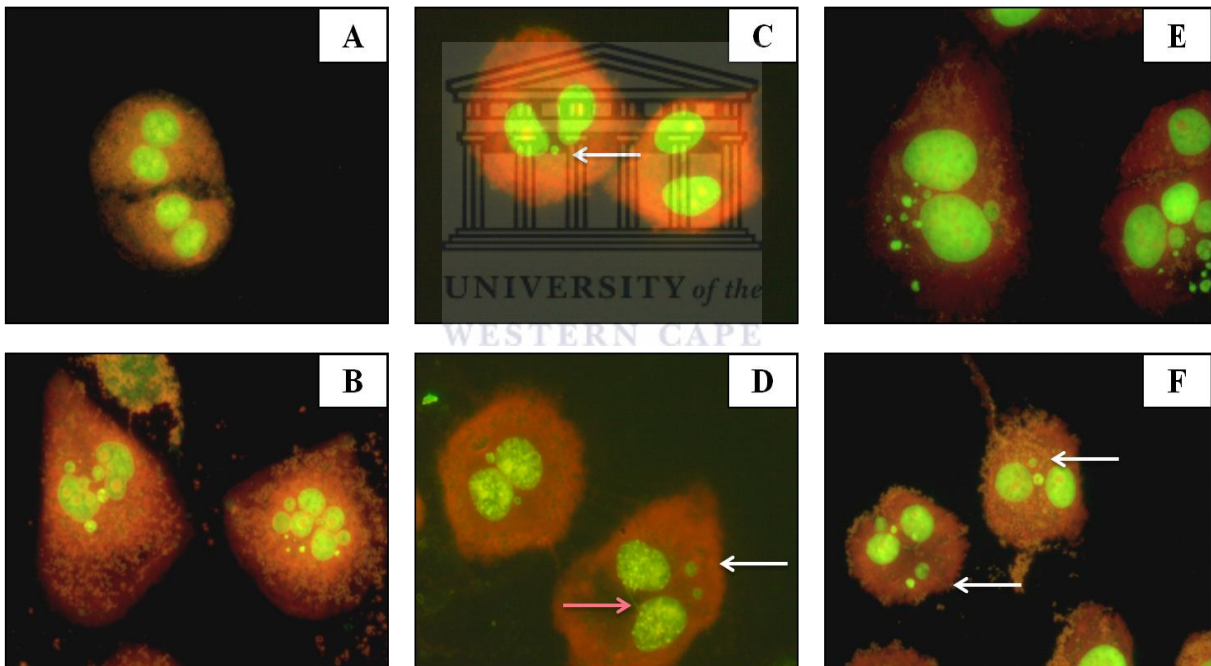


Figure 3.17: MCF-7 cells after CBMN assay, wherein (A) illustrates two BNCs, (B) a number of MNi with BNCs, (C) two BNCs; one cell containing one MNi, (D) two BNCs both having two MNi, (E) a number of MNi with BNC, and (F) two BNCs with two and four MNi, respectively. White arrows indicate MNi within BNCs and the pink arrow indicates an anaphase bridge.

Multiple cells showing characteristic apoptotic features were observed in CHO-K1 cells (Fig. 3.16 B) due to high-LET exposure. Based on the stained images of CHO-K1 and MCF-7 cells treated with non-irradiated or irradiated 10 nm AuNPs (Fig. 3.16 E, F & Fig. 3.17 E, F), resulted in more MNi, than cells treated with non-irradiated or irradiated 5 nm AuNPs (Fig. 3.16 C, D & Fig. 3.17 C, D).

3.3.2 Quantification of cellular kinetics and MNi

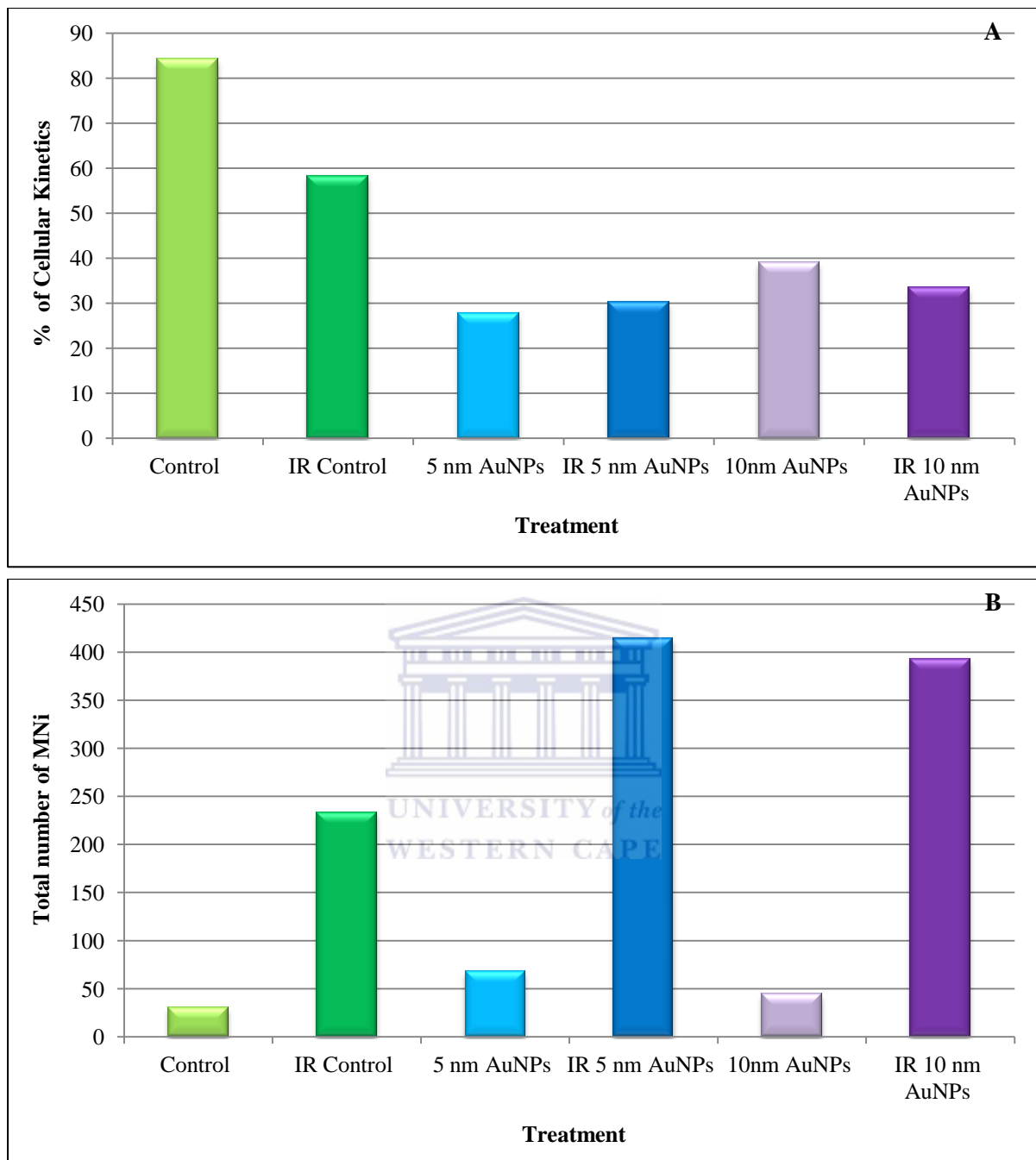


Figure 3.18: (A) Cellular kinetics of the CHO-K1 cells was determined by scoring 400 AO stained BNCs and expressed as a percentage (%). Cells treated with 50 $\mu\text{g/ml}$ AuNPs and/or irradiated with 2 Gy X-rays showed an overall decrease in cellular kinetics in comparison to the control. (B) Mean cumulative frequency of MNi present determined via the CBMN assay in CHO-K1 cells after 4 hour incubation with 50 $\mu\text{g/ml}$ AuNPs followed by 2 Gy X-ray radiation. Control cells treated with AuNPs showed a small number of MNi, whilst significant increase of MNi within cells treated with AuNPs and radiated with 2 Gy X-rays was apparent. The interaction indices for AuNPs and 6 MV X-rays in CHO-K1 cells are 1.6 to 1.7, thus $>$ Unity (Unity = 1).

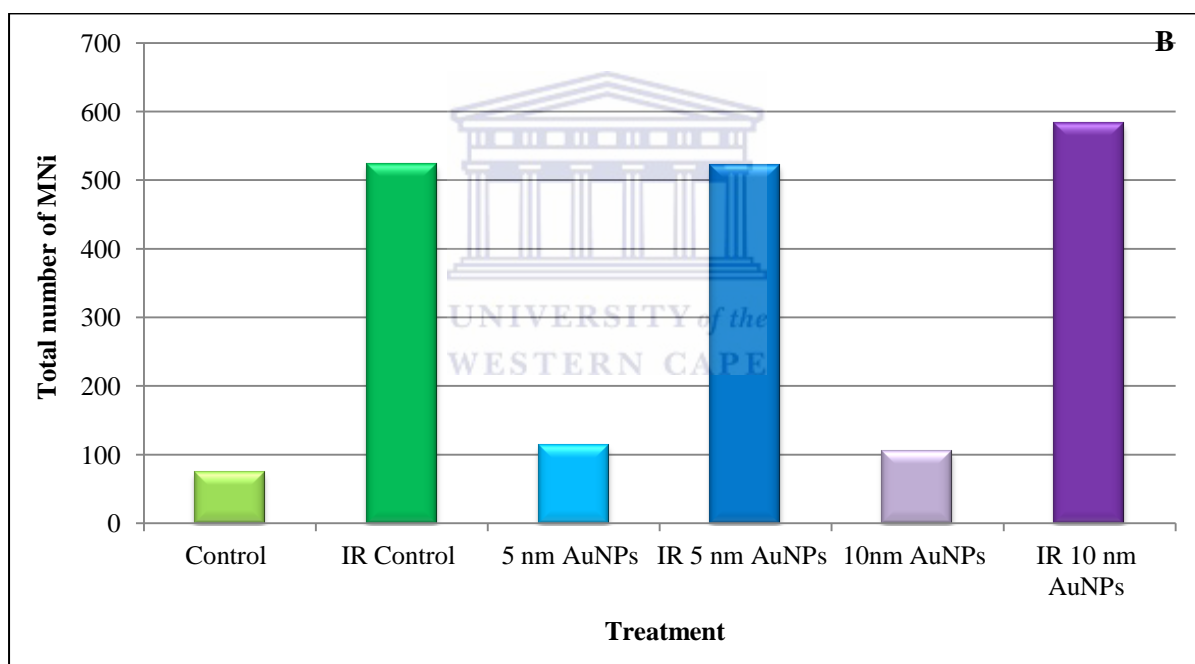
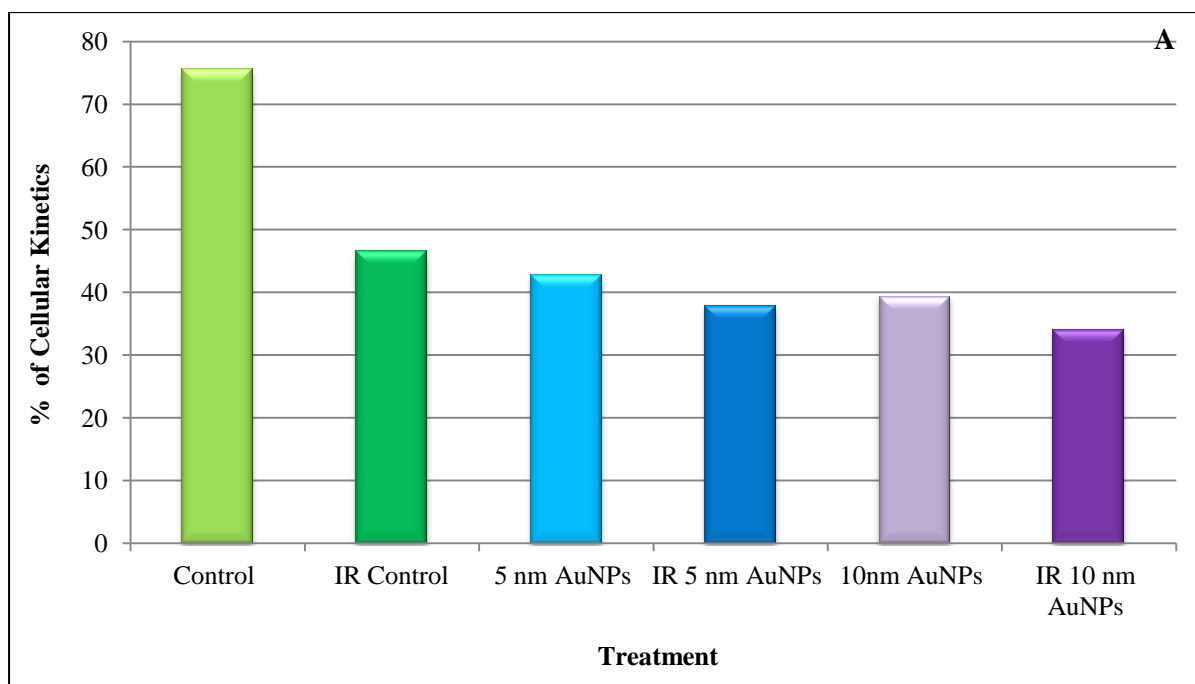


Figure 3.19: (A) Cellular kinetics of the BEnd5 cells was determined by scoring 400 AO stained BNCs and expressed as a percentage (%). Cells treated with 50 $\mu\text{g/ml}$ AuNPs and/or irradiated with 2 Gy X-rays showed an overall decrease in cellular kinetics in comparison to the control. (B) Mean cumulative frequency of MNi present determined via the CBMN assay in BEnd5 cells after 4 hour incubation with 50 $\mu\text{g/ml}$ AuNPs followed by 2 Gy X-ray radiation. Control cells treated with AuNPs showed a negligible number of MNi, whilst a noticeable increase of MNi within cells treated with AuNPs and radiated with 2 Gy X-rays was apparent. The interaction indices for AuNPs and 6 MV X-rays of 0.92 to 1.06 determined for BEnd5 cells was differed from Unity (Unity = 1).

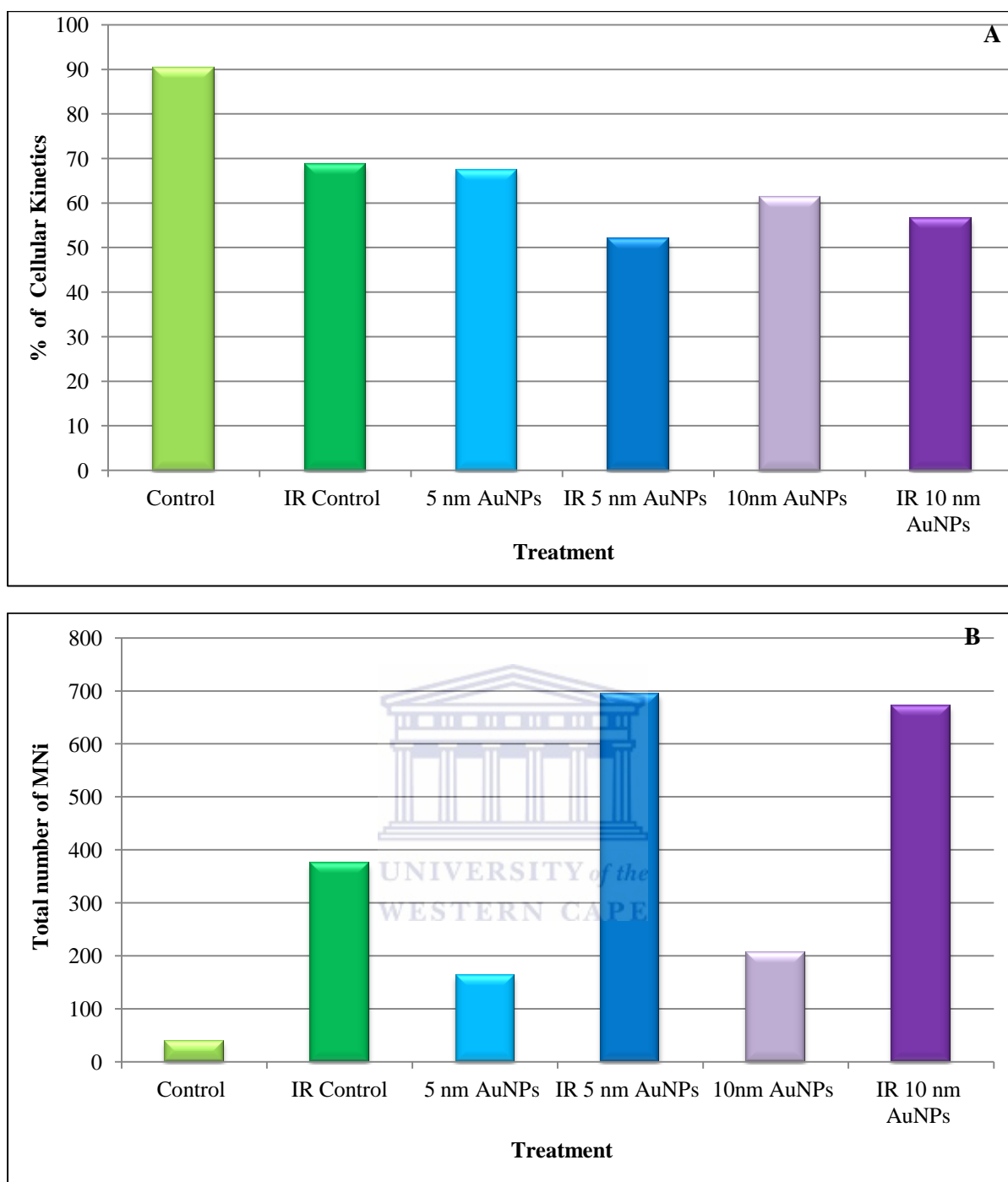


Figure 3.20: (A) Cellular kinetics of MCF-7 cells was determined by scoring 400 AO stained BNCs and expressed as a percentage (%). Cells treated with 50 $\mu\text{g/ml}$ AuNPs and/or irradiated with 2 Gy X-rays showed an overall decrease in cellular kinetics in comparison to the control. (B) Mean cumulative frequency of MNi present determined via the CBMN assay in MCF-7 cells after 4 hour incubation with 50 $\mu\text{g/ml}$ AuNPs followed by 2 Gy X-ray radiation. Control cells treated with AuNPs displayed an insignificant number of MNi, whilst an outspoken increase of MNi within cells treated with AuNPs and radiated with 2 Gy X-rays was apparent. The interaction indices for AuNPs and 6 MV X-rays of 1.3 to 1.4 were determined for MCF-7 cells, which is > Unity (Unity = 1).

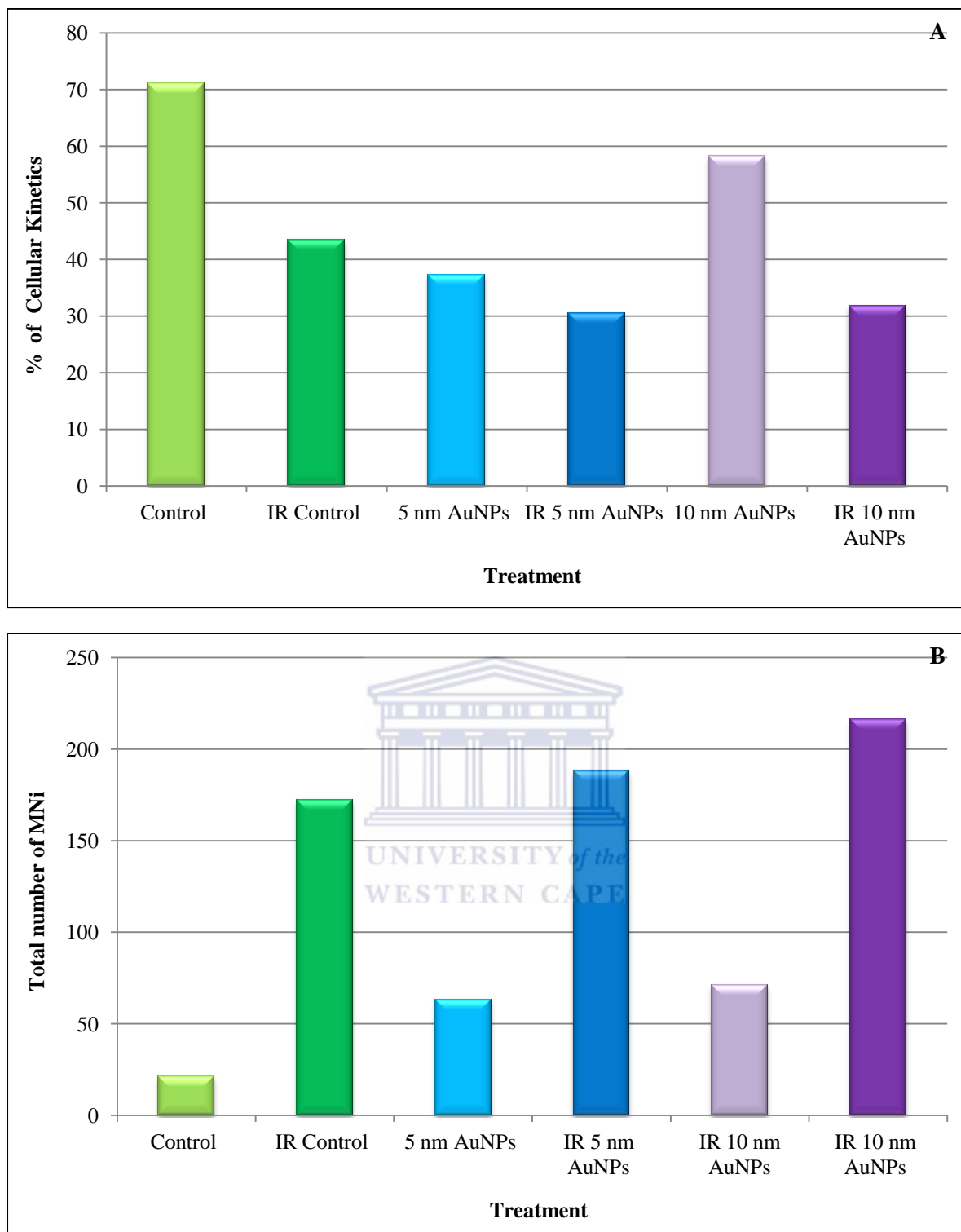
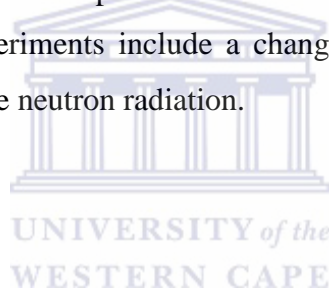


Figure 3.21: (A) Cellular kinetics of MCF-10A cells was determined by scoring 400 AO stained BNCs and expressed as a percentage (%). Cells treated with 50 $\mu\text{g/ml}$ AuNPs, excluding cells treated with 10 nm AuNPs and/or irradiated with 2 Gy X-rays showed an overall decrease in cellular kinetics in comparison to the control. (B) Mean cumulative frequency of MNi present determined via the CBMN assay in MCF-10A cells after 4 hour incubation with 50 $\mu\text{g/ml}$ AuNPs followed by 2 Gy X-ray radiation. Control cells treated with AuNPs showed an insignificant number of MNi in control, whilst a noticeable increase of MNi within cells treated with AuNPs and irradiated with 2 Gy X-rays was apparent. The interaction indices for AuNPs and 6 MV X-rays of 0.87 to 0.97 determined for MCF-10A cells, which is $<$ Unity (Unity = 1).

Cellular kinetics of abovementioned cells (Fig. 3.18 A, 3.19 A, 3.20 A & 3.21 A) decreased in the presence of 50 µg/ml AuNPs. The 5 nm AuNPs decreased the cellular kinetics of CHO-K1 cells by 57.5%, followed by the MCF-10A cells (33.75%), the BEnd5 cells (32.75%), and with the lowest effect (23%) on the MCF-7 cells. The 10 nm had the greater effect (46.25%) on CHO-K1 cells and a lesser effect on MCF-10A cells (12.75%). Overall, irradiated control and irradiated AuNPs yielded a great number of MNi in comparison with non-irradiated samples (Fig. 3.18 B, 3.19 B, 3.20 B & 3.21 B).

An interaction is determined, as follow, MNi numbers are higher when induced by a combination treatment of radiation and AuNPs compared to the additive sum of MNi numbers noted in samples exposed to AuNPs and radiation separately. Interaction indices can also be known as enhancement factor. A significant interaction between the scattered 6 MV 2 Gy X-rays and AuNPs was only seen in CHO-K1 (non-malignant) and MCF-7 cells (malignant). For this reason, further experiments on radiation damage were conducted in these cell lines only. These experiments include a change in AuNPs concentration, X-ray dose and the inclusion of p(66)/Be neutron radiation.



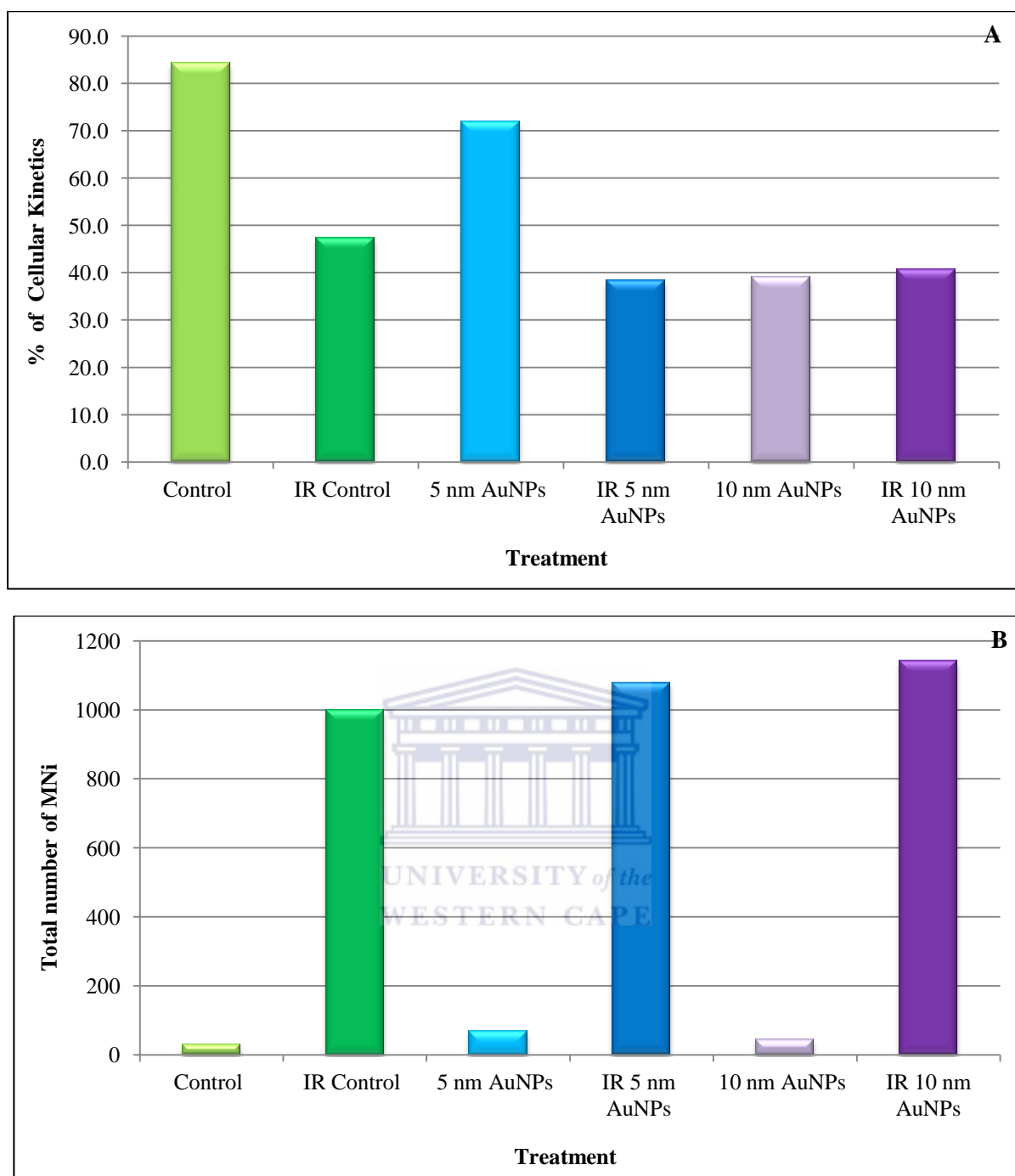


Figure 3.22: (A) Cellular kinetics of CHO-K1 cells was determined by scoring 400 AO stained BNCs and expressed as a percentage (%). Cells treated with 50 $\mu\text{g/ml}$ AuNPs and/or irradiated with 4 Gy X-rays showed an overall decrease in cellular kinetics in comparison to the control. (B) Mean cumulative frequency of MNi present determined via the CBMN assay in CHO-K1 cells after 4 hour incubation with 50 $\mu\text{g/ml}$ AuNPs followed by 4 Gy X-ray radiation. Control cells treated with AuNPs caused an insignificant number of MNi, whilst a clear increase of MNi within cells treated with AuNPs and radiated with 4 Gy X-rays was observed. The interaction indices for AuNPs and 6 MV 4 Gy X-rays of 1.04 to 1.13 have been determined for CHO-K1 cells is lower than the interaction indices after 2 Gy, in comparison to 2 Gy X-rays.

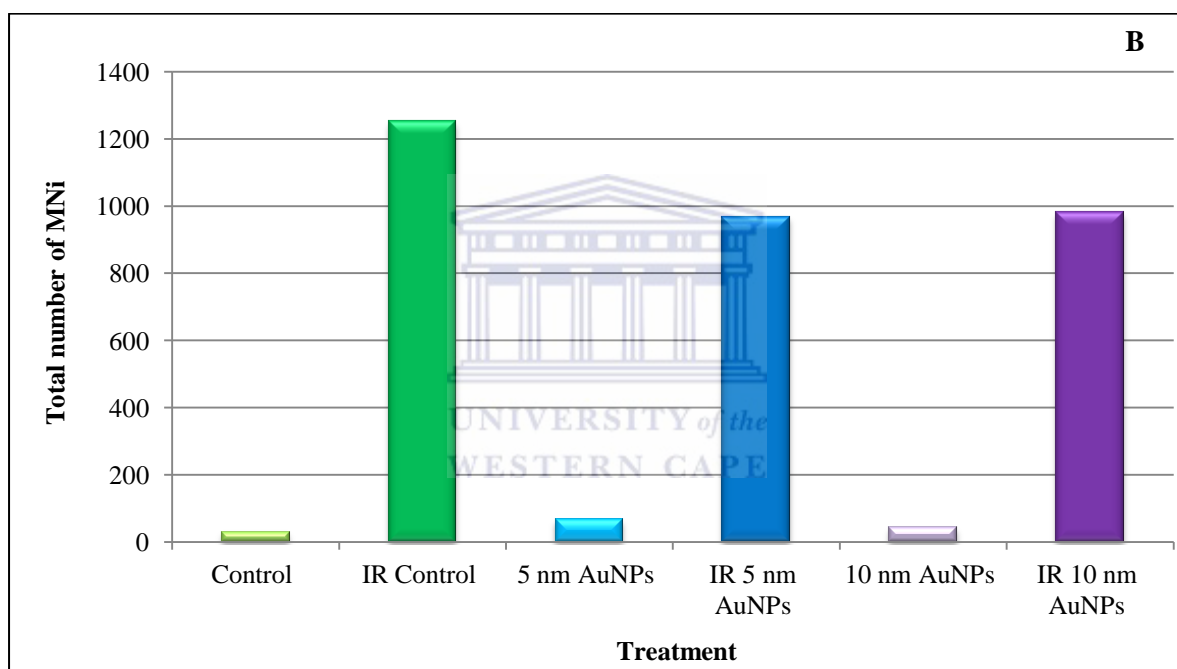
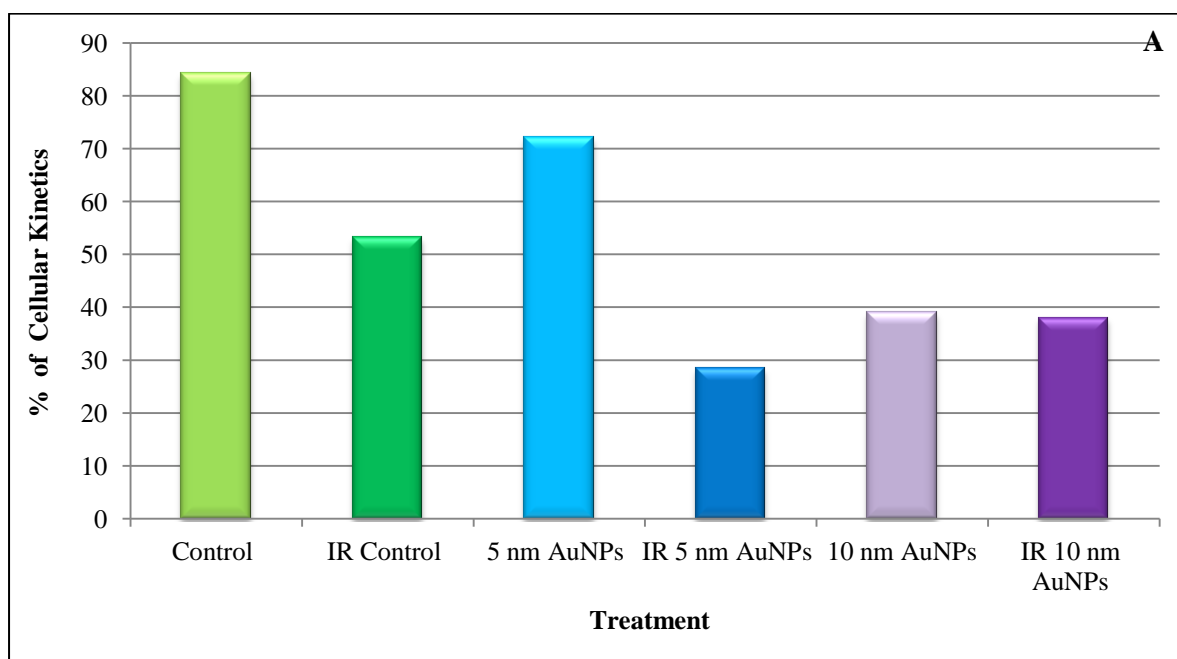


Figure 3.23: (A) Cellular kinetics of MCF-7 cells was determined by scoring 400 AO stained BNCs and expressed as a percentage (%). Cells treated with 50 $\mu\text{g/ml}$ AuNPs and/or irradiated with 4 Gy X-rays showed an overall decrease in cellular kinetics in comparison to the control. (B) Mean cumulative frequency of MNi present determined via the CBMN assay in MCF-7 cells after 4 hour incubation with 50 $\mu\text{g/ml}$ AuNPs followed by 4 Gy X-ray radiation. Control cells treated with AuNPs displayed a few caused MNi, whilst an observable increase of MNi within cells treated with AuNPs and radiated with 4 Gy X-rays was apparent. The interaction indices for AuNPs and 4 Gy X-rays of 0.74 to 0.77 is lower than the interaction indices after 2 Gy X-rays.

The 4 Gy dose of X-ray radiation had similar effects on the cellular kinetics of CHO-K1 and MCF-7 cells in comparison to the 2 Gy X-rays. Control cells treated with AuNPs displayed a few MNi, whilst an increase of MNi within BNCs incubated with irradiated AuNPs was apparent. However, the notable interaction between AuNPs and 2 Gy scattered X-ray

radiation in CHO-K1 and MCF-7 (Fig. 3.18 B & 3.20 B) did not exist in addition to a higher radiation dose of 4 Gy X-rays (Fig. 3.22 B & 3.23 B).

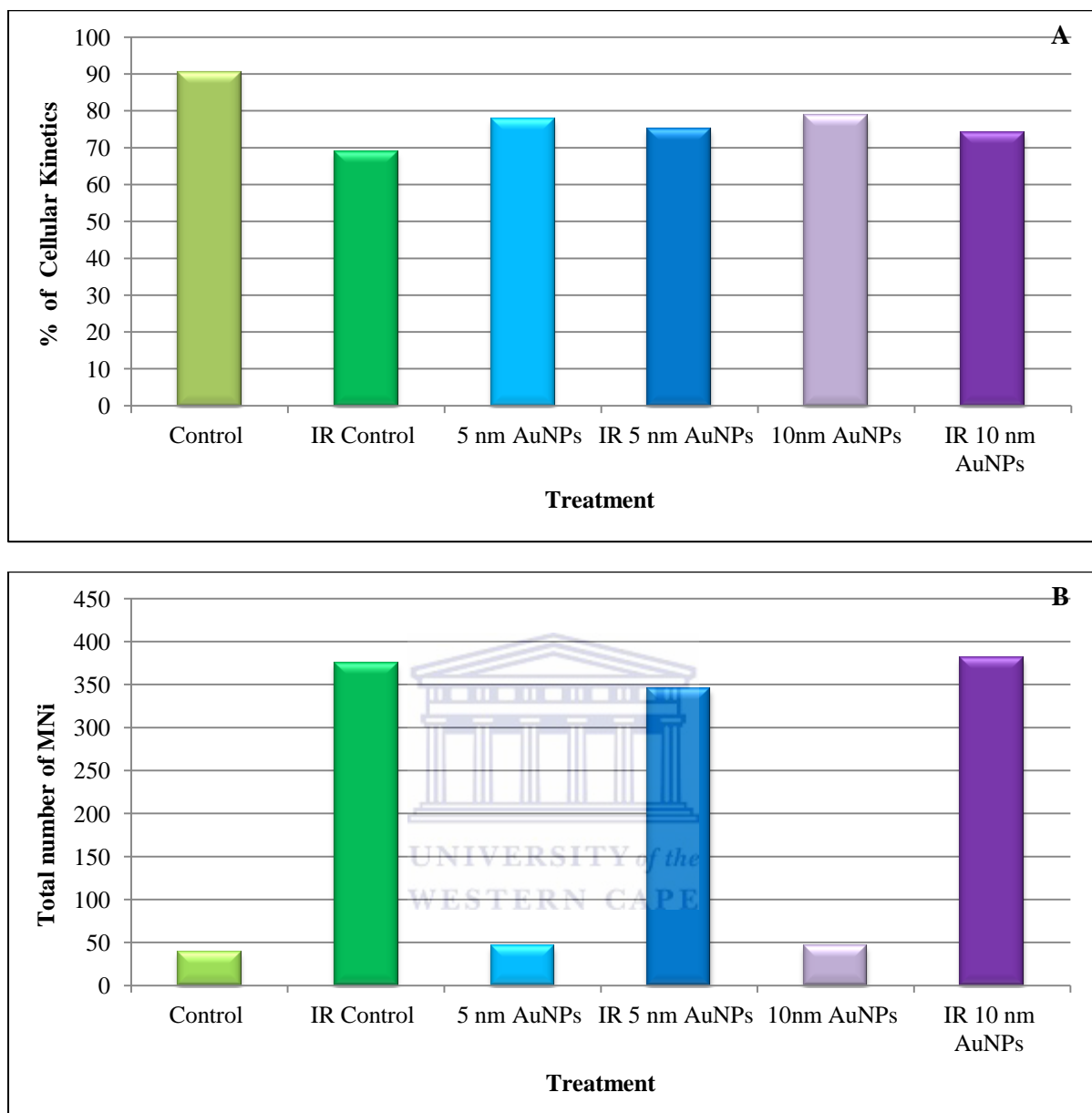


Figure 3.24: (A) Cellular kinetics of CHO-K1 cells was determined by scoring 400 AO stained BNCs and expressed as a percentage (%). Cells treated with 2.5 $\mu\text{g/ml}$ AuNPs and/or irradiated with 2 Gy X-rays showed no change in cellular kinetics in comparison to the control. (B) Mean cumulative frequency of MNi present determined via the CBMN assay in CHO-K1 cells after 4 hour incubation with 2.5 $\mu\text{g/ml}$ AuNPs followed by 2 Gy X-ray radiation. The radiated samples treated with AuNPs showed a number of MNi, but no difference between the control and the AuNP treated samples were observed. The interaction indices for AuNPs and 2 Gy X-rays of 0.89 to 1.00 is lower than the interaction indices after 50 $\mu\text{g/ml}$ AuNPs.

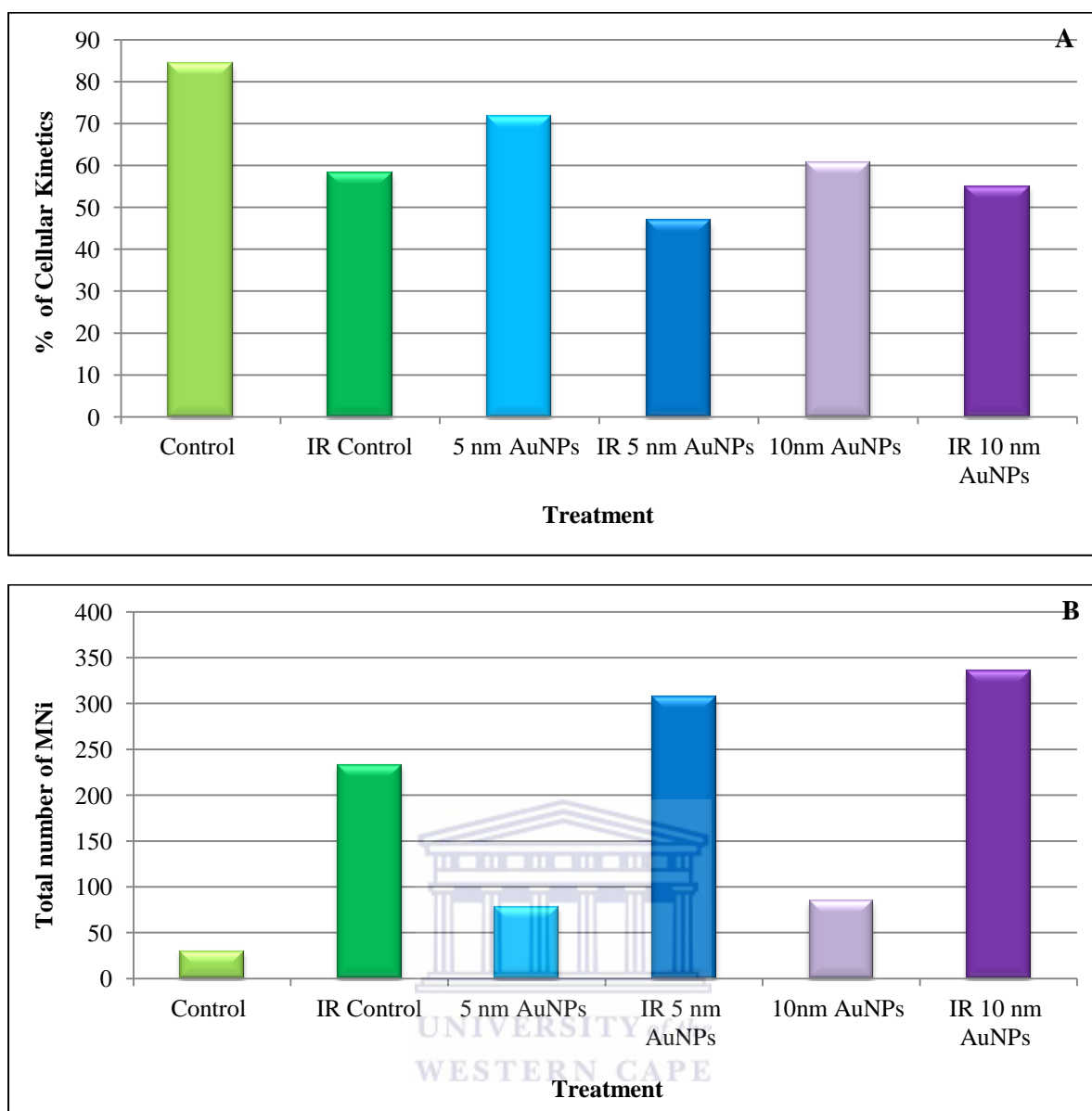


Figure 3.25: (A) Cellular kinetics of MCF-7 cells was determined by scoring 400 AO stained BNCs and expressed as a percentage (%). Cells treated with 2.5 $\mu\text{g/ml}$ AuNPs and/or irradiated with 2 Gy X-rays showed no change in cellular kinetics in comparison to the control. (B) Mean cumulative frequency of MNi present determined via the CBMN assay in MCF-7 cells after 4 hour incubation with 2.5 $\mu\text{g/ml}$ AuNPs followed by 2 Gy X-ray radiation. A visible increase of MNi within cells treated with AuNPs and radiated with 2 Gy X-rays was evident in comparison to the radiated control. The interaction indices for AuNPs and 2 Gy X-rays of 1.10 to 1.19 are lower than the interaction indices after 50 $\mu\text{g/ml}$ AuNPs.

A previous study conducted by Jain et al (2011) used a lower concentration of 12 μM of AuNPs and AuNPs radiosensitisation was observed in MDA-MB-231 cells (human breast cancer cell line) at 6 MV photon energies. The experiments by Jain et al. (2011) were carried out at 12 μM AuNP concentrations with 24 hour incubation. For this reason, lower concentration with longer exposure period could result in enhanced interaction between AuNPs and scattered 6 MV 2 Gy X-ray radiation. The irradiated 5 nm AuNPs (2.5 $\mu\text{g/ml}$) reduced the cellular kinetics of CHO-K1 was reduced by 16% (Fig. 3.24A), whereas the

cellular kinetics of MCF-7 was reduced between 30–38% (Fig. 3.25A). CHO-K1 and MCF-7 cells were treated with a lower concentration of AuNPs (2.5 µg/ml) followed by 2 Gy X-ray radiation to determine if the interaction between AuNPs and X-ray radiation would still exist. The interaction indices were less than Unity (Unity = 1), in comparison to the 50 µg/ml of AuNPs.

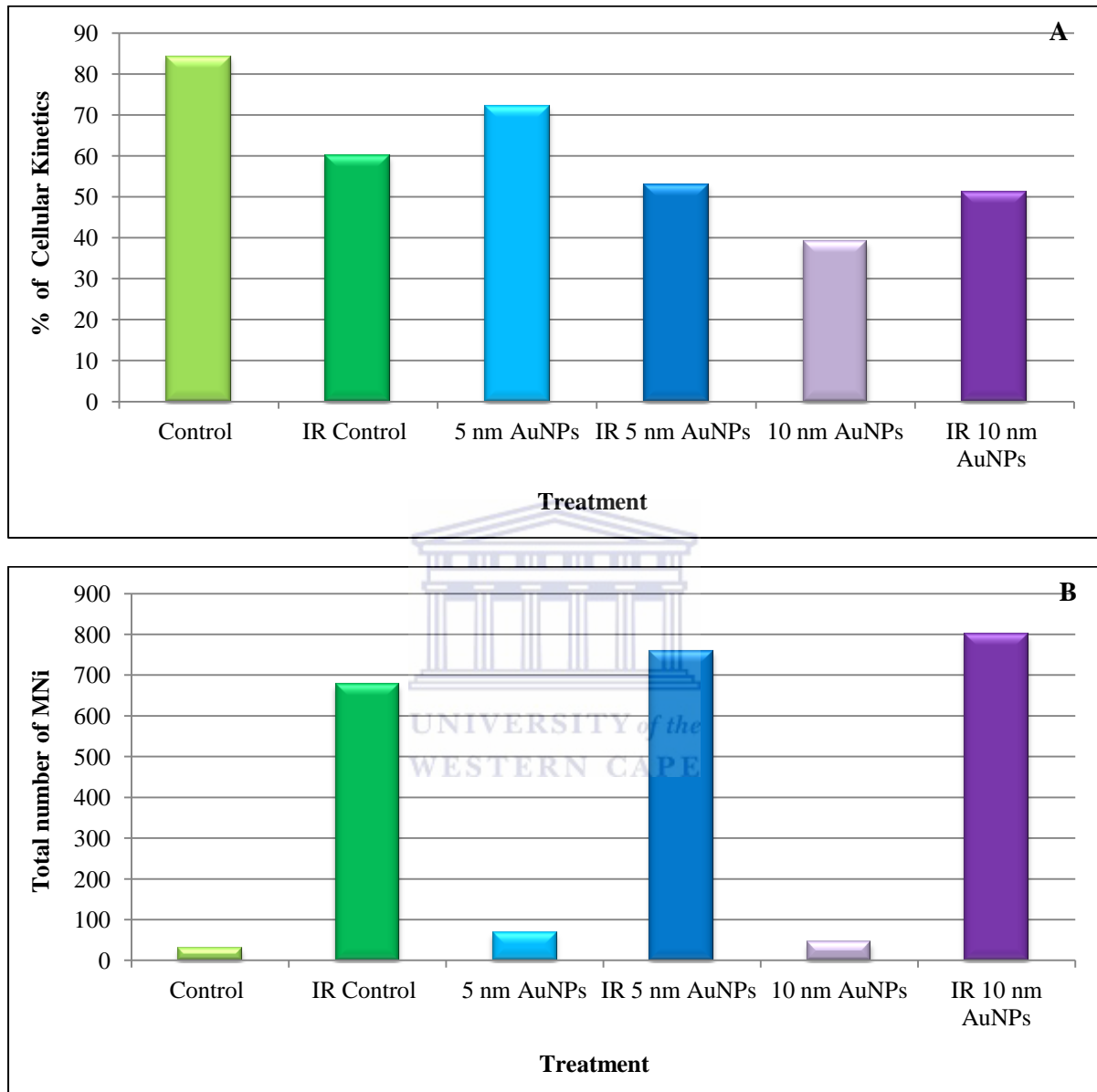


Figure 3.26: Cellular kinetics and MNi frequency of CHO-K1 cells. (A) Cellular kinetics of CHO-K1 cells was determined by scoring 400 AO stained BNCs and expressed as a percentage (%). Cells treated with 50 µg/ml AuNPs and/or irradiated with 1 Gy p(66)/Be neutrons showed an overall decrease in cellular kinetics in comparison to the control. (B) Mean cumulative frequency of MNi present were determined via the CBMN assay in CHO-K1 cells after 4 hour incubation with 50 µg/ml AuNPs followed by 1 Gy p(66)/Be neutrons. Control cells treated with AuNPs displayed an insignificant number of MNi, whilst a visible increase of MNi within cells treated with AuNPs and radiated with 1 Gy p(66)/Be neutrons was evident. The interaction indices for AuNPs and 1 Gy p(66)/Be neutrons of 1.06 to 1.16 is lower than the interaction indices after 2 X-rays.

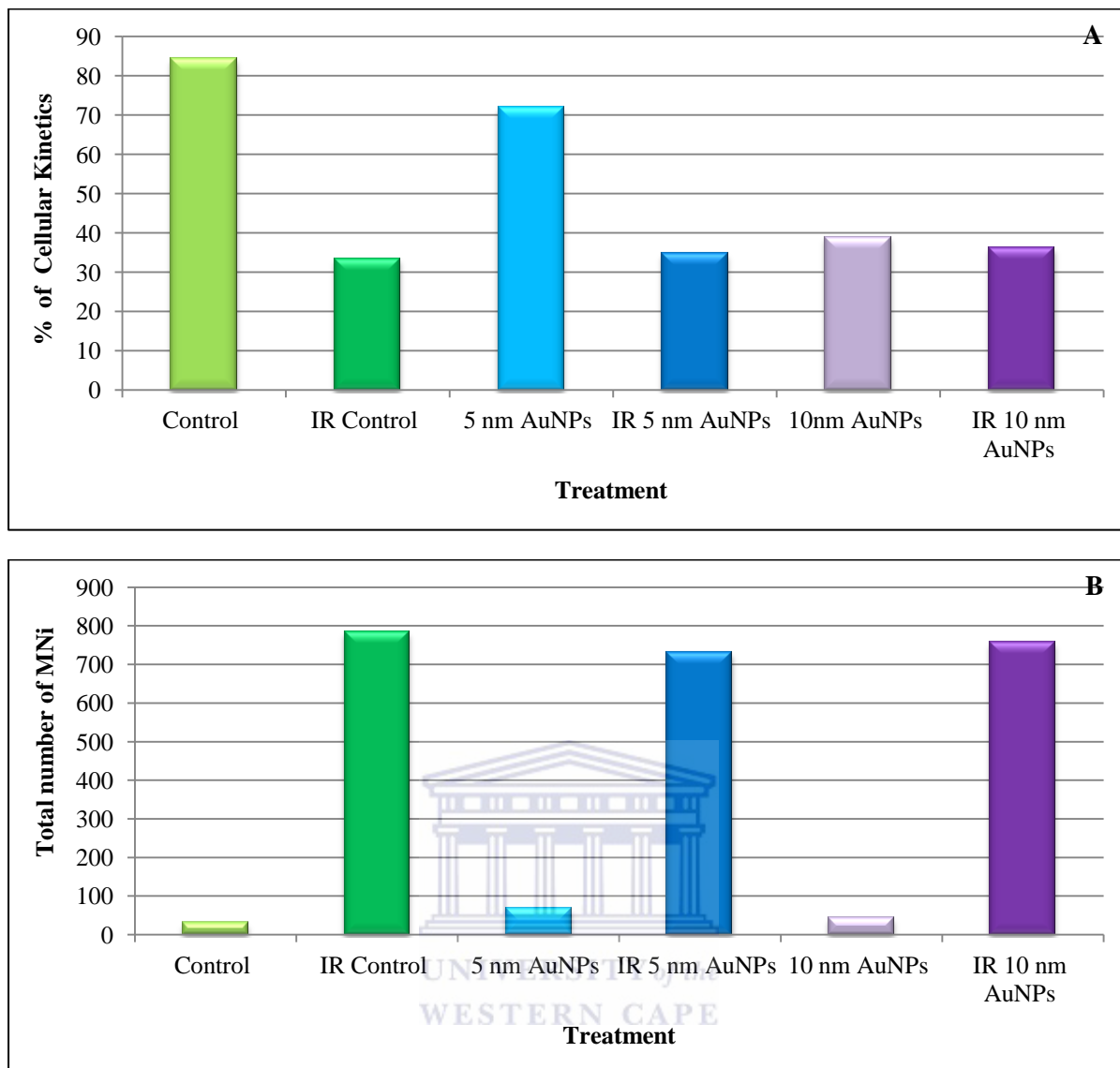


Figure 3.27: (A) Cellular kinetics of MCF-7 cells was determined by scoring 400 AO stained BNCs and expressed as a percentage (%). Cells treated with 50 $\mu\text{g/ml}$ AuNPs showed a decrease in cellular kinetics in comparison to the control, whilst the irradiated cells with 1 Gy p(66)/Be neutrons did not differ from the radiated control. (B) Mean cumulative frequency of MNi present determined via the CBMN assay in MCF-7 cells after 4 hour incubation with 50 $\mu\text{g/ml}$ AuNPs followed by 1 Gy p(66)/Be neutrons. No difference in the number of MNi within cells treated with AuNPs and radiated with 1 Gy p(66)/Be neutrons and the radiated control was noticeable. The interaction indices for AuNPs and 1 Gy p(66)/Be neutrons of 0.88 to 0.95 is lower than the interaction indices after 2 Gy X-rays.

The cellular kinetics of CHO-K1 and MCF-7 were not affected as expected and observed in Fig. 3.14 & Fig. 3.15. Control cells treated with AuNPs displayed an insignificant number of MNi, whilst a visible increase of MNi within cells treated with irradiated (1 Gy p(66)/Be neutrons) AuNPs was evident. However, the interaction between the irradiated in CHO-K1 (non-malignant) and MCF-7 cells (malignant) was not significant (Fig. 3.26 B & 3.27 B).

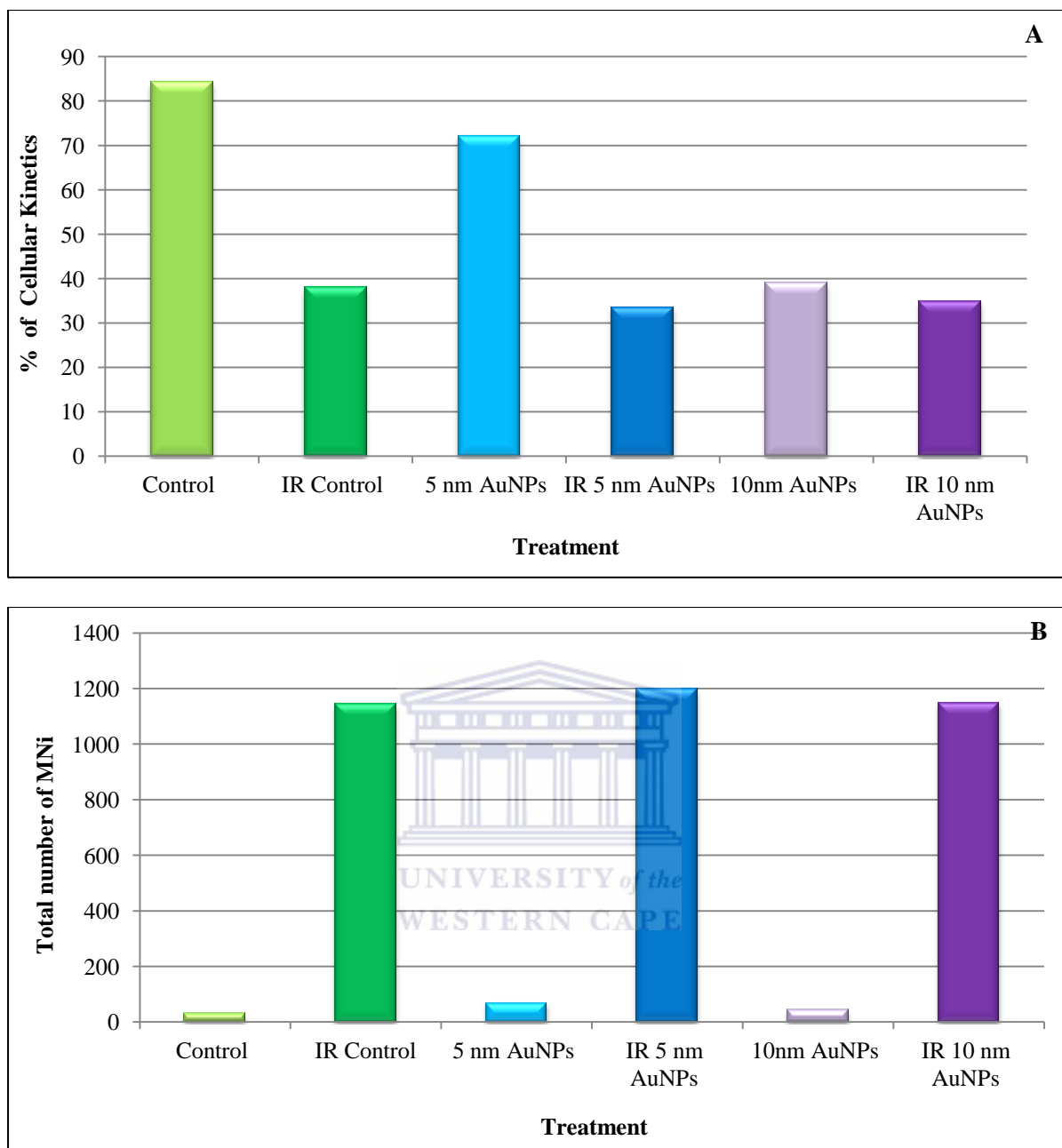


Figure 3.28: (A) Cellular kinetics of CHO-K1 cells was determined by scoring 400 AO stained BNCs and expressed as a percentage (%). Cells treated with 50 $\mu\text{g/ml}$ AuNPs and/or irradiated with 2 Gy p(66)/Be neutrons showed an overall decrease in cellular kinetics in comparison to the control. (B) Mean cumulative frequency of MNi present determined via the CBMN assay in CHO-K1 cells after 4 hour incubation with 50 $\mu\text{g/ml}$ AuNPs followed by 2 Gy p(66)/Be neutrons. All the samples radiated with 2 Gy p(66)/Be neutrons showed an increase in the number of MNi, however no clear increase was observed in the samples treated with AuNPs. The interaction indices for AuNPs and 2 Gy p(66)/Be neutrons of 1.00 to 1.02 is lower than the interaction indices after 2 Gy X-rays.

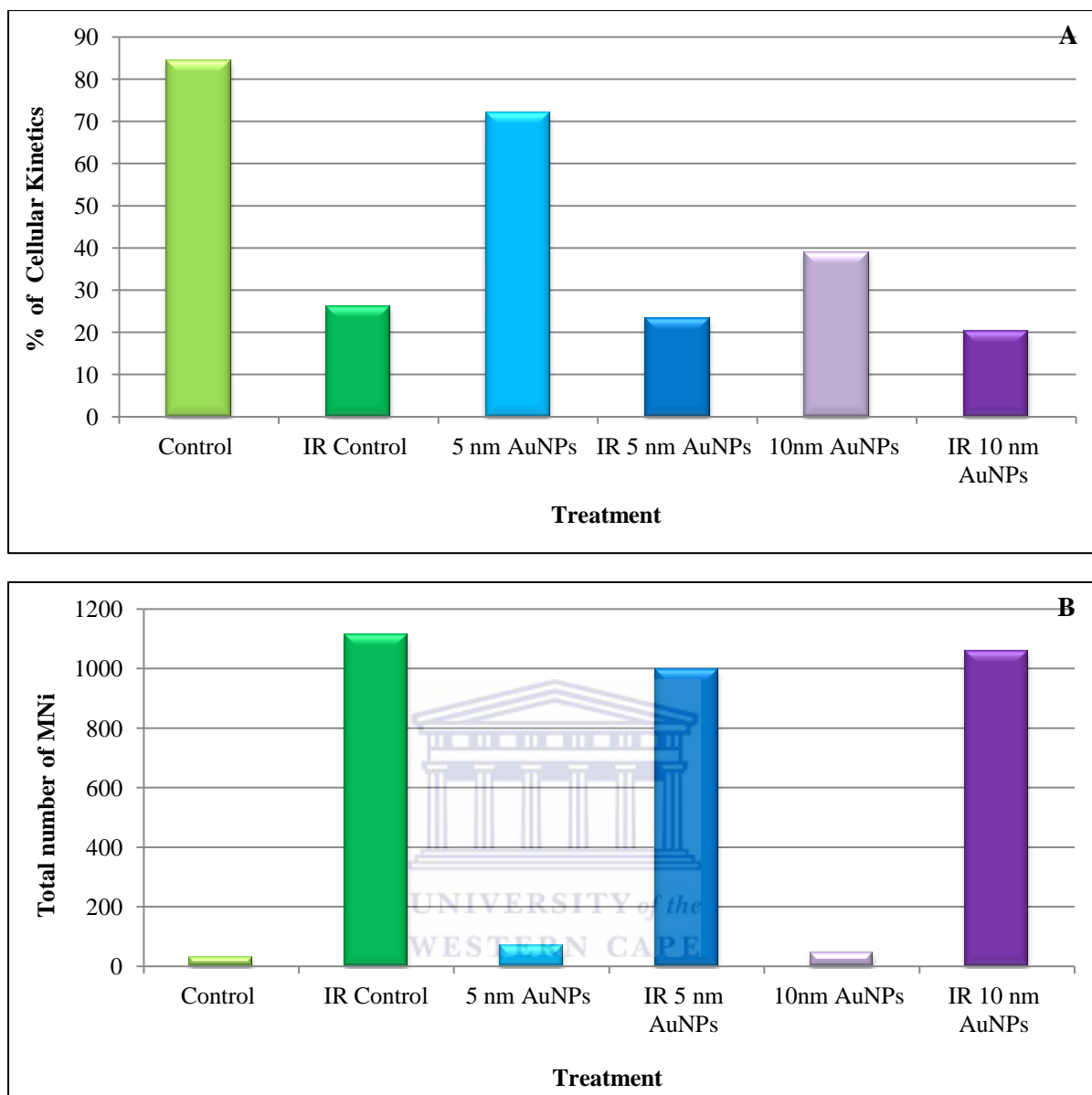


Figure 3.29: (A) Cellular kinetics of MCF-7 cells was determined by scoring 400 AO stained BNCs and expressed as a percentage (%). Cells treated with 50 $\mu\text{g/ml}$ AuNPs and/or irradiated with 2 Gy p(66)/Be neutrons showed a small decrease in cellular kinetics in comparison to the control. (B) Mean cumulative frequency of MNi present determined via the CBMN assay in MCF-7 cells after 4 hour incubation with 50 $\mu\text{g/ml}$ AuNPs followed by 2 Gy p(66)/Be neutrons. Control cells treated with AuNPs showed an irrelevant number of MNi. No difference between the radiated control and the AuNPs samples after 2 Gy p(66)/Be neutrons – was obvious. The interaction indices for AuNPs and 2 Gy p(66)/Be neutrons of 0.86 to 0.94 is lower than the interaction indices after 2 Gy X-rays.

The interaction indices between AuNPs and 2 Gy p(66)/Be neutrons is lower (Fig. 3.28 B & 3.29 B), in comparison to the interaction indices between AuNPs and 2 Gy X-rays, as p(66)/Be neutrons do not interact with AuNPs. Thus, no interaction was observed between AuNPs and p(66)/Be neutron radiation (Loveland et al., 2006; De Beer, 2015).

3.4 Cell viability assays

The MTT assay was used to assess the overall toxicity of the AuNPs on the CHO-K1, BEnd5, MCF-7 and MCF-10A cell lines.

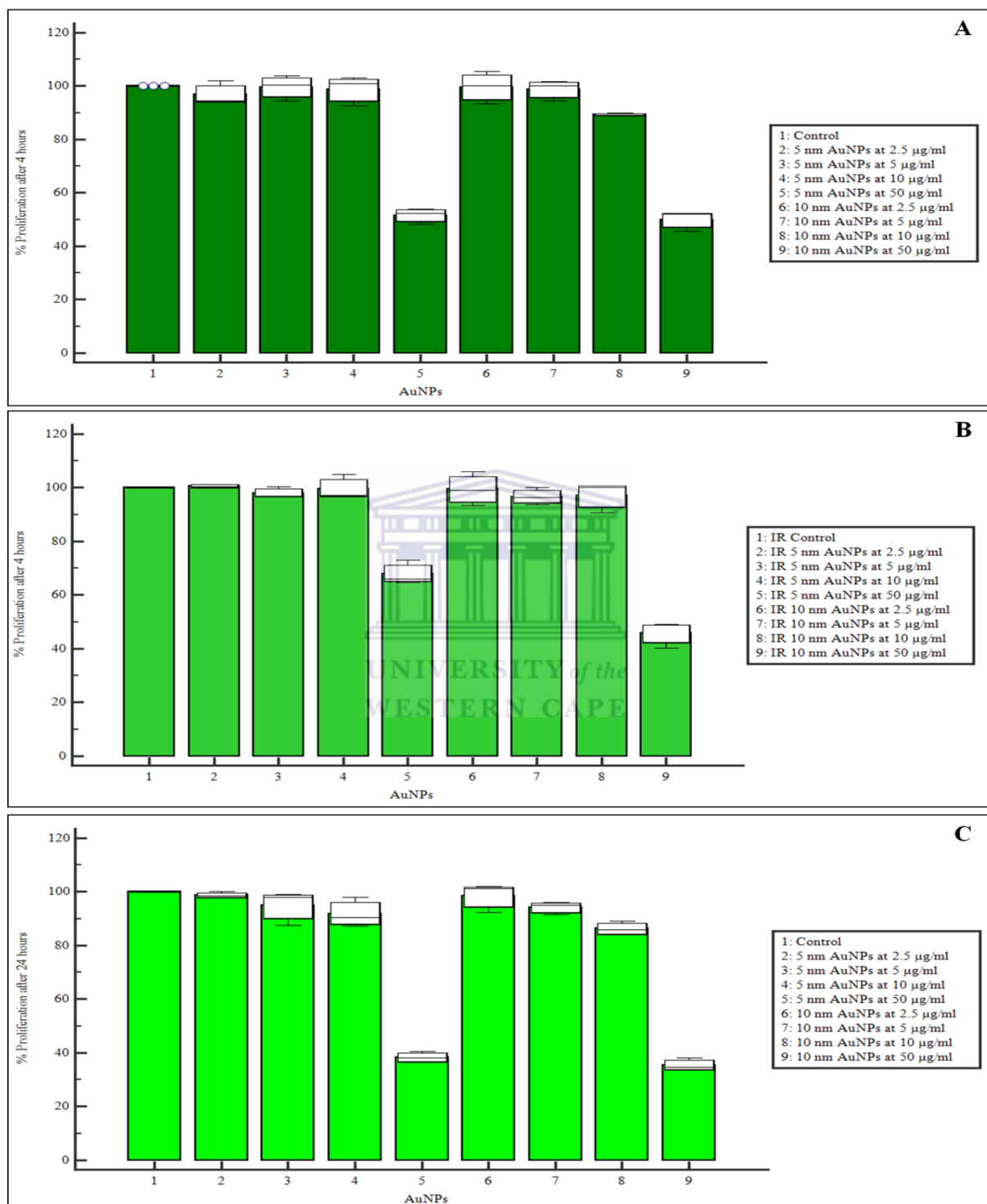


Figure 3.30: Box-and-Whisker plots showing the % cell viability in CHO-K1 cells as determined by MTT in 96 well plates. (A) Cells incubated with AuNPs for 4 hours, (B) cells incubated with AuNPs for 4 hours followed by 4 Gy 6 MV X-ray radiation, and (C) cells incubated with AuNPs for 24 hours. 5 and 10 nm AuNPs, at 50 µg/ml, caused a significant decrease in cell proliferation ($p < 0.05$) in all three different conditions, namely A, B and C (Addendum: Tables 5.4–5.6).

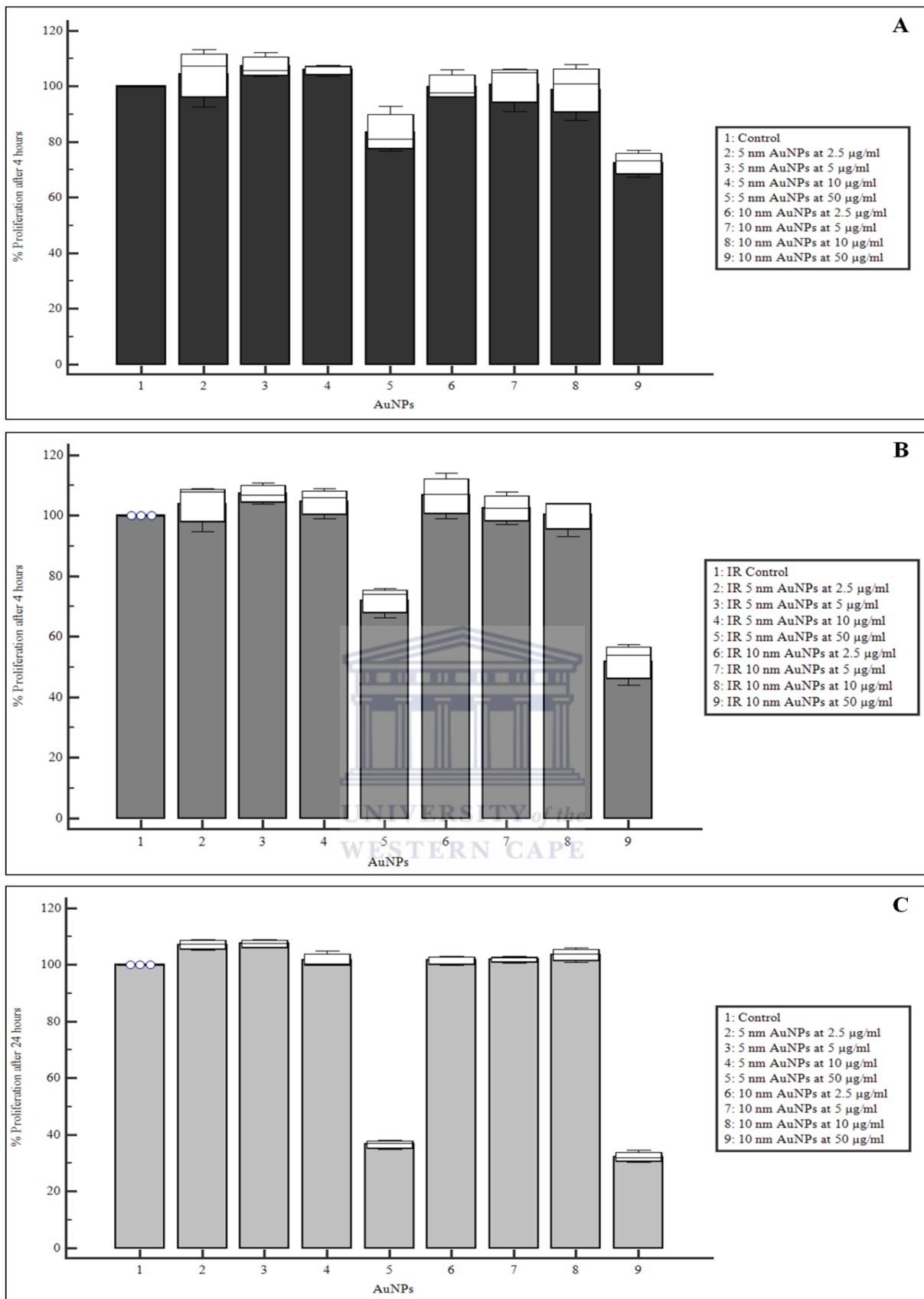


Figure 3.31: Box-and-Whisker plots showing the % cell viability in CHO-K1 cells as determined by MTT in 96 well plates. (A) Cells incubated with AuNPs for 4 hours, (B) cells incubated with AuNPs for 4 hours followed by 4 Gy X-ray radiation, and (C) cells incubated with AuNPs for 24 hours. 5 and 10 nm AuNPs, at 50 µg/ml, caused a significant decrease in cell proliferation ($p < 0.05$) in all three different conditions, namely A, B and C (Addendum: Tables 5.7–5.9).

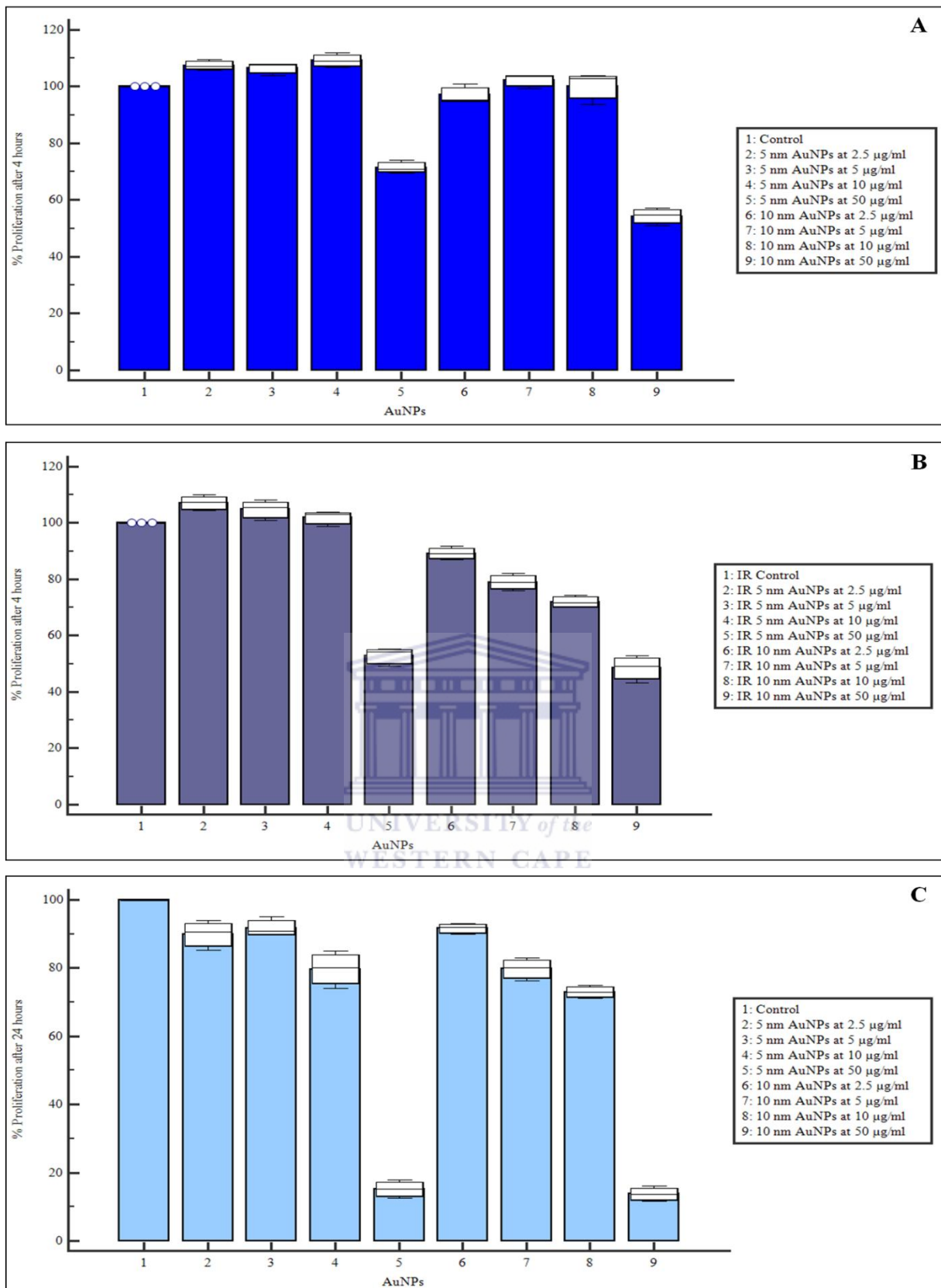


Figure 3.32: Box-and-Whisker plots showing the % cell viability in MCF-7 cells as determined by MTT in 96 well plates. (A) Cells incubated with AuNPs for 4 hours, (B) cells incubated with AuNPs for 4 hours followed by 4 Gy X-ray radiation, and (C) cells incubated with AuNPs for 24 hours. 5 and 10 nm AuNPs, at 50 µg/ml, caused a significant decrease in cell proliferation ($p < 0.05$) in all three different conditions, namely A, B and C (Addendum: Tables 5.10–5.12).

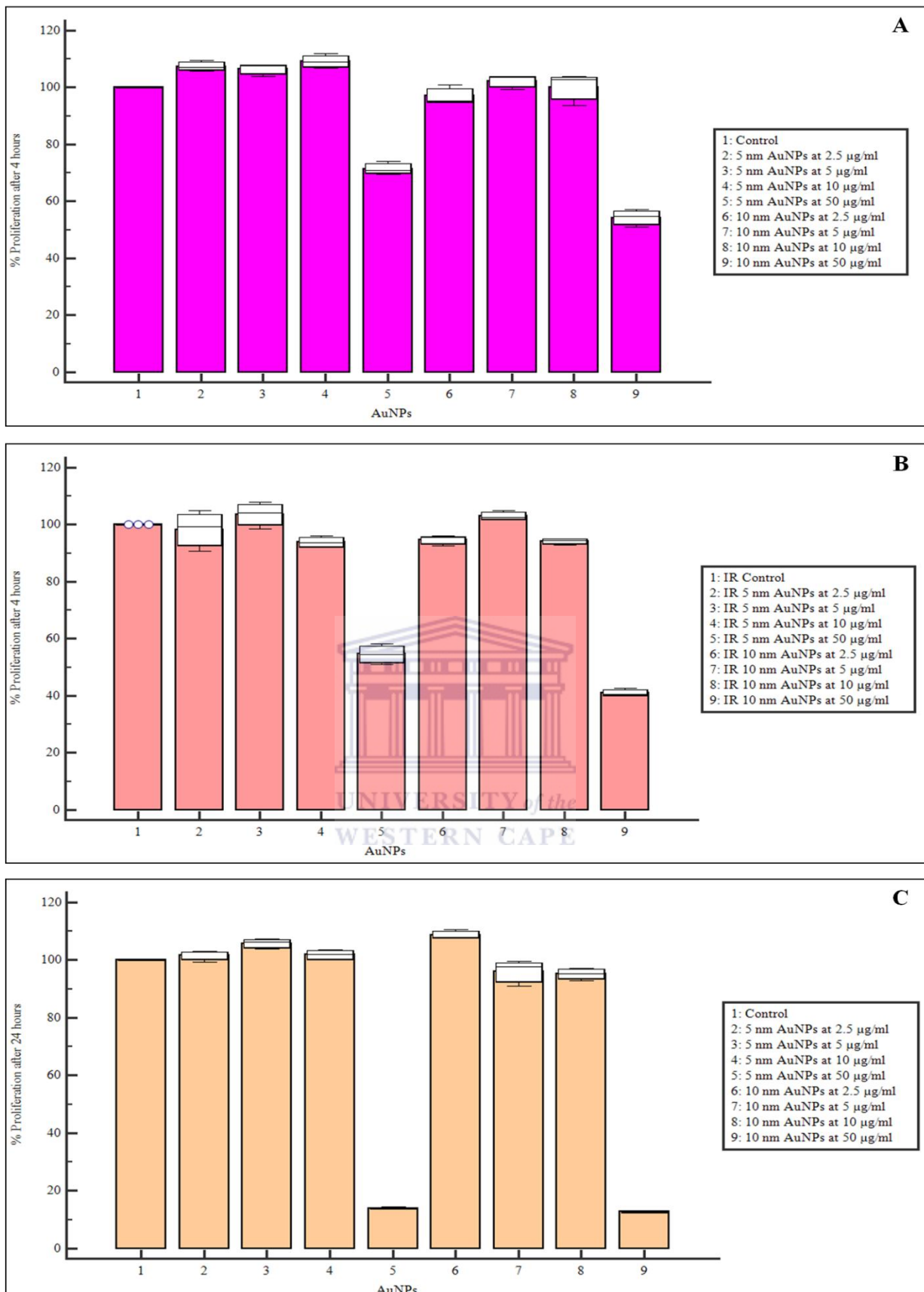


Figure 3.33: Box-and-Whisker plots showing the % cell viability in MCF-10A cells as determined by MTT in 96 well plates. (A) Cells incubated with AuNPs for 4 hours, (B) cells incubated with AuNPs for 4 hours followed by 4 Gy X-ray radiation, and (C) cells incubated with AuNPs for 24 hours. 5 and 10 nm AuNPs, at 50 µg/ml, caused a significant decrease in cell proliferation ($p < 0.05$), except in condition C (Addendum: Tables 5.13–5.15).

Based on results from Fig. 3.30–3.33 a decreased in cell toxicity was observed in each cell lines exposed to 50 $\mu\text{g/ml}$ of both types of AuNPs for 4 hours and followed by 4 Gy X-ray radiation. A significant decreased in cell survival was observed in each cell lines exposed to 50 $\mu\text{g/ml}$ of both types of AuNPs for 24 hours (Addendum: Table 5.3–5.13).

3.5 Flow cytometry

Flow cytometry was employed to analyse the effect of AuNPs alone, and with 2 Gy X-ray radiation on the cell cycle progression of CHO-K1, BEnd5, MCF-7 and MCF-10A cells (Fig. 3.34–3.37). The investigation was conducted by ethanol fixation and propidium iodide (PI) staining of cells. PI was utilised to stain the nucleus in order to determine the amount of DNA present. Tables 3.1–3.4 show the percentage cells in various cell cycle phases.

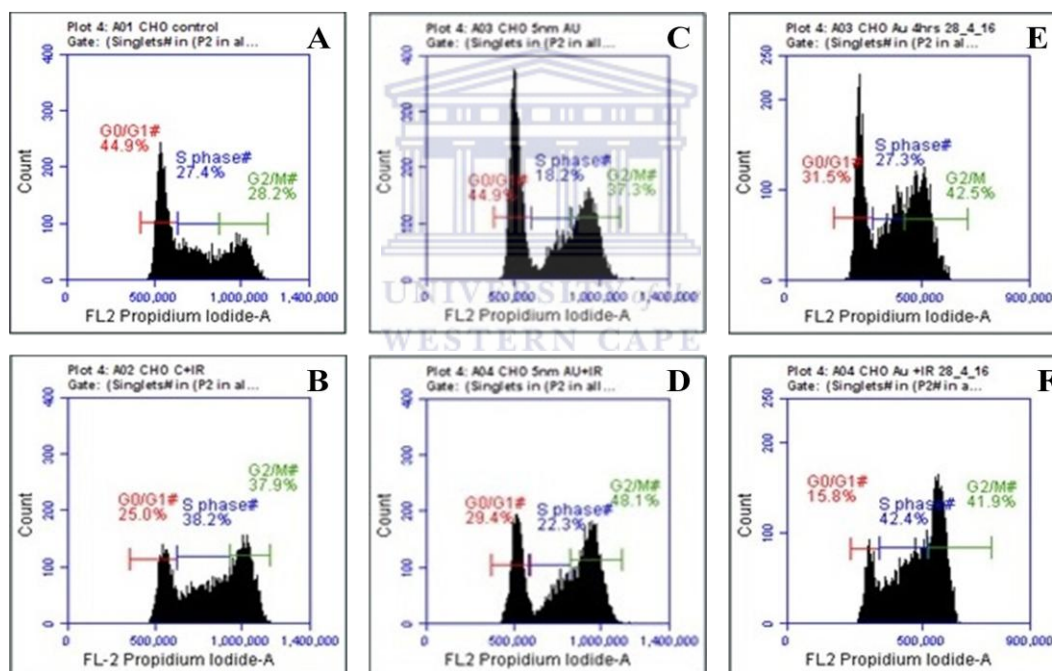


Figure 3.34: Flow cytometry was used to investigate the cell cycle progression in CHO-K1 cells. The DNA histograms show the effect of AuNPs on the CHO-K1 cells after a 4 hour exposure period, followed by 2 Gy X-ray radiation. (A) non-radiated control, (B) irradiated control, (C) non-radiated cells with 50 $\mu\text{g/ml}$ of 5 nm AuNPs, (D) cells with 50 $\mu\text{g/ml}$ irradiated 5 nm AuNPs, (E) non-radiated cells with 50 $\mu\text{g/ml}$ of 10 nm AuNPs and (F) cells with 50 $\mu\text{g/ml}$ irradiated 10 nm AuNPs.

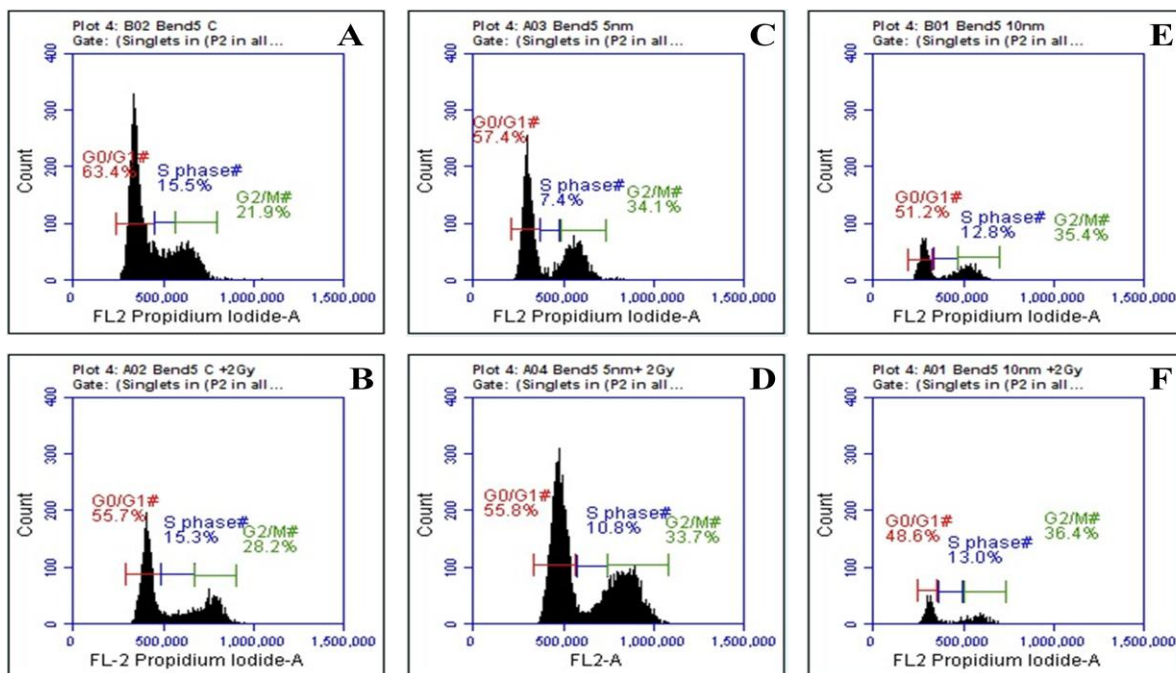


Figure 3.35: Flow cytometry was used to investigate the cell cycle progression in BEnd5 cells. The DNA histograms show the effect of AuNPs on the BEnd5 cells after a 4 hour exposure period, followed by 2 Gy X-ray radiation. (A) non-radiated control, (B) irradiated control, (C) non-radiated cells with 50 µg/ml of 5 nm AuNPs, (D) cells with 50 µg/ml irradiated 5 nm AuNPs, (E) non-radiated cells with 50 µg/ml of 10 nm AuNPs and (F) cells with 50 µg/ml irradiated 10 nm AuNPs.

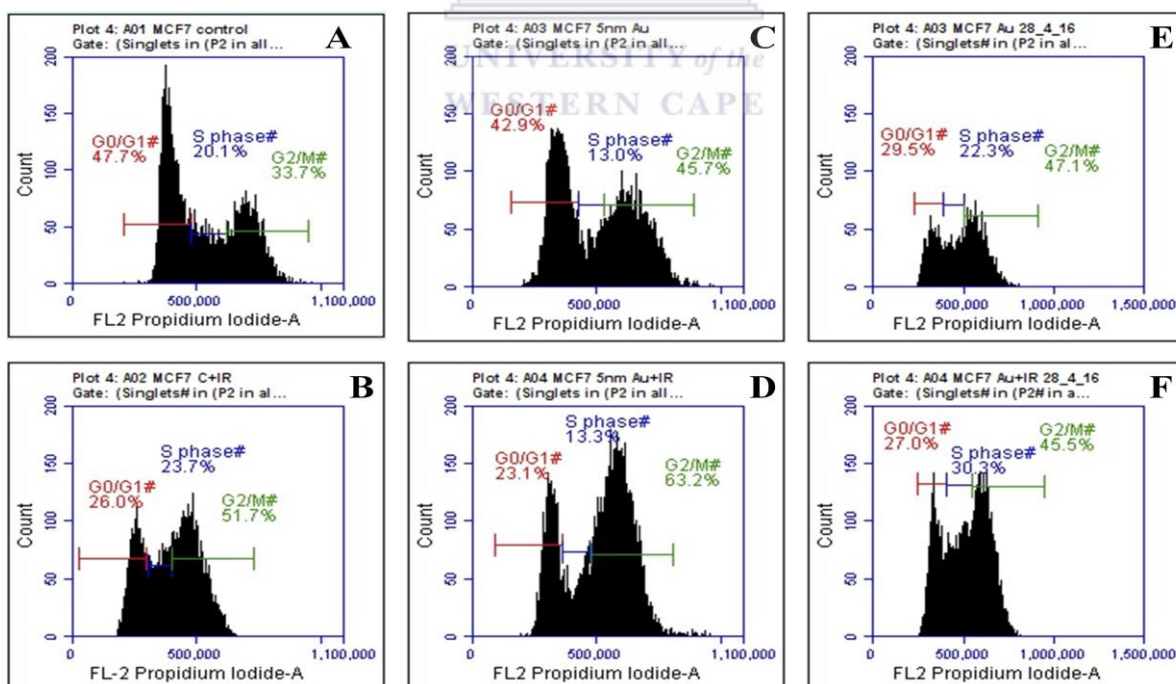


Figure 3.36: Flow cytometry was used to investigate the cell cycle progression in MCF-7 cells. The DNA histograms show the effect of AuNPs on the MCF-7 cells after a 4 hour exposure period, followed by 2 Gy X-ray radiation. (A) non-radiated control, (B) irradiated control, (C) non-radiated cells with 50 µg/ml of 5 nm AuNPs, (D) cells with 50 µg/ml irradiated 5 nm AuNPs, (E) non-radiated cells with 50 µg/ml of 10 nm AuNPs and (F) cells with 50 µg/ml irradiated 10 nm AuNPs.

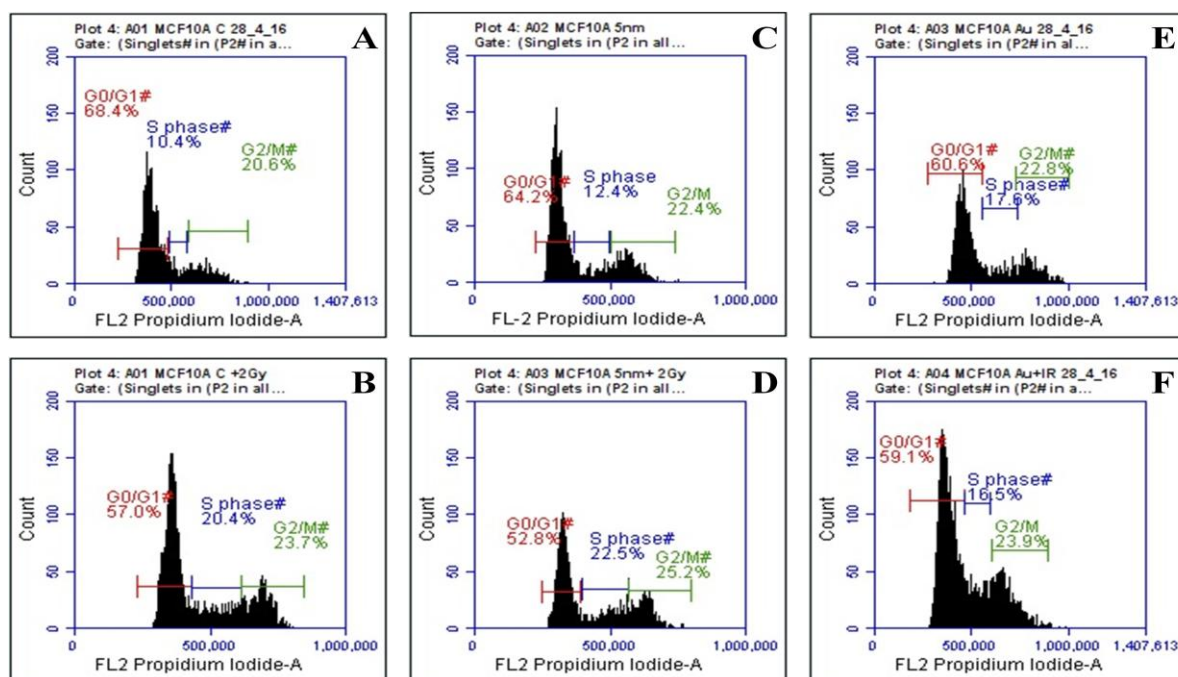


Figure 3.37: Flow cytometry was used to investigate the cell cycle progression in MCF-10A cells. The DNA histograms show the effect of AuNPs on the MCF-10A cells after a 4 hour exposure period, followed by 2 Gy X-ray radiation. (A) non-radiated control, (B) irradiated control, (C) non-radiated cells with 50 µg/ml of 5 nm AuNPs, (D) cells with 50 µg/ml irradiated 5 nm AuNPs, (E) non-radiated cells with 50 µg/ml of 10 nm AuNPs and (F) cells with 50 µg/ml irradiated 10 nm AuNPs.

Table 3.1: Shows the percentage distribution of CHO-K1 controls, AuNPs and irradiated AuNPs treated cells in the different cell cycle phases. PI staining detected by flow cytometry was utilized to investigate the effects of AuNPs and X-ray radiation on the cell cycle distribution. DNA content analysis showed a significant increase in the number of CHO-K1 cells in the S phase (38.2%) and in the G₂/M phase (37.9%), after radiation, when compared to the control cells in S (27.4%) and G₂/M (28.2%) (Fig. 3.34 A & B). Exposure to 5 and 10 nm AuNPs respectively increased the number of cells in G₂/M (37.3% and 42.5%) when compared to control cells (Fig 3.34 C & E). Radiated cells with 5 nm AuNPs increased the number of cells in the G₂/M phase even more (48.1%) and the cells treated with 10 nm AuNPs showed an increase in the S phase (42.4%).

Cell types	Time	Cell cycle phase	Control	Irradiated (IR) control	50 µg/ml of 5 nm AuNPs	50 µg/ml of IR 5 nm AuNPs	50 µg/ml of 10 nm AuNPs	50 µg/ml of IR 10 nm AuNPs
CHO-K1	4 H	G ₁	44.9	25.0	44.9	29.4	31.5	15.8
		S	27.4	38.2	18.2	22.3	27.3	42.4
		G ₂	28.2	37.9	37.3	48.1	42.5	41.9

Table 3.2: Shows the percentage distribution of BEnd5 controls, AuNPs and irradiated AuNPs treated cells in the different cell cycle phases. DNA content analysis displayed a significant increase in the number of BEnd5 cells in the G₂/M phase (28.2%) after radiation when compared to the control cells in G₂/M (21.9%) (Fig. 3.35 A & B). No major difference in number of cells in S phase (15.3%), after radiation, when compared to control cells were observed (Fig. 3.34 A & B). Exposure to 5 and 10 nm AuNPs respectively increased the number of cells in G₂/M (34.1% and 35.4%) when compared to control cells (Fig 3.35 C & E).

Cell types	Time	Cell cycle phase	Control	Irradiated (IR) control	50 µg/ml of 5 nm AuNPs	50 µg/ml of IR 5 nm AuNPs	50 µg/ml of 10 nm AuNPs	50 µg/ml of IR 10 nm AuNPs
BEnd5	4 H	G ₁	63.4	55.7	57.4	55.8	51.2	48.6
		S	15.5	15.3	7.4	10.8	12.8	13.0
		G ₂	21.9	28.2	34.1	33.7	35.4	36.4

Table 3.3: Shows the percentage distribution of MCF-7 controls, AuNPs and irradiated AuNPs treated cells in the different cell cycle phases. PI staining detected by flow cytometry was utilized to investigate the effects of AuNPs and X-ray radiation on the cell cycle distribution. DNA content analysis showed a significant increase in the number of MCF-7 cells in the G₂/M phase (51.7%), after radiation, when compared to the control cells G₂/M (33.7%) (Fig. 3.36 A & B). Exposure to 5 and 10 nm AuNPs respectively increased the number of cells in G₂/M (45.7% and 47.1%) when compared to control cells in G₂/M phase (33.7%). Cells incubated with 5 nm AuNPs, followed by 2 Gy X-ray radiation showed a significant increased the number of cells in the G₂/M phase (63.2%) when compared to control cells in G₂/M phase (33.7%). Cells exposed to 10 nm AuNPs and irradiated 10 nm AuNPs displayed a small decrease in the number of cells (47.5% and 45.5%, respectively) (Fig. 3.36 E & F).

Cell types	Time	Cell cycle phase	Control	Irradiated (IR) control	50 µg/ml of 5 nm AuNPs	50 µg/ml of IR 5 nm AuNPs	50 µg/ml of 10 nm AuNPs	50 µg/ml of IR 10 nm AuNPs
MCF-7	4 H	G ₁	47.7	26.0	42.9	23.1	29.5	27.0
		S	20.1	23.7	13.0	13.3	22.3	30.3
		G ₂	33.7	51.7	45.7	63.2	47.1	45.5

Table 3.4: Shows the percentage distribution of MCF-10A controls, AuNPs and irradiated AuNPs treated cells in the different cell cycle phases. DNA content analysis showed a significant increase in the number of MCF-10A cells in the S phase (20.4%) after radiation when compared to the control cells in S (10.4%) (Fig. 3.37 A & B). Exposure to 5 and 10 nm AuNPs respectively increased the number of cells in G₂/M (37.3% and 42.5%) when compared to control cells (Fig 3.34 C & E). Radiated cells with 5 nm and 10 nm AuNPs respectively increased the number of cells in the S phase (22.5% & 17.6 %) when compared to the control S phase (10.4%).

Cell types	Time	Cell cycle phase	Control	Irradiated (IR) control	50 µg/ml of 5 nm AuNPs	50 µg/ml of IR 5 nm AuNPs	50 µg/ml of 10 nm AuNPs	50 µg/ml of IR 10 nm AuNPs
MCF-10A	4 H	G ₁	68.4	57.0	64.2	52.8	60.6	59.1
		S	10.4	20.4	12.4	22.5	17.6	16.5
		G ₂	20.6	23.7	22.4	25.2	22.8	23.9

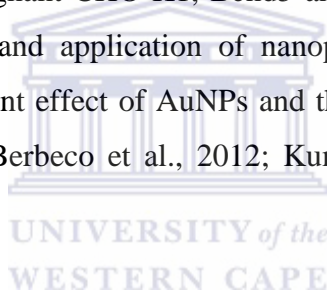


CHAPTER 4:

DISCUSSION

4.1 Introduction

The main aspect of this study was to investigate and contrast the effect of AuNPs between breast cancer cells and non-malignant CHO-K1, Bend5 and MCF-10A cells. The focus has been turned to the preparation and application of nanoparticles for cancer therapy with emphasis on the dose enhancement effect of AuNPs and the therapeutic potential of AuNPs in radiation therapy of cancer (Berbeco et al., 2012; Kumar et al., 2013; Abolfazli et al., 2015).



Dose enhancements can be accomplished by introducing a high atomic (Z) mass contrast agent, such as gold, that provide the greatest probability for photo interactions by photoelectric effect, when radiated by low energy X-rays (Spiers, 1949; Matsudaira et al., 1980). The photoelectric interactions produce photoelectrons and Auger electrons which introduce a localised dose enhancement in cells. The Auger effect is greatest in atoms of medium and high atomic mass, wherein the Auger electrons act as α -particles producing high local ionisation density damage. In this study, cellular uptake of AuNPs and their effect on cell viability was investigated. In order to demonstrate a possible interaction between the X-rays and AuNPs, an exceptionally high concentration of AuNPs was used and the chromosomal damage and changes in cellular kinetics were studied.

4.2 Characterisation of AuNPs

The characterisation of AuNPs is significant to evaluate the nature of the AuNPs. Since, the interaction of ANPs plays an important role in their properties.

4.2.1 UV-visible (vis) absorption spectrometry

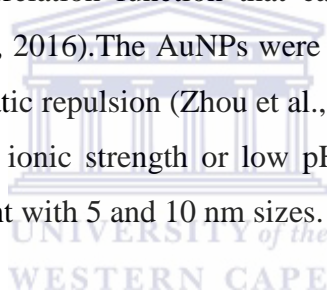
Surface plasmon resonance (SPR) is determined from absorption and scattering spectroscopy and is found to depend on the shape, size, and dielectric constants of both the metal and the surrounding material (Eutis & El-Sayed, 2005). Thus, increased particle size is noticeable with a peak shifting to a longer wavelength, whilst increased width of absorption spectra corresponds to the size distribution range (Verma et al., 2014; Peng et al., 2015). A slight peak shift of 10 nm AuNPs was observed, when compared to the peak of 5 nm AuNPs (Fig. 3.1).

The absorbance profile of 5 nm and 10 nm AuNPs as measured using UV-vis spectrophotometry is shown in Fig. 3.1. The λ_{\max} was between 500–565 nm, with SPR at 525 nm for both types of AuNPs. The UV-vis absorption peaks observed corresponded to the excitation of SPR in AuNPs and provides as an affirmation of their presence. This gives a brilliant red colour to the AuNPs, which varies in relation to their size.

4.2.2 Zeta (Z) potential dynamic light scattering (DLS) and polydispersity index (PDI)

Z-potential provides essential information on the dispersion of nanoparticles, as the charge is an indication of the repulsion forces between particles that can be utilised to predict long-term stability of the nanoparticles in suspension. Z-potential, DLS and PDI determination was used to assess the charge and hydrodynamic size as well as the size distribution width of the citrate-coated AuNPs (Fig. 3.2.1). The negative Z-potential charge of the AuNPs (from -24.5 mV for 5 nm AuNPs to -23.2 mV for 10 nm AuNPs) represents the necessary repulsive forces for the particles to remain stable in solution (Addendum: Fig. 5.1). PDI data was employed to determine the size width distribution of the AuNPs. The PDI measurements ranged from 0.202–0.329 suggested that the AuNPs were uniform in size (Fig. 3.2.2). The Z-average size/DLS (diameter in nm) was 38.12 nm and 48.50 nm, respectively for 5 nm and 10

nm AuNPs (Fig. 3.2.2) (Addendum: Fig. 5.2). It is known that smaller AuNPs tend to aggregate (Bhirde et al., 2014; Collado-González et al., 2015) and the hydrodynamic size of the 10 nm AuNPs (Fig. 3.2.2) was greater than the core size measured by TEM (Fig 3.3 G). The aggregates seen in TEM images could be attributed to the drying process during sample preparation. DLS measures the hydrodynamic radius of the AuNPs, whereas by TEM measurement is an estimated value of the projected area diameter. As a dispersed AuNP moves through a liquid medium, a thin electric dipole layer of the solvent adheres to its surface. This layer influences the movement of the particle in the medium as a result the hydrodynamic diameter provided information of the inorganic core along with any coating material and the solvent layer attached to the AuNP as it moved under the influence of Brownian motion, whereas the hydration layer is not present in the TEM measurement. Thus, only measurement of the inorganic core of AuNPs was obtained. Larger particles will diffuse slower than smaller particles and the DLS instrument measures the time dependence of the scattered light to generate a correlation function that can be mathematically linked to a particle size (Kumar & Kumbhat, 2016). The AuNPs were coated with citrate ions which act as stabilising agents via electrostatic repulsion (Zhou et al., 2009), but could still aggregate in a solution with sufficiently high ionic strength or low pH (Jia et al., 2014; Pamiés et al., 2014), thus possible and consistent with 5 and 10 nm sizes.



4.2.3 Transmission electron microscopy (TEM)

The transmission electron microscopy confirmed that 10 nm AuNPs were indeed 0.01 μm (10 nm) (Fig. 3.3 G) and that the AuNPs were in a monodispersional state, presumably due to negatively charged citrate ions on the surface of the nanoparticles. The internalisation of AuNPs can occur in various ways such as, phagocytosis, micropinocytosis and receptor-mediated endocytosis depending on size, type, cell receptors and cellular signalling cascades of AuNPs (Conner & Schmid, 2003; Chithrani et al., 2006). These mechanisms for nanoparticle internalisation include the formation of AuNP-protein complexes, recognition by cell membrane receptors, engulfment into a vesicle by the cells, being transported or penetrating into cells, the activation of signal pathways, and storage or removal of AuNPs by cells (Wang et al., 2015).

Vesicle transportation of AuNPs (Fig. 3.3 A–L) was observed in both the MCF-7 and MCF-10A cells. Previous studies found that the intracellular uptake of AuNPs into cells are highly reliant on nanoparticles properties such as size, shape and surface coatings (Chithrani et al., 2006; Chithrani, 2010; Freese et al., 2012; Neshatian et al., 2014; Kodiha et al., 2015). Extensive vesicle formation or possible autophagosomes containing AuNPs were observed in MCF-10A cells (Fig. 3.3 H, I & L), whereas in the MCF-7 cells AuNPs were observed only in the cytoplasm and in close proximity to the nuclear membrane (Fig. 3.3 E & F) implicating cellular damage, but no damage to the nucleus of the cell.

Nanoparticles with sizes larger than 500 nm have been known to enter phagocytic cells via phagocytosis pathways and smaller particles enter via the receptor-mediated endocytosis (RME) pathways (Dobrovolskaia and McNeil 2007; Hess and Tseng 2007; Oh & Park, 2014). However, a contradicting study reported that the internalisation of AuNPs smaller than 100 nm also occurred via phagocytosis (França et al., 2011). Ryan et al. (2007) investigated the ability of 5 nm citrate-coated AuNPs to enter the nucleus of HeLa cells. Only 25% of the internalised AuNPs were able to enter the nucleus. After conjugating a nuclear-penetrating peptide to the AuNPs, 50% of internalised AuNPs were able to enter the nucleus in HeLa cells. Nanoparticles with a negative Z-potential have been reported to exhibit no cellular internalisation of nanoparticles (Gratton et al., 2008). The AuNPs used in this study were negatively charged, regarded as anionic AuNPs and expected to show minor or no interaction with the negatively charged surface of the cell. Internalisation of AuNPs was observed in both the MCF-7 and MCF-10A cells indicating that anionic AuNP's uptake was mediated by non-specific adsorption of serum proteins onto the gold surface (protein corona), which allowed the nanoparticles to enter the cells via receptor-mediated endocytosis (Yen et al., 2009; Logan, 2013; Cheng et al., 2015). Another factor that influences the internalisation of AuNPs, besides size and Z-potential, is the temperature. Cellular uptake of nanoparticles decreases by 70% at 4 °C, when compared 37 °C. At 4 °C, nanoparticles form clusters on the outer cell membrane because endocytotic actions starts to cease, whereas at 37 °C nanoparticles begin to accumulate intracellular compartments of the cell (Luciani et al., 2009). All cells incubated with AuNPs in this study were incubated at 37 °C, 5% CO₂ air and relative humidified atmosphere.

AuNPs distributed in a biological fluid quickly bind to biomolecules, such as proteins and lipids, forming a protein corona on the AuNPs surface (Aggarwal et al., 2009; Monopoli et

al., 2012). These corona biomolecules can interact with membrane receptors to induce cell-signalling (Deng et al., 2011). Nanoparticle uptake commences with an initial adhesion of the nanoparticles to the cell and interactions with the lipids, proteins, and other components of the cell membrane followed by the activation of an energy-dependent uptake mechanism (Chithrani et al., 2006; Dausend et al., 2008) which allows the nanoparticles to be internalised into the cell and additionally trafficked to different sub-cellular areas, normally ending in lysosomal accumulation (Lesniak et al., 2012) (Fig. 3.3 B, D & F). Lysosomes are central for degradation and recycling of macromolecules delivered by endocytosis, phagocytosis and autophagy (Appelqvist et al., 2013). Once the particles are endocytosed, they may be degraded in the endolysosomal compartment, or can trigger binding of nanoparticles to intracellular targets, thus causing disturbances in cellular signalling, motility and metabolism (Pan et al., 2007; Baudoin et al., 2013; Xiang & Zhang, 2013; Paunescu et al., 2014). A variety of nanoparticles (e.g. quantum dots, iron oxide, gold, silica, titanium dioxide and carbon) have been reported to induce autophagy (Stern et al., 2012; Peynshaert et al., 2014). In the mechanism of autophagy, a double-membrane structure engulfs protein aggregates, damaged organelles and other cellular components to form an autophagosome which fuses with lysosomes causing the formation of autolysosomes (Huang et al., 2015). Autophagy maintains cellular homeostasis under stressful conditions (e.g. nutrient deprivation, oxidative stress and hypoxia) to help the cells survive (Mizushima & Komatsu, 2011; Murrow & Debnath, 2013).

Taking into consideration the various reports of AuNPs resulting in the induction of reactive oxygen species (ROS) in cells, it is possible that elevated ROS can result in mitochondrial swelling, mitochondrial depolarisation and DNA damage leading to necrosis or apoptosis (Tiwari et al., 2002; Peng & Jou, 2004; Butterworth et al., 2010; Yildirim et al., 2011; Zorov et al., 2014). Swollen mitochondria were noted in the MCF-10A cells (Fig. 3.3 H–J), but not in MCF-7 cells. This is possibly due to oxidative stress and cytotoxicity of the AuNPs as it has been shown that AuNPs sometimes impair mitochondrial function (Wang et al., 2013; Ding et al., 2014). Taggart et al. (2014) demonstrated that 1.9 nm AuNPs (500µg/ml) caused oxidation of the mitochondrial membrane protein, cardiolipin and cell specific disruption of mitochondrial membrane potential. The oxidation of cardiolipin initiates the intrinsic apoptotic pathway by releasing cytochrome c into the cytosol (Jiang et al., 2008). Both MDA-MB-231 (human breast adenocarcinoma) and T98G (human glioblastoma multiforma tumour) cells showed oxidation of cardiolipin in the presence of AuNPs. The

effect of AuNPs on the mitochondria might also be directly related to DNA damage upon the exposure to AuNPs, as mitochondria have been shown to play a role in the induction of DNA damage (Tartiet et al., 2007).

4.3 γ -H2AX foci assay

Previous studies reported that DNA DSBs induces H2AX phosphorylation and the number of γ H2AX foci is directly related to the number of radiation-induced DNA DSBs (Hudson et al., 2011; Murray et al., 2016). γ H2AX foci formation can be considered as a consistent and quantitative marker of radiation-induced DNA DSBs (Vignard et al., 2013). H2AX is one of several genes coding for histone H2A, which can undergo phosphorylation, acetylation and ubiquitination to regulate the cellular events (Kumar et al., 2012). γ -H2AX phosphorylation assay is a quantification technique by definite immunofluorescent staining that has been widely used to visualise the individual amount of DNA DSBs and is described as a highly sensitive method to monitor DSB induction and kinetics repair (Vujacic et al., 2011).

Isolated lymphocytes incubated with AuNPs were irradiated with low doses (1 Gy X-ray and 1 Gy p(66)/Be neutron) to prevent over-expression of foci, which can result in inaccurate automated scoring of foci per cell. The number of foci per cell increased slightly compared to the control. A significant increase in the number of foci was noticeable for cells treated with AuNPs followed by X-ray and p(66)/Be neutron radiation, respectively, compared to the control (Fig 3.4 & Fig. 3.5; Addendum: Table 5.3).

A study conducted by Wiwanitkit et al. (2009) demonstrated that 9 nm citrate-coated AuNPs could enter lymphocytes. Since lymphocytes have no phagocytosis activity (Salaberria et al., 2013) the known mechanism is the direct penetration of AuNPs into the cytoplasm of the lymphocyte (Wiwanitkit et al., 2009) substantiating the usefulness of nanoparticles as novel drug delivery systems to lymphocytes (Fahmy et al., 2007). According to this study, intracellular AuNPs could be observed in about $90.4 \pm 8.5\%$ of lymphocytes with no morphology changes when compared to control lymphocytes. However, the AuNPs could be seen in the cytoplasm, but not in the nucleus. In our study, the AuNPs could be seen mainly in the cytoplasm of MCF-7 and MCF-10A cells (Fig. 3.3 A–L). Wiwanitkit et al. (2009) suggested further researched into the penetration mechanism of AuNPs into the cytoplasm of

isolated lymphocytes as the lymphocyte membrane pore size at 4 nm x 2.5 nm, which was much smaller than the 9 nm AuNPs employed in the study.

4.4 Cytokinesis-Block Micronucleus (CBMN) assay

AuNPs are of interest for *in vitro* and *in vivo* applications in radiotherapy due to their well-known biocompatibility (Klhebtsov et al., 2011; Jain et al., 2012) and effectiveness as radiosensitisers of low energy photons for the activation of the high K-edge of gold (80 keV) that can lead to the emission of short-range photoelectrons upon irradiation (200–500 kV range) (Berbeco et al., 2012; Hashmi et al., 2014). Hainfeld et al. (2004) was the first to show that intravenously administered 1.9 nm untargeted AuNPs accumulated and enhanced the radiation-induced death of mammary carcinomas in mice models when combined with kilovolt (kV) photon radiation. A Monte Carlo study predicted that the theoretical dose enhancement achieved by gold radiosensitisation is up to 200% or more (Cho, 2005; Hainfeld et al., 2008).

Radiation induced damage can be measured by the CBMN assay. The visualisation of MNi within BNCs is represented in Figures 3.6–3.17. The consequences radiation induced DSBs may be observed as MNi containing acentric fragments from DNA. MNi are small, extracellular bodies resulting from chromosome breaks or lagging chromosomes during anaphase. Quantification of MNi within BNCs incubated for 4 hours with AuNPs and subsequently radiated with X-rays or p(66)/Be neutrons are shown in Figures 3.18 A–3.29 A. The percentage of cellular kinetics indicates the level of cellular division or growth rate undergone by each AuNPs treated sample with and without radiation.

As expected, AuNPs reduced the cellular kinetics of CHO-K1, BEnd5, MCF-7 and MCF-10A cell lines. MNi numbers for the non-radiated control samples were negligible, for all four cell lines. In the event of a radiosensitisation effect, the number of MNi of radiated cells treated with AuNPs should be higher than the controls (Fig. 3.18–3.21). Results showed that the non-malignant CHO-K1, BEnd5 and MCF-10A cells, as well as the malignant MCF-7 cells incubated with AuNPs, were more sensitive to radiation damage. However, the CHO-K1 and MCF-7 displayed significantly different interaction indices between the control cells and the 50 µg/ml AuNPs treated and radiated (scattered 6 MV 2 Gy X-ray) (Fig 3.6–3.9)

cells. Therefore, only CHO-K1 and MCF-7 cell lines were used for further experiments in this study.

A higher dose of 4 Gy X-ray with 50 µg/ml of AuNPs in these two cell lines resulted in a high number of MNi in both the control and AuNP treated cultures, indicating that no interaction between AuNPs and 4 Gy X-rays took place (Fig 3.22–3.23). Corresponding fluorescent micrographs, Figures 3.10 and 3.11 displayed blebbing of cell membranes and the possible presence of apoptotic bodies. As the same phenomenon was not observed in the MCF-7 cells exposed to 2 Gy radiation (Fig. 3.8), it is possible that the presence of apoptosis is due to the higher radiation (4 Gy) dose. Apoptosis, or programmed cell death (PCD), is characterised by loss of cell to cell contact, detachment, cell shrinkage (loss of K⁺ and water) nuclear condensation, internucleosomal DNA cleavage (CAD-activation), nuclear fragmentation, membrane blebbing and cell-self-fragmentation into apoptotic bodies (Ouyang et al., 2012; Jain et al., 2013). In contrast to apoptosis (a non-physiological cell death), necrosis can lead to cytoplasm mitochondria swelling resulting in ATP depletion due to mitochondrial dysfunction (Denecker et al., 2001; Brenner & Moulin, 2012; Hayat, 2013). Mitochondria swelling were noted in MCF-10A cells incubated with 50 µg/ml of 10 nm AuNPs in TEM micrographs (Fig. 3.3 H–J), which could be indicative of the start of necrosis in these cells. The concentration of AuNPs used in this study was exceptionally high as determination of the radiation interaction indices with gold was the main aim. However, the high concentrations (50 µg/ml of AuNPs) did have a detrimental effect on cell morphology, as mentioned above, and cell viability especially in the 24 hour exposure periods, as shown in the MTT studies (Fig. 3.30–3.33).

For comparison, CHO-K1 and MCF-7 cells were incubated for 4 hours with a much lower concentration of AuNPs (2.5 µg/ml) as employed in a study by Jain et al. (2011) to establish if a similar radiation interaction between AuNPs and the X-rays could be obtained. No significant interaction indices were present (Fig 3.24 & 3.25). This finding differs from the results obtained using the high concentration of AuNPs (50 µg/ml) suggesting that a significant interaction between AuNPs and X-rays were obtained, especially in the CHO-K1 and MCF-7 cells. Dividing CHO-K1 cells were observed after AuNPs treatment, illustrating that the low concentration did not affect the cellular division (Fig 3.12 C & F) compared to the higher concentration, while Figure 3.13 displayed a minute number of MNi within BNCs

of MCF-7. The low concentration AuNPs did not affect the cell division of either the non-malignant CHO-K1 cells or the malignant MCF-7 cells.

Ionising radiation (IR) interacts with DNA either directly or indirectly (Fig. 1.6), which damages cells either directly or indirectly through the production of free radicals causing DNA single or double-stranded breaks (DSBs). High-LET radiation damages the DNA directly by breaking hydrogen bonds connecting base pairs, whereas low-LET damages the DNA indirectly through radicals and reactive molecules (Hall & Giaccia, 2006). As a cell consists of 80% of water, IR often generates water radicals, as previously mentioned, by splitting a water molecule (H_2O) into hydrogen ions (H^+), hydroxyl radicals (OH^\cdot) or hydrogen peroxide (H_2O_2), which could initiate harmful chemical reactions in cells. High levels of ROS can cause damage to macromolecules, such as lipids, nucleic acids and proteins, leading to the induction lipid peroxidation (Cummings, 2006; Hernández et al., 2015). A differential damage was expected, when AuNP-treated cells were irradiated with different doses of X-ray or neutron radiation.

Figures 3.26–3.29 show a high number of MNi within BNCs of CHO-K1 and MCF-7 for both treatments of 50 $\mu\text{g}/\text{ml}$ with 1 Gy or 2 Gy p(66)/Be neutron radiation (energy mean of 29 MeV), respectively. No significant interaction was observed between the AuNPs and neutron radiation. Both, CHO-K1 and MCF-7 cells, after being treated with AuNPs (5 and 10 nm) followed by 2 Gy p(66)/Be neutron radiation displayed many MNi (Fig. 3.17 B & E) and characteristic features of apoptosis, such as apoptotic bodies (Fig. 3.16 B) and cell blebbing (Fig 3.16 B). In this study, Auger electrons were definitely inferred, as well as free radicals and charged species (ROS). Low-LET X-ray-induced Auger electrons expected to be in the cells treated with 50 $\mu\text{g}/\text{ml}$ of AuNPs, but a significant interaction between X-rays and AuNPs was only seen in CHO-K1 and MCF-7 cells. Auger electrons, which are weakly bound electrons cast out as a result of electronic shell rearrangements, can produce high local ionisation density. Several Auger electrons are generally emitted from the same atom simultaneously causing highly concentrated localised damage (Hainfeld et al., 2008; Kumar, 2010). However, they travel much shorter distances, usually ~ 10 nm. The Auger effect is greater in atoms of medium and high Z, such as gold (Hainfeld et al., 2008).

Different mechanisms of interaction between X-rays and nanoparticles, and neutrons and nanoparticles are expected according to the chemical nature of the nanoparticles, in this case

AuNPs. Gold (Au) has a high atomic number ($Z=79$) that enhances the photoelectric and thus the subsequent emissions of secondary electrons to increase conventional radiation therapy efficacy when bombarded with low voltage X-rays (Retif et al., 2015). The attenuation coefficient (cm^{-1}) for 125 kV X-rays for gold is 35.95 and only 6.23 for neutrons (De Beer, 2015). X-ray photons interact with the orbital electrons of atoms of the absorbing matter, namely AuNPs, and give off fast electrons. In contrast, neutrons interact with the nuclei of atoms of the absorbing matter (AuNPs) and set fast recoil protons, α -particles and heavier nuclear fragments in motion (Hall & Giaccia, 2006; Aktolun & Goldsmith, 2012). Thus, the lack of interaction between the AuNPs and the neutrons was expected (Loveland et al., 2006; De Beer, 2015).

4.5 Cell viability assay

Cell viability assays evaluate the overall toxicity of treatments such as AuNPs on cultured cells, by establishing cell survival and proliferation (Hillegas et al., 2010). It is important to know the dose of treatment required for a specific treatment. Many studies have reported non-toxicity of AuNPs (Conner et al., 2005; Shukla et al., 2005), but other researchers found AuNPs to have a toxic effect on cells (Goodman et al., 2004; Pan et al., 2007). It is known that metallic Au is non-toxic, but gold chloride or potassium gold cyanide is toxic to organs (Panyala et al., 2009). AuNPs are considered to be non-toxic as its core is inert (Bahadar et al., 2016). Previous studies suggest that cytotoxicity associated with AuNPs are dependent on concentrations, side chains, the stabiliser used, surface modifications, type of toxicity assay, cell line, and physical/chemical properties (Alkilany & Murphy, 2010; Arvizo et al., 2010; Yildirimer et al., 2011; Zhang et al., 2012; Yah, 2013; Favi et al., 2015; Pivodová et al., 2015; Bahadar et al., 2016). The variation in toxicity with respect to different cell lines has been observed in a human lung and liver cancer cell line (Patra et al., 2007). AuNPs have many side-effects due to the interaction with cell membranes, mitochondria or the nucleus (Pivodová et al., 2015).

Numerous drugs/medications are beneficial at low doses and toxic to cells at high doses. Several studies reported that the cytotoxicity of AuNPs is dose-dependent (Vajacic et al., 2011; Freese et al., 2012; Vecchio et al., 2012; Fratoddi et al., 2014). In this study, AuNPs were found to have similar toxicity effects on the non-malignant cells (CHO-K1, BEnd5 and

MCF-10A) when compared to the malignant cell line (MCF-7). At a high concentration of AuNPs (50 µg/ml) a significant reduction ($p < 0.05$) in cell viability was seen in all four cell lines (Addendum: Tables 5.4, 5.7, 5.10 & 5.13). At lower concentrations (2.5, 5 and 10 µg/ml) both the 5 and 10 nm AuNPs have no effect on the non-malignant cells (Fig. 3.30 A, 3.31 A, 3.32 A & 3.33 A), but caused a slight decrease in the proliferation of MCF-7 cells (Fig. 3.31). Therefore, AuNPs might aid as a therapeutic advantage in breast cancer

Cells incubated with 50 µg/ml AuNPs followed by 4 Gy X-ray radiation displayed a significant decrease ($p < 0.05$) (Addendum: Tables 5.3, 5.4, 5.9 & 5.12) in the cell viability of all the cell lines compared to the untreated control, (Fig. 3.30 B, 3.31 B, 3.32 B & 3.33 B). Overall, a significant ($p < 0.05$) decrease in cell viability was noted after 24 hour incubation with 50 µg/ml of AuNPs (Fig. 3.30 C, 3.31 C, 3.32 C & 3.33 C) in CHO-K1, BEnd5, MCF-7 and MCF-10A cells (Addendum: Tables 5.6, 5.9, 5.12 & 5.15).

Pivodová et al. (2015) conducted a cytotoxicity study of negatively charged AuNPs (-23.4 mV) by a cell viability MTT assay. It was shown that AuNPs do not have a significant cytotoxic effect on normal human dermal fibroblasts (NHDF) and normal human epidermal keratinocytes (NHEK). However, in our study the negatively charged AuNPs had a significant increase in cell death at 50 µg/ml after 4 and 24 hours (Fig. 3.30–3.33). Previous studies reported that spherical citrate capped AuNPs (21 nm) do not have a toxic effect on human breast-cancer cell lines (MCF-7) or human prostate-cancer cell lines (PC-3), as well as the spherical citrate capped AuNPs (10–50 nm) are not toxic to human leukemic cells (K562) (Vijayakumar & Ganesan, 2012; Yah, 2013).

Possible lysosomal bodies are illustrated in Fig. 3.3 B, D and F for MCF-7 cells as showed via TEM imaging. The latter was noted in cells treated with 50 µg/ml of 10 nm AuNPs. The observation led to the belief that the AuNPs were taken up via receptor-mediated endocytosis. Possible autophagosomes are also observed in MCF-7 (Fig. 3.3 A, D & E) and MCF-10A (Fig. 3.3 I & K). It is uncertain if the goal of these autophagosomes was cell survival or ultimately cell death, as it is known that a link between autophagy and apoptosis exists (Chen & Klionsky, 2011). Results of the MTT assay shows AuNPs can adversely affect cellular proliferation, probably by interacting with essential cell components including the nuclear membrane of the cell, mitochondria or nucleus. Adverse effects include organelle or DNA

damage, oxidative stress, apoptosis mutagenesis and protein up/down regulation (Alkilany et al., 2010; Söderstjerna et al., 2014; Khanna et al., 2015).

4.6 Flow cytometry (Propidium iodide)

Propidium iodide (PI) staining detected by flow cytometry was utilised to investigate the effects of 5 and 10 nm AuNPs followed by scattered 6 MV 2 Gy X-ray radiation. The latter allowed for the quantification of DNA content. Table 4.1 shows the cell progressions of the abovementioned cells, expressed as a percentage (%).

Table 4.1: Flow cytometry. This latter was used to investigate cell cycle progression in CHO-K1, BEnd5, MCF-7 and MCF-10A cells.

Cell types	Time	Cell cycle phase	Control	Irradiated (IR) control	50 µg/ml of 5 nm AuNPs	50 µg/ml of IR 5 nm AuNPs	50 µg/ml of 10 nm AuNPs	50 µg/ml of IR 10 nm AuNPs
CHO-K1	4 H	G ₁	44.9	25.0	44.9	29.4	31.5	15.8
		S	27.4	38.2	18.2	22.3	27.3	42.4
		G ₂	28.2	37.9	37.3	48.1	42.5	41.9
BEnd5	4 H	G ₁	63.4	55.7	57.4	55.8	51.2	48.6
		S	15.5	15.3	7.4	10.8	12.8	13.0
		G ₂	21.9	28.2	34.1	33.7	35.4	36.4
MCF-7	4 H	G ₁	47.7	26.0	42.9	23.1	29.5	27.0
		S	20.1	23.7	13.0	13.3	22.3	30.3
		G ₂	33.7	51.7	45.7	63.2	47.1	45.5
MCF-10A	4 H	G ₁	68.4	57.0	64.2	52.8	60.6	59.1
		S	10.4	20.4	12.4	22.5	176	16.5
		G ₂	20.6	23.7	22.4	25.2	22.8	23.9

G₂/M phase is the most sensitive phase to irradiation and certain treatment can cause cells to accumulate in this phase leading to an increase in radiosensitisation (Choy et al., 1993;

Pawlik & Keyomarsi, 2004; Roa et al., 2009; Soule et al., 2010; Raviraj et al., 2014). In this study, cell cycle analysis by flow cytometry revealed cell cycle arrest of only CHO-K1 and MCF-7 cells in G₂/M after 4 hour exposure to 50 µg/ml AuNPs (Fig. 3.34 B–C & Fig. 3.36 B–F). A cell cycle synchronisation or arrest was observed at the G₂/M phase in the cell cycle of irradiated 5 nm AuNPs CHO-K1 and MCF-7 cells (Fig. 3.34), but no cell cycle arrest was noted in BEnd5 and MCF-10A cells (Fig. 3.35 & 3.37). The G₂/M cell cycle arrest can be associated with the interaction between the AuNPs and X-ray radiation, since only CHO-K1 and MCF-7 cells displayed an interaction (Fig. 3.18 & Fig. 3.20). DNA content analysis showed a significant increase in the number of 10 nm AuNPs treated CHO-K1 cells in the S phase (42.4%) and in the G₂/M phase (48.1%) after radiation (Fig. 3.34; Table 3.1 & 4.1). Exposure to 5 and 10 nm AuNPs respectively increased the number of cells in G₂/M phase (45.7% and 47.1%) of the MCF-7 cell cycle, when compared to control cells in G₂/M phase (33.7%) (Fig. 3.36 B & C). However, a significant increase (63.2%) was observed in the G₂/M phase of the MCF-7 cells treated with 5 nm AuNPs and radiated (Table 3.3 & 4.1). According to Roa et al. (2009), AuNPs accumulated in prostate cancer cells (DU-145 cells) at the G₂/M phase via the activation of both checkpoint kinases (CHK1 and CHK2). Thus, these results suggested that AuNPs may be utilised to enhance radiotherapeutic sensitisation effect in cancer therapy. p53, cyclin E, cyclin A and cyclin B were identified as being the major mediators of AuNPs-induced cell cycle changes resulting in a significantly increased expression of cyclin E and cyclin B1, and decreased expression of cyclin A.

Cyclin E is a G₁ cyclin and is the foremost regulator of the G₁/S transition, wherein Cyclin E binds to CDK 2 leading to the formation of cyclin E-CDK 2 complex, which progresses the cell from the G₁ to the S phase, described as the G₁/S transition (Sanford & Parshad, 1999; Gérard & Goldbeter, 2009; Roa et al., 2009; Bertoli et al., 2013). As cells become dedicated to initiate division, the cells commence DNA replication and proceed to the S phase. These cells rely on specific checkpoints, as mentioned in Chapter 1, and can delay mitotic entry. DNA synthesis is mediated by the ATM and ATR protein kinases and CHK1 and/or CHK2, in which CHK1 is activated at the replication fork arrest in the S phase, whilst CHK2 is activated by damaged DNA detected during interphase (Jackson & Bartek, 2009; Brabzei & Foiani, 2010; Sorensen & Syljuasen, 2012). The CHK1 is necessary to avoid DNA damage with regards to replication stress during the S phase, whilst CHK2 is vital for the detection and repairing of DNA damage during interphase (Bartek & Lucas, 2003). The checkpoint

kinases caused the arrest of cell cycle progression via the regulation of cyclin-CDK activation (Bertoli et al., 2013).

As a result, AuNPs (5 and 10 nm) in this study could have inhibited the expression of cyclin E to accelerate the G₀/G₁ phase and consecutively caused the accumulation of cells in the G₂/M phase. After Roa et al. (2009) treated the DU-145 cells with glucose capped AuNPs (Glu-AuNPs), the expression of cyclin B1 by the cells was significantly increased ($p < 0.05$). This increase in cyclin B1 formed a cell accumulation in the G₂/M phase (Roa et al, 2009). The build up in the G₂/M phase was noted by the induction of 5 and 10 nm AuNPs that led to DNA damage. DNA damage activates the ‘guardian of the cell’, namely p53, which inhibits cyclin B expression and causes cell cycle arrest in the G₂/M phase. A therapeutic agent, such as AuNPs, can be utilised to cause an accumulation in the G₂/M phase to enhance radiation sensitivity (Roa et al., 2009; Babaei, M. & Ganjalikhani, 2014; Zhu et al., 2015). Furthermore, Saberi et al. (2016) observed no cell cycle arrest of HT-29 cells G₂/M after 24 h exposed to 80 μ M AuNPs possibly due to low AuNP concentration exposure. Consistently, Jain et al. (2011) showed that AuNPs do not affect the cell cycle arrest in MDA-MB-231 cells. Conversely, SK-OV-3 cells that were incubated with 14.37 nm Glu-AuNPs were arrested in the G₂/M phase (Geng et al., 2011). In contradiction, Liu et al. (2014) demonstrated that 5 nm AuNPs arrested the cell cycle at the G₀/G₁ phase in two lung cancer cell lines, namely A549 and 95D. Overall these data suggest that the effect of AuNPs on the cell cycle progression depend on the AuNPs size, concentration and the type of cells which is treated with AuNPs.

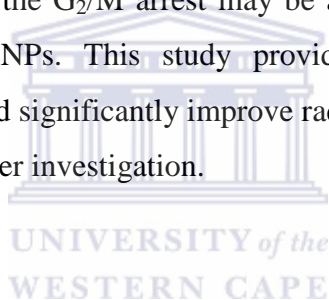
SUMMARY AND CONCLUSION

In this study, the citrate-capped AuNPs of different sizes (5 nm and 10 nm) were investigated on the cytotoxicity in different cell lines, namely CHO-K1, BEnd5, MCF-7 and MCF-10A, and the possible AuNPs interaction with X-ray and/or p(66)/Be neutron radiation for the enhancement of radiotherapy. X-rays are a low LET radiation type, which were scattered by using a Shonka chamber to obtain lower energy X-rays to interact with the AuNPs. At 50 µg/ml of AuNPs followed by scattered 6 MV 2 Gy X-rays only the CHO-K1 (non-malignant) and MCF-7 (malignant) cells showed an interaction above Unity ($U > 1$) implicating that AuNPs enhanced radiotherapy, whilst that for the other cell types used in the study were not different from Unity. The interaction was not present in CHO-K1 and MCF-7 cells, after a lower dose AuNPs (2.5 µg/ml) and/or higher X-ray radiation dose (4 Gy). Furthermore, the interaction did not exist after 1 and 2 Gy 66)/Be neutron radiation exposure with AuNPs, respectively. However, the higher MNi frequencies were induced by a combination treatment of AuNPs and radiation compared to the additive sum noted in samples exposed to AuNPs and radiation separately. Still, the interaction indices were not present in some conditions. Although this experimental set-up was to exploit the generation of Auger electrons to increase MNi frequency, the results are not consistent with the DNA damage associated with Auger electron damage. This could be due to the fact that none of the AuNPs penetrated the nuclear membrane and some AuNPs were 'captured' in lysosomal and autophagosome bodies. The latter caused the AuNPs not to be close enough to the DNA to cause DNA damage associated with the α -particle like Auger electrons.

The cellular kinetics of CHO-K1, BEnd5, MCF-7 and MCF-10A was reduced in all experimental conditions in comparison to the untreated control. Overall, the high concentration (50 µg/ml) of AuNPs reduced the cellular proliferation, whereas lower concentrations (2.5, 5 and 10 µg/ml) did not affect the cellular proliferation of the CHO-K1, BEnd5, MCF-7 and MCF-10A. The flow cytometry results showed that AuNPs caused a

G₂/M arrest and it is known that cells in the G₂/M phase is significantly more sensitive to irradiation. DNA damage activates the ‘guardian of the cell’, namely p53, which inhibits cyclin B expression and causes cell cycle arrest in G₂/M phase. A therapeutic agent, such as AuNPs, can be utilised to cause an accumulation in the G₂/M phase to enhance radiation sensitivity.

The findings of this study demonstrated that AuNPs have a remarkable potential to enhance the radiosensitivity of CHO-K1 and MCF-7 cells at MV energy. In addition, the G₂/M cell cycle arrest can be associated with the interaction between the AuNPs and X-ray radiation, since only CHO-K1 and MCF-7 cells displayed an interaction. Based on the results, the following conclusions were drawn: First, nanoparticle size is an essential variable affecting cellular kinetics, MNi frequency, DSBs in lymphocytes and cell progression. Second, in addition to particle size, cell type is also an essential aspect affecting the interaction between the AuNPs and radiation. Third, the G₂/M arrest may be associated with radiotherapy dose enhancement by means of AuNPs. This study provides useful information on dose enhancement by AuNPs that could significantly improve radiotherapy outcomes, although the molecular mechanisms need further investigation.



REFERENCES

- Aaseth, J., Haugen, M. & Forre, O. (1998). Rheumatoid arthritis and metal compounds- perspectives on the role of oxygen radical detoxification. *Analyst*. 123 (1), pp. 3– 6.
- Abbott, S. (Prof.) (2014). Zeta Potential. *AbottApps*. Available from: <http://www.stevenabbott.co.uk/PracticalSolunility/Zeta.html>.
- Abolfazli, M.K., Mahdavi, S.R. & Ataei, Gh. (2015) Studying Effects of Gold Nanoparticle on Dose Enhancement in Megavoltage Radiation. *Journal of Biommedical Physics & Engineering*. 5 (4), pp. 185–190.
- Aggarwal, P., Hal, J.B., McLeland, C.B., et al. (2009). Nanoparticle interaction with plasma proteins as it relates to particle biodistribution, biocompatibility and therapeutic efficacy. *Advanced Drug Delivery Reviews*. 61 (6), pp. 428–437.
- Ahmed, A., Tamimi, D.M.A., Isab, A.A., et al. (2012). Histological Changes in Kidney and Liver of Rats Due to Gold (III) Compound $[\text{Au}(\text{en})\text{Cl}_2]\text{Cl}$. *PLoS One*. 7 (12), pp. 1–11.
- Aillon, K.L., Xie, Y. , El-Gendy, N. et al. (2009). Nanomaterials physiochemical properties on *in vivo* toxicity. *Advanced drug Delivery Reviews*. 61 (8), pp. 457–466.
- Aktolun, C. & Goldsmith, S.J. (2012). Nuclear Medicine Therapy: Principles and Clinical Applications. *Springer*.

- Al-Ejeh, F., Kumar, R., Wiegmanns, A., et al. (2010). Harnessing the complexity of DNA-damage response pathways to improve cancer treatment outcomes. *Oncogene*. 29, pp. 6085–6098.
- Alkilany, A.M. & Murphy, C.J. (2010). Toxicity and cellular uptake of gold nanoparticles: what we have learned so far? *Journal of Nanoparticle Research*. 12, pp. 2313–2333.
- American Cancer Society (2016). Cancer Facts and Figures 2016. Atlanta, Ga: American Cancer Society, 2016. Available from: <https://www.cancer.gov/types/common-cancers>.
- American Cancer Society. (2013). Cancer Facts and Figures for African Americans 2013–2014. Available from: <https://www.cancer.org/content/dam/cancer-org/research/cancer-facts-and-statistics/cancer-facts-and-figures-for-african-americans/cancer-facts-and-figures-for-african-americans-2013-2014.pdf>
- American Cancer Society. (2015). What are the key statistics about breast cancer? | American Cancer Society. Available from: <http://www.cancer.org/cancer/breastcancer/detail-edguide/breast-cancer-key-statistics>.
- Apostolou, P. & Fostira, F. (2013). Hereditary Breast Cancer: The Era of New Susceptibility Genes. *BioMed Research International*. pp. 1–11.
- Appelqvist, H., Wäster, P., Kågedal, K., et al. (2013). The lysosome: from waste bag to potential therapeutic target. *Journal of Molecular Cell Biology*. 5, pp. 214–226.
- Arvizo, R., Bhattacharya, R. & Mukherjee, P. (2010). Gold nanoparticles: Opportunities and Challenges in Nanomedicine. *Expert Opinion on Drug Delivery*. 7 (6), pp. 753–763.

- Azeemi, S.T.Y. & Raza, S.M. (2005). A Critical Analysis of Chromotherapy and Its Scientific Evolution. *Evidence-Based Complementary and Alternative Medicine*. 2 (4), pp. 481–488.
- Babaei, M. & Ganjalikhani, M. (2014). The potential effectiveness of nanoparticles as radio sensitizers for radiotherapy. *Bioimpacts*. 4 (1), pp. 15–20.
- Bahadar, H., Maqbool., F., et al. (2016). Toxicity of Nanoparticles and an Overview of Current Experimental Models. *Iranian Biomedical Journal*. 20 (1), pp. 1–11.
- Balasubramanian, S.K., Jittiwat, J., Manikandan, J., et al. (2010). Biodistribution of gold nanoparticles and gene expression changes in the liver and spleen after intravenous administration in rats. *Biomaterials*. 31 (8), pp. 2034–2042.
- Barchanski, A. (2016). Laser-Generated Functional Nanoparticle Bioconjugates: Design for Application in Biomedical Science and Reproductive Biology. *Springer*.
- Barendsen, G.W. (1994). RBE LET relationships for different types of lethal radiation-damage in mammalian-cells - comparison with DNA DSB and an interpretation of differences in radiosensitivity. *International Journal of Radiation Biology*. 66 (5), pp. 433–436.
- Barnum, K.J. & O'Connell, M. (2014). Cell Cycle Regulation by Checkpoints. *Methods in Molecular Biology*. 1170, pp. 29–40.
- Bartek, J. & Lukas, J. (2003). Chk1 and Chk2 kinases in checkpoint control and cancer. *Cancer Cell*. 3, pp. 421–429.
- Baudoin, J.P., Jerome, W.G., Kübel, C., et al. (2013). Whole-Cell Analysis of Low-Density Lipoprotein Uptake by Macrophages Using STEM Tomography. *PLoS ONE*. 8 (1), pp. 1–8.

- Berbeco, R.I. et al. (2012). DNA Damage Enhancement from Gold Nanoparticles for Clinical MV photon Beams. *Radiation Research*. 178 (6), pp. 604–608.
- Berride, M.J. (2012). Cell Cycle and Proliferation. *Cell Signalling Biology*. Module 9, pp. 1–42.
- Bertoli, C., Skotheim, J.M. & De Bruin, R.A.M. (2013). Control of cell cycle transcription during G1 and S phases. *Nature Reviews Molecular Cell Biology*. 14 (8), pp. 518–528.
- Bhattacharya, R., & Mukherjee, P. (2008). Biological properties of "naked" metal nanoparticles. *Advanced Drug Delivery Reviews*. 60, pp. 1289–1306.
- Bhirde, A.A., Hassan, S.A., Harr, E., et al. (2014). Role of Albumin in the Formation and Stabilization of Nanoparticle Aggregates in Serum Studied by Continuous Photon Correlation Spectroscopy and Multiscale Computer Simulations. *The Journal of Physical Chemistry C, Nanomaterials and Interfaces*. 118 (29), pp. 16199–16208.
- Bingham, D., Gardin, I. & Hoyes, K.P. (2000). The Problem of Auger Emitters for Radiological Protection. *Radiation Protection Dosimetry*. 93, pp. 219–228.
- Blow, J. J. & Tanaka, T. U. (2005). The chromosome cycle: coordinating replication and segregation. *EMBO reports*. 6 (11), pp. 1028–1034.
- Branzei, D. & Foiani, M. (2010). Maintaining genome stability at the replication fork. *Nature Reviews Molecular Cell Biology*. 11, pp. 208–219.
- Brenner, C & Moulin, M (2012). Physiological Roles of the Permeability Transition Pore. *Circulation Research*. 111, pp. 1237–1247.

Britten, R.A. & Murray, D. (1997). Constancy of the relative biological effectiveness of 42 MeV (p->Be+) neutrons among cell lines with different DNA repair proficiencies. *Radiation Research*. 148 (4), pp. 308–316.

Brown, M. & Wittwer, C. (2002). Flow Cytometry: Principles and Clinical Applications in Hematology. *Clinical Chemistry*, 46 (8), pp. 1221–1229.

Burda, C., Chen, X., Narayanan, R. & El-Sayed, M.A. (2005). Chemistry and properties of nanocrystals of different shapes. *Chemical Reviews*. 105 (4), pp. 1025–1102.

Butterworth, K.T., Coulter, J.A., Jain, S., et al. (2010). Evaluation of cytotoxicity and radiation enhancement using 1.9 nm gold particles: potential application for cancer therapy. *Nanotechnology*. 21 (29), pp. 1–18.

Cai, W. & Chen, X. (2007). Nanoplatfoms for targeted molecular imaging in living subjects. *Small*. 3, pp. 1840–1854.

Cai, W., Gao, T., Hong, H. & Sun, J. (2008). Applications of gold nanoparticles in cancer nanotechnology. *Journal of Nanotechnology, Science and Applications*. 1, pp. 1–27.

Carter, J.D., Cheng, N.N., Qu, Y., et al. (2007). Nanoscale energy deposition by X-ray absorbing nanostructures. *The Journal of Physical Chemistry B*. 111, pp. 11622–11625.

Charrier-Savournin, F.B., et al. (2004). p21-Mediated Nuclear Retention of Cyclin B1-Cdk1 in Response to Genotoxic Stress. *Molecular Biology of the Cell*. 15, pp. 3965–3976.



- Chen, H., Dorrigan, A., Saad, S., et al. (2013). In Vivo Study of Spherical Gold Nanoparticles: Inflammatory Effects and Distribution in Mice. *PLoS ONE*. 8 (2), pp. 1–8.
- Chen, Y. & Klionsky, D.J. (2011). The regulation of autophagy – unanswered questions. *Journal of Cell Science*. 124, pp. 161–170.
- Chen, W.Y., Rosner, B., Hankinson, S.E., Colditz, G.A. & Willett, W.C. (2011). Moderate alcohol consumption during adult life, drinking patterns, and breast cancer risk. *Jama*. 306 (17), pp. 1884–1890.
- Cheng, X., Tian, X., Wu, A., et al. (2015). Protein Corona Influences Cellular Uptake of Gold Nanoparticles by Phagocytic and Nonphagocytic Cells in a Size-Dependent Manner. *ACS Applied Materials & Interfaces*. 7, pp. 20568–20575.
- Chithrani, B.D. (2010). Intracellular uptake, transport, and processing of gold nanostructures, *Molecular Membrane Biology*. 27, pp. 299–311.
- Chithrani, B.D., Ghazani, A.A. & Chan, W.C.W. (2006). Determining the Size and Shape Dependence of Gold Nanoparticle Uptake into Mammalian Cells. *NANO LETTERS*. 6 (1), pp. 662–668.
- Cho, S. H. (2005). Estimation of tumour dose enhancement due to gold nanoparticles during typical radiation treatments: a preliminary Monte Carlo study. *Physics in Medicine & Biology*. 50, pp. 163–173.
- Cho, K., Xu, W., Nie, S., et al. (2008). Therapeutic Nanoparticles for Drug Delivery in Cancer. *Clinical Cancer Research*. 14 (5), pp. 1310–1316.
- Choy, H., Rodriguez, F., Koesfer, S., et al. (1993). Investigation of Taxol as a Potential Radiation Sensitizer. *Cancer*. 71 (11), pp. 3774–3778.

- Christensen, D.M., Jenkins, M.S., Sugarman, S.L., et al. (2014). Management of Ionizing Radiation Injuries and Illnesses, Part 1: Physics, Radiation Protection, and Radiation Instrumentation. *The Journal of the American Osteopathic Association*. 114, pp. 189–199.
- Clogston, J.D. & Patri, A.K. (2011). Zeta potential measurement. *Methods in Molecular Biology*. 697, pp. 63–70.
- Cobrinik, D. (2005). Pocket proteins and cell cycle control. *Oncogene*. 24, pp. 2796–2809.
- Collado-González, M., et al. (2015). Aggregation behaviour of gold nanoparticles in presence of chitosan. *Journal of Nanoparticle Research*. 17 (6), pp. 1–10.
- Coller, H.A. (2007). What's taking so long? S-phase entry from quiescence versus proliferation. *Nature Reviews Molecular Cell Biology*. 8, pp. 667–670.
- Conner, S.D. & Schmid, S.L. (2003). Regulated portals of entry into the cell. *Nature*. 422, pp. 37–44.
- Connor, E.E., Mwamuka, J., Gole, A., et al. (2005). Gold nanoparticles are taken up by human cells but do not cause acute cytotoxicity. *Small*. 1, pp. 325–327.
- Cooper, S. (1998). On the proposal of a G₀ phase and the restriction point. *The FASEB Journal*. 12 (3), pp. 367–373.
- Cummings, M. (2006). Human Heredity: Principles and Issues. Chapter 11. 7th Edition, p. 250.
- Curtis, E., Quale, C., Haggstrom, D. & Smith-Bindman, R. (2008). Racial and ethnic differences in breast cancer survival: how much is explained by screening, tumor severity, biology, treatment, comorbidities, and demographics? *Cancer*. 112, pp. 171–180.

- D' Adda di Fagagna, F. (2008). Living on a break: cellular senescence as a DNA-damage response. *Nature Reviews Cancer*. 8, pp. 512–552.
- Daignan-Fornier, B. & Sagot, I. (2011). Proliferation/Quiescence: When to start? Where to stop? What to stock? *Cell Division*. 6 (20), pp. 1–5.
- Dalton, S. (1998). Cell cycle control of chromosomal DNA replication. *Immunology and Cell Biology*. 76, pp. 467–472.
- Danforth, D.N. Jr. (2013). Disparities in breast cancer outcomes between Caucasian and African American women: a model for describing the relationship of biological and nonbiological factors [serial online]. *Breast Cancer Research*. 15, p. 208.
- Daniel, M.C. & Astruc, D. (2004). GNPs: assembly, supramolecular chemistry, quantum-size related properties, and applications toward biology, catalysis, and nanotechnology. *Chemical Reviews*. 104, pp. 293–346.
- Darzynkiewicz, Z., Zhao, H., Zhang, S., et al. (2015). Initiation and termination of DNA replication during S phase in relation to cyclins D1, E and A, p21WAF1, Cdt1 and the p12 subunit of DNA polymerase δ revealed in individual cells by cytometry. *Oncotarget*. 6 (14), pp. 11735–11750.
- Dausend, J., Musyanovych, A., Dass, M., et al. (2008). Uptake mechanism of oppositely charged fluorescent nanoparticles in HeLa cells. *Macromolecular Bioscience*. 8 (12), pp.1135–1143.
- De Beer, F.C. (2015). Neutron- and X-ray radiography/ tomography: non-destructive analytical tools for the characterization of nuclear materials. *The Journal of The Southern African Institute of Mining and Metallurgy*. 115, pp. 913–924.

- Debnath, P., Muthuswamy, S. & Brugge, J. (2003). Morphogenesis and oncogenesis of MCF-10A mammary epithelial acini grown in three-dimensional basement membrane cultures. *Methods*. 30, pp. 256–268.
- De Jong, W.H. & Borm, P.J.A. (2008). Drug delivery and nanoparticles: Applications and hazards. *International Journal of Nanomedicine*. 3 (2), pp. 133–149.
- Denecker, G., Vercammen, D., Steemans, M., et al. (2001). Death receptor-induced apoptotic and necrotic cell death: differential role of caspases and mitochondria. *Cell Death Differ*. 8, pp. 829–840.
- Deng, Z.J., Liang, M., Monteiro, M., Toth, I. & Minchin, R.F. (2011). Nanoparticle-induced unfolding of fibrinogen promotes Mac-1 receptor activation and inflammation. *Nature Nanotechnology*. 6, pp. 39–44.
- Ding, F., Li, Y., Liu, J., et al. (2014). Overendocytosis of gold nanoparticles increases autophagy and apoptosis in hypoxic human renal proximal tubular cells. *International Journal of Nanomedicine*. 9, pp. 4317–4330.
- DiScipio, R.G. (1996). Preparation of Colloidal Gold Particles of Various Sizes Using Sodium Borohydride and Sodium Cyanoborohydride. *Analytical Biochemistry*. 236 (1), pp. 168–170.
- Dobrovolskaia, M.A. & McNeil, S.E. (2007). Immunological properties of engineered nanomaterials. *Nature Nanotechnology*. 2, pp. 469–478.
- Dorée, M. & Galas, S. (1994). The cyclin-dependent protein kinases and the control of cell division. *The FASEB Journal*. 8 (14), pp. 1114–1121.
- Dubravka, D. & Scott, D.W. (2000). Regulation of the G1 phase of the mammalian cell cycle. *Cell Research*. 10, pp. 1–16.

- Dykman, L.A. & Khlebtsov, N.G. (2011). Gold Nanoparticles in Biology and Medicine: Recent Advances and Prospects. *ACTA NATURAE*. 3 (2), pp. 34–55.
- Elhissi, A.M.A., Ahmed, W., Hassan, I.U., et al. (2012). Carbon Nanotubes in Cancer Therapy and Drug Delivery. *Journal of Drug Delivery*. pp. 1–10.
- Ema, M., Kobayashi, N., Naya, M., et al. (2010). Reproductive and developmental toxicity studies of manufactured nanomaterials. *Reproductive Toxicology*. 30 (3), pp. 343–352.
- Eustis, S. & El-Sayed, M.A. (2005). Why gold nanoparticles are more precious than pretty gold: Noble metal surface plasmon resonance and its enhancement of radiative and nonradiative properties of nanocrystals of different shapes. *The Royal Society of Chemistry*. 35, pp. 209–217.
- Fahmy, T.M., Fong, P.M., Park, J., et al. (2007). Nanosystems for simultaneous imaging and drug delivery to T cells. *AAPS Journal*. 9, pp. 171–180.
- Favi, P.M., Gao, M., Arango, L.J.S., et al. (2015). Shape and surface effects on the cytotoxicity of nanoparticles: Gold nanospheres versus gold nanostars. *Journal of Biomedical Materials Research*. 103 (11), pp. 3449–3462.
- Fenech, M. (2000). The in vitro micronucleus technique. *Mutation Research*. 455, pp. 81–95.
- Fenech, M., Chang, W. & Kirsch-Volders, M., et al. (2003). HUMN project: detailed description of the scoring criteria for the cytokinesis-block micronucleus assay using isolated human lymphocyte cultures. *Mutation Research*. 534, pp. 65–75.
- Fourie, S.J., McMaster, A., Mothilal, R., Maart, K. (2014). A Phase IV Clinical Trial of Patients with Solid Tumors Receiving Lenograstim as Primary Prophylaxis for Chemotherapy-Induced Neutropenia, in a Docetaxel-Based Regimen. *Journal of Cancer Research*. pp. 1–7.

- França, A., Aggarwal, P., Barsov, E.V., et al. (2011). Macrophage scavenger receptor A mediates the uptake of gold colloids by macrophages in vitro. *Nanomedicine (Lond)*. 6, pp. 1175–1188.
- Franken, N.A.P. et al. (2011). Comparison of RBE values of high-LET α -particles for the induction of DNA-DSBs, chromosome aberrations and cell reproductive death. *Radiation Oncology*. 6 (64), pp. 1–8.
- Freedman, R.A., Virgo, K.S., Labadie, J. et al. (2012). Receipt of locoregional therapy among young women with breast cancer. *Breast Cancer Research Treatment*. 135, pp. 893–906.
- Freeman, W.H. & Co. (2004). Life: The Science of Biology, 7th Edition, Fig. 9.4 Cyclin-Dependent Kinase and Cyclins Trigger Transitions in Cell Cycle.
- Freese, C., Uboldi, C., Gibson, M.I., et al. (2012). Uptake and cytotoxicity of citrate-coated gold nanospheres: Comparative studies on human endothelial and epithelial cells. *Particle and Fibre Toxicology*. 9 (23), pp. 1–11.
- Frens, G. (1973). Controlled nucleation for the regulation of the particle size in monodisperse gold suspensions. *Nature Physical Science*. 241, pp. 20–22.
- Fricker, S.P. & Buckley, R.G. (1996). Comparison of two colorimetric assays as cytotoxicity endpoints for an in vitro screen for antitumour agents. *Anticancer Research*. 16, pp. 3755–3760.
- Gamper, N., Stockand, J.D. & Shapiro, M.S. (2005). The use of Chinese hamster ovary (CHO) cells in the study of ion channels. *Journal of Pharmacological and Toxicological Methods*. 51 (3), pp. 117–183.

- Gao, X., Cui, Y., Levenson, R.M. et al. (2004). In vivo cancer targeting and imaging with semiconductor quantum dots. *Nature Biotechnology*. 22, pp. 969–967.
- Gayek, A.S. & Ohi, R. (2016). CDK-1 Inhibition in G2 Stabilizes Kinetochores-Microtubules in the following Mitosis. *PLoS ONE*. 11 (6).
- Geng, F., Song, K., Xing, J.Z., et al. (2011). Thio-glucose bound gold nanoparticles enhance radio-cytotoxic targeting of ovarian cancer. *Nanotechnology*. 22 (28).
- Gérard, C & Goldbeter, A. (2009). Temporal self-organization of the cyclin/Cdk network driving the mammalian cell cycle. *Proceedings of the National Academy of Sciences*. 106 (51), pp. 21643–21648.
- Gherardini, L., Ciuti, G., Tognarelli, S. & Cinti, C. (2014). Searching for the perfect wave: The effect of radiofrequency electromagnetic fields on cells. *International Journal of Molecular Science*. 15, pp. 5366–5387.
- Glennas, A., Kvien, T.K., Andrup, O., et al. (1997). Auranofin is safe and superior to placebo in elderly-onset rheumatoid arthritis. *British Journal of Rheumatology*. 36, pp. 870–877.
- Goodman, C.M., Mccusker, C.D., Yilmaz, T., Rotello, V.M. (2004). Toxicity of Gold Nanoparticles Functionalized with Cationic and Anionic Side Chains. *Bioconjugate Chemistry*. 15, pp. 897–900.
- Gratton, S.E.A., Ropp, P.A., Pohlhaus, P.D., et al. (2008). The effect of particle design on cellular internalization pathways. *Proceedings of the National Academic of Science of the United States of America*. 105 (33), pp. 11613–11618.
- Grodzinski, P., Silver, M. & Molnar, L.K. (2006). Nanotechnology for cancer diagnostics: promises and challenges. *Expert Review of Molecular Diagnostics*. 6, pp. 307–318.

- Hall, E.J., & Giaccia, A.J. (2006). *Radiobiology for the Radiobiologist*. 6th Edition. Lippincott Williams & Wilkins, Philadelphia.
- Hainfeld, J.F., Dilmanian, F. A., Slatkin, D.N., et al. (2008). Radiotherapy enhancement with gold nanoparticles. *Journal of Pharmacy and Pharmacology*. 60, pp. 977–985.
- Hainfeld, J.F., Slatkin, D.N., Focella, T.M. & Smilowitz, H.M. (2006). Gold nanoparticles: a new X-ray contrast agent. *The British Institute of Radiology*. 79 (939), pp. 248–253.
- Hainfeld, J.F., Slatkin, D.N. & Smilowitz, H.M. (2004). The use of gold nanoparticles to enhance radiotherapy in mice. *Physics in Medicine and Biology*. 49, pp. 309–315.
- Hashmi, G., Imtiaz, M.H. & Rafique, S. (2014). Gold Nano Particles (GNPs): An Emerging Solution of Cancer. *Universal Journal of Biomedical Engineering*. 2 (3), pp. 41–46.
- Hayat, M.A. (2013). Stem Cells and Cancer Stem Cells. Therapeutic Applications in Disease and Injury. Volume 10, p. 39.
- Heiligtag, F.J. & Niederberger, M. (2013). The fascinating world of nanoparticle research. *Materials Today*. 16, (7 – 8), pp. 262–271.
- Hernández, L., Terradas, M., Camps, J., et al. (2015). Aging and radiation: bad companions. *Aging Cell*. 14, pp. 153–161.
- Herold, D.M., Das, I.J., Stobbe, C.C., et al. (2000). Gold microspheres: a selective technique for producing biologically effective dose enhancement. *International Journal of Radiation Biology*. 76, pp. 1357–1364.
- Hess, H. & Tseng, Y. (2007). Active intracellular transport of nanopartides: opportunity or threat? *ACS Nano*. 1, pp. 390–392.

- Hill, M.A. (1999). Radiation damage to DNA: The importance of track structure. *Radiation Measurements*. 31 (1 – 6), pp. 15–23.
- Hillegas, J.M., Shukla, A., Lathrop, S.A., et al. (2010). Assessing nanotoxicity in cells in vitro. *Wiley Interdisciplinary Reviews: Nanomedicine and Nanobiotechnology*. 2 (3), pp. 219–231.
- Hochegger, H., Takeda, S. & Hunt, T. (2008). Cyclin-dependent kinases and cell-cycle transitions: does one fit all? *Nature Reviews Molecular Cell Biology*. 9, pp. 910–916.
- Howlader, N., Noone, A.M., Krapcho, M., et al. (2015). SEER Cancer Statistics Review, 1975–2012. seer.cancer.gov/csr/1975_2012/ (based on November 2014 SEER data submission). Bethesda, MD: National Cancer Institute.
- Huanga, X. & El-Sayed, M.A. (2010). Gold nanoparticles: Optical properties and implementations in cancer diagnosis and photothermal therapy. *Journal of Advanced Research*. 1, pp. 13–28.
- Huang, W.C., Tsai, P.J. & Chen, Y.C. (2007). Functional gold nanoparticles as photothermal agents for selective killing of pathogenic bacteria. *Nanomedicine*. 2 (6), pp. 395–402.
- Huang, D., Zhou, H. & Gao, J. (2015). Nanoparticles modulate autophagic effect in a dispersity-dependent manner. *Scientific Reports*. 5, pp. 1–10.
- Hudson, D., Kovalchuk, I., Koturbash, I., et al. (2011). Induction and persistence of radiation-induced DNA damage is more pronounced in young animals than in old animals. *Aging*. 3 (6), pp. 609–620.
- Hwang, A. & Muschel, R.J. (1998). Radiation and the G2 Phase of the Cell Cycle. *Radiation Research*. 150 (5), pp. S52–S59.

- Hyun, S-Y. & Jang, Y-J. (2015). p53 activates G1 checkpoint following DNA damage by doxorubicin during transient mitotic arrest. *Oncotarget*. 6 (7), pp. 4804–4815.
- Imbalzano, K.M., Tatarkova, I., Imbalzano, A.N. & Nickerson, J.A. (2009). Increasingly transformed MCF-10A cells have a progressively tumor-like phenotype in three-dimensional basement membrane culture. *Cancer Cell International*. 9 (7), pp. 1–11.
- Imoto, Y., Yoshida, Y., Yagisawa, F., et al. (2011). The cell cycle, including the mitotic cycle and organelle division cycles, as revealed by cytological observations. *Journal of Electron Microscopy*. 60 (1), pp. 117–136.
- Jackson, S.P. & Bartek, J. (2009). The DNA-damage response in human biology and disease. *Nature*. 461, pp. 1071–1078.
- Jain, S., Coulter, J.A., Hounsell, A.R., et al. (2011). Cell-Specific Radiosensitization by Gold Nanoparticles at Megavoltage Radiation Energies. *International Journal of Radiation Oncology, Biology, Physics*. 79 (2), pp. 531–539.
- Jain, S., Hirst, D.G. & O’Sullivan, J.M. (2012). Gold nanoparticles as novel agents for cancer therapy. *The British Journal of Radiology*. 85, pp. 101–113.
- Jain, M.V., Paczulla, A.M., Klonisch, T., et al. (2013). Interconnections between apoptotic, autophagic and necrotic pathways: implications for cancer therapy development. *Journal of Cellular and Molecular Medicine*. 17 (1), pp. 12–29.
- Jatoi, I., & Proschan, M.A. (2005). Randomized trials of breast-conserving therapy versus mastectomy for primary breast cancer: a pooled analysis of updated results. *American Journal of Clinical Oncology*. 28, pp. 289–294.
- Jemal, A., Bray, F., Center, M.M., et al. (2011). Global cancer statistics. *CA: A Cancer Journal for Clinicians*. 61 (2), pp. 69–90.

Jemal, A., Siegel, R., Ward, E., et al. (2009). Cancer Statistics. *CA: A Cancer Journal for Clinicians*. 59 (4), pp. 225–249.

Jia, L., Zhu, J., & Ma, Y. (2014). Stability and cytocompatibility of silk fibroin-capped gold nanoparticles. *Materials and Engineering*. 43, pp. 231–236.

Jiang, J., Huang, Z., Zhao, Q., et al. (2008). Interplay between bax, reactive oxygen species production, and cardiolipin oxidation during apoptosis. *Biochemical and Biophysical Research Communications*. 368 (1), pp. 145–150.

Jones, L.A. & Chilton, J.A. (2000). Impact of Breast Cancer on African American Women: Priority Areas for Research in the Next Decade. *American Journal of Public Health*. 92 (4), pp. 539–542.

Kattou, S., Nikopoulos, D., Vogianis, E., et al. (2014). How Safe is the Environmental Electromagnetic Radiation? *Journal of Physical Chemistry & Biophysics*. 4 (3), pp. 1–10.

Kean, W.F., Gerecz, E. & Hogan, M.G. (1987). Gold therapy II. Historical, chemical, pharmacological and biological profile of anti-arthritic gold compounds. *Singapore Medical Journal*. 28 (2), pp. 117–25.

Khan, F.M. (2003). Khan's The Physics of Radiation Therapy. 3rd Edition.

Khanna, P., Ong, C, Bay, B.H., et al. (2015). Nanotoxicity An Interplay of Oxidative Stress, Inflammation and Cell Death. *Nanomaterials*. 5, pp. 1163–1180.

Khlebtsov, N. & Dykman, L. (2011). Biodistribution and toxicity of engineered gold nanoparticles: a review of in vitro and in vivo studies. *Chemical Society Reviews*. 40, pp. 1647–1671.

- Kobayashi, H. & Brechbiel, M.W. (2005). Nano-sized MRI contrast agents with dendrimer cores. *Advanced Drug Delivery Reviews*. 57, pp. 2271–2286.
- Kodiha, M., Wang, Y.M., Hutter, E., et al. (2015). Off to the Organelles - Killing Cancer Cells with Targeted Gold Nanoparticles. *Theranostics*. 5 (4), pp. 357–370.
- Kong, T., Zeng, J., Wang, X., et al. (2008). Enhancement of radiation cytotoxicity in breast-cancer cells by localized attachment of gold nanoparticles. *Small*. 4, pp. 1537–1543.
- Krishan, A. (1975). Rapid flow cytofluorometric analysis of mammalian cell cycle by propidium iodide staining. *The Journal of Cell Biology*. 66, pp. 188–193.
- Krpetic, Z., Nativo, P., Francesca, P., et al. (2009). A multidentate peptide for stabilization and facile bioconjugation of gold nanoparticles. *Bioconjugate Chemistry*. 20, pp. 619–624.
- Kumar, R., Horikoshi, N., Singh, M., et al. (2012). Chromatin modifications and the DNA damage response to ionizing radiation. *Frontiers in Oncology*. 2 (214), pp. 1–9.
- Kumar, N. & Kumbhat, S. (2016). Essentials in Nanoscience and Nanotechnology. Available from: <https://books.google.co.za/books?isbn=1119096138>.
- Kwatra, D., Venugopal, A. & Anant, S. (2013). Nanoparticles in radiation therapy: a summary of various approaches to enhance radiosensitization in cancer. *Translational Cancer Research*. 2 (4), pp. 330–342.
- LaTorre Travis, E. (1989). Primer of Medical Radiobiology. Mosby-Year Book, Inc., St Louis, 2nd Edition.

- Lee, A.V., Oesterreich, S. & Davidson, N.E. (2015). MCF-7 Cells—Changing the Course of Breast Cancer Research and Care for 45 Years. *Journal of the National Cancer Institute*. 107 (7), pp. 1–4.
- Lehnert, S. (2008). *Biomolecular Action of Ionizing Radiation*. Taylor and Francis group, New York.
- Lesniak, A., Salvati, A., Santos-Martinez, M.J. (2012). Nanoparticle Adhesion to the Cell Membrane and Its Effect on Nanoparticle Uptake Efficiency. *Journal of American Chemical Society*. pp. A–G.
- Li, L., Story, M. & Legerski, R.J. (2001). Cellular responses to ionizing radiation damage. *International Journal of Radiation Oncology, Biology, Physics*. 49 (4), pp. 1157–1162.
- Lim, E.K., Jang, E., Le, K., et al. (2013). Delivery of Cancer Therapeutics Using Nanotechnology. *Pharmaceutics*. 5 (2), pp. 294–317.
- Lim, S. & Kaldis, P. (2013). Cdks, cyclins and CKIs: roles beyond cell cycle regulation. *Development*. 140 (15), pp. 3079–3093.
- Lim, Z-Z. J., Li, J-E. J., et al. (2011). Gold nanoparticles in cancer therapy. *Acta Pharmacologica Sinica*. 32, pp. 983–990.
- Lindqvist, A., Rodriguez-Bravo, V. & Medema, R.H. (2009). The decision to enter mitosis: feedback and redundancy in the mitotic entry network. *The Journal of Cellular Biology*. 185 (2), pp. 193–202.
- Litieri, S., Werutsky, G., Fentiman, I.S., et al. (2012). Breast conserving therapy versus mastectomy for stage I-II breast cancer: 20 year follow-up of the EORTC 10801 phase 3 randomised trial. *The Lancet Oncology*. 13, pp. 412–419.

- Liu, Z., Wu, Y., Guo, Z., et al. (2014) Effects of Internalized Gold Nanoparticles with Respect to Cytotoxicity and Invasion Activity in Lung Cancer Cells. *PLOS ONE*. 9 (6).
- Logan, T. & Ly, M. (2013). Gold Nanoparticle Interaction with Cell Membranes. *Worcester Polytechnic Institute*. pp. 1–102.
- Loveland, W.D., Morrissey, D.J. & Seaborg, G.T. (2006). Interaction of Radiation with Matter. *Modern Nuclear Chemistry*. pp. 497–535.
- Luciani, N., Gazeau, F. & Wilhelm, C. (2009). Reactivity of the monocyte/macrophage system to superparamagnetic anionic nanoparticles. *Journal of Materials Chemistry*. 19, pp. 6373–6380.
- Maeda, H. (2010). Tumor-selective delivery of macromolecular drugs via the EPR effect: background and future prospects. *Bioconjugate Chemistry*. 21, pp. 797–802.
- Maeda, H., Wu, J., Sawa, T. et al. (2000). Tumor vascular permeability and the EPR effect in macromolecular therapeutics: a review. *Journal of Control Release*. 65, pp. 271–284.
- Malam, Y., Loizidou, M. & Seifalian, A.M. (2009). Liposomes and nanoparticles: nanosized vehicles for drug delivery in cancer. *Trends in pharmacological sciences*. 30 (11), pp. 592–599.
- Murray, P.J., Cornelissen, B., Vallis, R.A., et al (2016). DNA double-strand break repair: a theoretical framework and its application. *Journal of the Royal Society*. 13 (114), pp. 1–11.
- Matsudaira, H., Ueno, A.M., Furuno, I. (1980). Iodine contrast medium sensitizes cultured mammalian cells to X rays but not to gamma rays. *Radiation Research*. 84 (1), pp. 144–148.

- McFarland, A.D., Haynes, C.L., Mirkin, C.A., et al. (2004). Color My Nanoworld. *Journal of Chemical Education*. 81 (4), p. 544.
- McGuire, K.P., Santillan, A.A., Kaur, P., et al. (2009). Are mastectomies on the rise? A 13-year trend analysis of the selection of mastectomy versus breast conservation therapy in 5865 patients. *The Annals of Surgical Oncology*. 16, pp. 2682–2690.
- McLean, J.R., Chaix, D., Ohi, M.D. & Gould, K.L. (2011). State of the APC/C: organization, function, and structure. *Critical Reviews in Biochemistry and Molecular Biology*. 46 (2), pp. 118–136.
- Medema, R.H. & Macurek, L. (2012). Checkpoint control and cancer. *Oncogene*. 31, pp. 2601–2613.
- Medina, L.A., et al. (2008). Use of an orthovoltage X-ray treatment unit as a radiation research system in a small-animal cancer model. *Journal of Experimental & Clinical Cancer Research*. 27 (57), pp. 1–11.
- Mello, R.S., Callisen, H., Winter, J., et al. (1983). Radiation dose enhancement in tumors with iodine. *Medical Physics*. 10, pp. 75–78.
- Mesa, A.V., Norman, A., Solberg, T.D., et al. (1999). Dose distributions using kilovoltage x-rays and dose enhancement from iodine contrast agents. *Physics in Medicine and Biology*. 44, pp. 1955–1968.
- Mesbahi, A. (2010). A review on gold nanoparticles radiosensitization effect in radiation therapy of cancer. *Reports of Practical Oncology & Radiotherapy*. 15 (6), pp. 176–180.
- Meunier, S. & Vernos, I. (2012). Microtubule assembly during mitosis – from distinct origins to distinct functions? *Journal of Cell Science*. 125, pp. 2805–2814.

- Michalet, X., Pinaud, F.F., Bentolila, L.A., Tsay, J.M, et al. (2005). Quantum Dots for Live Cells, in Vivo Imaging, and Diagnostics. *Science*. 307 (5709), pp. 538–544.
- Miller, K.D., Siegel, R.L., Lin, C.C., et al. (2016). Cancer treatment and survivorship statistics, 2016. *CA: A Cancer Journal for Clinicians*. 66 (4), pp. 271–289.
- Mizushima, N. & Komatsu, M. (2011). Autophagy: Renovation of cells and tissues. *Cell*. 147, pp. 728–741.
- Monopoli, M.P., Aberg, C., Salvati, A. & Dawson, R.A. (2012). Biomolecular coronas provide the biological identity of nanosized materials. *Nature Nanotechnology*. 7 (12), pp. 779–786.
- Mombach, J.C.M., Bugs, C.A. & Chaouiya, C. (2014). Modelling the onset of senescence at the G1/S cell cycle checkpoint. *BMC Genomics*. 15 (7), pp. 1–11.
- Morhason-Bello, I. O., Odedina, F., Rebbeck, T., et al. (2013). Challenges and opportunities in cancer control in Africa: a perspective from the African Organisation for Research and Training in Cancer. *The Lancet Oncology*. 14 (4), pp. 142–151.
- Mousavie Anijdan, S.H., Shirazim, A., Mahdavi, S.R. (2012). Megavoltage dose enhancement of gold nanoparticles for different geometric set-ups: Measurements and Monte Carlo simulation. *International Journal of Radiation Research*. 10, (3–4), pp. 183–186.
- Murrow, L. & Debnath, J. (2013). Autophagy as a stress-response and quality-control mechanism: Implications for cell injury and human disease. *Annual Review of Pathology: Mechanisms of Disease*. 8, pp. 105–137.
- National Cancer Institute. (2014). *Prophylactic Mastectomy*. Available from: www.breastcancer.org/treatment/surgery/prophylactic-mast.

- Neshatian, M., Chung, S, Yohan, D., et al. (2014). Determining the Size Dependence of Colloidal Gold Nanoparticle Uptake in a Tumor-like Interface (Hypoxic). *Colloids and Interface Science Communications*. 1, pp. 57–61.
- Neuberger, T., Schöpf, B., Hofmann, H., et al. (2005). Superparamagnetic nanoparticles for biomedical applications: Possibilities and limitations of a new drug delivery system. *Journal of Magnetism and Magnetic Materials*. 293 (1), pp. 483–496.
- Ngwa, W., Kumar, R., Sridhar, S., et al. (2014). Targeted radiotherapy with gold nanoparticles: current status and future perspectives. *Nanomedicine*. 9 (7), pp. 1063–1082.
- Niederhuber, J.E., Armitage, J.O., Dorrshow, J.H., et al. (2013). *Abeloff's Clinical Oncology*. 5th Edition.
- Nishitani, H., Taraviras, S., Lygerou, Z. & Nishimoto, T. (2001). The human licensing factor for DNA replication Cdt1 accumulates in G1 and is destabilized after initiation of S-phase. *The Journal of Biological Chemistry*. 276, pp. 44905–44911.
- Nurse, P. (1994). Ordeing S phase and M phase in the cell cycle. *Cell*. 79 (4), pp. 547–550.
- Oberdörster, G. (2010). Safety assessment for nanotechnology and nanomedicine: Concepts of nanotoxicology. *Journal of International Medicine*. 267, pp. 89–105.
- Oh, N. & Park, J-H. (2014). Endocytosis and exocytosis of nanoparticles in mammalian cells. *International Journal of Nanomedicine*. 9 (1), pp. 51–63.
- Olive, P.L. & Banath, J.P. (2004). Phosphorylation of histone H2AX as a measure of radiosensitivity. *International Journal of Radiation Oncology, Biology, Physics*. 58 (2), pp. 331–335.

- Ouyang, L., Shi, Z., Zhao, S., et al. (2012). Programmed cell death pathways in cancer: a review of apoptosis, autophagy and programmed necrosis. *Cell Proliferation*. 45, pp. 487–498.
- Qu, Y., Han, B., Yu, Y., et al. (2015). Evaluation of MCF-10A as a Reliable Model for Normal Human Mammary Epithelial Cells. *PLoS ONE*. 10 (7).
- Pamiés, R., Hernández Cifre, J.G., Fernández Espín, V., et al. (2014). Aggregation behaviour of gold nanoparticles in saline aqueous media. *Journal of Nanoparticle Research*. 16 (2376), pp. 1–11.
- Pan, Y.S., Neuss, A., Leifert, M. et al. (2007). Size-dependent cytotoxicity of gold nanoparticles. *Small*. 3, pp. 1941–1949.
- Panchangam, R.B.S & Dutta, S. (2015). Engineered Nanoparticles for the Delivery of Anticancer Therapeutics. *Journal of Pharmaceutics & Drug Delivery Research*. 4 (1), pp. 1–16.
- Panyala, N.R., Pena-Mendez, E.M. & Havel, J. (2009). Gold and nano-gold in medicine: overview, toxicology and perspectives. *Journal of Applied Medicine*. 7 (2), pp. 75–91.
- Park, Y.S., Liz-Marzán, L.M., Kasuya, A., et al. (2006). X-ray absorption of gold nanoparticles with thin silica shell. *Journal of Nanoscience and Nanotechnology*. 6, pp. 3503–3506.
- Patra, H.K., Banerjee, S., Chaudhuri, U., et al. (2007). Cell selective response to gold nanoparticles. *Nanomedicine: nanotechnology, biology and medicine*. 3 (2), pp. 111–119.



- Paunescu, V., Bojin, F.M., Gavriiliuc, O.I., et al. (2014). Enucleation: a possible mechanism of cancer cell death. *Journal of Cellular and Molecular Medicine*. 18 (6), pp. 962–965.
- Pawlik, T. & Keyomarsi, K. (2004). Role of Cell Cycle in Mediating Sensitivity to Radiotherapy. *International Journal of Radiation Oncology, Biology and Physics*. 59 (4), pp. 928–942.
- Peng, T.I & Jou, M.J. (2004). Mitochondrial swelling and generation of reactive oxygen species induced by photoirradiation are heterogeneously distributed. *Annals of the New York Academy of Sciences*. 1011, pp. 112–122.
- Peng, X., Qi, W., Huang, R. et al. (2015). Elucidating the Influence of Gold Nanoparticles on the Binding of Salvianolic Acid B and Rosmarinic Acid to Bovine Serum Albumin. *PLoS ONE*. pp. 1–23.
- Pernodet, N., Fang, X., Sun, Y., et al. (2006). Adverse effects of citrate/gold nanoparticles on human dermal fibroblasts. *Small*. 2, pp. 766–773.
- Peynshaert, K., Manshian, B.B., Joris, F., et al. (2014). Exploiting intrinsic nanoparticle toxicity: The pros and cons of nanoparticle-induced autophagy in biomedical research. *Chemical Reviews*. 114, pp. 7581–7609.
- Pivodová, V., Franková, J., Galandáková, A., et al. (2015) *In Vitro* AuNPs' Cytotoxicity and Their Effect on Wound Healing. *Nanobiomedicine*. 2 (7), pp. 1–7.
- Podhorecka, M., et al. (2010). H2AX Phosphorylation: Its Role in DNA Damage Response and Cancer Therapy. *Journal of Nucleic Acids*. pp. 1–9.
- Praetorius, N.P. & Mandal, T.K. (2007). Engineered nanoparticles in cancer therapy. *Recent Patents on Drug Delivery & Formulation*. 1, pp. 37–51.

- Preethi, P.S, Suganya, M., Suganya, K. & Nanthini, U.R. (2016). METAL NANOPARTICLES - PAST TO PRESENT. *International Journal of Pharmaceutical Sciences and Business Management*. 4 (6), pp. 1–6.
- Prise, K.M., Folkard, M., Newman, H.C. & Michael, B.D. (1994). Effect of radiation quality on lesion complexity in cellular DNA. *International Journal of Radiation Biology*. 66 (5), pp. 537–542.
- Rahman, W.N., Bishara, N., Ackerly, T., et al. (2009). Enhancement of radiation effects by gold nanoparticles for superficial radiation therapy. *Nanomedicine: Nanotechnology, Biology, and Medicine*. 5, pp. 136–142.
- Raviraj, J., Bokkasam, V.K., Kumar, V.S., et al. (2014). Radiosensitizers, radioprotectors, and radiation mitigators. *Indian Journal of Dental Research*. 25 (1), pp. 83–90.
- Retif, P., Pinel, S., Toussaint, M., et al. (2015). Nanoparticles for Radiation Therapy Enhancement: the Key Parameters. *Theranostics*. 5 (9), pp. 1030–1044.
- Rhind, N., & Russell, P. (2012). Signaling Pathways that Regulate Cell Division. *Cold Spring Harbor Perspectives in Biology*. 4 (10), pp. 1–15.
- Rialland, M., Sola, F. & Santocanale, C (2002). Essential role of human CDT1 in DNA replication and chromatin licensing. *Journal of Cell Science*. 115, pp. 1435–1440.
- Riss, T.L., Moravec, R.A., Niles, A.L., et al. (2013). Cell Viability Assays. [Updated 2016 Jul 1]. In: Sittampalam GS, Coussens NP, Brimacombe K, et al., editors. Assay Guidance Manual [Internet]. Bethesda (MD): Eli Lilly & Company and the National Center for Advancing Translational Sciences; 2004-. Available from: <https://www.ncbi.nlm.nih.gov/books/NBK144065/>.
- Roa, W., Zhang, X., Guo, L., et al. (2009). Gold nanoparticle sensitize radiotherapy of prostate cancer cells by regulation of the cell cycle. *Nanotechnology*. 20, pp. 1–10.

- Robar, J.L., Riccio, S.A. & Martin, M.A. (2002). Tumour dose enhancement using modified megavoltage photon beams and contrast media. *Physics in Medicine and Biology*. 47, pp. 2433–2449.
- Robertson, D.J. Stukel, T.A., Gottlieb, D.J., et al. (2009). Survival after hepatic resection of colorectal cancer metastases: a national experience. *Cancer*. 115, 752–759.
- Rohiman, A., Anshri, I., Surawijaya, A. & Idris, I. (2011). Study of Colloidal Gold Synthesis Using Turkevich Method. *Academic Journal. AIP Conference Proceedings*. 1415, (39).
- Ryan, J.A., Overton, K.W., Speight, M.E. et al. (2007). Cellular uptake of gold nanoparticles passivated with BSA-SV40 large T antigen conjugates. *Analytical Chemistry*. 79, pp. 9150–9159.
- Saberi, A., et al. (2016). Gold nanoparticles in combination with megavoltage radiation energy increased radiosensitization and apoptosis in colon cancer HT-29 cells. *International Journal of Radiation Biology*. 92 (11), pp. 1–9.
- Sacristan, C. & Kops, G.J. (2015). Joined at the hip: kinetochores, microtubules, and spindle assembly checkpoint signaling. *Trends in Cell Biology*. 25 (1), pp. 21–28.
- Sahoo, S.K., Parveen, S. & Panda, J.J. (2007). The present and future of nanotechnology in human health care. *Nanomedicine*. 3, pp. 20–31.
- Salaberria, C., Muriel, J., De Luna, M., et al. (2013). The PHA Test as an Indicator of Phagocytic Activity in a Passerine Bird. *PLoS ONE*. 8 (12), pp. 1–7.
- Sanford, K.K. & Parshad, R. (1999). The contribution of deficient DNA repair to chromosomal radiosensitivity of CHO cells after G2 irradiation *Cancer Genet. Cytogenetics*. 108, pp. 38–41.
- Saqcena, M. (2014). Metabolic Checkpoints in Cancer Cell Cycle. *CUNY Academic Works*.

- Schaeublin, N.M., Braydich-Stolle, L.K., Schrand, A.M. et al. (2011). Surface charge of gold nanoparticles mediates mechanism of toxicity. *Nanoscale*. 3, pp. 410–420.
- Schlebusch, C.M., Dreyer, G., Sluiter, M.D. (2010). Cancer prevalence in 129 breast-ovarian cancer families tested for BRCA1 and BRCA2 mutations. *South African Medical Journal*. 100 (2), pp. 113–117.
- Shaw, I.C. (1999). Gold-based therapeutic agents. *Chemical Reviews*. 99 (9), pp. 2589–2600.
- Shedbalkar, U., Singh, R., Wadhvani, S., et al. (2014). Microbial synthesis of gold nanoparticles: Current status and future prospects. *Advances in Colloid and Interface Science*. 209, pp. 40–48.
- Sherr, C.J. (1994). G1 phase progression: cycling on cue. *Cell*. 79 (4), pp. 551–555.
- Sherr C.J., Roberts J.M. (1999). CDK inhibitors: positive and negative regulators of G1 phase progression. *Genes & Development*. 13, pp. 1501–1512.
- Shukla, R., Bansal, V., Chaudhary, M. et al. (2005). Biocompatibility of gold nanoparticles and their endocytotic fate inside the cellular compartment: A microscopic overview. *Langmuir: The ACS Journal of Surfaces and Colloids*. 21, pp. 10644–10654.
- Siegel, R.L., Miller, K.D. & Jemal, A. (2016). Cancer statistics, 2016. *CA: A Cancer Journal for Clinicians*. 66 (1), pp. 7–30.
- Silver, D.P. & Livingston, D.M. (2012). Mechanisms of BRCA 1 Tumor Suppression. *Cancer Discovery*. 2 (8), pp. 679–684.
- Spiers, F.W. (1949). The influence of energy absorption and electron range on dosage in irradiated bone. *British Journal of Radiology*. 22 (261), pp. 521–533.

- Söderstjerna, E., Bauer, P., Cedervall, T., et al. (2014). Silver and Gold Nanoparticles Exposure to In Vitro Cultured Retina – Studies on Nanoparticle Internalization, Apoptosis, Oxidative Stress, Glial- and Microglial Activity. *PLoS ONE*. 9 (8), pp. 1–16.
- Soenen, S.J., Rivera-Gil, P., Montenegro, J-M., et al. (2011). Cellular toxicity of inorganic nanoparticles: Common aspects and guidelines for improved nanotoxicity evaluation. *Nanotoday*. 6, pp. 446–465.
- Sonavan, G., Tomado, K., Makino, K. (2008). Biodistribution of colloidal gold nanoparticles after intravenous administration: effect of particle size. *Colloids Surface B Biointerfaces*. 66 (2), pp. 274–280.
- Sorensen, C.S. & Syljuasen, R.G. (2012). Safeguarding genome integrity: the checkpoint kinases ATR, CHK1 and WEE1 restrain CDK activity during normal DNA replication. *Nucleic Acids Research*. 40, pp. 477–486.
- Soria, G. & Gottifredi, V. (2010). PCNA-coupled p21 degradation after DNA damage: The exception that confirms the rule? *DNA Repair (Amst)*. 9, pp. 358–336.
- Soule, B.P., Simone, N.L., DeGraff, W.G., et al. (2010). Loratadine dysregulates cell cycle progression and enhances the effect of radiation in human tumor cell lines. *Radiation Oncology*. 5 (8), pp. 1–12.
- Steiner, O., Coisne, C., Engelhardt, B. & Lyck, R. (2011). Comparison of immortalized bEnd5 and primary mouse brain microvascular endothelial cells as in vitro blood–brain barrier models for the study of T cell extravasation. *Journal of Cerebral Blood Flow & Metabolism*. 31 (1), pp. 315–327.
- Stern, S., Adisheshaiah, P. & Crist, R. (2012). Autophagy and lysosomal dysfunction as emerging mechanisms of nanomaterial toxicity. *Particle & Fibre Toxicology*. 9, pp. 1–20.

- Strober, W. (2001). Trypan blue exclusion test of viability. *Current Protocols in Immunology*. Appendix 3.
- Su, X.Y., Liu, P.D., Wu, H. & Gu, N. (2014). Enhancement of radiosensitization by metal-based nanoparticles in cancer radiation therapy. *Cancer Biology & Medicine*. 11 (2), pp. 86–91.
- Surveillance, Epidemiology, and End Results (SEER) Program. SEER cancer Statistics Review (2013). [Online]. Available from: www.seer.cancer.gov/statfacts/html/breast/html.
- Suryadinata, R., Sadowski, M. & Sarcevic, B. (2010). Control of cell cycle progression by phosphorylation of cyclin-dependent kinase (CDK) substrates. *Bioscience Reports*. 30 (4), pp. 243–255.
- Taggart, L.E., McMahon, S.J., Currell, F.J., et al. (2014). The role of mitochondrial function in gold nanoparticle mediated radiosensitisation. *Cancer Nanotechnology*. 5 (5), pp. 1–12.
- Tartier, L., Gilchrist, S., Burdak-Rothkamm, S., et al. (2007). Cytoplasmic irradiation induces mitochondrial-dependent 53BP1 protein relocalization in irradiated and bystander cells. *Cancer Research*. 67 (12), pp. 5872–5879.
- Teyssier, F., Bay, J.O, Dionet, C. & Verrelle, P. (1999). Cell cycle regulation after exposure to ionizing radiation. *Bulletin du cancer*. 86 (4), pp. 345–357.
- Tiwari, B.S., Belenghi, B., & Levine, A. (2002). Oxidative Stress Increased Respiration and Generation of Reactive Oxygen Species, Resulting in ATP Depletion, Opening of Mitochondrial Permeability Transition, and Programmed Cell Death. *Plant Physiology*. 128 (4), pp. 1271–1281.

- Tiwari, P.M., Vig, K., Dennis, V.A. & Singh, S.R. (2011). Functionalized Gold Nanoparticles and Their Biomedical Applications. *Nanomaterials*. 1 (1), pp. 31–63.
- Torres-Chavolla, E., Ranasinghe, R.J. & Alocilja, E.C. (2010). Characterization and Functionalization of Biogenic. *IEEE Transactions On Nanotechnology*. pp. 533–538.
- Turkevich, J., Stevenson, P.C. & Hillier, J. (1951). A study of the nucleation and growth processes in the synthesis of colloidal gold. *Discuss Faraday Society*. 11, pp. 55–75.
- Tyner, A.L. (2009). A new year, a new role for p21. *Cell Cycle*. 8 (2), pp. 183–184.
- Vandersickel, V. et al. (2010). The radiosensitizing effect of Ku70/80 knockdown in MCF-10A cells irradiated with X-rays and p(66)+Be(49) neutrons. *Radiation Oncology*. 5 (1), p. 30.
- Vandevoorde, C., Vral, A., Vandekerckhove, B. et al. (2016). Radiation Sensitivity of Human CD34+ Cells Versus Peripheral Blood T Lymphocytes of Newborns and Adults: DNA Repair and Mutagenic Effects. *Radiation Research*. 185 (6), pp. 580–590.
- Vecchio, G., Galeone, A., Brunetti, V., et al. (2012). Concentration-Dependent, Size-Independent Toxicity of Citrate Capped AuNPs in *Drosophila melanogaster*. *PLoS ONE*. 1 (7), pp. 1–11.
- Verma, H.N., Singh, P. & Chavan, R.M. (2014). Gold nanoparticles: synthesis and characterization. *Veterinary World*. 7 (2), pp. 72–77.
- Vignard, J., Mirey, G. Salles, B. (2013). Ionizing-radiation induced DNA double-strand breaks: A direct and indirect lighting up. *Radiotherapy and Oncology*. 108 (3), pp. 362–369.

- Vijayakumar, S. & Ganesan, S. (2012). In Vitro cytotoxicity assay on gold nanoparticles with different stabilizing agents. *Journal of Nanomaterials*. pp. 1–9.
- Vona-Davis, L. & Rose, D.P. (2009). The influence of socioeconomic disparities on breast cancer tumor biology and prognosis: a review. *Journal of Women's Health (Larchmt)*. 18, pp. 883–893.
- Vral, A., Fenech, M. & Thierens, H. (2011). The micronucleus assay as a biological dosimeter of in vivo ionising radiation exposure. *Mutagenesis*. 26 (1), pp.11–17.
- Vujacic, A., et al. (2011). Particle Size and Concentration Dependent Cytotootoxicity of Citrate Capped Gold Nanoparticle. *Digest Journal of Nanomaterials and Biostructures*. 6 (3), pp. 1367–1376.
- Wang, S., Lawson, R., Ray, P.C. & Yu, H. (2011). Toxic effects of gold nanoparticles on *Salmonella typhimurium* bacteria. *Toxicity and Industrial Health*. pp. 547–554.
- Wang, P., Wang, X., Wang, L., et al. (2015). Interaction of gold nanoparticles with proteins and cells. *Science and Technology of Advanced Materials*. 16, pp. 1–15.
- Wang, Y., Yang, F., Zhang, H-X., et al. (2013). Cuprous oxide nanoparticles inhibit the growth and metastasis of melanoma by targeting mitochondria. *Cell Death and Disease*. 4, pp. 1–10.
- Welsh, P.L. & King, M. (2001). BRCA 1 and BRCA 2 and the genetics of breast and ovarian cancer. *Human Molecular Genetics*. 10 (7), pp. 705–713.
- Wiwanitkit, V., Sereemasun, A. & Rojanathanes, R. (2009). Identification of gold nanoparticle in lymphocytes: a confirmation of direct intracellular penetration effect. *Turkish Journal of Hematology*. 26, pp. 29–30.

Wolfe, T., Chatterjee, D., Lee, J., et al. (2015). Targeted Gold Nanoparticles Enhance Sensitization of Prostate Tumors to Megavoltage Radiation Therapy *in vivo*. *Nanomedicine*. 11 (5), pp. 1277–1283.

World Health Organization (WHO). (2008). The Global Burden of Disease: 2004 Update. Geneva: WHO; 2008.

Xiang, S. & Zhang, X. (2013). Cellular Uptake Mechanism of Non-Viral Gene Delivery and Means for Improving Transfection Efficiency. *Gene Therapy - Tools and Potential Applications. Chapter 4*. pp. 71–90.

Yah, C.S. (2013). The toxicity of Gold Nanoparticles in relation to their physiochemical properties. *Biomedical Research*. 24 (3), pp. 400–413.

Yen, H.J., Hsu, S.H. & Tsai, C.L. (2009). Cytotoxicity and immunological response of gold and silver nanoparticles of different sizes. *Small*. 5, pp. 1553–1561.

Yildirimer, L., Thanh, N.T.K., Loizidou, M., et al. (2011). Toxicological considerations of clinically applicable nanoparticles. *Nanotoday*. 6 (6), pp. 585–607.

Yoon, D.S., Wersto, R.P., Zhou, W., et al. (2002). Variable levels of chromosomal instability and mitotic spindle checkpoint defects in breast cancer. *The American Journal of Pathology*. 161, pp. 391–397.

Yu, Y.P., Mahaney, B.L., Yano, K.I., et al. (2008). DNA-PK and ATM phosphorylation sites in XLF/cernunnos are not required for repair of DNA double strand breaks. *DNA Repair*. 7 (10), pp. 1680–1692.

Yu, Y.P., Wang, W., Ding, Q., et al. (2003). DNA-PK phosphorylation sites in XRCC4 are not required for survival after radiation or for v(d)j recombination. *DNA Repair*. 2 (11), pp. 1239–1252.

- Yukihara, E.G. & McKeever, S.W.S. (2011). *Optically Stimulated Luminescence: Fundamentals and Applications*. John Wiley & Sons Ltd, United Kingdom.
- Zhanga, X., Menga, L., Lua, Q., et al. (2009). Targeted delivery and controlled release of doxorubicin to cancer cells using modified single wall carbon nanotubes. *Biomaterials*. 30 (30), pp. 6041–6047.
- Zhang, X.D., Wu, D., Shen, X., et al. (2011). Size-dependent in vivo toxicity of PEG-coated gold nanoparticles. *International Journal of Nanomedicine*, 6, pp. 2071–2081.
- Zhang, Y., Xu, D., Li, W., et al. (2012). Effect of Size, Shape, and Surface Modification on Cytotoxicity of Gold Nanoparticles to Human HEp-2 and Canine MDCK Cells. *Journal of Nanomaterials*. pp. 1–7.
- Zhao, F., Zhao, Y., Liu, Y. (2011). Cellular uptake, intracellular trafficking, and cytotoxicity of nanomaterials. *Small*. 7 (10), pp. 1322–1337.
- Zhou, J., Ralston, J., Sedev, R., & Beattie, D. (2009). Functionalized gold nanoparticles: synthesis, structure and colloid stability. *Journal of Colloid and Interface Stability*. 331, pp. 251–262.
- Zhu, C-D., Zheng, Q., Wang, L-X., et al. (2015). Synthesis of novel galactose functionalized gold nanoparticles and its radiosensitizing mechanism. *Journal of Nanobiotechnology*. 13 (67), pp. 1–11.
- Zorov, D.B., Juhaszova, M., & Sollott, S.J. (2014). Mitochondrial Reactive Oxygen Species (ROS) and ROS-Induced ROS Release. *Physiological Reviews*. 94 (3), pp. 909–950.

ADDENDUM

<p style="text-align: right;">A</p> <p>Expert Advice v2.0</p> <p>Malvern Instruments Ltd - © Copyright 2008</p> <hr/> <p>Zeta potential measurements ----- Distribution data good.</p>	
<p>Expert Advice v2.0</p> <p>Malvern Instruments Ltd - © Copyright 2008</p> <hr/> <p>Zeta potential measurements ----- Distribution data poor - increase number of sub runs per measurement. Flare from cell wall - check for bubbles, increase sample concentration.</p>	 

Figure 5.1: Expert advice for the zeta potential measurements of AuNPs using Malvern Instruments' Zetasizer Nano ZS. (A) represents the 5 nm AuNPs and (B) the 10 nm AuNPs.

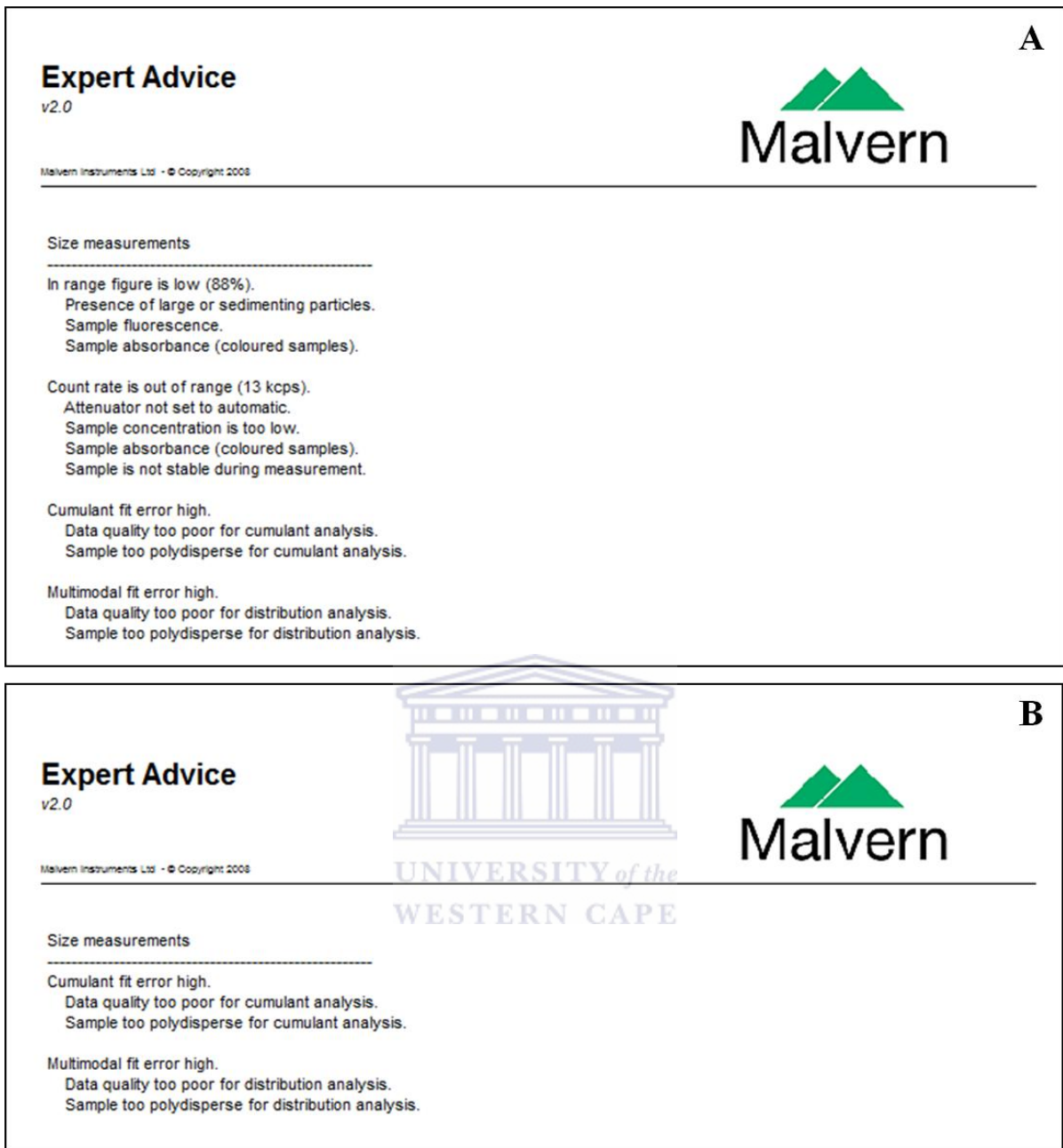


Figure 5.2: Expert advice for the size measurements of AuNPs using Malvern Instruments' Zetasizer Nano ZS. (A) represents the 5 nm AuNPS and (B) the 10 nm AuNPs.

Table 5.3: Average number of foci per isolated human lymphocytes incubated with 50 µg/ml AuNPs for 4 hours. Kruskal-Wallis test was used to determine the significant difference between the control means and experimental groups.

Data	Mean no. of foci cell
Factor codes	AuNPs
Sample size	78
Test statistic	68,3632
Corrected for ties Ht	68,3649
Degrees of Freedom (DF)	8
Significance level	$P < 0,000001$

Factor	n	Average Rank	Different ($P < 0,05$) from factor nr
(1) 1	11	7,77	(2)(3)(4)(5)(6)(7)(8)(9)
(2) 2	16	22,28	(1)(3)(4)(5)(6)(7)(8)(9)
(3) 3	13	29,62	(1)(2)(4)(5)(6)(8)(9)
(4) 4	11	48,82	(1)(2)(3)(5)(6)(8)(9)
(5) 5	12	62,42	(1)(2)(3)(4)(7)
(6) 6	9	68,44	(1)(2)(3)(4)(7)
(7) 7	2	41,50	(1)(2)(5)(6)(8)(9)
(8) 8	2	61,50	(1)(2)(3)(4)(7)
(9) 9	2	73,00	(1)(2)(3)(4)(7)

Table 5.4: % of cell viability in CHO-K1 cells incubated with 50 µg/ml AuNPs for 4 hours. Kruskal-Wallis test was used to determine the significant difference between the control means and experimental groups.

Data	% Proliferation
Factor codes	AuNPs
Sample size	27
Test statistic	18,3704
Corrected for ties Ht	18,5059
Degrees of Freedom (DF)	8
Significance level	$P = 0,017737$

Factor	n	Average Rank	Different ($P < 0,05$) from factor nr
(1) 1	3	18,00	(5)(8)(9)
(2) 2	3	16,67	(5)(9)
(3) 3	3	20,33	(5)(8)(9)
(4) 4	3	19,00	(5)(8)(9)
(5) 5	3	4,00	(1)(2)(3)(4)(6)(7)
(6) 6	3	18,67	(5)(8)(9)
(7) 7	3	18,33	(5)(8)(9)
(8) 8	3	8,00	(1)(3)(4)(6)(7)
(9) 9	3	3,00	(1)(2)(3)(4)(6)(7)

Table 5.5: % of cell viability in CHO-K1 cells incubated with 50 µg/ml AuNPs for 4 hours followed by 4 Gy X-ray radiation. Kruskal-Wallis test was used to determine the significant difference between the control means and experimental groups.

Data	% Proliferation
Factor codes	AuNPs
Sample size	27
Test statistic	16,1376
Corrected for ties Ht	16,3219
Degrees of Freedom (DF)	8
Significance level	P = 0,037998

Factor	n	Average Rank	Different (P<0,05) from factor nr
(1) 1	3	18,50	(5)(9)
(2) 2	3	22,00	(5)(9)
(3) 3	3	15,33	(5)(9)
(4) 4	3	17,50	(5)(9)
(5) 5	3	5,00	(1)(2)(3)(4)(6)(8)
(6) 6	3	16,67	(5)(9)
(7) 7	3	12,50	(9)
(8) 8	3	16,50	(5)(9)
(9) 9	3	2,00	(1)(2)(3)(4)(6)(7)(8)

Table 5.6: % of cell viability in CHO-K1 cells incubated with 50 µg/ml AuNPs for 24 hours. Kruskal-Wallis test was used to determine the significant difference between the control means and experimental groups.

Data	% Proliferation
Factor codes	AuNPs
Sample size	27
Test statistic	21,7169
Corrected for ties Ht	21,7968
Degrees of Freedom (DF)	8
Significance level	P = 0,005307

Factor	n	Average Rank	Different (P<0,05) from factor nr
(1) 1	3	23,50	(3)(4)(5)(7)(8)(9)
(2) 2	3	20,17	(4)(5)(8)(9)
(3) 3	3	16,50	(1)(5)(8)(9)
(4) 4	3	13,17	(1)(2)(5)(6)(9)
(5) 5	3	4,50	(1)(2)(3)(4)(6)(7)
(6) 6	3	22,33	(4)(5)(7)(8)(9)
(7) 7	3	14,67	(1)(5)(6)(9)
(8) 8	3	8,67	(1)(2)(3)(6)
(9) 9	3	2,50	(1)(2)(3)(4)(6)(7)

Table 5.7: % of cell viability in BEnd5 cells incubated with 50 µg/ml AuNPs for 4 hours. Kruskal-Wallis test was used to determine the significant difference between the control means and experimental groups.

Data	% Proliferation
Factor codes	AuNPs
Sample size	27
Test statistic	23,0476
Corrected for ties Ht	23,1040
Degrees of Freedom (DF)	8
Significance level	P = 0,003233

Factor	n	Average Rank	Different (P<0,05) from factor nr
(1) 1	3	12,00	(2)(3)(4)(5)(9)
(2) 2	3	22,67	(1)(5)(6)(7)(8)(9)
(3) 3	3	21,67	(1)(5)(6)(7)(8)(9)
(4) 4	3	24,33	(1)(5)(6)(7)(8)(9)
(5) 5	3	5,00	(1)(2)(3)(4)(7)(8)
(6) 6	3	10,33	(2)(3)(4)(9)
(7) 7	3	14,67	(2)(3)(4)(5)(9)
(8) 8	3	13,33	(2)(3)(4)(5)(9)
(9) 9	3	2,00	(1)(2)(3)(4)(6)(7)(8)

Table 5.8: % of cell viability in BEnd5 cells incubated with 50 µg/ml AuNPs for 4 hours followed by 4 Gy X-ray radiation. Kruskal-Wallis test was used to determine the significant difference between the control means and experimental groups.

Data	% Proliferation
Factor codes	AuNPs
Sample size	27
Test statistic	16,2275
Corrected for ties Ht	16,2573
Degrees of Freedom (DF)	8
Significance level	P = 0,038842

Factor	n	Average Rank	Different (P<0,05) from factor nr
(1) 1	3	13,00	(9)
(2) 2	3	18,50	(5)(9)
(3) 3	3	20,83	(5)(9)
(4) 4	3	17,67	(5)(9)
(5) 5	3	5,00	(2)(3)(4)(6)(7)
(6) 6	3	19,67	(5)(9)
(7) 7	3	15,50	(5)(9)
(8) 8	3	13,83	(9)
(9) 9	3	2,00	(1)(2)(3)(4)(6)(7)(8)

Table 5.9: % of cell viability in BEnd5 cells incubated with 50 µg/ml AuNPs for 24 hours. Kruskal-Wallis test was used to determine the significant difference between the control means and experimental groups.

Data	% Proliferation
Factor codes	AuNPs
Sample size	27
Test statistic	22,8915
Corrected for ties Ht	22,9265
Degrees of Freedom (DF)	8
Significance level	P = 0,003460

Factor	n	Average Rank	Different (P<0,05) from factor nr
(1) 1	3	9,00	(2)(3)(7)(8)(9)
(2) 2	3	23,67	(1)(4)(5)(6)(7)(9)
(3) 3	3	24,67	(1)(4)(5)(6)(7)(8)(9)
(4) 4	3	14,33	(2)(3)(5)(9)
(5) 5	3	5,00	(2)(3)(4)(6)(7)(8)
(6) 6	3	13,50	(2)(3)(5)(9)
(7) 7	3	15,17	(1)(2)(3)(5)(9)
(8) 8	3	18,67	(1)(3)(5)(9)
(9) 9	3	2,00	(1)(2)(3)(4)(6)(7)(8)

Table 5.10: % of cell viability in MCF-7 cells incubated with 50 µg/ml AuNPs for 4 hours. Kruskal-Wallis test was used to determine the significant difference between the control means and experimental groups.

Data	% Proliferation
Factor codes	AuNPs
Sample size	27
Test statistic	23,0476
Corrected for ties Ht	23,1040
Degrees of Freedom (DF)	8
Significance level	P = 0,003233

Factor	n	Average Rank	Different (P<0,05) from factor nr
(1) 1	3	12,00	(2)(3)(4)(5)(9)
(2) 2	3	22,67	(1)(5)(6)(7)(8)(9)
(3) 3	3	21,67	(1)(5)(6)(7)(8)(9)
(4) 4	3	24,33	(1)(5)(6)(7)(8)(9)
(5) 5	3	5,00	(1)(2)(3)(4)(7)(8)
(6) 6	3	10,33	(2)(3)(4)(9)
(7) 7	3	14,67	(2)(3)(4)(5)(9)
(8) 8	3	13,33	(2)(3)(4)(5)(9)
(9) 9	3	2,00	(1)(2)(3)(4)(6)(7)(8)

Table 5.11: % of cell viability in MCF-7 cells incubated with 50 µg/ml AuNPs for 4 hours followed by 4 Gy X-ray radiation. Kruskal-Wallis test was used to determine the significant difference between the control means and experimental groups.

Data	% Proliferation
Factor codes	AuNPs
Sample size	27
Test statistic	24,9101
Corrected for ties Ht	24,9405
Degrees of Freedom (DF)	8
Significance level	P = 0,001591

Factor	n	Average Rank	Different (P<0,05) from factor nr
(1) 1	3	18,00	(2)(3)(5)(6)(7)(8)(9)
(2) 2	3	25,00	(1)(4)(5)(6)(7)(8)(9)
(3) 3	3	23,33	(1)(4)(5)(6)(7)(8)(9)
(4) 4	3	19,67	(2)(3)(5)(6)(7)(8)(9)
(5) 5	3	4,33	(1)(2)(3)(4)(6)(7)(8)
(6) 6	3	14,00	(1)(2)(3)(4)(5)(8)(9)
(7) 7	3	11,00	(1)(2)(3)(4)(5)(9)
(8) 8	3	8,00	(1)(2)(3)(4)(5)(6)(9)
(9) 9	3	2,67	(1)(2)(3)(4)(6)(7)(8)

Table 5.12: % of cell viability in MCF-7 cells incubated with 50 µg/ml AuNPs for 24 hours. Kruskal-Wallis test was used to determine the significant difference between the control means and experimental groups.

Data	% Proliferation
Factor codes	AuNPs
Sample size	27
Test statistic	24,3492
Corrected for ties Ht	24,3790
Degrees of Freedom (DF)	8
Significance level	P = 0,001979

Factor	n	Average Rank	Different (P<0,05) from factor nr
(1) 1	3	26,00	(2)(3)(4)(5)(6)(7)(8)(9)
(2) 2	3	19,33	(1)(4)(5)(7)(8)(9)
(3) 3	3	20,33	(1)(4)(5)(7)(8)(9)
(4) 4	3	12,33	(1)(2)(3)(5)(6)(9)
(5) 5	3	4,00	(1)(2)(3)(4)(6)(7)(8)
(6) 6	3	20,33	(1)(4)(5)(7)(8)(9)
(7) 7	3	12,33	(1)(2)(3)(5)(6)(9)
(8) 8	3	8,33	(1)(2)(3)(5)(6)(9)
(9) 9	3	3,00	(1)(2)(3)(4)(6)(7)(8)

Table 5.13: % of cell viability in MCF-10A cells incubated with 50 µg/ml AuNPs for 4 hours. Kruskal-Wallis test was used to determine the significant difference between the control means and experimental groups.

Data	% Proliferation
Factor codes	AuNPs
Sample size	27
Test statistic	23,0476
Corrected for ties Ht	23,1040
Degrees of Freedom (DF)	8
Significance level	P = 0,003233

Factor	n	Average Rank	Different (P<0,05) from factor nr
(1) 1	3	12,00	(2)(3)(4)(5)(9)
(2) 2	3	22,67	(1)(5)(6)(7)(8)(9)
(3) 3	3	21,67	(1)(5)(6)(7)(8)(9)
(4) 4	3	24,33	(1)(5)(6)(7)(8)(9)
(5) 5	3	5,00	(1)(2)(3)(4)(7)(8)
(6) 6	3	10,33	(2)(3)(4)(9)
(7) 7	3	14,67	(2)(3)(4)(5)(9)
(8) 8	3	13,33	(2)(3)(4)(5)(9)
(9) 9	3	2,00	(1)(2)(3)(4)(6)(7)(8)

Table 5.14: % of cell viability in MCF-10A cells incubated with 50 µg/ml AuNPs for 4 hours followed by 4 Gy X-ray radiation. Kruskal-Wallis test was used to determine the significant difference between the control means and experimental groups.

Data	% Proliferation
Factor codes	AuNPs
Sample size	27
Test statistic	21,2884
Corrected for ties Ht	21,3209
Degrees of Freedom (DF)	8
Significance level	P = 0,006342

Factor	n	Average Rank	Different (P<0,05) from factor nr
(1) 1	3	20,00	(4)(5)(6)(8)(9)
(2) 2	3	16,83	(5)(9)
(3) 3	3	22,67	(4)(5)(6)(8)(9)
(4) 4	3	11,67	(1)(3)(7)(9)
(5) 5	3	5,00	(1)(2)(3)(6)(7)
(6) 6	3	12,67	(1)(3)(5)(7)(9)
(7) 7	3	23,50	(4)(5)(6)(8)(9)
(8) 8	3	11,67	(1)(3)(7)(9)
(9) 9	3	2,00	(1)(2)(3)(4)(6)(7)(8)

Table 5.15: % of cell viability in MCF-10A cells incubated with 50 µg/ml AuNPs for 24 hours. Kruskal-Wallis test was used to determine the significant difference between the control means and experimental groups.

Data	% Proliferation
Factor codes	AuNPs
Sample size	27
Test statistic	24,6217
Corrected for ties Ht	24,6971
Degrees of Freedom (DF)	8
Significance level	P = 0,001749

Factor	n	Average Rank	Different (P<0,05) from factor nr
(1) 1	3	15,50	(3)(5)(6)(7)(8)(9)
(2) 2	3	17,00	(3)(5)(6)(7)(8)(9)
(3) 3	3	23,00	(1)(2)(4)(5)(7)(8)(9)
(4) 4	3	18,17	(3)(5)(6)(7)(8)(9)
(5) 5	3	5,00	(1)(2)(3)(4)(6)(7)(8)
(6) 6	3	26,00	(1)(2)(4)(5)(7)(8)(9)
(7) 7	3	10,33	(1)(2)(3)(4)(5)(6)(9)
(8) 8	3	9,00	(1)(2)(3)(4)(5)(6)(9)
(9) 9	3	2,00	(1)(2)(3)(4)(6)(7)(8)

